INFORMATION TO USERS

This reproduction was made from a copy of a document sent to us for microfilming. While the most advanced technology has been used to photograph and reproduce this document, the quality of the reproduction is heavily dependent upon the quality of the material submitted.

The following explanation of techniques is provided to help clarify markings or notations which may appear on this reproduction.

1. The sign or "target" for pages apparently lacking from the document photographed is "Missing Page(s)". If it was possible to obtain the missing page(s) or section, they are spliced into the film along with adjacent pages. This may have necessitated cutting through an image and duplicating adjacent pages to assure complete continuity.

2. When an image on the film is obliterated with a round black mark, it is an indication of either blurred copy because of movement during exposure, duplicate copy, or copyrighted materials that should not have been filmed. For blurred pages, a good image of the page can be found in the adjacent frame. If copyrighted materials were deleted, a target note will appear listing the pages in the adjacent frame.

3. When a map, drawing or chart, etc., is part of the material being photographed, a definite method of "sectioning" the material has been followed. It is customary to begin filming at the upper left hand corner of a large sheet and to continue from left to right in equal sections with small overlaps. If necessary, sectioning is continued again—beginning below the first row and continuing on until complete.

4. For illustrations that cannot be satisfactorily reproduced by xerographic means, photographic prints can be purchased at additional cost and inserted into your xerographic copy. These prints are available upon request from the Dissertations Customer Services Department.

5. Some pages in any document may have indistinct print. In all cases the best available copy has been filmed.

University Microfilms International
300 N. Zeeb Road
Ann Arbor, MI 48106

Swift, James William

BIFURCATION AND SYMMETRY IN CONVECTION

University of California, Berkeley PH.D. 1985

PLEASE NOTE:

In all cases this material has been filmed in the best possible way from the available copy. Problems encountered with this document have been identified here with a check mark __√__.

1. Glossy photographs or pages _____
2. Colored illustrations, paper or print _____
3. Photographs with dark background _____
4. Illustrations are poor copy _____
5. Pages with black marks, not original copy _____
6. Print shows through as there is text on both sides of page _____
7. Indistinct, broken or small print on several pages __√__
8. Print exceeds margin requirements _____
9. Tightly bound copy with print lost in spine _____
10. Computer printout pages with indistinct print _____
11. Page(s) _____ lacking when material received, and not available from school or author.
12. Page(s) _____ seem to be missing in numbering only as text follows.
13. Two pages numbered _____. Text follows.
14. Curling and wrinkled pages _____
15. Dissertation contains pages with print at a slant, filmed as received _____
16. Other _____

_____

_____

University
Microfilms
International

Bifurcation and Symmetry in Convection

By

James William Swift

A.B. (University of California, Santa Cruz) 1978

DISSERTATION

Submitted in partial satisfaction of the requirements for the degree of

DOCTOR OF PHILOSOPHY

in

Physics

in the

GRADUATE DIVISION

OF THE

UNIVERSITY OF CALIFORNIA, BERKELEY

Approved: 12/10/84
Chairman Date
..... 12/10/84
..... 12/6/84

.....

Bifurcation and Symmetry in Convection

James W. Swift

Abstract

The theory of bifurcation with symmetry is applied to the onset of convection in a fluid layer heated from below. Doubly diffusive convection illustrates the general theory, which describes selection between the possible cellular patterns: rolls, hexagons, triangles, squares, and rectangles. Double periodicity in the horizontal plane is imposed, thus allowing only a finite number of convection rolls to become unstable at the onset of convection. Each roll has a time-dependent complex amplitude and the center manifold theorem allows a complete description of the dynamics near the instability in terms of an ordinary differential equation for the critical amplitudes. These ordinary differential equations are called *normal forms*. For the cases discussed here there are 1, 2, 3, 4, or 6 complex amplitudes (i.e. rolls) which go unstable simultaneously. The normal forms have a high degree of symmetry which allows a complete characterization of the dynamics in terms of a few parameters which cannot be eliminated through scaling. These parameters are evaluated for doubly diffusive convection. A classification of all possible generic bifurcations is given for the simplest realization of each type of double periodicity. Some degenerate bifurcations and their unfoldings are classified. Since the classification does not rely on the details of the problem, this work is relevant to any bifurcation problem with the spatial symmetry of the plane when the instability has a preferred wavelength which is neither zero nor infinity.

Table of Contents

Acknowledgements

Here I wish to acknowledge my gratitude to those who have contributed to this work, directly or indirectly. Many great men in the field have been influential and encouraging, particularly: Marty Golubitsky, Fritz Busse, John Guchenheimer, and Jerry Marsden. First and foremost, however, I owe my thanks to my advisor, Edgar Knobloch, for his thorough scrutiny of the entire manuscript, as well as his continuing advice, support, and criticism. Thanks also to the other members of my dissertation committee, Alan Kaufman and Jerry Marsden, for their prompt and valuable comments. Several colleagues to whom I owe my gratitude have been: Ken Rimey, who was invaluable as a consultant on UNIX and vaxima (the computer operating system and the symbolic algebra program), Kurt Wiesenfeld, who has shared an office as well as an advisor, an my house mate Albert Stebbins. In the final days of this work, Constance Eldridge has encouraged me when things looked discouraging, and helped with the figures and xeroxing. I am grateful that Colin Sparrow and the Fellows of King's College have been so patient and understanding in these final months of preparation. And finally, I want to thank my parents for all their love, support, and encouragement.

Introduction

In recent years there has been an explosion of interest in nonlinear dynamics. The modern theory of dynamical systems asks qualitative questions about the behavior of nonlinear systems, where exact solutions are difficult to find. One aspect of nonlinear dynamics is bifurcation theory, which is concerned with the branching of solutions as a parameter is varied. In this dissertation bifurcation theory is used to investigate pattern selection between two- and three-dimensional convection in a fluid layer heated from below.

In this introduction a short description of convection is given, followed by a brief summary of previous work done in this field and the overall philosophy of the bifurcation theory approach. Then the techniques used in the calculations are described, followed by an outline of the dissertation.

When a fluid layer is heated from below, the fluid near the bottom expands and becomes less dense than the fluid near the top. The warm fluid has a tendency to rise, but viscosity (internal fluid friction) serves to damp any fluid motion. These competing forces are measured by a non-dimensional parameter, the *Rayleigh number*, which is proportional to the temperature difference and inversely proportional to the viscosity. For small Rayleigh numbers, all fluid motion decays due to viscosity, and the heat is transferred across the fluid layer by molecular *conduction*. (The Rayleigh number is also inversely proportional the the coefficient of thermal conductivity, which determines the effectiveness of conductive heat transport.) As the Rayleigh number is increased there is a *critical* Rayleigh number beyond which the fluid motion is not effectively damped by viscosity, and convection sets in. *Convection* is the transport of heat through bulk fluid motion.

The simplest example of convection, in which only velocity and tempera-

ture are dynamical fields, is called Rayleigh-Bénard convection. When a solute is added and a solute gradient is maintained, there are buoyancy effects which are analogous to those caused by thermal expansion. This is called thermohaline convection when the solute is salt, and the name doubly diffusive convection refers to the more general case. More complicated examples of convection include magnetoconvection, when a magnetic field is present and the fluid is electrically conducting, and convection in a rotating fluid layer. The symmetry of Rayleigh-Bénard or doubly diffusive convection is different from that of convection in a rotating fluid layer, because the rotation introduces a handedness to the problem. When the imposed magnetic field is vertical, the critical modes of magnetoconvection have the same symmetry as Rayleigh-Bénard convection (Busse & Clever, 1982).

With the idealizations of an infinite plane layer and uniform heating from below, the convection equations have the symmetry of all rotations and translations in the horizontal plane. This symmetry is necessarily broken when convection occurs, because the fluid must flow up in some places and down in others. The pattern of upward and downward fluid flow, as viewed from above, is called the *planform*. The possible planforms include rolls, hexagons, rectangles, and squares. In rolls, the fluid circulates in counter-rotating cylinders. This is a two-dimensional pattern, because the velocity and temperature fields do not change in the direction of the roll axis. The roll planform consists of alternating stripes of upward and downward flow. Bénard (1901) observed hexagonal cells, with the flow up at the centers and down on the sides of a honeycomb pattern. The three-dimensional patterns, rectangles, squares and hexagons, are approximated (at small amplitude) by a linear superposition of rolls oriented in different directions. Any superposition of rolls of the same wavelength is treated equally by the linearized convection equations; therefore

nonlinear interactions are responsible for pattern selection.

Due to Bénard's observations, the early work on the nonlinear pattern selection tried to understand why hexagons are the preferred planform. Two papers which appeared almost simultaneously, Gor'kov (1958) and Malkus & Veronis (1958), used rather different approaches toward this end. Gor'kov tacitly assumed that the solution has hexagonal symmetry, and then showed that two patterns, hexagons and regular triangles, are possible. The paper by Malkus & Veronis uses a more general approach to the problem. They consider rolls, hexagons, squares and rectangles; however, they incorrectly assert that two-dimensional roll solutions are not physically realizable.

Both papers, however, used the Boussinesq equations as their starting point. It was later found (Block, 1956, Palm 1960, Segel & Stuart 1962, Busse 1962, Busse 1967) that deviations from the Boussinesq approximation were responsible for the stability of the hexagons.

While Gor'kov (1958) made some fundamental mistakes, his paper is insightful; he stresses the importance of the coupling of $\mathbf{k}$ vectors in the horizontal plane, and the symmetry of the solutions. This paper has been largely ignored in the West, where most workers follow Malkus & Veronis (1958). The amplitude expansion of Malkus & Veronis finds the Rayleigh number as function of the amplitude ε of the fluid motion:

$$R = R_c + R_1\varepsilon + R_2\varepsilon^2 + \cdots , \tag{1}$$

where R_c is the critical Rayleigh number, at which linear theory predicts the convective instability. This relation can be inverted to determine the amplitude as a function of $R-R_c$.

The symmetry implied by the Boussinesq approximation, which is discussed at length here, forces all the odd coefficients, R_1, R_3, etc., to be zero. The sign of R_2 then determines whether the convection solutions exist supercritically

(for $R > R_c$) or subcritically (for $R < R_c$). When three-dimensional patterns are studied, each pattern has its own R_2. For all patterns but hexagons, the symmetry in the horizontal plane forces R_1, R_3, etc., to be zero even if the Boussinesq approximation is not valid.

As mentioned above, Malkus & Veronis (1958) incorrectly asserted that the roll solutions cannot be realized in practice. This is corrected by Schlüter, Lortz, & Busse (1965), who extended the work of Malkus & Veronis. For Rayleigh-Bénard convection in the Boussinesq approximation they found that the only stable small amplitude solutions are the two-dimensional rolls. However, three-dimensional patterns, such as squares and hexagons, can be stable given the general structure of the problems, even when the Boussinesq approximation is valid. Hence, a difficult calculation must be performed in order to determine which patterns are stable. The calculation of the stable pattern has been done in the following cases:

- Nagata & Thomas (1983) calculated R_2 for the three-dimensional patterns in doubly diffusive convection. The techniques they use cannot establish the stability of the patterns, although the stability can be inferred from a knowledge of R_2 for the various patterns. The calculation of the stable pattern is done in this dissertation using different techniques. The details of the results for R_2 are slightly different in the two calculations; unlike the calculations of Nagata & Thomas (1983), those obtained here agree with Schlüter *et al.* (1965) in the limit of Rayleigh-Bénard convection. The result is that rolls are the only stable small amplitude solutions in doubly diffusive convection. These calculations are done for Boussinesq convection with the simplest boundary conditions: stress-free boundaries for the velocity field, and fixed temperature and solute at the boundaries.

- Busse & Clever (1982) performed the calculation for convection in a verti-

cal magnetic field with stress-free boundaries, in the limit when the magnetic diffusivity is much larger than the other diffusion coefficients. They found that rolls are the only stable small amplitude solution in this limiting case.

• For rotating convection with free boundaries and infinite Prandtl number, Küppers & Lortz (1969) calculated that rolls are stable when the rotation rate is below a critical value. For larger rotation rates, the rolls are unstable to perturbations in the form of rolls oriented preferentially at 58° in the direction of rotation. No stable steady state solution exists in this regime. Later, Küppers (1970) found numerically that the results are similar for the more realistic rigid boundaries when the Prandtl number is of order one or larger. At small Prandtl numbers the rolls can be subcritical ($R_2 < 0$), and the instability can be oscillatory as well. The case of convection in a rotating fluid layer with free boundaries and *finite* Prandtl number is unusual; the rolls are unstable at *any* nonzero rotation rate (Swift, in preparation). A roll is always unstable to other rolls oriented at small enough angles in the direction of rotation. This is due to a vertical vorticity mode which is forbidden with rigid boundary conditions.

• When the thermal conductivity of the boundaries is small, rolls are *not* stable to three-dimensional disturbances. (The usual assumption is that the thermal conductivity of the boundaries is infinite.) Busse & Riahi (1980) showed that for nearly insulating boundaries, squares (and many rectangles) are stable relative to rolls. This is the first known example of a convection system with vertical symmetry where three-dimensional patterns are preferred. Riahi (1983) numerically computed the stability of rolls, squares, and hexagons for convection in a porous layer with finite conducting boundaries. Hexagons are never stable in this system, and squares are preferred when the conductivity is small enough.

The bifurcation theory approach, pioneered by Joseph (1976) and Sat-

tinger (1979), attempts to derive as much information as possible from the symmetry of the problem, without reference to the particular equations. The questions of interest are:

- What are the possible patterns of convective motion?
- What are the stability properties of the solutions?
- What is the role of symmetry?

The result of the bifurcation analysis is a *normal form*. This is the simplest system which contains all of the essential features of the original problem. The normal form is an ordinary differential equation for the amplitudes of the critical rolls. These critical rolls have the preferred wavelength of the instability. The three-dimensional patterns are linear superpositions of critical rolls in different orientations. The normal forms contain coefficients which are not determined by the symmetry, but depend on the specifics of the physical problem.

The results are summarized in the *bifurcation diagrams*. These diagrams plot the heat transport of the solutions as a function of the Rayleigh number. They show which solutions exist, whether they are subcritical or supercritical, and their stability. The determination of which of the possible bifurcation diagrams actually applies to a given physical situation requires a calculation of the coefficients in the normal form.

For technical reasons, the number of critical rolls described by the normal form must be finite. This is accomplished by imposing double periodicity in the horizontal plane. Doubly periodic solutions are represented by a Fourier series instead of a Fourier integral. Each different example of double periodicity, such as the square lattice and the hexagonal lattice, must be treated separately. Only the doubly periodic solutions can be studied using this approach, although others exist. Indeed, Busse (1978) showed that spatially

quasiperiodic solutions of the third order equations exist, although there are technical difficulties at higher order.

The power of the bifurcation theory approach to convection is that the results depend only on the symmetry of the problem. The same results apply to Rayleigh-Bénard convection, doubly diffusive convection, and magnetoconvection.

Bifurcation theory gives a way to determine when the truncation of the perturbation expansion is justified. The normal forms can be analyzed as dynamical systems to test whether they are structurally stable, that is, whether the addition of higher order terms will change their qualitative behavior. Traditionally, the expansions have been carried out to third order. Buzano & Golubitsky (1983), and Golubitsky *et al.* (1984) found that fifth order terms are necessary for convection on a hexagonal lattice. Even when rolls are stable, these higher order terms are necessary from a mathematical point of view, although they are not physically important.

Furthermore, bifurcation theory is a *dynamical* theory. The solution types and their stability is described by the normal forms. Two separate calculations are necessary with the amplitude expansion technique. As a dynamical theory, the analyses of both steady state bifurcations and oscillatory bifurcations are possible using the same techniques.

The classification of the possible bifurcations has intrinsic mathematical interest, but from the point of view of a physicist, the calculation of the coefficients is more important. Therefore a major portion of this dissertation is devoted to an efficient calculation of the coefficients in doubly diffusive convection.

The calculational techniques used here are based on the center manifold theorem, as is the bifurcation theory. The methods are simpler than those of

Malkus & Veronis (1958) or Schlüter *et al.* (1965), but they only work with stress-free boundary conditions. With the more realistic boundary conditions, however, numerical calculations are necessary. The simpler techniques are therefore applicable whenever an analytic calculation can be done.

The main features of the calculational techniques are:

• The partial differential equations of convection are reduced to an infinite set of ordinary differential equations. The degrees of freedom which contribute to the normal form at a given order are determined, using symmetry considerations, and the system is truncated. The analysis proceeds using the finite set of ordinary differential equations.

• Complex notation is used throughout. Traditionally, the vertical eigenfunctions are written as sines and cosines (for the simplest boundary conditions). The use of complex exponentials makes the calculations easier.

• The equations of doubly diffusive convection are written so that the symmetry between heat and solute is explicit. This symmetry is exploited fully in the calculations.

• The depth of the fluid is normalized to π rather than one. This has the effect of eliminating bothersome factors of π in the calculations.

Outline of the Dissertation

Chapter One contains an introduction to the equations describing Rayleigh-Bénard convection, doubly diffusive convection, and convection in a rotating fluid layer. The symmetry of these equations is discussed.

Chapter Two begins with a review of bifurcation theory. Then, the normal form for bifurcation in the plane with the symmetry of a square is derived as an example of bifurcation with symmetry. It is then shown that this example describes the possible steady state bifurcation behavior of convection on a

square or rhombic lattice. On the hexagonal lattice, the bifurcations are more complicated; the behavior depends on whether or not the Boussinesq approximation is valid. These two cases are treated separately, and the connection between them is made.

In Chapter Three, Hopf bifurcations in convection are discussed. The two-dimensional oscillatory solutions can be either traveling waves or standing waves, and the normal form is derived which describes the selection between these two patterns. This bifurcation equivalent to the original example of bifurcation in the plane with the symmetry of a square. Three-dimensional oscillatory convection is sufficiently complicated that the normal forms have not yet been determined, although the most general ordinary differential equations with the correct symmetry are derived here.

Chapter Four contains the calculation, for doubly diffusive convection, of the coefficients in the normal forms derived in Chapter Two. A detailed discussion of the symmetry of the infinite dimensional ordinary differential equations of convection in a doubly periodic domain is included. The treatment of the nonlinear terms is general enough to apply to magnetoconvection and convection in a rotating fluid layer.

In Chapter Five, the third order coefficients of the normal forms for two-dimensional, oscillatory, doubly diffusive convection are calculated. The third order result is degenerate, so one of the degenerate bifurcations analyzed in Chapter Two is relevent.

Finally, the Conclusion gives a summary of the present results and a program for future research.

Three appendices follow. Appendix A lists the notation used throughout the dissertation. Appendix B is a reprint of "Convection in a rotating fluid layer" (Swift, 1984). This paper describes the effect of non-Boussinesq terms

added to the cubic truncation of the ordinary differential equations describing rotating convection on the hexagonal lattice. Appendix C describes an efficient technique for calculating the sub- or supercriticality of Hopf bifurcations with three fold rotational symmetry. Such bifurcations occur at finite amplitude in the Boussinesq and non-Boussinesq cases of rotating convection.

Chapter One

The Convection Equations

In this chapter three examples of convection are introduced: Rayleigh-Bénard convection, doubly diffusive convection, and convection in a rotating fluid layer. The linear stability analysis of the conduction state is carried out in the cases where the Boussinesq approximation holds, and stress free boundary conditions are applied to the top and bottom plate. These idealizations, which are discussed in detail, are not necessary for the normal form results of Chapters Two and Three. However they make the powerful calculation techniques of Chapter Four and Five possible. What goes wrong with other boundary conditions is described, and the chapter ends with a discussion of the symmetries of the partial differential equations. The results of linear theory are not new, but they are necessary for the remainder of the dissertation.

1.1. The Fundamental Equations

Consider a fluid layer of thickness d heated uniformly from below; the bottom and top plates are held at fixed temperatures T_0 and T_1 respectively. Let

$$\mathbf{x} = (x_1, x_2, x_3) = (x, y, z) \tag{1-1}$$

be the position, and

$$\mathbf{u} = (u_1, u_2, u_3) = (u, v, w) \tag{1-2}$$

be the velocity of the fluid.

The continuity equation, expressing the conservation of mass, is:

$$\left(\frac{\partial}{\partial t} + \mathbf{u}\cdot\nabla\right)\rho = -\rho\nabla\cdot\mathbf{u}, \tag{1-3}$$

where ρ is the density of the fluid. The combination

$$\frac{\partial}{\partial t} + \mathbf{u}\cdot\nabla \tag{1-4}$$

is the convective derivative, or total time derivative for a comoving fluid

element. For an incompressible fluid the equation of continuity reduces to

$$\nabla\cdot\mathbf{u} = 0. \tag{1-5}$$

The conservation of momentum is:

$$\rho\left(\frac{\partial}{\partial t}+\mathbf{u}\cdot\nabla\right)u_i = -\frac{\partial}{\partial x_i}p - \rho g\,\delta_{i,3} + \sum_{j=1}^{3}\frac{\partial}{\partial x_j}(\mu e_{i,j}) - \frac{\partial}{\partial x_i}\frac{2}{3}\mu(\nabla\cdot\mathbf{u}), \tag{1-6}$$

where p is the dynamic pressure, g is the acceleration of gravity, μ is the coefficient of viscosity, and

$$e_{i,j} = \frac{1}{2}\left[\frac{\partial u_i}{\partial x_j}+\frac{\partial u_j}{\partial x_i}\right]. \tag{1-7}$$

The viscous stress term, containing μ, is complicated; however for an incompressible fluid with constant viscosity, equation (1-6) reduces to the Navier-Stokes equation:

$$\rho\left(\frac{\partial}{\partial t}+\mathbf{u}\cdot\nabla\right)\mathbf{u} = -\nabla p + \rho\mathbf{g} + \mu\nabla^2\mathbf{u}. \tag{1-8}$$

The conservation of energy is

$$\left(\frac{\partial}{\partial t}+\mathbf{u}\cdot\nabla\right)(\rho c_V T) = \nabla\cdot(k\nabla T) - p\,\nabla\cdot\mathbf{u} + \Phi, \tag{1-9}$$

where c_V is the specific heat at constant volume, T is the temperature, and k is the coefficient of heat conduction. The rate at which energy is dissipated by viscosity,

$$\Phi = \sum_{i=1}^{3}\sum_{j=1}^{3} 2\mu e_{i,j}e_{i,j} \tag{1-10}$$

can be neglected because it is extremely small; for water it is about $d(\mathrm{cm})\cdot 10^{-8}$ times the contribution of the convection of heat. (It is difficult to heat water by stirring it.)

In order to close the system of equations (1-5, 1-8, 1-9) an equation of state is needed, fixing ρ as a function of p and T. The simplest equation of state which includes buoyancy due to thermal expansion is:

$$\rho = \rho_0[1-\alpha(T-T_{ref})] \tag{1-11}$$

where α is the coefficient of thermal expansion and T_{ref} is the temperature

where $\rho = \rho_0$. More general expressions for ρ are discussed in the next section.

The transport coefficients, μ and k, depend on temperature in general. The viscosity of fluids tends to decrease as temperature is increased (as with heated syrup). Less familiar from everyday experience is the fact that the effect is typically reversed in gases. The partial differential equations obtained with temperature dependent μ, κ, and c_v are contained in Busse's Thesis (1962). These equations are complicated, and for the most part this temperature dependence will be neglected. In some cases (see Chapter Two), however, this dependence introduces qualitative effects.

1.2. The Boussinesq Approximation

In many cases the variation in density across the layer is small; α is of the order 10^{-3} to 10^{-4} per °C for most liquids and gases (Chandrasekhar, 1961). The variation of density can therefore be ignored except in the buoyancy term ($\rho\mathbf{g}$). If the variations of c_v, k and μ are small, these quantities can be assumed constant. This is the *Boussinesq approximation*. The Boussinesq approximation also requires that the velocities are sufficiently subsonic.

For a deep fluid layer the assumption of equation (1-11) that the density is independent of pressure breaks down. Spiegel & Veronis (1960) consider an ideal gas and find that, if the depth of the layer is much less than any scale height, the Boussinesq approximation is valid if c_p replaces c_v and the temperature gradient is replaced by its excess over the adiabatic.

The fluid equations, in the Boussinesq approximation, are:

$$\left(\frac{\partial}{\partial t} + \mathbf{u}\cdot\nabla\right)\mathbf{u} = -\frac{\nabla p}{\rho_0} + \frac{\rho}{\rho_0}\mathbf{g} + \nu\nabla^2\mathbf{u}, \tag{1-12}$$

$$\left(\frac{\partial}{\partial t} + \mathbf{u}\cdot\nabla\right)T = \kappa\nabla^2 T, \tag{1-13}$$

$$\nabla\cdot\mathbf{u} = 0, \tag{1-14}$$

where

$$\nu = \frac{\mu}{\rho_0} \text{ is the kinematic viscosity, and}$$
$$\kappa = \frac{k}{\rho_0 c_v} \text{ is the coefficient of thermometric conductivity.} \tag{1-15}$$

When there is no fluid motion, and the bottom and top boundaries are held at fixed temperatures T_0 and T_1 the temperature equation is $\nabla^2 T = 0$ which has the solution:

$$T = T_0 - \frac{\Delta T}{d} z \text{ , where } \Delta T = T_0 - T_1 > 0. \tag{1-16}$$

The density is therefore

$$\rho = \rho_0 \left(1 + \alpha \frac{\Delta T}{d} z\right). \tag{1-17}$$

The Navier-Stokes equation (1-8) reduces to:

$$\frac{\nabla p}{\rho_0} = \left(1 + \alpha \frac{\Delta T}{d} z\right)(-g\,\hat{\mathbf{z}}), \tag{1-18}$$

and the pressure distribution is

$$p = p_0 - \rho_0 g z - \tfrac{1}{2} \rho_0 \frac{\Delta T}{d} g z^2. \tag{1-19}$$

This is the *conduction* solution; it describes the transport of heat across the layer by molecular conduction.

Let ϑ be the variation from the linear temperature profile:

$$T = T_0 - \frac{\Delta T}{d} z + \vartheta \tag{1-20}$$

and let p be the variation of the pressure from the conduction solution. The Boussinesq equations (1-12, 1-13) become:

$$\left(\frac{\partial}{\partial t} + \mathbf{u}\cdot\nabla\right)\mathbf{u} = -\frac{\nabla p}{\rho_0} + \alpha \vartheta g\,\hat{\mathbf{z}} + \nu \nabla^2 \mathbf{u} \tag{1-21}$$

$$\left(\frac{\partial}{\partial t} + \mathbf{u}\cdot\nabla\right)\vartheta - \mathbf{u}\cdot\hat{\mathbf{z}}\,\frac{\Delta T}{d} = \kappa \nabla^2 \vartheta \tag{1-22}$$

$$\nabla\cdot\mathbf{u} = 0. \tag{1-23}$$

These equation can be non-dimensionalized. The dimensionless position coordinate is chosen to be

$$\mathbf{x}' = \mathbf{x}\frac{\pi}{d}, \tag{1-24}$$

so that the new boundaries are at $z' = 0$ and $z' = \pi$.

There are two logical choices for the time scale: the thermal diffusion time and the viscous diffusion time. The thermal diffusion time scale gives

$$\begin{aligned} t' &= t\frac{\pi^2\kappa}{d^2} \\ \mathbf{u}' &= \mathbf{u}\frac{d}{\pi\kappa} \\ \vartheta' &= \vartheta\frac{\pi}{\Delta T} \\ p' &= p\frac{d^3}{\rho_0\pi^3\kappa\nu}. \end{aligned} \tag{1-25}$$

Dropping the primes, the non-dimensional equations in the thermal diffusion scaling are

$$\left(\frac{\partial}{\partial t} + \mathbf{u}\cdot\nabla\right)\mathbf{u} = \sigma(-\nabla p + R\vartheta\hat{\mathbf{z}} + \nabla^2\mathbf{u}) \tag{1-26}$$

$$\left(\frac{\partial}{\partial t} + \mathbf{u}\cdot\nabla\right)\vartheta = \mathbf{u}\cdot\hat{\mathbf{z}} + \nabla^2\vartheta \tag{1-27}$$

$$\nabla\cdot\mathbf{u} = 0, \tag{1-28}$$

where

$$\begin{aligned} &R \equiv \frac{\alpha g \Delta T d^3}{\nu\kappa\pi^4} \text{ is the } \textit{Rayleigh number}, \text{ and} \\ &\sigma \equiv \frac{\nu}{\kappa} \text{ is the } \textit{Prandtl number}. \end{aligned} \tag{1-29}$$

The vertical viscous diffusion time scale gives:

$$\begin{aligned} t'' &= t\frac{\pi^2\nu}{d^2} = \sigma t' \\ \mathbf{u}'' &= \frac{\mathbf{u}'}{\sigma} \\ \vartheta'' &= \frac{\vartheta'}{\sigma} \\ p'' &= \frac{p'}{\sigma}. \end{aligned} \tag{1-30}$$

Dropping the double primes, the viscous time scale equations are

$$\left(\frac{\partial}{\partial t}+\mathbf{u}\cdot\nabla\right)\mathbf{u} = -\nabla p + R\vartheta\hat{\mathbf{z}}+\nabla^2\mathbf{u} \tag{1-31}$$

$$\left(\frac{\partial}{\partial t}+\mathbf{u}\cdot\nabla\right)\vartheta = \frac{1}{\sigma}(\mathbf{u}\cdot\hat{\mathbf{z}}+\nabla^2\vartheta) \tag{1-32}$$

$$\nabla\cdot\mathbf{u} = 0. \tag{1-33}$$

Other scalings of the equations are possible. The above scalings, based on equation (1-24), are not standard since the depth of the layer is usually set to 1 rather than π. Consequently, the Rayleigh number defined here is $1/\pi^4$ times the usual Rayleigh number. The Rayleigh number defined in equation (1-29) is denoted as R_1 by Chandrasekhar (1961). The advantage of this scaling is that the eigenfunctions have a vertical dependence $\sin(z)$ rather than $\sin(\pi z)$. The nonlinear calculations of Chapters Four and Five would have hundreds of factors of π strewn about with the usual scaling, but they would all cancel out in the end. (I am indebted to John Salmon and Ken Rimey for pointing this out to me.)

1.3. Boundary Conditions

The partial differential equations (1-26 ff) or (1-31 ff) must be supplemented by boundary conditions. Since the temperature is specified at the two plates

$$\vartheta = 0 \text{ at } z = 0, \pi. \tag{1-34}$$

This assumes that the boundaries are perfectly conducting.

There are two types of boundary conditions used for the velocity field: *rigid* and *free*. The more realistic rigid (or no slip) boundaries satisfy

$$\mathbf{u} = 0 \text{ at } z = 0, \pi, \tag{1-35}$$

which implies, using $\nabla\cdot\mathbf{u} = 0$, that

$$\frac{\partial w}{\partial z} = 0 \text{ at } z = 0, \pi, \tag{1-36}$$

$$\text{where } \mathbf{u} \equiv (u,v,w). \tag{1-37}$$

At (stress) free boundaries the tangential viscous stress vanishes:

$$\mu\left(\frac{\partial u}{\partial z}+\frac{\partial w}{\partial x}\right)=\mu\left(\frac{\partial v}{\partial z}+\frac{\partial w}{\partial y}\right)=0 \text{ at } z=0,\pi. \tag{1-38}$$

In addition, the vertical velocity vanishes because the fluid cannot go through the boundary:

$$w=0 \text{ at } z=0,\pi, \tag{1-39}$$

which implies that

$$\frac{\partial w}{\partial x}=\frac{\partial w}{\partial y}=0 \text{ at } z=0,\pi. \tag{1-40}$$

Substituting (1-40) into (1-38), and using the fact that the velocity field is divergence free, one finds

$$\frac{\partial u}{\partial z}=\frac{\partial v}{\partial z}=\frac{\partial^2 w}{\partial z^2}=0 \text{ at } z=0,\pi. \tag{1-41}$$

Free boundaries are relevant when two fluids are in contact or when the upper surface is air. Realistically, such boundaries can move, but such free boundary problems are notoriously difficult. The non-deformable free boundaries used here greatly simplify the mathematical calculations, although they are somewhat artificial.

The boundary conditions listed above are the same on the top and bottom plate, but this is not necessary. In Bénard's experiments, for example, there were rigid boundaries on the bottom plate and free boundaries on the top plate. When the boundary conditions are the same on the top and bottom, they are said to be *symmetric*.

1.4. Doubly Diffusive Convection

There can be buoyancy in fluids due to other effects besides thermal expansion. In the ocean, for instance, the concentration of salt is higher at the surface due to the evaporation of fresh water. Salty water is denser than fresh water, thus convection can be driven by concentration gradients in the absence

of a temperature gradient. The equations for solutal convection are found by analogy to (1-31)-(1-33). In place of $\alpha\Delta T$ there is $\Delta\rho \equiv \rho_{top} - \rho_{bottom}$. In place of κ there is κ_S, the coefficient of solute diffusion. In terms of the viscous time scale, and using the Boussinesq approximation, the equations are:

$$\left(\frac{\partial}{\partial t}+\mathbf{u}\cdot\nabla\right)\mathbf{u} = -\nabla p + R_S\xi\hat{\mathbf{z}}+\nabla^2\mathbf{u} \tag{1-42}$$

$$\left(\frac{\partial}{\partial t}+\mathbf{u}\cdot\nabla\right)\xi = \frac{1}{\sigma_S}(\mathbf{u}\cdot\hat{\mathbf{z}}+\nabla^2\xi) \tag{1-43}$$

$$\nabla\cdot\mathbf{u} = 0\,, \tag{1-44}$$

where

$$R_S \equiv \frac{g\,\Delta\rho\,d^3}{\nu\kappa_S\pi^4} \text{ and } \sigma_S \equiv \frac{\nu}{\kappa_S}. \tag{1-45}$$

Here ξ is the solute analog of ϑ (see equation (1-20)), and R_S and σ_S are the solute Rayleigh and Prandtl numbers. (σ_S is also called the Schmidt number.)

Both temperature and solute gradients are present in *doubly diffusive convection*. The basic equations are, with the viscous time scale:

$$\left(\frac{\partial}{\partial t}+\mathbf{u}\cdot\nabla\right)\mathbf{u} = -\nabla p + R_T\vartheta\hat{\mathbf{z}}+R_S\xi\hat{\mathbf{z}}+\nabla^2\mathbf{u} \tag{1-46}$$

$$\left(\frac{\partial}{\partial t}+\mathbf{u}\cdot\nabla\right)\vartheta = \frac{1}{\sigma_T}(\mathbf{u}\cdot\hat{\mathbf{z}}+\nabla^2\vartheta) \tag{1-47}$$

$$\left(\frac{\partial}{\partial t}+\mathbf{u}\cdot\nabla\right)\xi = \frac{1}{\sigma_S}(\mathbf{u}\cdot\hat{\mathbf{z}}+\nabla^2\xi) \tag{1-48}$$

$$\nabla\cdot\mathbf{u} = 0\,. \tag{1-49}$$

The generalization to more solutes is obvious. The symmetry between heat and solute in these equations is delicate. Any departure from the Boussinesq approximation is likely to break this symmetry.

The study of doubly diffusive convection is relatively recent. It began as the "oceanographic curiosity" of Stommel *et al.*(1956), and the linear theory was studied throughly by Baines & Gill (1969). The nonlinear aspects of doubly diffusive convection have been the subject of many papers, including Veronis (1959, 1966, 1968b), Huppert & Moore (1976), and Knobloch & Proctor (1981).

The above scaling emphasizes the symmetry between temperature and solute, but is nonstandard. Usually the solute Rayleigh number is defined as

$$\widetilde{R}_S \equiv \frac{-g\,\Delta\rho\, d^3}{\nu\kappa_T} \tag{1-50}$$

and the ratio $\tau = \kappa_S / \kappa_T$ is used rather than σ_T. Note that a negative value of $\widetilde{R}_S$ indicates a destabilizing solute gradient. Pearlstein (1981) uses the symmetric definitions given here in equation (1-45).

The standard boundary conditions are to specify the concentration at the top and bottom:

$$\xi = 0 \text{ at } z = 0, \pi, \tag{1-51}$$

although these are hard to realize in practice. The formal symmetry between heat and solute requires that the boundary conditions for ξ and ϑ are the same. The solute boundary conditions used here (1-51) are the same as the temperature boundary conditions for perfectly conducting boundaries (1-34).

1.5. Convection in a Rotating Fluid Layer

Consider a fluid layer rotating at a constant rate Ω_{dim} (the subscript stands for "dimensional".) The dimensional equation of motion (1-21) must be modified to include the centrifugal and Coriolis forces:

$$\left(\frac{\partial}{\partial t} + \mathbf{u}\cdot\nabla\right)\mathbf{u} = \frac{-\nabla p}{\rho_0} + \alpha\vartheta g\,\hat{\mathbf{z}} + \mu\nabla^2\mathbf{u} + \nabla\left(\tfrac{1}{2}|\,\Omega_{dim}\times\mathbf{x}|^2\right) + 2\mathbf{u}\times\Omega_{dim}\,, \tag{1-52}$$

where the origin of the coordinate system is on the rotation axis. The pressure increases radially to balance the centrifugal force. It is possible to incorporate the centrifugal force into a modified pressure:

$$p' \equiv p - \tfrac{1}{2}\rho_0\,|\,\Omega\times\mathbf{x}|^2. \tag{1-53}$$

Thus, *the centrifugal force has no significance, only the Coriolis force is important.* As a consequence, the center of rotation is not singled out, and the equations are symmetric with respect to translations in the horizontal plane. Of course, the pressure does affect the fluid properties far away from the center

of rotation, thus violating the translational symmetry.

The non-dimensional rotation vector is

$$\Omega = \frac{2\Omega_{dim}\, d^2}{\nu\pi^2}. \tag{1-54}$$

With the thermal time scaling, the equation of motion (1-52) becomes

$$\left(\frac{\partial}{\partial t} + \mathbf{u}\cdot\nabla\right)\mathbf{u} = \sigma(-\nabla p + R\vartheta\hat{\mathbf{z}} + \mathbf{u}\times\Omega + \nabla^2\mathbf{u}). \tag{1-55}$$

When the viscous time scale is used, the Prandtl number σ is absent in the equation of motion, but the non-dimensional Ω is defined the same way.

1.6. The Velocity Field Expansion

While the velocity field has three scalar components, only two are independent because $\nabla\cdot\mathbf{u} = 0$. Since the vertical direction is singled out, scalar fields related to the vertical velocity and vertical vorticity will be used. The vertical velocity has already been defined:

$$w = \mathbf{u}\cdot\hat{\mathbf{z}}. \tag{1-56}$$

The vorticity is the curl of the velocity,

$$\omega \equiv \nabla\times\mathbf{u}, \tag{1-57}$$

and the vertical vorticity is

$$\zeta \equiv \omega\cdot\hat{\mathbf{z}}. \tag{1-58}$$

A general divergence free vector field can be written as

$$\mathbf{u}(\mathbf{x}, t) = \sum_{n=-\infty}^{\infty} \int d^2\mathbf{k}\left[w_{\mathbf{k},n}(t)\,\mathbf{W}_{\mathbf{k},n} + \zeta_{\mathbf{k},n}(t)\,\mathbf{Z}_{\mathbf{k},n}\right], \tag{1-59}$$

where $w_{\mathbf{k},n}$ and $\zeta_{\mathbf{k},n}$ are time-dependent amplitudes of the vertical velocity modes and vertical vorticity modes, respectively defined as:

$$\mathbf{W}_{\mathbf{k},n} \equiv (-\mathbf{k}n + |\mathbf{k}|^2\hat{\mathbf{z}})e^{i(\mathbf{k}\cdot\mathbf{x}+nz)} \tag{1-60}$$

$$\mathbf{Z}_{\mathbf{k},n} \equiv (\hat{\mathbf{z}}\times\mathbf{k})e^{i(\mathbf{k}\cdot\mathbf{x}+nz)}, \tag{1-61}$$

where $\mathbf{k}$ is a wave vector in the horizontal plane:

$$\mathbf{k}\cdot\hat{\mathbf{z}} = 0 . \tag{1-62}$$

Since $\mathbf{u}$ is real,

$$w_{\mathbf{k},n} = \overline{w}_{-\mathbf{k},-n} , \text{ and } \zeta_{\mathbf{k},n} = -\overline{\zeta}_{-\mathbf{k},-n} , \tag{1-63}$$

where the overbar denotes complex conjugation.

In the literature the velocity field decomposition is often written as

$$\mathbf{u} = \nabla\times(\psi\hat{\mathbf{z}}) + \nabla\times\nabla\times(\varphi\hat{\mathbf{z}}). \tag{1-64}$$

The correspondence between the two representations, (1-59) and (1-64) is

$$\psi = i \sum_{n=-\infty}^{\infty} \int d^2\mathbf{k}\, \zeta_{\mathbf{k},n} e^{i(\mathbf{k}\cdot\mathbf{x}+nz)}, \tag{1-65}$$

$$\varphi = i \sum_{n=-\infty}^{\infty} \int d^2\mathbf{k}\, w_{\mathbf{k},n} e^{i(\mathbf{k}\cdot\mathbf{x}+nz)}. \tag{1-66}$$

In terms of the vertical velocity and vertical vorticity fields, the boundary conditions on the velocity field are

$$w = \frac{\partial^2 w}{\partial z^2} = \frac{\partial \zeta}{\partial z} = 0 \text{ at a free boundary, and} \tag{1-67}$$

$$w = \frac{\partial w}{\partial z} = \zeta = 0 \text{ at a rigid boundary.} \tag{1-68}$$

The boundary conditions must be satisfied by each $\mathbf{k}$ mode separately. For free boundaries at top and bottom,

$$w = 0 \text{ at } z = 0, \pi \text{ implies } \sum_{n=-\infty}^{\infty} w_{\mathbf{k},n} = \sum_{n=-\infty}^{\infty} (-1)^n w_{\mathbf{k},n} = 0 \tag{1-69}$$

$$\frac{\partial^2 w}{\partial z^2} = 0 \text{ at } z = 0, \pi \text{ implies } \sum_{-\infty}^{\infty} n^2 w_{\mathbf{k},n} = \sum_{-\infty}^{\infty} (-1)^n n^2 w_{\mathbf{k},n} = 0 \tag{1-70}$$

$$\frac{\partial \zeta}{\partial z} = 0 \text{ at } z = 0, \pi \text{ implies } \sum_{-\infty}^{\infty} n\, \zeta_{\mathbf{k},n} = \sum_{-\infty}^{\infty} (-1)^n n\, \zeta_{\mathbf{k},n} = 0 . \tag{1-71}$$

For these symmetric boundary conditions the even and odd terms in the sum can be separated:

$$\sum_{even\ n} w_{\mathbf{k},n} = \sum_{odd\ n} w_{\mathbf{k},n} = 0 \tag{1-72}$$

$$\sum_{even} n^2 w_{\mathbf{k},n} = \sum_{odd} n^2 w_{\mathbf{k},n} = 0 \tag{1-73}$$

$$\sum_{even} n\, \zeta_{\mathbf{k},n} = \sum_{odd} n\, \zeta_{\mathbf{k},n} = 0\,. \tag{1-74}$$

For rigid boundaries at top and bottom the vertical velocity condition is the same, but the other two boundary conditions are:

$$\frac{\partial w}{\partial z} = 0 \text{ at } z = 0,\, \pi \text{ implies } \sum_{even\ n} n\, w_{\mathbf{k},n} = \sum_{odd\ n} n\, w_{\mathbf{k},n} = 0 \tag{1-75}$$

$$\zeta = 0 \text{ at } z = 0,\, \pi \text{ implies } \sum_{even} \zeta_{\mathbf{k},n} = \sum_{odd} \zeta_{\mathbf{k},n} = 0\,. \tag{1-76}$$

For free boundaries the boundary conditions can be satisfied by the infinite set of relations:

$$w_{\mathbf{k},n} = -w_{\mathbf{k},-n} \tag{1-77}$$

$$\zeta_{\mathbf{k},n} = \zeta_{\mathbf{k},-n}\,. \tag{1-78}$$

For rigid boundaries the situation is more complicated. No single pair of $\pm n$ terms can satisfy both of the vertical velocity conditions. Furthermore, an initial condition which satisfies the boundary conditions does not automatically satisfy the boundary conditions at later times. (See section 1.8 on Lagrange multipliers.) The Fourier expansion technique does not work very well for rigid boundaries.

1.7. Linear Stability Theory

If the temperature difference, *i.e.* the Rayleigh number, is large enough, the motionless conduction state becomes unstable to overturning fluid motion. In this section, the stability of the conduction solution is described. The question is, will small perturbations grow or decay? Because the conduction solution satisfies

$$\mathbf{u} = \vartheta = \xi = 0\,, \tag{1-79}$$

its stability to infinitesimal perturbations can be computed by neglecting the nonlinear terms. The linear stability of finite amplitude solutions is more

difficult to compute because the solutions are not known exactly.

The linearized equations can be represented by a matrix $\mathbf{L}$ of differential operators,

$$\frac{d}{dt}\begin{bmatrix}\mathbf{u}\\ \vartheta\\ \xi\end{bmatrix} = \mathbf{L}\begin{bmatrix}\mathbf{u}\\ \vartheta\\ \xi\end{bmatrix}. \tag{1-80}$$

The goal of the linear analysis is to find eigenfunctions and eigenvalues of these linearized equations. The eigenfunctions and corresponding eigenvalues λ_j are defined by

$$\mathbf{L}\begin{bmatrix}\mathbf{u}(\mathbf{x})\\ \vartheta(\mathbf{x})\\ \xi(\mathbf{x})\end{bmatrix}_{\lambda_j} = \lambda_j \begin{bmatrix}\mathbf{u}(\mathbf{x})\\ \vartheta(\mathbf{x})\\ \xi(\mathbf{x})\end{bmatrix}_{\lambda_j}, \tag{1-81}$$

where the eigenfunctions must satisfy the boundary conditions.

The general solution to the linearized equations is

$$\begin{bmatrix}\mathbf{u}(\mathbf{x},t)\\ \vartheta(\mathbf{x},t)\\ \xi(\mathbf{x},t)\end{bmatrix} = \sum_j c_j e^{\lambda_j t}\begin{bmatrix}\mathbf{u}(\mathbf{x})\\ \vartheta(\mathbf{x})\\ \xi(\mathbf{x})\end{bmatrix}_{\lambda_j}, \tag{1-82}$$

where the coefficients c_j are arbitrary. If any of the eigenvalues has positive real part, then the conduction solution is *unstable*. because some perturbations will grow exponentially, until the nonlinear terms are important. On the other hand, the conduction solution is *stable* if all of the eigenvalues have negative real part, that is

$$\mathrm{Re}(\lambda_j) < 0, \text{ for all } j. \tag{1-83}$$

Because the coefficients of the partial differential equation are independent of the horizontal coordinates, the eigenfunctions have an exponential spatial dependence:

$$\begin{bmatrix}\mathbf{u}(\mathbf{x})\\ \vartheta(\mathbf{x})\\ \xi(\mathbf{x})\end{bmatrix}_{\lambda_j} = \begin{bmatrix}\mathbf{u}(z)\\ \vartheta(z)\\ \xi(z)\end{bmatrix}_{\lambda_j} e^{i\mathbf{k}\cdot\mathbf{x}}. \tag{1-84}$$

The eigenvalue depends on R, as well as $|\mathbf{k}|^2$, where $\mathbf{k}$ is the wave vector in the horizontal plane ($\mathbf{k}\cdot\hat{\mathbf{z}} = 0$).

When the Boussinesq approximation is valid, the equations for the vertical eigenfunctions also have constant coefficients. In this case the vertical eigenfunctions are sums of exponential functions. With rigid boundaries, the vertical eigenfunctions are sums of hyperbolic and sinusoidal functions (see Chandrasekhar, 1961), and their Fourier expansion includes an infinite number of terms.

On the other hand, with free boundaries, the eigenfunctions are of the form

$$\sin(z)e^{i\mathbf{k}\cdot\mathbf{x}} = \frac{1}{2i}\left(e_{\mathbf{k},n} - e_{\mathbf{k},-n}\right) \tag{1-85}$$

for w, ϑ, and ξ, and

$$\cos(z)e^{i\mathbf{k}\cdot\mathbf{x}} = \frac{1}{2}\left(e_{\mathbf{k},n} + e_{\mathbf{k},-n}\right) \tag{1-86}$$

for ζ, where

$$e_{\mathbf{k},n} \equiv e^{i(\mathbf{k}\cdot\mathbf{x}+nz)}. \tag{1-87}$$

Because differentiation of $e_{\mathbf{k},n}$ only introduces a multiplicative constant, the linear operator $\mathbf{L}$ is block diagonal in the basis where the functions have spatial dependence $e_{\mathbf{k},n}$. The operator, restricted to these functions, is called $\mathbf{L}_{\mathbf{k},n}$. The linear analysis can therefore be done separately for each subspace of functions of the form

$$\begin{aligned} \mathbf{u} = \mathbf{u}_{\mathbf{k},n} &\equiv w_{\mathbf{k},n}\mathbf{W}_{\mathbf{k},n} + \zeta_{\mathbf{k},n}\mathbf{Z}_{\mathbf{k},n} \\ \vartheta &= \vartheta_{\mathbf{k},n}e_{\mathbf{k},n} \\ \xi &= \xi_{\mathbf{k},n}e_{\mathbf{k},n}\,, \end{aligned} \tag{1-88}$$

where the complex amplitudes $w_{\mathbf{k},n}$, $\zeta_{\mathbf{k},n}$, $\vartheta_{\mathbf{k},n}$, and $\xi_{\mathbf{k},n}$ are time-dependent. While these functions (1-88) do not satisfy the boundary conditions, the boundary conditions are satisfied if the following constraints hold:

$$\begin{aligned} w_{\mathbf{k},n} &= -w_{\mathbf{k},-n} \\ \zeta_{\mathbf{k},n} &= \zeta_{\mathbf{k},-n} \\ \vartheta_{\mathbf{k},n} &= -\vartheta_{\mathbf{k},-n} \\ \xi_{\mathbf{k},n} &= -\xi_{\mathbf{k},-n} \,. \end{aligned} \tag{1-89}$$

With free boundaries, only the $e_{\mathbf{k},n}$ terms need be considered, since these constraints are automatically preserved by the dynamics. With rigid boundaries, Lagrange multipliers must be introduced to ensure that the boundary conditions satisfied. This introduces a coupling between the different $e_{\mathbf{k},n}$ modes, and the operator $\mathbf{L}$ is not separable into a direct sum of $\mathbf{L}_{\mathbf{k},n}$ operators (see section 1.8).

The pressure field has not been included in (1-88) since it can be eliminated by taking repeated curls of the velocity equation and dotting with $\hat{\mathbf{z}}$. This has the effect of separating the vertical velocity and vertical vorticity amplitudes. Using this technique, Bénard convection is described by four scalar equations:

$$\hat{\mathbf{z}}\cdot\nabla\times\left[\left(\frac{\partial}{\partial t}+\mathbf{u}\cdot\nabla\right)\mathbf{u}\right] = \hat{\mathbf{z}}\cdot\nabla\times\left[\sigma(-\nabla p + R\vartheta\hat{\mathbf{z}}+\nabla^2\mathbf{u})\right] \tag{1-90}$$

$$\hat{\mathbf{z}}\cdot\nabla\times\nabla\times\left[\left(\frac{\partial}{\partial t}+\mathbf{u}\cdot\nabla\right)\mathbf{u}\right] = \hat{\mathbf{z}}\cdot\nabla\times\nabla\times\left[\sigma(-\nabla p + R\vartheta\hat{\mathbf{z}}+\nabla^2\mathbf{u})\right] \tag{1-91}$$

$$\left(\frac{\partial}{\partial t}+\mathbf{u}\cdot\nabla\right)\vartheta = (\mathbf{u}\cdot\hat{\mathbf{z}}+\nabla^2\vartheta) \tag{1-92}$$

$$\nabla\cdot\mathbf{u} = 0\,. \tag{1-93}$$

The linearized equations are easily written in terms of the time-dependent amplitudes. The pure exponential notation simplifies the evaluation of the curls. Each "∇" can be replaced by the *vector*, $i(\mathbf{k}+n\hat{\mathbf{z}})$. The following useful relations are derived using only vector identities:

$$\hat{\mathbf{z}}\cdot\nabla\times\mathbf{u}_{\mathbf{k},n} = i\,|\mathbf{k}|^2\zeta_{\mathbf{k},n} \tag{1-94}$$

$$\hat{\mathbf{z}}\cdot\nabla\times\nabla\times\mathbf{u}_{\mathbf{k},n} = |\mathbf{k}|^2(|\mathbf{k}|^2+n^2)w_{\mathbf{k},n} \tag{1-95}$$

$$\nabla^2 e_{\mathbf{k},n} = -(|\mathbf{k}|^2+n^2)e_{\mathbf{k},n} \tag{1-96}$$

$$\nabla^2 \mathbf{u}_{\mathbf{k},n} = -(|\mathbf{k}|^2+n^2)\mathbf{u}_{\mathbf{k},n} \tag{1-97}$$

$$\hat{\mathbf{z}}\cdot\nabla\times(e_{\mathbf{k},n}\hat{\mathbf{z}}) = 0 \tag{1-98}$$

$$\hat{\mathbf{z}}\cdot\nabla\times\nabla\times(e_{\mathbf{k},n}\hat{\mathbf{z}}) = |\mathbf{k}|^2 \tag{1-99}$$

$$\mathbf{u}_{\mathbf{k},n}\cdot\hat{\mathbf{z}} = |\mathbf{k}|^2 w_{\mathbf{k},n} \tag{1-100}$$

$$\nabla\cdot\mathbf{u}_{\mathbf{k},n} = 0\,. \tag{1-101}$$

The first two equations imply that equation (1-91) gives the time derivative of the vertical velocity amplitude $w_{\mathbf{k},n}$, and equation (1-90) gives the time derivative of the vertical vorticity amplitude $\zeta_{\mathbf{k},n}$. For example, the linear equation for the time derivative of $w_{\mathbf{k},n}$ is found by evaluating equation (1-91) using the identities above:

$$\frac{d}{dt}\left(|\mathbf{k}|^2(|\mathbf{k}|^2+n^2)w_{\mathbf{k},n}\right) = \sigma R|\mathbf{k}|^2\vartheta_{\mathbf{k},n} - \sigma|\mathbf{k}|^2(|\mathbf{k}|^2+n^2)^2 w_{\mathbf{k},n}\,, \tag{1-102}$$

which reduces to

$$\frac{d}{dt}w_{\mathbf{k},n} = \frac{\sigma R}{(|\mathbf{k}|^2+n^2)}\vartheta_{\mathbf{k},n} - \sigma(|\mathbf{k}|^2+n^2)w_{\mathbf{k},n}\,. \tag{1-103}$$

1.7.1. Rayleigh-Bénard convection

For Bénard convection with the thermal time scale, the linear equations are

$$\frac{d}{dt}\begin{pmatrix} w_{\mathbf{k},n} \\ \zeta_{\mathbf{k},n} \\ \vartheta_{\mathbf{k},n} \end{pmatrix} = \begin{pmatrix} -\sigma(|\mathbf{k}|^2+n^2) & 0 & \dfrac{\sigma R}{(|\mathbf{k}|^2+n^2)} \\ 0 & -\sigma(|\mathbf{k}|^2+n^2) & 0 \\ |\mathbf{k}|^2 & 0 & -(|\mathbf{k}|^2+n^2) \end{pmatrix}\begin{pmatrix} w_{\mathbf{k},n} \\ \zeta_{\mathbf{k},n} \\ \vartheta_{\mathbf{k},n} \end{pmatrix}. \tag{1-104}$$

The vertical vorticity amplitude is not coupled to the other two amplitudes, and it decays away as

$$\zeta_{\mathbf{k},n} \sim e^{-\sigma(|\mathbf{k}|^2+n^2)t}\,. \tag{1-105}$$

The vertical vorticity is not important for the linear analysis of Bénard convection at any nonzero Prandtl number. However, equation (1-105) indicates that the limit $\sigma \to 0$ is singular.

For rigid boundaries, the boundary condition (1-68) requires that $\zeta_{\mathbf{k}0}=0$. The $n=0$ mode of vertical vorticity is allowed with free boundaries, and the decay rate can be arbitrarily small as $|\mathbf{k}|^2\to 0$. The limiting case is a uniform horizontal velocity field which is not damped at all; these modes must be eliminated by appropriately choosing the coordinate system.

A *roll* is defined as the velocity and temperature field corresponding to an eigenvector of the matrix

$$\mathbf{L}_{\mathbf{k},n}=\begin{bmatrix} -\sigma(|\mathbf{k}|^2+n^2) & \dfrac{\sigma R}{(|\mathbf{k}|^2+n^2)} \\ |\mathbf{k}|^2 & -(|\mathbf{k}|^2+n^2) \end{bmatrix}. \tag{1-106}$$

The growth rate of the roll solutions is given by the eigenvalues λ of the matrix. These eigenvalues are solutions of the characteristic equation,

$$\mathrm{Det}\,(\mathbf{L}_{\mathbf{k},n}-\lambda\mathbf{I})=0\,. \tag{1-107}$$

Therefore

$$\lambda^2+(1+\sigma)(|\mathbf{k}|^2+n^2)\lambda+\sigma\left[(|\mathbf{k}|^2+n^2)^2-\frac{|\mathbf{k}|^2R}{(|\mathbf{k}|^2+n^2)}\right]=0\,. \tag{1-108}$$

As R is varied, the instability of the conduction solution is due to an eigenvalue passing through zero. When $\lambda=0$, the characteristic equation reduces to $\mathrm{Det}\,(\mathbf{L}_{\mathbf{k},n})=0$, which implies that

$$R=\frac{(|\mathbf{k}|^2+n^2)^3}{|\mathbf{k}|^2}. \tag{1-109}$$

For fixed n, the minimum Rayleigh number occurs when

$$\frac{\partial R}{\partial(|\mathbf{k}|^2)}=0\,, \tag{1-110}$$

which implies that

$$|\mathbf{k}|^2=\tfrac{1}{2}n^2. \tag{1-111}$$

The minimum Rayleigh number, as a function of n, is

$$R_{\min}(n)=\tfrac{27}{4}n^4. \tag{1-112}$$

As the Rayleigh number is increased, the instability occurs first for $n=1$. The

critical Rayleigh number is therefore $R_c \equiv \frac{27}{4}$, and the *critical wavenumber* is $|\mathbf{k}|^2_c \equiv k_c^2 \equiv \frac{1}{2}$. These results were first found by Rayleigh (1916); Chandrasekhar (1961) gives a complete treatment of the linear problem.

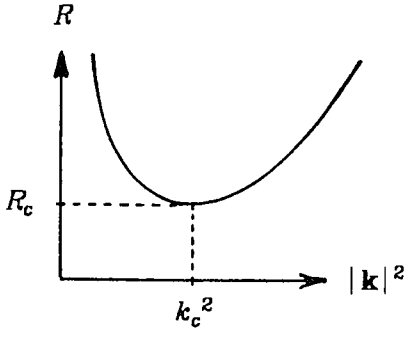

Fig. 1-1. The neutral curve for Bénard convection (equation (1-109), with $n = 1$). According to linear theory, rolls grow exponentially with time above the neutral curve and decay exponentially below it. As the Rayleigh number is increased, the instability first occurs at $R = R_c = \frac{27}{4}$, with a wavelength of $|\mathbf{k}|^2 = k_c^2 = \frac{1}{2}$.

The sum of the two eigenvalues of (1-106) is $-(1+\sigma)(|\mathbf{k}|^2+n^2)$, which is always negative. Therefore it is impossible to have $\lambda = \pm i\omega$, with ω real, in Bénard convection. In other convection examples it is possible for the conduction solution to go unstable when a complex conjugate pair of eigenvalues of $\mathbf{L}_{\mathbf{k},n}$ crosses into the right half plane. This is called *overstability* in the fluid mechanics literature, a term which is descriptive of the growing oscillations of the linearized equations. When the nonlinear terms are included, this phenomenon is called *Hopf bifurcation* in the Mathematics literature. The nonlinear terms damp the exponential growth, and lead to finite amplitude periodic solutions. The steady state bifurcation which typically occurs in convection when an eigenvalue crosses through zero is called a *pitchfork bifurcation.* These bifurcations are discussed in section 2.1.

1.7.2. Doubly diffusive convection

For doubly diffusive convection the vertical vorticity mode decays away, as it does in Bénard convection. The linear equations for the other three

amplitudes, using the viscous time scale, are:

$$\frac{d}{dt}\begin{bmatrix} w_{\mathbf{k},n} \\ \vartheta_{\mathbf{k},n} \\ \xi_{\mathbf{k},n} \end{bmatrix} = \begin{bmatrix} -(|\mathbf{k}|^2+n^2) & \dfrac{R_T}{(|\mathbf{k}|^2+n^2)} & \dfrac{R_S}{(|\mathbf{k}|^2+n^2)} \\ \dfrac{1}{\sigma_T}|\mathbf{k}|^2 & -\dfrac{1}{\sigma_T}(|\mathbf{k}|^2+n^2) & 0 \\ \dfrac{1}{\sigma_S}|\mathbf{k}|^2 & 0 & -\dfrac{1}{\sigma_S}(|\mathbf{k}|^2+n^2) \end{bmatrix} \begin{bmatrix} w_{\mathbf{k},n} \\ \vartheta_{\mathbf{k},n} \\ \xi_{\mathbf{k},n} \end{bmatrix}. \quad (1\text{-}113)$$

The characteristic equation is

$$\begin{aligned} 0 = {} & \lambda^3+\lambda^2(|\mathbf{k}|^2+n^2)\left(1+\frac{1}{\sigma_T}+\frac{1}{\sigma_S}\right) \\ & +\lambda\left((|\mathbf{k}|^2+n^2)^2\left(\frac{1}{\sigma_T}+\frac{1}{\sigma_S}+\frac{1}{\sigma_T\sigma_S}\right)-\frac{|\mathbf{k}|^2}{(|\mathbf{k}|^2+n^2)}\left(\frac{R_T}{\sigma_T}+\frac{R_S}{\sigma_S}\right)\right) \\ & +\frac{1}{\sigma_T\sigma_S}\left[(|\mathbf{k}|^2+n^2)^3-(R_T+R_S)|\mathbf{k}|^2\right]. \end{aligned} \quad (1\text{-}114)$$

At the onset of steady convection $\lambda = 0$; therefore

$$(R_T+R_S) = \frac{(|\mathbf{k}|^2+n^2)^3}{|\mathbf{k}|^2}. \quad (1\text{-}115)$$

By analogy to the Bénard case the critical wavenumber and Rayleigh number are:

$$k_c^2 = \tfrac{1}{2}\ ,\ (R_T+R_S)_c = \tfrac{27}{4}. \quad (1\text{-}116)$$

The onset of oscillatory convection occurs when $\lambda = \pm i\omega$. The real and imaginary parts of equation (1-114) give:

$$0 = -\omega^2(|\mathbf{k}|^2+n^2)\left(1+\frac{1}{\sigma_T}+\frac{1}{\sigma_S}\right)+\frac{1}{\sigma_T\sigma_S}\left[(|\mathbf{k}|^2+n^2)^3-(R_T+R_S)|\mathbf{k}|^2\right] \quad (1\text{-}117)$$

$$0 = -\omega^2+\left\{(|\mathbf{k}|^2+n^2)^2\left(\frac{1}{\sigma_T}+\frac{1}{\sigma_S}+\frac{1}{\sigma_T\sigma_S}\right)-\frac{|\mathbf{k}|^2}{(|\mathbf{k}|^2+n^2)}\left(\frac{R_T}{\sigma_T}+\frac{R_S}{\sigma_S}\right)\right\}. \quad (1\text{-}118)$$

Eliminating ω^2, these equations reduce to

$$R_T\frac{\sigma_S^2}{(1+\sigma_S)}+R_S\frac{\sigma_T^2}{(1+\sigma_T)} = \frac{(|\mathbf{k}|^2+n^2)^3}{|\mathbf{k}|^2}(\sigma_S+\sigma_T). \quad (1\text{-}119)$$

The right hand side has a minimum at $|\mathbf{k}|^2 = \frac{1}{2}$, $n = 1$. The condition for overstability is therefore

$$R_T \frac{{\sigma_S}^2}{(1+\sigma_S)} + R_S \frac{{\sigma_T}^2}{(1+\sigma_T)} = \frac{27}{4}(\sigma_S+\sigma_T). \tag{1-120}$$

In addition, ω^2 must be positive. From equation (1-117), this implies

$$R_T+R_S < \frac{27}{4}. \tag{1-121}$$

There are four parameters needed to describe doubly diffusive convection. At a Hopf bifurcation, only three are needed to specify the system. It is convenient in the calculations to use ω^2 as the third parameter, along with R_S and R_T. The Rayleigh numbers at the Hopf bifurcation can be recovered as follows:

$$\begin{aligned} R_T &= \frac{27}{4}\frac{(1+\sigma_S)}{(\sigma_S-\sigma_T)}\left(1+\tfrac{4}{9}\omega^2{\sigma_T}^2\right) \\ R_S &= \frac{27}{4}\frac{(1+\sigma_T)}{(\sigma_T-\sigma_S)}\left(1+\tfrac{4}{9}\omega^2{\sigma_S}^2\right). \end{aligned} \tag{1-122}$$

The curves of the steady and oscillatory instability meet in a codimension-two bifurcation when $\omega^2 = 0$, which is at

$$R_T = \frac{27}{4}\frac{(1+\sigma_S)}{(\sigma_S-\sigma_T)}, \quad \text{and} \quad R_S = \frac{27}{4}\frac{(1+\sigma_T)}{(\sigma_T-\sigma_S)}. \tag{1-123}$$

For salt water $\sigma_S \approx 700$ and $\sigma_T \approx 7$. In the limit that $\sigma_S \gg \sigma_T$ the overstability line is

$$R_T = \frac{27}{4}, \quad R_S < 0. \tag{1-124}$$

Note that overstability can occur even when the fluid is denser on the bottom ($R_S+R_T < 0$). Fig. 1-2 shows the stability regions for doubly diffusive convection at various fixed parameter values. The first treatment of the linear theory of doubly diffusive convection is found in Baines & Gill (1969).

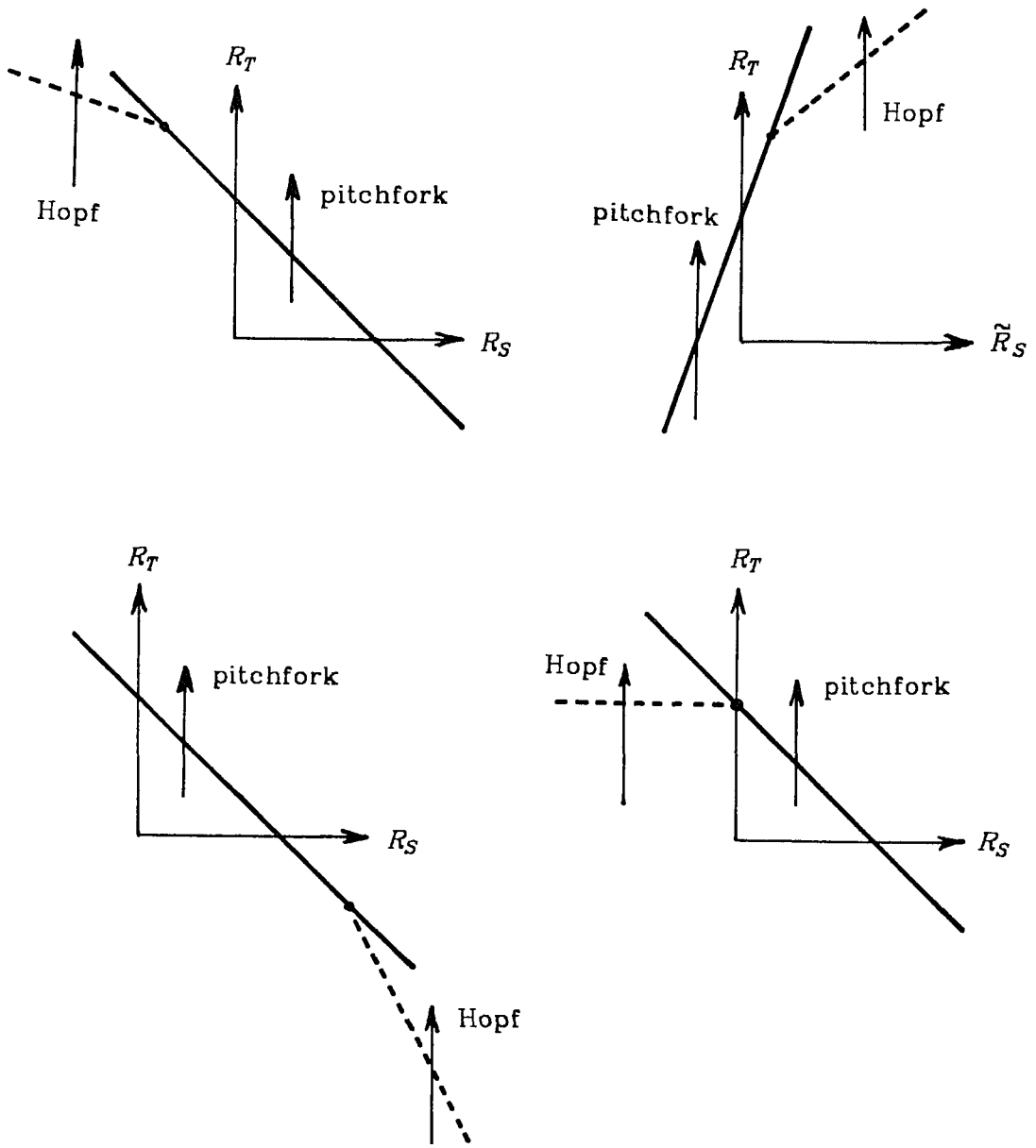

Fig. 1-2. The lines of neutral stability in the R_S-R_T (solutal Rayleigh number - Thermal Rayleigh number) plane, for fixed values of the Prandtl numbers. The pitchfork bifurcation occurs at $R_S+R_T = \frac{27}{4}$, where one of the eigenvalues of $\mathbf{L}_{\mathbf{k},n}$ (with $|\mathbf{k}|^2 = \frac{1}{2}$, $n = 1$) passes through zero. The condition for Hopf bifurcation, where a complex conjugate pair of eigenvalues of $\mathbf{L}_{\mathbf{k},n}$ crosses into the right half plane (with $|\mathbf{k}|^2 = \frac{1}{2}$, $n = 1$ as before), is given by equations (1-120) and (1-121). The solid line indicates pitchfork bifurcation, and the dotted line indicates Hopf bifurcation. In a typical experiment, R_S is held constant as R_T is increased. This experiment is indicated by arrows in the figures, although other paths through R_S-R_T space are possible. Fig. (b) corresponds to the same Prandtl numbers as fig. (a), but in fig. (b) the standard definition of the solutal Rayleigh number ($\tilde{R}_S$) is used (see equation (1-50).) Fig. (d) shows the limiting case of the Prandtl numbers appropriate for salt water.

1.7.3. Convection in a rotating fluid layer

The Coriolis force terms needed for convection in a rotating layer can be calculated for the single $\mathbf{u}_{\mathbf{k},n}$ velocity mode of equation (1-88) using vector identities. They are

$$\hat{\mathbf{z}}\cdot\nabla\times(\mathbf{u}_{\mathbf{k},n}\times\Omega) = i(n|\mathbf{k}|^2\Omega\cdot\hat{\mathbf{z}}+|\mathbf{k}|^2\Omega\cdot\mathbf{k})w_{\mathbf{k},n} \tag{1-125}$$

$$\hat{\mathbf{z}}\cdot\nabla\times\nabla\times(\mathbf{u}_{\mathbf{k},n}\times\Omega) = -(n|\mathbf{k}|^2\Omega\cdot\hat{\mathbf{z}}+|\mathbf{k}|^2\Omega\cdot\mathbf{k})\zeta_{\mathbf{k},n}\,. \tag{1-126}$$

The viscous time scale is somewhat simpler since there are fewer σs in the linear equations:

$$\frac{d}{dt}\begin{pmatrix} w_{\mathbf{k},n} \\ \zeta_{\mathbf{k},n} \\ \vartheta_{\mathbf{k},n} \end{pmatrix} = \begin{pmatrix} -(|\mathbf{k}|^2+n^2) & \dfrac{-(n\,\Omega\cdot\hat{\mathbf{z}}+\Omega\cdot\mathbf{k})}{(|\mathbf{k}|^2+n^2)} & \dfrac{R}{(|\mathbf{k}|^2+n^2)} \\ n\,\Omega\cdot\hat{\mathbf{z}}+\Omega\cdot\mathbf{k} & -(|\mathbf{k}|^2+n^2) & 0 \\ \dfrac{|\mathbf{k}|^2}{\sigma} & 0 & \dfrac{-(|\mathbf{k}|^2+n^2)}{\sigma} \end{pmatrix} \begin{pmatrix} w_{\mathbf{k},n} \\ \zeta_{\mathbf{k},n} \\ \vartheta_{\mathbf{k},n} \end{pmatrix}. \tag{1-127}$$

When the velocity is in the plane perpendicular to Ω the Coriolis force, as well as the centrifugal force, is balanced by the pressure gradient. Therefore, the component of Ω perpendicular to both $\hat{\mathbf{z}}$ and $\mathbf{k}$ does not have any effect.

It is useful to think of convection in a rotating layer as an approximation to convection in a rotating spherical shell heated from the inside. At the north pole Ω points along the $\hat{\mathbf{z}}$ axis, while at the equator Ω is in the horizontal plane. When $\mathbf{k}$ points East-West the linear problem is identical to convection at the North pole with a reduced rotation rate.

Consider first the case where the rotation vector is vertical. (The complications which arise when $\Omega\cdot\mathbf{k}\neq 0$ are discussed in the next section.) The characteristic equation is

$$\begin{aligned} 0 = {} & \lambda^3+\lambda^2(|\mathbf{k}|^2+n^2)\left(2+\frac{1}{\sigma}\right) \\ & +\lambda\left[(|\mathbf{k}|^2+n^2)^2\left(1+\frac{2}{\sigma}\right)+\frac{nT}{(|\mathbf{k}|^2+n^2)}-\frac{R|\mathbf{k}|^2}{(|\mathbf{k}|^2+n^2)}\right] \\ & +\frac{1}{\sigma}\left[(|\mathbf{k}|^2+n^2)^3+n^2T-R|\mathbf{k}|^2\right], \end{aligned} \tag{1-128}$$

where $T\equiv|\Omega|^2=(\Omega\cdot\hat{\mathbf{z}})^2$ is the Taylor number. In dimensional units, the Taylor

number is

$$T \equiv \frac{4|\Omega_{dim}|^2 d^4}{\nu^2 \pi^4}. \tag{1-129}$$

The reader is warned that the standard definition of the Taylor number does not include the factor of π^4. The scaling of equation (1-24) is responsible for the difference. Chandrasekhar (1961) defines the right hand side of (1-129) to be T_1.

The conduction solution is unstable to exponentially growing rolls when R exceeds

$$R = \frac{1}{|\mathbf{k}|^2}\left[(|\mathbf{k}|^2+n^2)^3+n^2 T\right]. \tag{1-130}$$

The minimum Rayleigh number occurs when $|\mathbf{k}|^2$ satisfies the cubic

$$2(|\mathbf{k}|^2)^3+3(|\mathbf{k}|^2)^2-n^6 = n^2 T. \tag{1-131}$$

There is an analytic expression for the critical wavenumber as a function of T, but it is rather lengthy. The wavenumber monotonically increases with T, so the critical wavelength goes to zero as $T \to \infty$.

The minimum Rayleigh number corresponds to $n = 1$, so for fixed T the critical wavenumber is given by the solution of the cubic equation:

$$T = (1+k_c^2)^2(2k_c^2-1). \tag{1-132}$$

The critical Rayleigh number for this Taylor number is

$$R_c = 3(1+k_c^2)^2. \tag{1-133}$$

Overstability occurs when

$$0 = -\omega^2+(|\mathbf{k}|^2+n^2)^2\left[\frac{2}{\sigma}+1+\frac{n^2 T}{(|\mathbf{k}|^2+n^2)^2}-\frac{R|\mathbf{k}|^2}{\sigma(|\mathbf{k}|^2+n^2)^3}\right] \tag{1-134}$$

and

$$0 = -\omega^2(|\mathbf{k}|^2+n^2)\left(2+\frac{1}{\sigma}\right)+\frac{1}{\sigma}\left[(|\mathbf{k}|^2+n^2)^3+n^2 T-R|\mathbf{k}|^2\right]. \tag{1-135}$$

Eliminating ω^2, this gives

$$R = 2(1+\sigma)\frac{1}{|\mathbf{k}|^2}\left((|\mathbf{k}|^2+n^2)^3+\frac{\sigma^2}{(1+\sigma)^2}n^2T\right). \tag{1-136}$$

The minimum Rayleigh number, for fixed Taylor number, occurs when $n = 1$ and $|\mathbf{k}|^2$ satisfies

$$\frac{\sigma^2}{(1+\sigma)^2}T = (1+k_c^2)^2(2k_c^2-1). \tag{1-137}$$

The corresponding Rayleigh number for overstability is

$$R_c = 6(1+\sigma)(1+k_c^2)^2, \tag{1-138}$$

provided $\omega^2 > 0$ (so that ω is real). A necessary condition for overstability is $\sigma < 1$.

The neutral curves, which plot R vs. $|\mathbf{k}|^2$, must be drawn for fixed T and σ. There are two neutral curves (assuming $n=1$): one for stationary convection (1-130), and one for oscillatory convection (1-136). Unlike the doubly diffusive case, the direct and oscillatory instabilities have different preferred wavelengths in rotating convection. Fig. 1-3(a) shows how the T-σ plane is divided into two regions, depending on whether the instability to stationary convection or to oscillatory convection occurs first as the Rayleigh number is increased.

The T-σ plane is separated into many regions where the neutral curves are qualitatively different. Only the most important division is shown in fig. 1-3(a). Within regions I and II there are several possible neutral curves, some of which are shown in figs. 1-3(b) through (e). The linear theory of rotating convection is sufficiently complicated that it is not possible to give a full treatment here. See Chandrasekhar (1961) or Weiss (1964) for details.

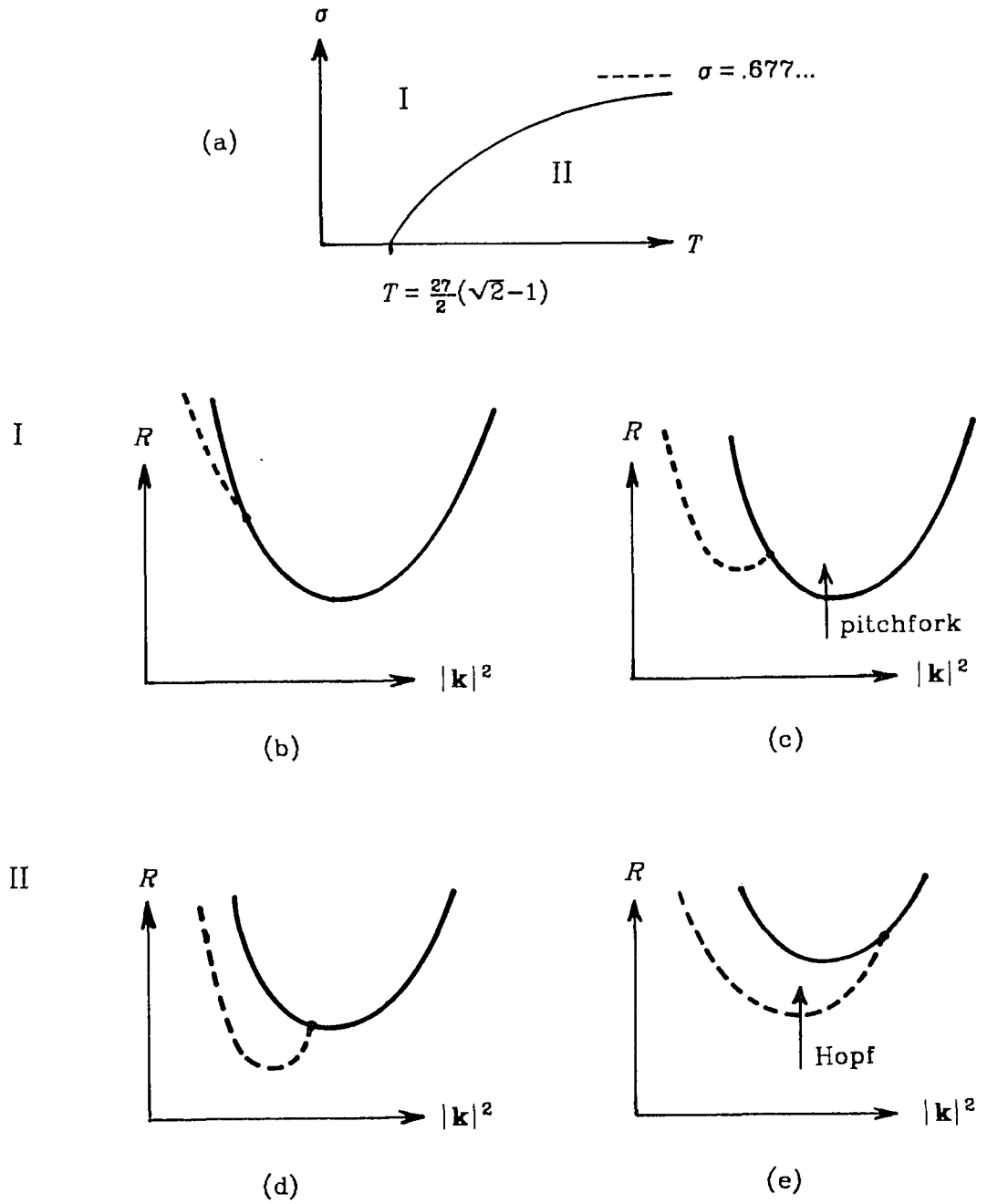

Fig. 1-3. In fig. (a), the σ-T (Prandtl number - Taylor number) plane is divided into two regions. In region I, the pitchfork bifurcation occurs before the Hopf bifurcation when the Rayleigh number R is increased for fixed T and σ. In region II, the Hopf bifurcation occurs first. For the parameter values on the boundary between regions I and II there is a codimension-two bifurcation. The equation describing this boundary is given in the appendix of Pearlstein (1981). In figs. (b) and (c), typical neutral curves for region I are shown. If figs. (d) and (e), typical neutral curves for region II are shown. The solid line indicates the pitchfork bifurcation (equation (1-130)), and the dotted line indicates the Hopf bifurcation (equation (1-136)).

1.8. Lagrange Multipliers

This section describes the modifications of the Fourier amplitude technique which are needed when the boundary conditions are not chosen "correctly".

With rigid boundaries, the linear equations (1-104) for Bénard convection do not preserve the boundary conditions. Given an initial condition satisfying the rigid boundary conditions, if R is slightly greater than $\frac{27}{4}$ all the modes except $n = \pm 1$ will decay away. This asymptotic state certainly does not satisfy the rigid boundary conditions.

A similar problem occurs when $\mathbf{k}\cdot\Omega$ is not zero in rotating convection. The linear equations (1-127) do not preserve the boundary conditions. Suppose the initial condition has only four modes, $(\pm\mathbf{k}, \pm n)$, related by the reality conditions (1-63) and the symmetries which satisfy the boundary conditions

$$\begin{aligned} w_{\mathbf{k},n} + w_{\mathbf{k},-n} &= 0 \\ \zeta_{\mathbf{k},n} - \zeta_{\mathbf{k},-n} &= 0 \\ \vartheta_{\mathbf{k},n} + \vartheta_{\mathbf{k},-n} &= 0 . \end{aligned} \tag{1-139}$$

If these boundary conditions hold at $t = 0$, the linear equations reduce to

$$\begin{aligned} \frac{d}{dt}(w_{\mathbf{k},n} + w_{\mathbf{k},-n}) &= \frac{-\Omega\cdot\mathbf{k}}{(|\mathbf{k}|^2 + n^2)}(\zeta_{\mathbf{k},n} + \zeta_{\mathbf{k},-n}) \\ \frac{d}{dt}(\zeta_{\mathbf{k},n} - \zeta_{\mathbf{k},-n}) &= \Omega\cdot\mathbf{k}(w_{\mathbf{k},n} - w_{\mathbf{k},-n}) \\ \frac{d}{dt}(\vartheta_{\mathbf{k},n} + \vartheta_{\mathbf{k},-n}) &= 0 . \end{aligned} \tag{1-140}$$

and the boundary conditions are immediately violated unless $\mathbf{u} = 0$. The nonlinear terms cannot preserve the boundary conditions since the argument is valid for arbitrarily small amplitudes.

Note that when Ω is vertical the boundary conditions *are* automatically preserved by the equations of motion, due to the n in the off diagonal terms linking $w_{\mathbf{k},n}$ and $\zeta_{\mathbf{k},n}$ in equation (1-127).

How can the equations fail to preserve the boundary conditions? The reso-

lution of the paradox is that, under certain conditions, the modal equations (1-104, 1-113, and 1-127) must be modified in order to preserve the boundary conditions. The boundary conditions are a *constraint* capable of exerting a force, similar to a bead constrained to a wire. There is a *Lagrange multiplier* for each of the constraints. Let the constraints be numbered 1 through 8: Equation (1-72) gives

$$C_{1\,(2)} = \sum_{odd\ (even)\ n} w_{\mathbf{k},n} = 0\,. \tag{1-141}$$

For free boundaries constraints 3 through 6 are derived from equations (1-73) and (1-74):

$$C_{3\,(4)} = \sum_{odd\ (even)\ n} n^2 w_{\mathbf{k},n} = 0 \tag{1-142}$$

$$C_{5\,(6)} = \sum_{odd\ (even)\ n} n\,\zeta_{\mathbf{k},n} = 0\,. \tag{1-143}$$

For rigid boundaries these constraints are [see (1-75) and (1-76)]:

$$C_{3\,(4)} = \sum_{odd\ (even)\ n} n\,w_{\mathbf{k},n} = 0 \tag{1-144}$$

$$C_{5\,(6)} = \sum_{odd\ (even)\ n} \zeta_{\mathbf{k},n} = 0\,. \tag{1-145}$$

The constraints from the temperature boundary condition (1-34) are:

$$C_{7\,(8)} = \sum_{odd\ (even)\ n} \vartheta_{\mathbf{k},n} = 0\,. \tag{1-146}$$

The linear equations must be modified to include an arbitrarily strong "force" in the directions perpendicular to the constraints:

$$\begin{aligned}
\frac{d}{dt} w_{\mathbf{k},n} &= \left(\frac{d}{dt} w_{\mathbf{k},n}\right)_{matrix} - \lambda_1 \frac{\partial C_1}{\partial w_{\mathbf{k},n}} - \cdots - \lambda_4 \frac{\partial C_4}{\partial w_{\mathbf{k},n}} \\
\frac{d}{dt} \zeta_{\mathbf{k},n} &= \left(\frac{d}{dt} \zeta_{\mathbf{k},n}\right)_{matrix} - \lambda_5 \frac{\partial C_5}{\partial \zeta_{\mathbf{k},n}} - \lambda_6 \frac{\partial C_6}{\partial \zeta_{\mathbf{k},n}} \\
\frac{d}{dt} \vartheta_{\mathbf{k},n} &= \left(\frac{d}{dt} \vartheta_{\mathbf{k},n}\right)_{matrix} - \lambda_7 \frac{\partial C_7}{\partial \vartheta_{\mathbf{k},n}} - \lambda_8 \frac{\partial C_8}{\partial \vartheta_{\mathbf{k},n}},
\end{aligned} \tag{1-147}$$

where the matrix subscript refers to equation (1-104) or (1-127). This introduces eight new variables (λ_1 through λ_8). There are also eight new equations which guarantee that the boundary conditions are preserved:

$$\frac{d}{dt} C_1 = 0, \cdots, \frac{d}{dt} C_8 = 0. \qquad (1\text{-}148)$$

Since the boundary conditions are the same on top and bottom, the even and odd problems separate. For the even solutions only amplitudes with n even are non-zero, and all the C_n, where n is odd, are zero. The odd solutions are similarly constructed.

With stress free, perfectly conducting boundaries, all of the Lagrange multipliers are zero; this is why these boundary conditions are so simple. With rigid boundaries, λ_3 and λ_4 are nonzero. When there are nonzero Lagrange multipliers, it is impractical to carry out the procedure described here. The purpose of this section is to give a novel view of what goes wrong when rigid boundary conditions are imposed.

It appears that no one has analytically solved the linear problem with free boundaries when $\boldsymbol{\Omega}\cdot\mathbf{k} \neq 0$. Hathaway *et al.* (1979) do the linear theory when the diffusion constants are set to zero. The only boundary condition that they impose is $w = 0$. Hathaway *et al.* (1980) numerically solve the linear problem with diffusion, but they impose rigid boundary conditions. In both cases, the rolls where $\mathbf{k}$ is pointing East-West (where $\mathbf{k}\cdot\boldsymbol{\Omega} = 0$) have the lowest critical Rayleigh number, because the interaction with the rotation suppresses convection.

1.9. Symmetries

In the next chapter, the possible bifurcation structure of the convection equations is found, using only their symmetries and the results of linear theory. Therefore it is important to understand the symmetries of these equations.

In an infinite plane layer the equations have the symmetry of the Euclidean group: all rotations and translations in the plane. The symmetry acts on the coordinate $\mathbf{x}$ by

$$\mathbf{x} \rightarrow \mathbf{x}' = \mathbf{R}\cdot\mathbf{x} + \mathbf{d}, \tag{1-149}$$

where $\mathbf{d}$ is a vector in the horizontal plane,

$$\mathbf{d}\cdot\hat{\mathbf{z}} = 0, \tag{1-150}$$

and $\mathbf{R}$ is an orthogonal matrix of the form

$$\mathbf{R} = \begin{bmatrix} \cos\varphi & \sin\varphi & 0 \\ -\sin\varphi & \cos\varphi & 0 \\ 0 & 0 & 1 \end{bmatrix}, \tag{1-151}$$

or

$$\mathbf{R} = \begin{bmatrix} -\cos\varphi & \sin\varphi & 0 \\ \sin\varphi & \cos\varphi & 0 \\ 0 & 0 & 1 \end{bmatrix}. \tag{1-152}$$

The matrices of the form (1-151) represent *proper* (orientation preserving) rotations, and those of the form (1-152) represent *improper rotations*, or reflections. For convection in a rotating fluid layer, only proper rotations are symmetries.

In conjunction with (1-149), the velocity field is transformed by the rotations,

$$\mathbf{u} \rightarrow \mathbf{u}' = \mathbf{R}\cdot\mathbf{u}, \tag{1-153}$$

and the temperature field, solute field, and pressure field are unchanged,

$$\begin{aligned} \vartheta &\rightarrow \vartheta' = \vartheta \\ \xi &\rightarrow \xi' = \xi \\ p &\rightarrow p' = p\,. \end{aligned} \tag{1-154}$$

The equations are *symmetric* under a transformation if they are identical when written in terms of the primed variables; for instance equations (1-26)-(1-28) become

$$\left(\frac{\partial}{\partial t} + \mathbf{u}'\cdot\nabla'\right)\mathbf{u}' = \sigma\left(-\nabla' p' + R\vartheta'\hat{\mathbf{z}} + (\nabla')^2\mathbf{u}'\right) \tag{1-155}$$

$$\left(\frac{\partial}{\partial t} + \mathbf{u}'\cdot\nabla'\right)\vartheta' = \mathbf{u}'\cdot\hat{\mathbf{z}} + (\nabla')^2\vartheta' \tag{1-156}$$

$$\nabla'\cdot\mathbf{u}' = 0, \tag{1-157}$$

where the fields now depend on the transformed variables,

$$\vartheta' = \vartheta'(\mathbf{x}', t)\,. \tag{1-158}$$

(The symmetries discussed here do not involve the time coordinate.)

When the Boussinesq approximation is valid and the boundary conditions are symmetric, the system has another symmetry, called the *Boussinesq symmetry*, The Boussinesq symmetry is a reflection in the horizontal midplane coupled with a reversal of the temperature and solute perturbations. The transformation of the coordinates is

$$\begin{aligned} x &\to x \\ y &\to y \\ z &\to \pi - z\,. \end{aligned} \tag{1-159}$$

The dependent variables transform as follows:

$$\begin{aligned} \mathbf{u} &\to \mathbf{R}\cdot\mathbf{u} \\ \vartheta &\to -\vartheta \\ \xi &\to -\xi \\ p &\to p\,, \end{aligned} \tag{1-160}$$

where

$$\mathbf{R} = \begin{bmatrix} 1 & 0 & 0 \\ 0 & 1 & 0 \\ 0 & 0 & -1 \end{bmatrix}. \tag{1-161}$$

In terms of the new variables, the equations for Bénard convection (1-26)-(1-28), doubly diffusive convection (1-46)-(1-49), and rotating convection when the rotation vector is vertical (1-55) and (1-27)-(1-28), remain unchanged. The full problem is specified by the equations *and* the boundary conditions. In addition the to the above transformations, the boundary conditions on the top and bottom are interchanged. The problem has the Boussinesq symmetry if, in addition to the validity of the Boussinesq approximation, the boundary conditions are the same on the top and bottom plates, and the average of the temperature of the top and bottom plates does not change with time (Krishnamurti, 1968).

Note that the sign of the z derivative is changed by the transformation (1-159),

$$\hat{\mathbf{z}}\cdot\nabla = \frac{\partial}{\partial z} \rightarrow \hat{\mathbf{z}}\cdot\nabla' = -\frac{\partial}{\partial z}, \tag{1-162}$$

but the vertical unit vector $\hat{\mathbf{z}}$ is unchanged. This is because z is an independent variable in the problem, while $\hat{\mathbf{z}}$ ($g\,\hat{\mathbf{z}}$) is a parameter which defines the system.

In addition to these symmetries, there are *pseudo-symmetries*. In pseudo-symmetries, the parameters of the problem can be transformed, whereas with true symmetries, only the dependent and independent variables are transformed. In doubly diffusive convection (1-46)-(1-49), there is the pseudo-symmetry between heat and solute:

$$\begin{aligned}
&\mathbf{x} \rightarrow \mathbf{x} \\
&\mathbf{u} \rightarrow \mathbf{u} \\
&\vartheta \rightarrow \xi \\
&\xi \rightarrow \vartheta \\
&[R_T \rightarrow R_S] \\
&[R_S \rightarrow R_T] \\
&[\sigma_T \rightarrow \sigma_S] \\
&[\sigma_S \rightarrow \sigma_T].
\end{aligned} \tag{1-163}$$

The transformation of the parameters is enclosed in square brackets to distinguish it from a transformation of the variables. This pseudo-symmetry will often by abbreviated by $[T \leftrightarrow S]$.

In rotating convection, when the rotation vector is vertical, there is also a pseudo-symmetry of reflections, coupled with a reversal of the sign of $\boldsymbol{\Omega}$:

$$\begin{aligned}
&\mathbf{x} \rightarrow \mathbf{R}\cdot\mathbf{x} \\
&\mathbf{u} \rightarrow \mathbf{R}\cdot\mathbf{u} \\
&\vartheta \rightarrow \vartheta \\
&p \rightarrow p \\
&[\boldsymbol{\Omega} \rightarrow -\boldsymbol{\Omega}],
\end{aligned} \tag{1-164}$$

where $\mathbf{R}$ is of the form (1-152). This pseudo-symmetry corresponds to changing from a right handed to a left handed coordinate system.

Note that the pseudo-symmetries can be considered to be true symmetries, by artificially including the parameters as new dependent variables. For

instance, in rotating convection Ω can be considered a dependent variable satisfying

$$\frac{\partial \Omega}{\partial t} = 0 . \tag{1-165}$$

The value of Ω is imposed as the initial condition for the new dependent variable. In this way, the transformation (1-164) becomes a symmetry, rather than a pseudo-symmetry.

The practical differences between the two types of symmetry are seen in the following chapters. Pseudo-symmetries do not directly affect the normal form results of Chapters Two and Three; however, they simplify the calculations of the coefficients of the normal forms and greatly influence the structure of the problem.

Chapter Two

Bifurcation Theory and Normal Forms

This chapter describes the bifurcations which can occur in convection when the horizontal planforms are doubly periodic. For the results of this chapter to hold, all that is required of a physical problem is that it be symmetric with respect to rigid motions in a two-dimensional plane, that the linear stability of the conduction solution has a real eigenvalue go through zero, and that the wavelength of the most unstable disturbance is neither zero nor infinity. The normal forms relevant to Hopf bifurcations, where the instability is due to a complex conjugate pair of eigenvalues crossing into the right half plane, are discussed in the next chapter.

The results of this chapter are based on the center manifold theorem. This theorem allows the partial differential equations of convection to be reduced, in certain cases, to a few ordinary differential equations. The chapter starts with a review of bifurcation theory, and the simplest bifurcations are introduced. An understanding of these simple bifurcations is a prerequisite for what follows.

In section 2.3, an example of bifurcation with symmetry is discussed. This example displays the essential behavior of many of the bifurcations which occur in convection. Then, the least degenerate (simplest) bifurcations of convection on a square or rhombic lattice are classified, using the correspondence to the example studied earlier.

Convection on a hexagonal lattice must be treated separately from convection on the other lattices. The Boussinesq approximation plays an important role in pattern selection on a hexagonal lattice. Four different normal forms are appropriate, depending on the degree to which the Boussinesq symmetry is valid.

The chapter ends with a discussion of the lattice function, which displays the results of all the lattices.

An intuitive, physical approach to the theory is used whenever possible, rather than sophisticated mathematics.

2.1. A Quick Review of Bifurcation Theory

Bifurcation theory is the study of the branching of solutions of ordinary and partial differential equations. This branching is always accompanied by a change in the stability of the solutions. The stability properties of a stationary solution are found by linearizing the equations about the fixed point. This linearization is a linear operator. If the system is an ordinary differential equation, the linear operator can be represented by a matrix. The eigenvalues of this linear operator (or matrix) determine the linear stability. For the discussion below, assume that the system is an ordinary differential equation, hereafter referred to as an ODE. Define $\mathbf{X}_j$ and λ_j as the eigenvectors and corresponding eigenvalues of the matrix. (In the case of partial differential equations, the eigenvectors are replaced by eigenfunctions.) The general solution of the linearized equations is a linear superposition of

$$\mathbf{X}_j e^{\lambda_j t} . \tag{2-1}$$

If all the eigenvalues have negative real part then any perturbation decays and the fixed point is stable (to small enough perturbations). If any eigenvalue has a positive real part, then a perturbation along the corresponding eigenvector will grow exponentially, and the fixed point is unstable. If an eigenvalue has zero real part, then the nonlinear terms determine whether a perturbation along the corresponding eigenvector grows or decays.

The linear space defined by the set of eigenvectors whose eigenvalues have negative real part is called the *stable eigenspace*. Likewise, the *center*

(unstable) eigenspace is spanned by the eigenvectors corresponding to eigenvalues with zero (positive) real part.

The center manifold is an example of an *invariant manifold*: a subspace of the phase space which is invariant under the dynamics. The stable, unstable, and center manifolds are tangent to the stable, unstable, and center eigenspaces of a fixed point, respectively. It is not obvious that such invariant manifolds exist. The *center manifold theorem* states that such an invariant manifold does indeed exist. There are analogous theorems for the existence of the other invariant manifolds (see Hirsch *et al.* 1967). The book by Marsden & McCracken (1976) describes how the center manifold theorem is used in bifurcation theory. The following statement of the center manifold theorem is taken from Marsden & McCracken (1976, p. 47).

THEOREM: *Let Z be a smooth Banach space and let F_t be a C^0 semiflow defined in a neighborhood of $O \in Z$ for $0 \le t \le \tau$. Assume $F_t(O) = O$ and that for $t > 0$, $F_t(x)$ is C^{k+1} jointly in t and x. Assume that the spectrum of the linear semigroup $DF_t(O): Z \to Z$ is of the form $e^{t(\sigma_1 \cup \sigma_2)}$ where σ_1 lies on the imaginary axis and σ_2 lies in the left half plane* $\mathrm{Re}(\sigma_2) < -\sigma < 0$. *Let Y be the generalized eigenspace corresponding to the part of the spectrum on the unit circle. Assume* $\dim Y = d < \infty$.

Then there exists a neighborhood V of O in Z and a C^k submanifold $M \subset V$ of dimension d passing through O and tangent to Y at O such that

(a) (Local invariance): *If $x \in M$, $t > 0$, and $F_t(x) \in V$, then $F_t(x) \in M$.*

(b) (Local attractivity): *If $t > 0$ and $F_t^n(x)$ remains defined and in V for all $n = 0, 1, 2, \cdots$, then $F_t^n(x) \to M$ as $n \to \infty$.*

For what follows, it is not necessary to understand the details of this theorem. However, a few remarks are in order:

• The Banach space formulation is general enough to apply to the partial different equations of convection.

• The correspondence between the notation in the theorem and that used here is:

$$\begin{aligned} &\sigma_1 = \{\lambda_j \mid \mathrm{Re}(\lambda_j) = 0\}; \\ &\sigma_2 = \{\lambda_j \mid \mathrm{Re}(\lambda_j) < -\sigma < 0\}; \\ &Y = \mathrm{span}\{\mathbf{X}_j \mid \mathrm{Re}(\lambda_j) = 0\} \text{ is the center eigenspace;} \\ &M \text{ is the center manifold.} \end{aligned} \tag{2-2}$$

• The dimension of the center eigenspace must be less than infinity, and the stable part of the spectrum (σ_2) must be bounded away from zero. Both of these conditions are violated in convection, *unless* double periodicity is imposed.

Rather than present a rigorous mathematical treatment of bifurcation theory, an example is used to illustrate the ideas. Consider the following system of ODEs in the plane;

$$\dot{x} = \lambda x - x^3 + xy \tag{2-3}$$

$$\dot{y} = -y + ax^2, \tag{2-4}$$

where $(x, y) \in \mathbb{R}^2$, and λ and a are real, fixed parameters.

Note that this ODE is symmetric under the reflection through the y axis.

$$(x, y) \to (-x, y). \tag{2-5}$$

The point $x = y = 0$ is a stationary solution for all values of λ, and the linearization is

$$\dot{x} = \lambda x \tag{2-6}$$

$$\dot{y} = -y \tag{2-7}$$

When $\lambda < 0$ the stable eigenspace is the whole $x-y$ plane. When $\lambda > 0$ the stable eigenspace is the y axis and the unstable eigenspace is the x axis. At precisely $\lambda = 0$ the x axis is the center eigenspace.

The stable and unstable manifolds are both one-dimensional when $\lambda > 0$. These manifolds are invariant under the dynamics, and tangent to the stable and unstable eigenspaces. Note that the y axis, defined by $x = 0$, is invariant under the dynamics, since $\dot{x} = 0$ when $x = 0$. This result is forced by the symmetry (2-5); since the y axis is invariant under the reflection it is also invariant under the dynamics. The y axis is therefore the stable manifold.

The unstable manifold can be written as a Taylor expansion,

$$y = ax^2 + O(x^3), \tag{2-8}$$

where a must be determined. The fact that the unstable manifold is invariant under the flow implies that

$$\dot{y} = 2ax\dot{x} + O(x^3). \tag{2-9}$$

When the ODE (2-4) is substituted into this equation, one finds

$$-y + ax^2 = 2a\lambda x^2 + O(x^3), \tag{2-10}$$

which becomes

$$(-a + a)x^2 = 2a\lambda x^2 + O(x^3) \tag{2-11}$$

when equation (2-8) is substituted for y. The above equation determines a:

$$a = \frac{a}{(1+2\lambda)}. \tag{2-12}$$

The unstable manifold, which exists for $\lambda > 0$, is therefore

$$y = \frac{a}{(1+2\lambda)}x^2 + O(x^3). \tag{2-13}$$

When $\lambda = 0$, the center manifold can be found by the same procedure:

$$y = ax^2 + O(x^3). \tag{2-14}$$

It is natural to use x as the coordinate of the center manifold. This is done by projecting the center manifold onto the x axis. The dynamics *on* the center manifold are given by inserting (2-14) into equation (2-3):

$$\begin{aligned} \dot{x} &= -x^3 + x\left[ax^2 + O(x^3)\right] \\ &= (a-1)x^3 + O(x^4). \end{aligned} \tag{2-15}$$

Therefore the sign of $(a-1)$ determines the stability of the origin. This stability

(or instability) is very sensitive to perturbations in the equations, since any linear terms will dominate the cubic terms when x is small enough.

A fixed point is called *hyperbolic* if it has no eigenvalues with zero real part. The behavior of a hyperbolic fixed point is not sensitive to perturbations in the equations. A theorem due to Hartman (1973) says that there is a (nondifferentiable) change of coordinates which eliminates all the nonlinear terms in the neighborhood of a hyperbolic fixed point. When λ is fixed and nonzero, the qualitative behavior of the nonlinear ODE (2-6), (2-7) near $x=y=0$ is the same as the linearization (2-3), (2-4). When λ is small, however, the neighborhood of $x=y=0$ described in the theorem is also small.

In order to capture the transition from negative to positive λ, the system is extended to include λ as an independent variable, treated equally with with x and y. The resulting three-dimensional system of ODEs is

$$\dot{x} = \lambda x - x^3 + xy \tag{2-16}$$

$$\dot{y} = -y + ax^2 \tag{2-17}$$

$$\dot{\lambda} = 0. \tag{2-18}$$

Now the center manifold is *two-dimensional* when $\lambda = 0$, and one-dimensional otherwise. The center manifold at $\lambda = 0$ has coordinates (x, λ). The dynamics on the center manifold are

$$\dot{x} = \lambda x + (a-1)x^3 + O(x^5) + O(\lambda x^3) + O(\lambda^2 x) \tag{2-19}$$

$$\dot{\lambda} = 0. \tag{2-20}$$

Note that the coefficient of the cubic term can be calculated *at* $\lambda = 0$. This simplifies the calculations.

Assuming $a \neq 1$, the variable x can be scaled by

$$x \to \frac{x}{\sqrt{|a-1|}} \tag{2-21}$$

and the system can be truncated to give the *normal form* for the *pitchfork bifurcation*:

$$\dot{x} = \lambda x + x^3 \text{ when } a - 1 > 0, \text{ and} \tag{2-22}$$

$$\dot{x} = \lambda x - x^3 \text{ when } a - 1 < 0. \tag{2-23}$$

The pitchfork bifurcation is forced by the $x \to -x$ reflectional symmetry. The equation for $\dot{x}$ on the center manifold must have only odd order terms in x. The bifurcation is a pitchfork provided the coefficient of x^3 is nonzero.

In order to deserve the designation as a normal form, it must be demonstrated that the qualitative features of equation (2-22) or (2-23) are unchanged by adding higher order terms, such as

$$O(x^5),\ O(\lambda x^3),\ \text{and } O(\lambda^2 x). \tag{2-24}$$

The higher order terms do not change the qualitative features provided all of the fixed points are hyperbolic when $\lambda \neq 0$. The analysis of the normal form shows that the fixed points are indeed hyperbolic. In addition to the stationary solution at $x = 0$, there is a fixed point at

$$\lambda \pm x^2 = 0. \tag{2-25}$$

The upper sign is for equation (2-22), and the lower sign for equation (2-23). The linearization of the ODE about the new fixed point is

$$\left.\frac{\partial \dot{x}}{\partial x}\right|_{\lambda \pm x^2 = 0} = \pm 2x^2 \tag{2-26}$$

Therefore in the "+" version of the normal form (2-22), the nonzero solutions are unstable, and exist for $\lambda < 0$. This is called a *subcritical bifurcation*. Conversely, the normal form (2-23) corresponds to a *supercritical bifurcation*, where the nonzero solutions are stable and exist when $\lambda > 0$.

It is a general feature that subcritical solutions, i.e. those coexisting with a stable solution at the origin, are unstable. On the other hand, supercritical solutions have a stable eigenvector pointing in the direction towards the origin. Fig. 2-1 gives a pictorial description of the two bifurcations.

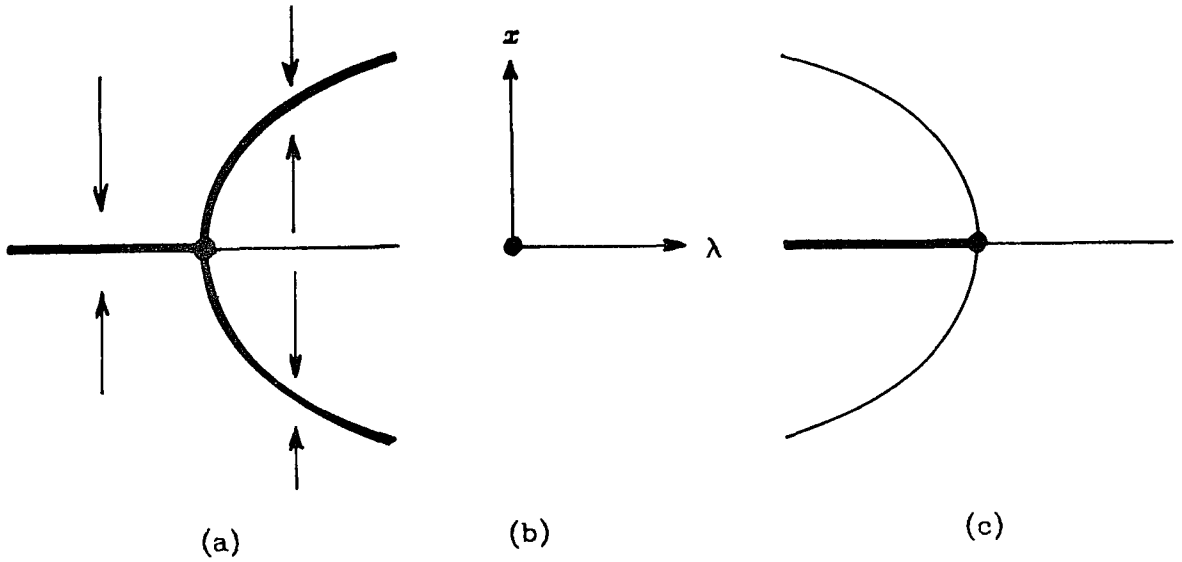

Fig. 2-1. The *bifurcation diagrams* for the two cases of the *pitchfork bifurcation*: (a) the supercritical bifurcation, equation (2-23), and (c) the subcritical bifurcation, equation (2-22). These diagrams plot the solutions as a function of the bifurcation parameter λ. The stable solutions are indicated by thick lines, and the unstable solutions by thin lines. The axes of (a) and (c) are shown in fig. (b). A few trajectories of the two-dimensional system in x and λ, equations (2-19) and (2-20), are drawn in fig. (a).

The *Hopf bifurcation* is closely related to the pitchfork bifurcation. It occurs when a complex conjugate pair of eigenvalues ($\lambda \pm i\omega$) crosses into the right half plane. The normal form for the Hopf bifurcation is

$$\dot{z} = (\lambda + i\omega)z + az\,|\,z\,|^2. \tag{2-27}$$

where the z and a are complex, and λ and ω are real. This normal form can be reduced to the pitchfork by writing z in polar coordinates,

$$z = re^{i\varphi}. \tag{2-28}$$

The time derivatives of z and $\bar{z}$ are

$$\dot{z} = \dot{r}e^{i\varphi} + i\dot{\varphi}re^{i\varphi}, \text{ and } \dot{\bar{z}} = \dot{r}e^{-i\varphi} - i\dot{\varphi}re^{-i\varphi}. \tag{2-29}$$

The time derivatives of r and φ can be isolated to give

$$\dot{r} = \frac{1}{2r}(\bar{z}\dot{z} + z\dot{\bar{z}})$$
$$\dot{\varphi} = \frac{1}{2ir^2}(\bar{z}\dot{z} - z\dot{\bar{z}}). \tag{2-30}$$

The Hopf bifurcation normal form (2-27), written in polar coordinates, is therefore

$$\dot{r} = \lambda r + \mathrm{Re}(a) r^3$$
$$\dot{\varphi} = \omega + \mathrm{Im}(a) r^2. \tag{2-31}$$

The equation for r is the same as the (unscaled) pitchfork bifurcation normal form. The nonzero solutions are called limit cycles. They are oscillatory solutions with a period of approximately ω. Nearby trajectories approach stable limit cycles, and diverge from unstable limit cycles, as time increases. The value of $\mathrm{Im}(a)$ is not important for the qualitative behavior of the system; it determines how the period changes with amplitude.

The bifurcation diagrams for the Hopf bifurcation are drawn in fig. 2-2. These diagrams should properly be three-dimensional; two dimensions for z and one for λ. This problem is avoided by using $|z|^2$ to represent the limit cycle solutions.

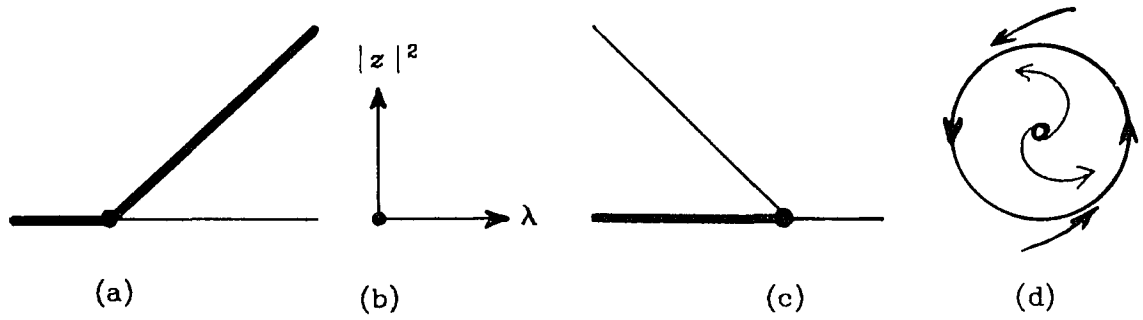

Fig. 2-2. The bifurcation diagrams for the Hopf bifurcation (2-31), with (a) $\mathrm{Re}(a) < 0$ and (c) $\mathrm{Re}(a) > 0$. Fig. (b) shows the axes used for the bifurcation diagrams and fig. (d) draws the phase portrait in z space for $\mathrm{Re}(a) < 0$ and $\lambda > 0$. Note that, if x^2 vs. λ had been plotted in fig. 2-2(a) and 2-2(c), then the diagrams would be identical to figs. (a) and (c) here.

A familiarity with two more bifurcations is assumed in this dissertation; the saddle-node and the transcritical bifurcations.

The saddle-node is the "typical" bifurcation which occurs when there are no symmetries. The normal form for the saddle-node bifurcation is

$$\dot{x} = \lambda + x^2 . \tag{2-32}$$

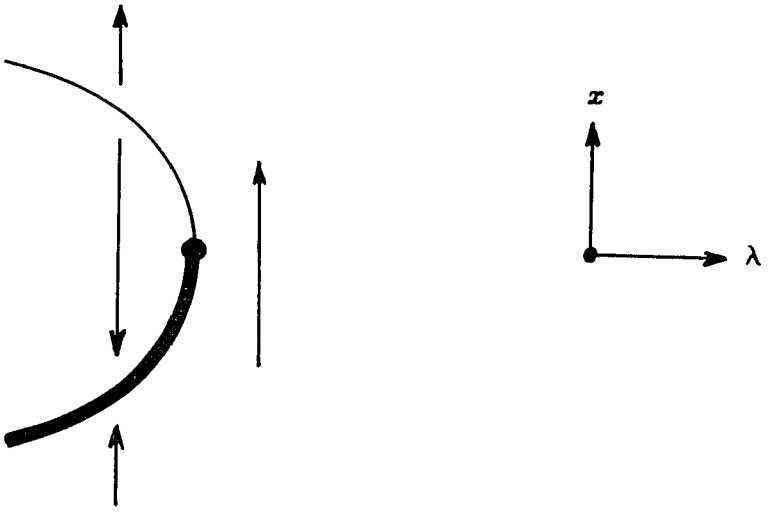

Fig. 2-3. Bifurcation diagram for the saddle-node bifurcation (2-32). If the phase space is two dimensional, and if the flow is attracting along the direction perpendicular to the page, then the unstable fixed point is a saddle, and the stable fixed point is a stable node: hence the name.

The transcritical bifurcation typically occurs when the origin ($x=0$) is constrained to be a fixed point, but there is *not* a reflection symmetry ($x \to -x$). The normal form for the transcritical bifurcation is

$$\dot{x} = \lambda x + x^2 . \tag{2-33}$$

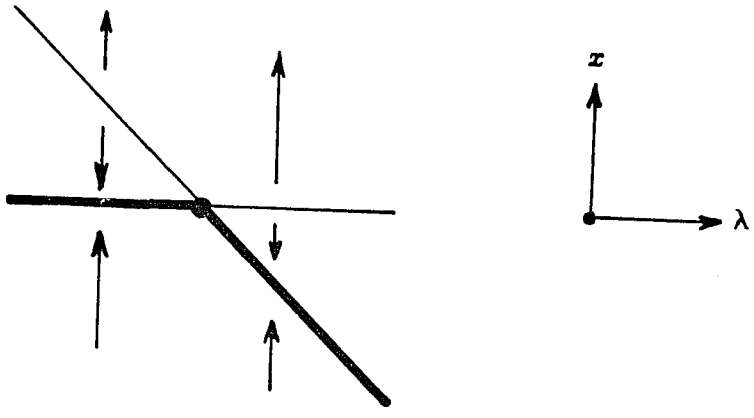

Fig. 2-4. Bifurcation diagram for the transcritical bifurcation (2-33).

2.2. Equivariant Vector Fields

The bifurcations mentioned above are the simplest cases which occur when a single eigenvalue goes through zero, or a single complex conjugate pair of eigenvalues crosses into the right half plane. When there is no symmetry in the problem, or if the symmetry is a reflection of a single coordinate (as in (2-5)), it is unlikely that *two* real eigenvalues go through zero simultaneously. If two eigenvalues happen to cross together, the system can be perturbed so that one eigenvalue crosses into the right hand plane before the other. On the other hand, symmetry can force multiple eigenvalues to cross into the right hand plane. Thus, the simplest bifurcations of vector fields with symmetry are often multiple bifurcations.

The symmetry of a vector field greatly influences what types of bifurcations are possible. The symmetry of an ODE (or vector field) is described by its *equivariance* under a transformation.

The first step of a bifurcation analysis in the presence of symmetry is to find the most general ODE with the given symmetry. Then the Taylor expansion of the ODE about the bifurcation point is truncated to obtain a candidate normal form. If this truncated ODE is structurally stable, then it is indeed a normal

form.

Assume that the system can be described by a point $\mathbf{a}$ in phase space, where $\mathbf{a}$ is either real or complex. For this section the phase space is assumed real,

$$\mathbf{a} \in \mathbb{R}^n , \tag{2-34}$$

but later the complex version is used. The dynamics of the system is given by an ODE,

$$\dot{\mathbf{a}} = \mathbf{f}(\mathbf{a}) , \tag{2-35}$$

where

$$\mathbf{f}: \mathbb{R}^n \to \mathbb{R}^n . \tag{2-36}$$

The system is symmetric if it is left unchanged by a transformation

$$\gamma: \mathbb{R}^n \to \mathbb{R}^n ; \mathbf{a} \to \gamma\mathbf{a}. \tag{2-37}$$

The set of all such transformations forms a group, called the symmetry group Γ.

The correct symmetry for an ODE is *equivariance*. The ODE is equivariant under Γ if

$$\gamma\mathbf{f}(\mathbf{a}) = \mathbf{f}(\gamma\mathbf{a}) \text{ or } \gamma \circ \mathbf{f} = \mathbf{f} \circ \gamma \text{ for all } \gamma \in \Gamma. \tag{2-38}$$

The equivariance condition simply says that $\mathbf{a}$ and $\dot{\mathbf{a}}$ transform the same way under γ. A more complicated definition of equivariance is needed if the transformation γ is nonlinear; however all symmetries discussed in this dissertation are linear.

If $\mathbf{f}$ is a linear ODE then it can be represented by a matrix $\mathbf{F}$,

$$\dot{\mathbf{a}} = \mathbf{f}(\mathbf{a}) = \mathbf{F} \cdot \mathbf{a}. \tag{2-39}$$

The equivariance condition says that the matrix $\mathbf{F}$ is unchanged under a similarity transformation by the matrix representation of γ:

$$\mathbf{F} = \gamma^{-1} \cdot \mathbf{F} \cdot \gamma. \tag{2-40}$$

2.3. Bifurcation in the Plane with the Symmetry of the Square

A fairly simple bifurcation with symmetry is presented in this section. The phase space is the real plane with the symmetry of the square. Many of the bifurcations which occur in convection are equivalent to this example. Convection on a square or rhombic lattice has the same normal form, except that the phase space is complex ($\mathbb{C}^2$) rather than real ($\mathbb{R}^2$). The competition between traveling waves and standing waves in oscillatory convection is also described by a similar normal form.

Let the real, two-dimensional plane be described by the coordinates $(x_1, x_2) \in \mathbb{R}^2$. The coordinates are naturally chosen so that the symmetries of the square are

$$
\begin{aligned}
&(x_1, x_2) \to (x_1, x_2)\\
&(x_1, x_2) \to (-x_1, x_2)\\
&(x_1, x_2) \to (x_1, -x_2)\\
&(x_1, x_2) \to (-x_1, -x_2)\\
&(x_1, x_2) \to (x_2, x_1)\\
&(x_1, x_2) \to (-x_2, x_1)\\
&(x_1, x_2) \to (x_2, -x_1)\\
&(x_1, x_2) \to (-x_2, -x_1).
\end{aligned}
\qquad (2\text{-}41)
$$

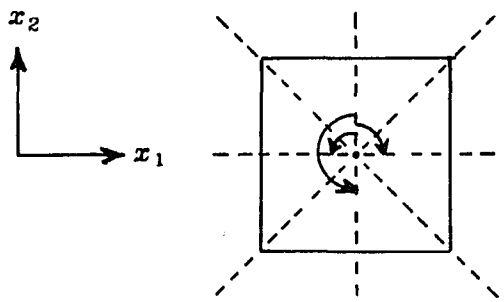

Fig. 2-5. The symmetries of a square in the x_1-x_2 plane ($\mathbf{D}_4$ symmetry). Each reflection is indicated by a dotted line, and the proper rotations are indicated by curved arrows.

The technique for finding the most general equivariant ODE is to look at each term in the Taylor expansion. The equivariance under $(x_1, x_2) \to (-x_1, x_2)$ gives

$$-\dot{x}_1(x_1, x_2) = \dot{x}_1(-x_1, x_2). \qquad (2\text{-}42)$$

Applied to a typical term in the Taylor expansion,

$$\dot{x}_1 = {x_1}^{n_1} {x_2}^{n_2}, \qquad (2\text{-}43)$$

this equivariance condition implies

$$-(x_1^{n_1}x_2^{n_2}) = (-x_1)^{n_1}x_2^{n_2} = (-1)^{n_1}(x_1^{n_1}x_2^{n_2}); \tag{2-44}$$

therefore n_1 must be odd. The equivariance under $(x_1, x_2) \to (x_1, -x_2)$ implies that n_2 is even. The general equivariant ODE is therefore

$$\dot{x}_1 = x_1 g(x_1^2, x_2^2), \tag{2-45}$$

where g is an arbitrary function of two variables:

$$g : \mathbb{R}^2 \to \mathbb{R}. \tag{2-46}$$

The interchange symmetry yields the equivariance condition

$$\dot{x}_2(x_1, x_2) = \dot{x}_1(x_2, x_1), \tag{2-47}$$

and therefore

$$\dot{x}_2 = x_2 g(x_2^2, x_1^2). \tag{2-48}$$

It can be verified that the system (2-45), (2-48) is equivariant under all the symmetries of the square.

The next step in the search for a normal form is to truncate the ODE, including the dependence on the bifurcation parameter λ. The scaling can be chosen so that λ is the eigenvalue of the trivial solution ($x_1 = x_2 = 0$). This gives a one parameter family of equivariant vector fields,

$$\dot{\mathbf{a}} = \mathbf{f}(\mathbf{a}, \lambda) = \lambda \mathbf{a} + \cdots. \tag{2-49}$$

The λ dependence of $\mathbf{f}$ can be more complicated in general, since λ represents the parameter which is adjusted in an experiment. Singularity theory (see Golubitsky & Schaeffer 1984) gives a method for treating cases such as

$$\dot{\mathbf{a}} = \lambda^2 \mathbf{a} + \cdots, \tag{2-50}$$

but this complication is ignored here.

The third order truncation of the general equivariant vector field with the symmetry of the square is

$$\begin{aligned} \dot{x}_1 &= x_1\left[\lambda + a x_2^2 + b(x_1^2 + x_2^2)\right] \\ \dot{x}_2 &= x_2\left[\lambda + a x_1^2 + b(x_1^2 + x_2^2)\right], \end{aligned} \tag{2-51}$$

where a and b are arbitrary real parameters. There are of course many ways

to write this result. This choice is motivated by the calculation of the coefficients a and b in the convection examples. The contributions to $\dot{x}_1$ naturally separate into the two terms shown.

2.3.1. The analysis of the normal form

The final step in the search for a normal form is to test this truncated system for structural stability. If it is structurally stable for all λ near zero, but excluding $\lambda = 0$, then it is a normal form.

Consider the vector field defined on a two-dimensional disk containing the origin. Such a vector field is structurally stable if (1) all of the fixed points and limit cycles are isolated and hyperbolic, and (2) if there are no saddle connections (Arnol'd 1983, pp. 94-95). By definition, the eigenvalues of the linear stability analysis of a hyperbolic fixed point have nonzero real part. Similarly, the Floquet exponents of a hyperbolic limit cycle have nonzero real parts, except for one exponent which is forced to be zero. The zero exponent corresponds to a perturbation in the direction of the flow. A consequence of structural stability, or robustness as it is often called, is that the higher order terms neglected in the truncation will not change the qualitative aspects of the system.

The truncation (2-51) is indeed a normal form. This is verified in the analysis of this section.

The fixed points are found by setting $\dot{x}_1 = \dot{x}_2 = 0$. It is useful to cross multiply the equations:

$$0 = x_1\dot{x}_2 - x_2\dot{x}_1 = bx_1x_2(x_1^2 - x_2^2). \tag{2-52}$$

Therefore either

$$b = 0, \text{ or } x_1x_2 = 0, \text{ or } x_1^2 = x_2^2. \tag{2-53}$$

If $b = 0$ there is a whole circle of solutions at $x_1^2 + x_2^2 = \lambda$, and the system is certainly not structurally stable. When $b \neq 0$, the possible solution types are

defined as follows;

$$\text{conduction}: \quad A^2 \equiv x_1^2 + x_2^2 = 0 \tag{2-54}$$

$$\text{rolls}: \quad x_1 x_2 = 0, \; A^2 \neq 0 \tag{2-55}$$

$$\text{squares}: \quad x_1^2 = x_2^2 \neq 0. \tag{2-56}$$

These names are chosen to correspond to the solution types of convection on a square lattice. The names "face" and "corner" would be more descriptive of the square, but there is an ambiguity; the x_1 and x_2 axes can point in the direction of a face *or* a corner of the square.

The simplest place to look for solutions of the ODE is on the lines of reflectional symmetry. These lines fall into two classes; the lines which contain the rolls,

$$x_2 = 0, \text{ and } x_1 = 0, \tag{2-57}$$

and the lines which contain the squares,

$$x_1 = x_2, \text{ and } x_1 = -x_2. \tag{2-58}$$

The amplitude of these two solution types, as a function of λ, is given by the solution of a single algebraic equation. The other equation is automatically satisfied as a consequence of the symmetry. The rolls with $x_1 \neq 0$ satisfy

$$0 = \lambda + b\, x_1^2. \tag{2-59}$$

The squares satisfy

$$0 = \lambda + (a + 2b) x_1^2. \tag{2-60}$$

It will soon become evident that it is best to express these results in term of the amplitude squared:

$$A^2 = x_1^2 + x_2^2. \tag{2-61}$$

For rolls,

$$A^2 = \frac{-\lambda}{b}, \tag{2-62}$$

and for squares,

$$A^2 = \frac{-\lambda}{\frac{1}{2}a+b}. \tag{2-63}$$

The stability of the stationary solutions to infinitesimal perturbations is found by computing the eigenvalues of the Jacobian matrix **J**, defined by

$$\mathbf{J} \equiv \mathrm{D}\mathbf{f} = \begin{pmatrix} \frac{\partial \dot{x}_1}{\partial x_1} & \frac{\partial \dot{x}_1}{\partial x_2} \\ \frac{\partial \dot{x}_2}{\partial x_1} & \frac{\partial \dot{x}_2}{\partial x_2} \end{pmatrix}. \tag{2-64}$$

This matrix gives the linearization of the system about a solution. Let

$$(x_1, x_2) = (\tilde{x}_1, \tilde{x}_2) + (\delta x_1, \delta x_2) \tag{2-65}$$

where $(\tilde{x}_1, \tilde{x}_2) \equiv \tilde{\mathbf{a}}$ is a stationary solution. The linearized equations for the perturbations are

$$\frac{d}{dt}\begin{pmatrix} \delta x_1 \\ \delta x_2 \end{pmatrix} = \mathbf{J}\big|_{\tilde{\mathbf{a}}} \cdot \begin{pmatrix} \delta x_1 \\ \delta x_2 \end{pmatrix}, \tag{2-66}$$

where the Jacobian matrix is evaluated at the stationary solution.

Only two of the elements of **J**,

$$\frac{\partial \dot{x}_1}{\partial x_1} = (\lambda + a x_2^2 + bA^2) + 2b x_1^2 \tag{2-67}$$

and

$$\frac{\partial \dot{x}_1}{\partial x_2} = 2(a+b) x_1 x_2, \tag{2-68}$$

need be calculated. This is because the symmetry of a solution restricts the form of the Jacobian matrix. When the equivariance condition,

$$\mathbf{f}(\gamma \mathbf{a}) = \gamma f(\mathbf{a}), \tag{2-69}$$

is differentiated, it follows from the chain rule that

$$\mathrm{D}\mathbf{f}\big|_{\gamma \mathbf{a}} \circ \gamma = \gamma \circ \mathrm{D}\mathbf{f}\big|_{\mathbf{a}}. \tag{2-70}$$

Therefore the matrix $\mathbf{J}\big|_{\tilde{\mathbf{a}}}$ commutes with all γ in the *isotropy subgroup* of $\tilde{\mathbf{a}}$, defined by

$$\Sigma_{\tilde{\mathbf{a}}} \equiv \{\gamma \in \Gamma \text{ such that } \gamma\tilde{\mathbf{a}} = \tilde{\mathbf{a}}\}. \tag{2-71}$$

The symmetry of a solution is described by its isotropy subgroup.

The isotropy subgroup of the conduction solution is the whole group Γ. Therefore the Jacobian matrix, evaluated at $x_1 = x_2 = 0$, commutes with all the matrices which correspond to the mappings (2-41). The result is that $\mathbf{J}$ is a multiple of the identity matrix,

$$\mathbf{J}_C = \begin{pmatrix} \lambda & 0 \\ 0 & \lambda \end{pmatrix}. \tag{2-72}$$

where

$$\lambda = \left.\frac{\partial \dot{x}_1}{\partial x_1}\right|_{[x_1 = x_2 = 0]}. \tag{2-73}$$

The conduction solution therefore has λ as a double eigenvalue.

The rolls (with $x_1 \neq 0$) are left invariant by the group element

$$(x_1, x_2) \to (x_1, -x_2), \text{ or } \begin{pmatrix} x_1 \\ x_2 \end{pmatrix} \to \begin{pmatrix} 1 & 0 \\ 0 & -1 \end{pmatrix}\begin{pmatrix} x_1 \\ x_2 \end{pmatrix}. \tag{2-74}$$

Therefore the matrix $\mathbf{J}$, evaluated at the rolls, commutes with the matrix

$$\begin{pmatrix} 1 & 0 \\ 0 & -1 \end{pmatrix}. \tag{2-75}$$

The consequence is that

$$\mathbf{J}_R = \begin{pmatrix} \alpha & 0 \\ 0 & \beta \end{pmatrix}, \tag{2-76}$$

where

$$\alpha = \left.\frac{\partial \dot{x}_1}{\partial x_1}\right|_{\left[\begin{smallmatrix} \lambda + b x_1^2 = 0 \\ x_2 = 0 \end{smallmatrix}\right]} = 2b x_1^2 = 2bA^2, \tag{2-77}$$

and

$$\beta = \left.\frac{\partial \dot{x}_2}{\partial x_2}\right|_{\left[\begin{smallmatrix} \lambda + b x_1^2 = 0 \\ x_2 = 0 \end{smallmatrix}\right]} = \left.\frac{\partial \dot{x}_1}{\partial x_1}\right|_{\left[\begin{smallmatrix} \lambda + b x_2^2 = 0 \\ x_1 = 0 \end{smallmatrix}\right]} = aA^2. \tag{2-78}$$

The eigenvalues of this matrix are clearly α and β.

The isotropy subgroup of the squares (with $x_1 = x_2$) is the group composed of the identity transformation and the mapping

$$\begin{bmatrix} x_1 \\ x_2 \end{bmatrix} \to \begin{bmatrix} 0 & 1 \\ 1 & 0 \end{bmatrix} \begin{bmatrix} x_1 \\ x_2 \end{bmatrix}. \tag{2-79}$$

Therefore the Jacobian matrix for the squares has the form

$$\mathbf{J}_S = \begin{bmatrix} \mu & \nu \\ \nu & \mu \end{bmatrix}, \tag{2-80}$$

where

$$\mu = \left. \frac{\partial \dot{x}_1}{\partial x_1} \right|_{\left[\begin{smallmatrix} \lambda + (a+2b) x_1^2 = 0 \\ x_1 = x_2 \end{smallmatrix} \right]} = 2b x_1^2 = b A^2, \tag{2-81}$$

and

$$\nu = \left. \frac{\partial \dot{x}_1}{\partial x_2} \right|_{\left[\begin{smallmatrix} \lambda + (a+2b) x_1^2 = 0 \\ x_1 = x_2 \end{smallmatrix} \right]} = 2(a+b) x_1 x_2 = (a+b) A^2. \tag{2-82}$$

The eigenvectors of $\mathbf{J}_S$ are

$$\begin{bmatrix} 1 \\ 1 \end{bmatrix}, \text{ and } \begin{bmatrix} 1 \\ -1 \end{bmatrix}, \tag{2-83}$$

and the eigenvalues are

$$\mu + \nu = (a+2b) A^2, \text{ and } \mu - \nu = -a A^2 \tag{2-84}$$

respectively.

There are no limit cycle solutions to the truncated system (51). This is because the ODE can be written as a gradient vector field;

$$\dot{x}_1 = \frac{\partial L(x_1, x_2)}{\partial x_1} \tag{2-85}$$

$$\dot{x}_2 = \frac{\partial L(x_1, x_2)}{\partial x_2}, \tag{2-86}$$

where

$$L(x_1, x_2) = \tfrac{1}{2}\lambda(x_1^2 + x_2^2) + \tfrac{1}{2} a x_1^2 x_2^2 + \tfrac{1}{4} b (x_1^2 + x_2^2)^2. \tag{2-87}$$

The proof is as follows: Along trajectories of the system under (2-85) and (2-86), L is strictly increasing (in other words it is a Liapunov function). If there were

a limit cycle, the value of L would have to increase over one period of the oscillation. On the other hand, since L is only a function of position it would have to repeat itself after one period. Since this is a contradiction, there can be no limit cycles.

It is worth noting that the general equivariant ODE (2-45), (2-48) *cannot* be written as a gradient system. The gradient of any invariant function,

$$L(x_1, x_2) = L(-x_1, x_2) = L(x_2, x_1), \tag{2-88}$$

is an equivariant vector field, but not all equivariant vector fields can be written as the gradient of some L. For example, the general fifth order terms in the ODE which are given by a gradient are

$$\dot{x}_1 = \frac{\partial}{\partial x_1}\left[\tfrac{1}{6}d(x_1^6+x_2^6)+\tfrac{1}{2}e(x_1^4x_2^2+x_1^2x_2^4)\right] \tag{2-89}$$

$$= x_1(dx_1^4+2ex_1^2x_2^2+ex_2^4). \tag{2-90}$$

This is more restricted than the general equivariant ODE, where the coefficients of all three quintic terms are arbitrary.

The last condition for structural stability of a two-dimensional vector field is that there are no saddle connections. A saddle connection is where a one-dimensional unstable manifold of a fixed point is also a stable manifold of the same or a different fixed point. This does not happen in (2-51) because rolls and squares never coexist as saddle points. (A saddle point has one positive and one negative eigenvalue.) Roll-roll or square-square saddle connections are impossible because one of the invariant manifolds of the saddle point is on the line of reflectional symmetry (see the phase portraits of fig. 2-6).

This completes the demonstration that the third order system (2-51) is structurally stable for fixed $\lambda \neq 0$ (and therefore the one parameter family $\mathbf{f}(\mathbf{a}, \lambda)$ is structurally stable), provided certain *non-degeneracy conditions* hold;

$$a \neq 0\,,\ b \neq 0\,,\ \text{and}\ a+2b \neq 0\,. \tag{2-91}$$

These conditions are inequalities, and are therefore satisfied for "most" values of a and b.

A fourth non-degeneracy condition is implicit in this treatment. It is required that the eigenvalue of the trivial solution (conduction) cross zero with nonzero speed as the bifurcation parameter is varied. In other words, the situation shown in equation (2-50) does not happen.

The conditions $b \neq 0$ and $a+2b \neq 0$ ensure that neither the roll nor square solutions satisfy

$$0 = \lambda + 0 \cdot A^2 + O(A^4)\,. \tag{2-92}$$

When this happens fifth order terms are needed.

The condition $a \neq 0$ ensures that the eigenvalues of the square and roll solutions are nonzero, and that there are no solutions other than conduction, squares, and rolls.

The following table summarizes the results for the least degenerate bifurcation with the symmetry of a square in the plane ($\mathbf{D}_4$ symmetry).

name	definition	amplitude	eigenvalues
conduction	$x_1 = x_2 = 0$	$A^2 = 0$	$\lambda,\ \lambda$
rolls	$x_1 x_2 = 0,\ A^2 \neq 0$	$A^2 = \dfrac{-\lambda}{b}$	$2bA^2,\ aA^2$
squares	$x_1^2 = x_2^2 \neq 0$	$A^2 = \dfrac{-\lambda}{\frac{1}{2}a+b}$	$(a+2b)A^2,\ -aA^2$

Table 2-1. Small amplitude solutions of equation (2-51).

These results are shown here in two ways. In fig. 2-6 the phase portraits are drawn for a, b, and λ fixed. The bifurcation diagrams, which plot A^2 vs. λ, for a and b fixed, are in figs. 2-7 and 2-8.

One of the parameters in the normal form (2-51) can be set to ± 1 by a scaling of the amplitudes. For instance, let

$$(x_1,x_2) \to \frac{1}{\sqrt{|b|}}(x_1,x_2) \tag{2-93}$$

and the normal form becomes

$$\dot{x}_1 = \lambda x_1 + \frac{a}{|b|} x_1 x_2^2 + \mathrm{sgn}(b)\, x_1 A^2. \tag{2-94}$$

Note that the sign of the coefficients cannot be changed, however. This scaling is discontinuous when b changes sign. A different way to scale the normal form is to set

$$a^2+b^2 = 1 \tag{2-95}$$

by the change of variables

$$(x_1,x_2) \to (a^2+b^2)^{-1/4}(x_1,x_2). \tag{2-96}$$

This scaling only becomes singular when both a and b are zero. This shows that the normal form has only one free parameter: the angle in the a-b plane.

The calculation of the coefficients in the normal form naturally give formulas for a and b. It is awkward to rescale the normal form if both a and b are complicated functions of the natural parameters in the problem. Therefore the results are presented here with both a and b retained in the normal form.

The qualitative features of the solutions depend only on the signs of a, b, and $a+2b$. Fig. 2-7 shows the six regions in the a-b plane which are defined by the non-degeneracy conditions, and fig. 2-8 shows the bifurcation diagrams for each of these regions.

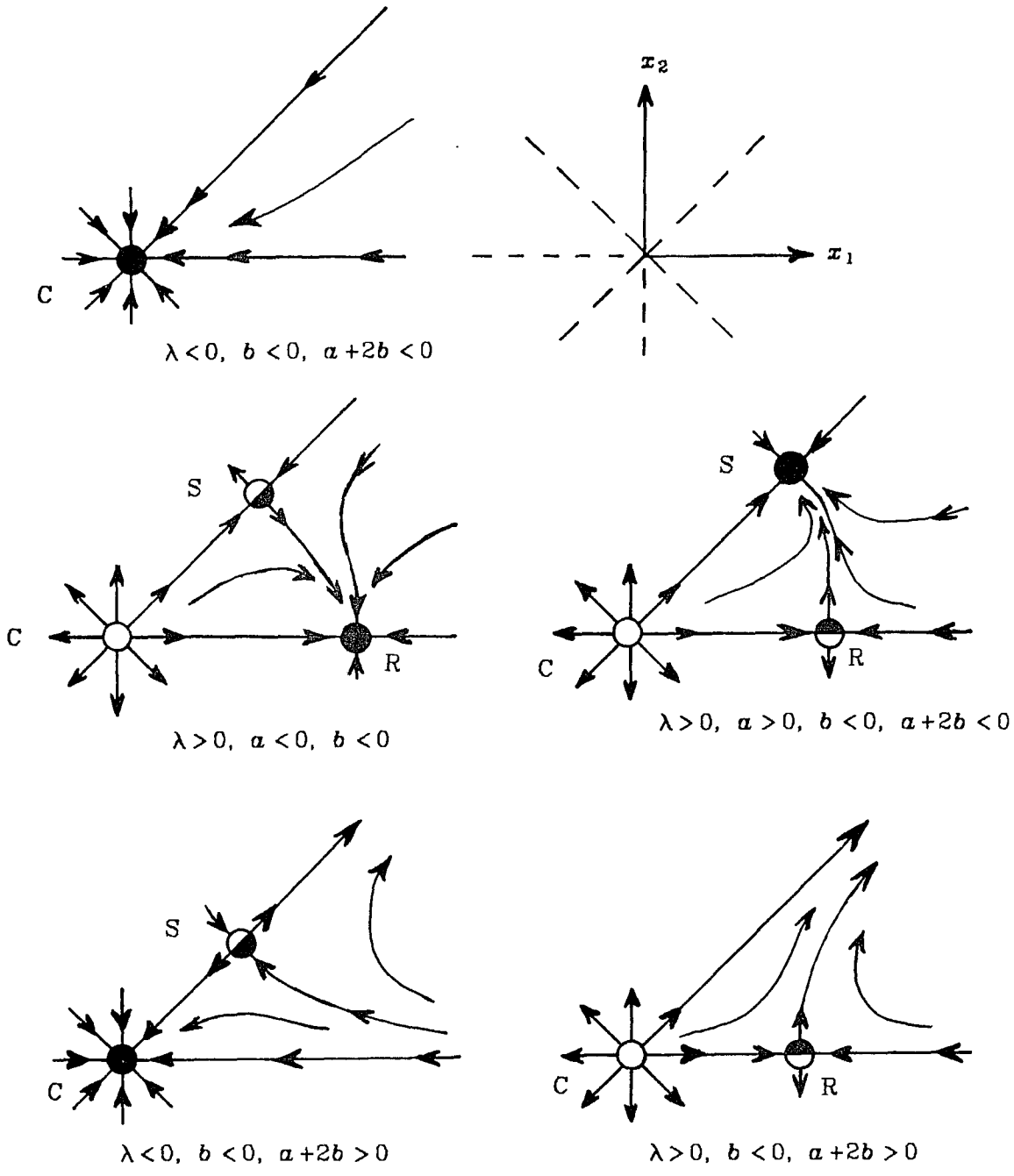

Fig. 2-6. Phase portraits of the normal form with $\mathbf{D}_4$ symmetry, equation (2-51), for fixed values of the coefficients λ, a, and b. The picture at the upper right shows axes of the phase portraits. Using the symmetries of the system, the phase portraits in the entire x_1-x_2 plane can be reconstructed from the regions pictured here. The roll solutions (R) are fixed points on the x_1 and x_2 axes, and the square solutions (S) are fixed points on the the lines defined by $x_1+x_2=0$ and $x_1-x_2=0$. The conduction solution (C) is at the origin, $x_1=x_2=0$. The nomenclature is due to the application of this normal form to convection. In these and all future phase portraits, unstable fixed points are indicated by an open circle, stable fixed points by a closed circle, and saddle points by a half-filled circle.

Bifurcation in the Plane with the Symmetry of the Square

$$\dot{x}_1 = x_1(\lambda + a x_2^2 + b A^2), \quad \dot{x}_1 = x_1(\lambda + a x_2^2 + b A^2), \quad A^2 \equiv x_1^2 + x_2^2$$

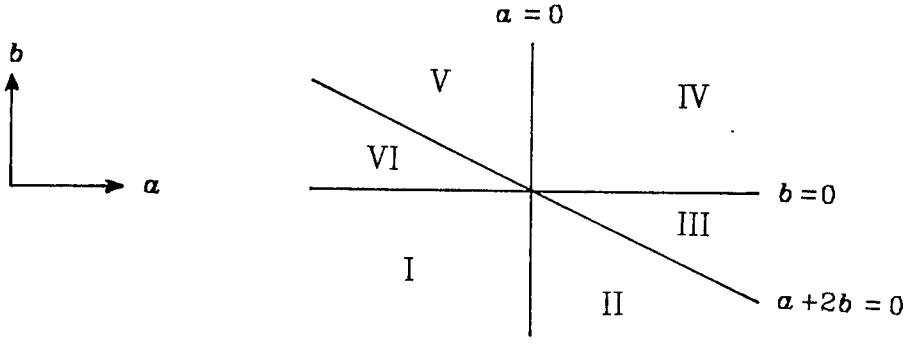

Fig. 2-7. The behavior of the normal form (2-51), listed above, depends on the coefficients a and b. The a-b plane is divided into six regions by the non-degeneracy conditions: $a \neq 0$, $b \neq 0$, and $a + 2b \neq 0$. Within each region, the qualitative behavior is similar.

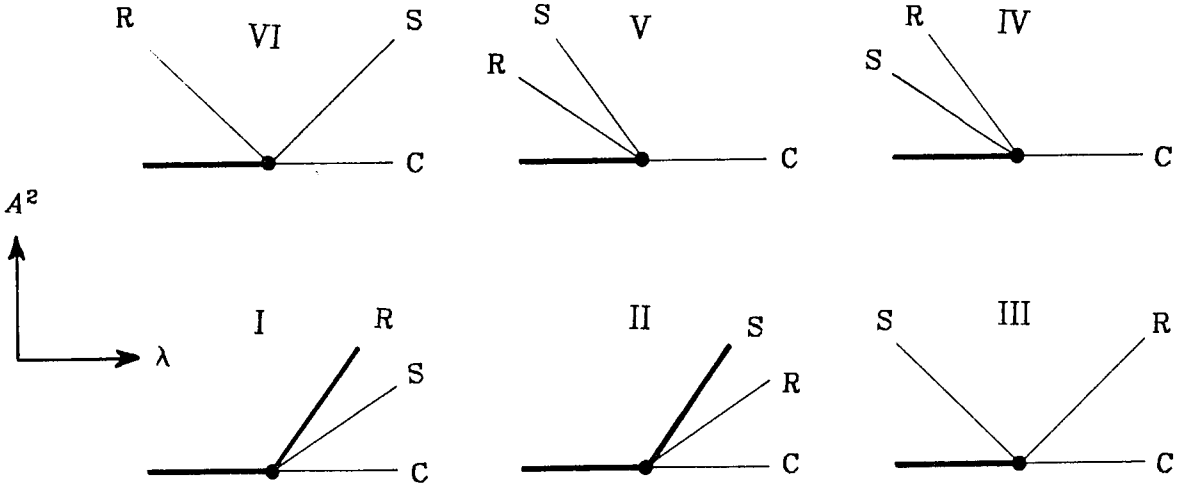

C : Conduction R : Rolls S : Squares

Fig. 2-8. The possible bifurcation diagrams, which plot A^2 vs. λ, for a and b within each of the regions shown above. A bold line represents stable solutions, a fine line represents unstable solutions. These diagrams are relevant to three different normal forms: (1) Bifurcation in the plane with the symmetry of the square, (2) Convection on a square or rhombic lattice (equation (2-151)), and (3) Hopf bifurcation in two-dimensional convection (equation (3-35)). Cases (2) and (3) are discussed later, in sections 2.7 and 3.2.

2.4. Bifurcation Theory Applied to Convection

The first step of the bifurcation analysis is to solve the linearized equations. This has been done in Chapter One; the essential elements of the linear analysis are repeated here.

When the lateral boundaries are sufficiently far away, the fluid layer can be considered infinite in the horizontal plane. The convection equations are then equivariant with respect to rigid motions in the plane, (that is, all translations and rotations). The coefficients of the partial differential equations are constant in the horizontal plane, but may depend on the vertical coordinate. With these assumptions the partial differential equations, linearized about the conduction solution, are separable. The eigenfunctions are of the form

$$f(z)e^{i\mathbf{k}\cdot\mathbf{x}}, \tag{2-97}$$

where z is the vertical direction and $\mathbf{k}$ is a two-dimensional vector in the horizontal plane. These eigenfunctions are called *rolls*, because the fluid circulates in counter rotating cylinders, as shown in fig. 2-9(a). The $\mathbf{k}$ vector of a roll is perpendicular to the roll axis, since the fields change in the direction of $\mathbf{k}$.

The linear stability analysis determines when an infinitesimal roll disturbance grows or decays with time. Because the system is linearized, the rolls have an exponential time dependence,

$$e^{\lambda_j t}, \tag{2-98}$$

where the eigenvalues (λ_j) depend on the Rayleigh number as well as $|\mathbf{k}|^2$. When the real part of λ_j is positive the corresponding disturbance grows and the conduction solution is unstable. Assume that the results of the linear stability analysis give a diagram similar to fig. 2-9(b). There is a *critical Rayleigh number*, R_c, below which all roll disturbances decay. At the critical Rayleigh number, the rolls with the *critical wavenumber*, $|\mathbf{k}|^2 = k_c^2$, are neutrally stable. This defines the circle of critical $\mathbf{k}$ vectors in the two-dimensional $\mathbf{k}$ space,

shown in fig. 2-9(c). For $R > R_c$, there is a range of wavenumbers, all of which are unstable.

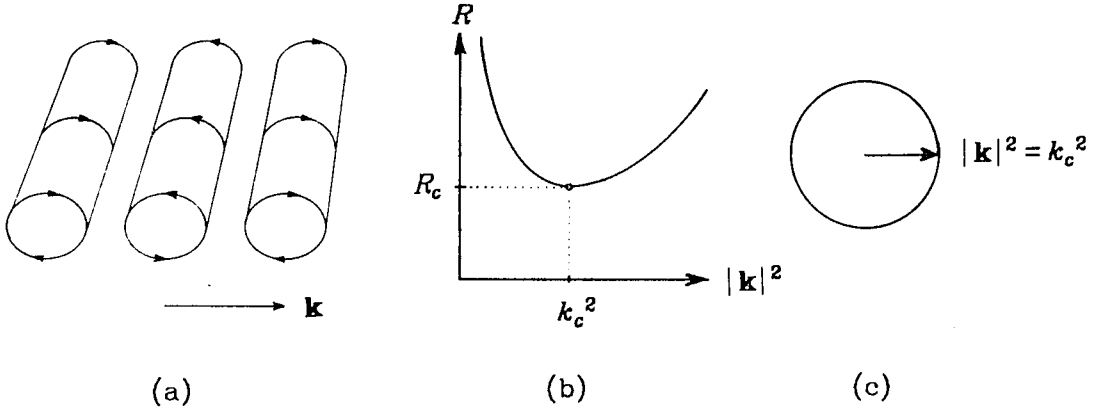

Fig. 2-9. (a) A roll and its associated $\mathbf{k}$ vector. (b) Linear stability analysis finds the critical Rayleigh number R_c and the corresponding critical wavenumber squared, k_c^2. (c) The circle of critical $\mathbf{k}$ vectors.

2.5. Doubly Periodic Convection

The crucial assumption of this work, which forces the number of critical rolls to be finite, is that all fields are doubly periodic in the horizontal plane. This means that there are two translation vectors $\mathbf{w}_1$ and $\mathbf{w}_2$ in the horizontal plane such that all fields satisfy

$$\psi(\mathbf{x}) = \psi(\mathbf{x} + n_1\mathbf{w}_1 + n_2\mathbf{w}_2) \tag{2-99}$$

for all integers n_1 and n_2. The vertical dependence of ψ is suppressed in the discussion of double periodicity. The Fourier transform of such doubly periodic functions is discrete:

$$\psi(\mathbf{x}) = \sum_{l,m=-\infty}^{\infty} \psi_{l,m} e^{i(l\mathbf{k}_1 + m\mathbf{k}_2)\cdot\mathbf{x}} \equiv \sum_{\mathbf{k}\in\mathbb{Z}^2} \psi_{\mathbf{k}} e^{i\mathbf{k}\cdot\mathbf{x}} \tag{2-100}$$

where

$$\psi_{\mathbf{k}} = \overline{\psi}_{-\mathbf{k}} \text{ and } \mathbf{k}_\alpha \cdot \mathbf{w}_\beta = \delta_{\alpha,\beta}. \tag{2-101}$$

The overbar denotes complex conjugation, the labels α and β run from 1 to 2,

and $\delta_{\alpha,\beta}$ is the Kronecker delta function. The sum on $\mathbf{k}$ ranges over a two-dimensional lattice, which can be identified with the ordered pairs of integers:

$$\mathbf{k} \in \{l\,\mathbf{k}_1 + m\,\mathbf{k}_2 \,|\, (l,m) \in \mathbb{Z}^2\}. \tag{2-102}$$

In the sums, e.g. (2-100), the range of $\mathbf{k}$ is abbreviated by

$$\mathbf{k} \in \mathbb{Z}^2. \tag{2-103}$$

When double periodicity is *not* imposed, the rotational degeneracy of the problem is troublesome, because there are an infinite number of eigenfunctions with zero eigenvalue at $R = R_c$, (one for each direction of $\mathbf{k}$). In addition, there are stable modes with an eigenvalue arbitrarily close to zero. This contradicts two of the hypotheses of the center manifold theorem: (1) dim $Y < \infty$, and (2) $\sigma_2 < -\sigma < 0$. These complications are avoided by imposing double periodicity in the horizontal plane. When all fields are doubly periodic, a finite number of eigenfunctions go unstable at the bifurcation, and the center manifold theorem allows a description of the dynamics near the bifurcation in terms of an ordinary differential equation for the critical amplitudes.

The assumption of doubly periodic convection is only partially justified physically. The most frequently observed patters (rolls, squares, and hexagons) are doubly periodic, although there are always defects in the patterns. Clearly, doubly periodic patterns must be understood before the defects can be studied. The disadvantage of imposing double periodicity is that defects in the cellular structure cannot be studied. Newell & Whitehead (1969), and Segel (1969) developed a method for studying defects by allowing the amplitudes to depend on a slow spatial scale. Work continues using the approach (see for example Cross & Newell (1984)). This method assumes that two-dimensional rolls are stable to three-dimensional disturbances in an infinite layer. If the doubly periodic analysis shows that squares or hexagons are stable instead of rolls, then the procedure for studying defects must be modified.

The choice of the two basis vectors in $\mathbf{k}$ space, $\mathbf{k}_1$ and $\mathbf{k}_2$ in equation (2-102), is not unique. However, the basis vector can always be chosen so that one of five sets of equalities and inequalities holds. This defines the five different types of $\mathbf{k}$ space lattices for double periodicity in the plane:

Hexagonal lattice

$$|\mathbf{k}_1|^2 = |\mathbf{k}_2|^2 \neq 0, \quad \mathbf{k}_1 \cdot \mathbf{k}_2 = -\tfrac{1}{2}|\mathbf{k}_1|^2 \tag{2-104}$$

Square lattice

$$|\mathbf{k}_1|^2 = |\mathbf{k}_2|^2 \neq 0, \quad \mathbf{k}_1 \cdot \mathbf{k}_2 = 0 \tag{2-105}$$

Rhombic lattice

$$|\mathbf{k}_1|^2 = |\mathbf{k}_2|^2 \neq 0, \quad \mathbf{k}_1 \cdot \mathbf{k}_2 \neq 0, \quad \mathbf{k}_1 \cdot \mathbf{k}_2 \neq \pm \tfrac{1}{2}|\mathbf{k}_1|^2 \tag{2-106}$$

Rectangular lattice

$$0 \neq |\mathbf{k}_1|^2 \neq |\mathbf{k}_2|^2 \neq 0, \quad \mathbf{k}_1 \cdot \mathbf{k}_2 = 0 \tag{2-107}$$

General lattice

None of the above are possible. (2-108)

Examples of these lattices are drawn in fig. 2-10.

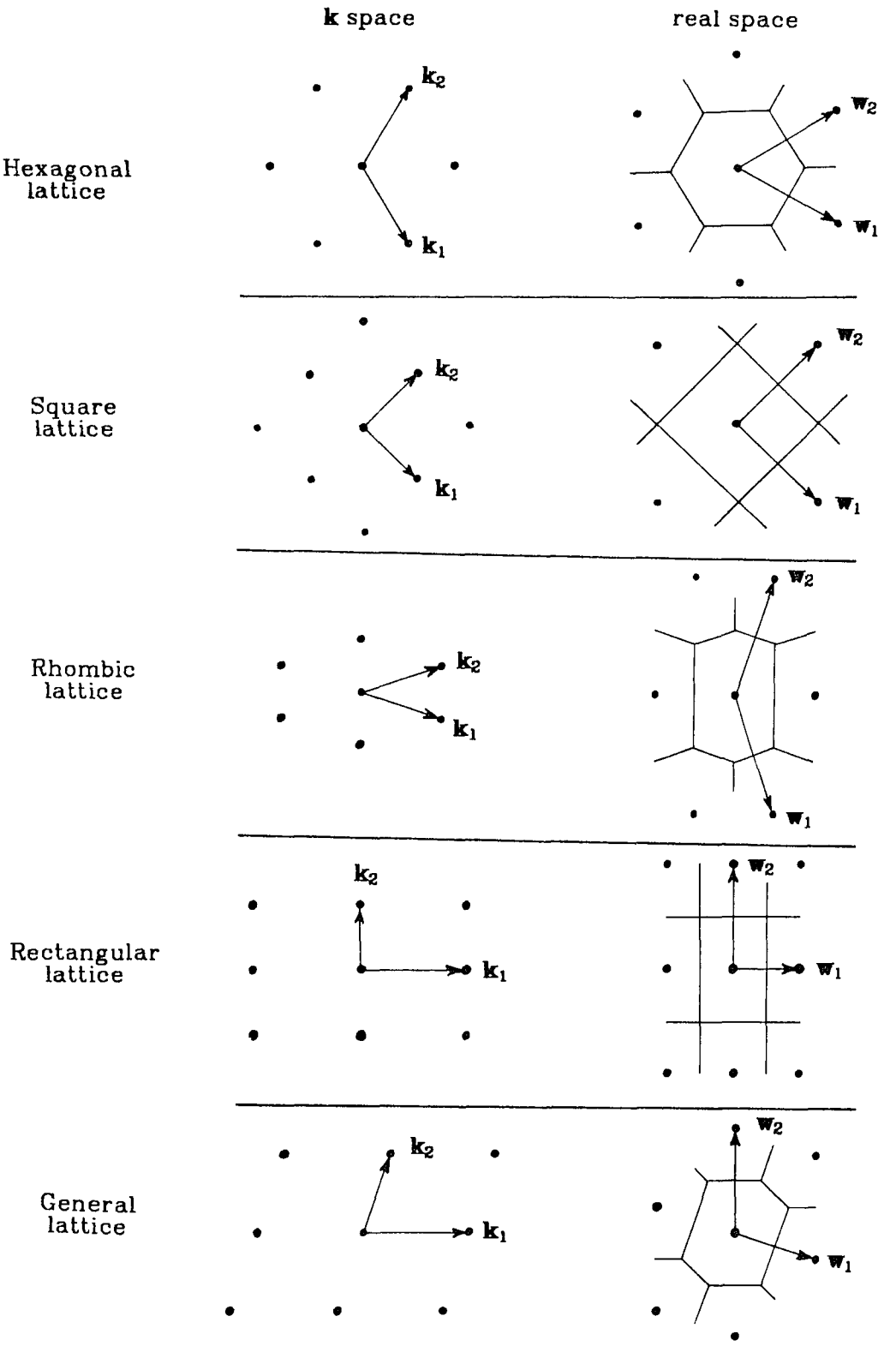

Fig. 2-10. The **k** space lattices representing the 5 types of double periodicity in the plane are shown in the first column; the corresponding real space lattices are in the second column. One fundamental region in each of the real space lattices is indicated. The fundamental region defines a tiling of the plane such that all fields are repeated exactly in each tile.

When the fields are doubly periodic, the partial differential equations can be reduced to an infinite-dimensional system of ordinary differential equation for the complex amplitudes, $\psi_{\mathbf{k},n}(t)$, where the fields are written as

$$\psi(\mathbf{x},t) = f_n(z) \sum_{\mathbf{k}\in\mathbb{Z}^2} \psi_{\mathbf{k},n}(t)\, e^{i\mathbf{k}\cdot\mathbf{x}} \tag{2-109}$$

Here the vertical eigenfunctions, $f_n(z)$, are labeled by a vertical "quantum number" n. The critical mode has $n = 1$.

At R_c, all the amplitudes $\psi_{\mathbf{k},n}(t)$ are linearly damped except the critical modes. As with the example of equation (2-3), (2-4), the damped degrees of freedom can be eliminated since the system is attracted to the center manifold. Then a normal form describes the dynamics on the center manifold.

When the two vectors $\mathbf{k}_\alpha$ have length equal to the critical wavenumber k_c the resulting $\mathbf{k}$ space lattices are either hexagonal, square, or rhombic. Sattinger (1979) found the normal forms for the least degenerate bifurcations on these lattices. He found that in the non-Boussinesq case on the hexagonal lattice the least degenerate bifurcation does not have any stable solutions near the origin. Sattinger's work has been extended in the hexagonal case by Buzano & Golubitsky (1983), using singularity theory. They found the normal form for a degenerate bifurcation, in the non-Boussinesq case, which has stable solutions in the local analysis. Golubitsky *et al.* (1984) then studied the onset of convection on the hexagonal lattice in the Boussinesq approximation, as well as the case in which all of the non-Boussinesq terms are small.

Busse has also considered the question of what patterns are possible, purely on the grounds of symmetry. In place of double periodicity, Busse (1978, etc.) introduces a more general superposition of N critical $\mathbf{k}$ vectors, and truncates the equations to third order. At least two classes of solution to this truncated system exist; regular patterns, where the critical $\mathbf{k}$ vectors are equally spaced around the circle, and semi-regular patterns, where the angle between $\mathbf{k}$

vectors

alternates between two values as one goes around the circle. In both cases each roll has equal amplitude. These patterns are quasi-periodic when there are three (or more) critical $\mathbf{k}$ vectors such that

$$n_1\mathbf{k}_1+n_2\mathbf{k}_2+n_3\mathbf{k}_3 = 0 \text{ implies } n_1 = n_2 = n_3 = 0. \qquad (2\text{-}110)$$

Quasi-periodic patterns introduce complications at higher order in the amplitude, since sums and differences of critical $\mathbf{k}$ vectors can excite modes which have $|\mathbf{k}|^2$ arbitrarily close to k_c^2. This introduces "small denominator" problems which prevent one from finding the normal form.

2.6. Translations and Rotations of Doubly Periodic Functions

The convection equations are equivariant with respect to the Euclidean group in the horizontal plane, that is, all combinations of translations and rotations (including reflections). The Euclidean group is technically a semi-direct product of these translations and rotations, because these two operations do not commute, but this is not an important distinction for what follows.

The translations $\mathbf{x} \to \mathbf{x}+\mathbf{d}$ transform the doubly periodic functions (2-100) as follows:

$$\psi(\mathbf{x}+\mathbf{d}) = \sum_{\mathbf{k}\in\mathbb{Z}^2} \psi_{\mathbf{k}} e^{i\mathbf{k}\cdot(\mathbf{x}+\mathbf{d})} = \sum_{\mathbf{k}\in\mathbb{Z}^2} \left(\psi_{\mathbf{k}} e^{i\mathbf{k}\cdot\mathbf{d}}\right) e^{i\mathbf{k}\cdot\mathbf{x}}. \qquad (2\text{-}111)$$

Therefore the translation $\mathbf{x} \to \mathbf{x}+\mathbf{d}$ corresponds to the phase shift

$$\psi_{\mathbf{k}} \to \psi_{\mathbf{k}} e^{i\mathbf{k}\cdot\mathbf{d}}. \qquad (2\text{-}112)$$

The domain of doubly periodic functions is a two-torus, and the translations can also be identified with a torus, with coordinates

$$(\mathbf{k}_1\cdot\mathbf{d},\ \mathbf{k}_2\cdot\mathbf{d}). \qquad (2\text{-}113)$$

The rotations act on the horizontal by a linear transformation

$$\mathbf{x} \to \mathbf{R}\cdot\mathbf{x}, \qquad (2\text{-}114)$$

where the transpose of $\mathbf{R}$ equals $\mathbf{R}^{-1}$. As a consequence,

$$\mathbf{k}\cdot(\mathbf{R}\cdot\mathbf{x}) = (\mathbf{R}^{-1}\cdot\mathbf{k})\cdot\mathbf{x}. \tag{2-115}$$

The notation used here is that rotations include reflections, so that

$$\mathrm{Det}\,\mathbf{R} = \pm 1. \tag{2-116}$$

The terms *proper rotations* and proper Euclidean group will be used when reflections are excluded.

The doubly periodic functions transform under rotations as

$$\psi(\mathbf{R}\cdot\mathbf{x}) = \sum_{\mathbf{k}\in\mathbb{Z}^2} \psi_{\mathbf{k}} e^{i\mathbf{k}\cdot(\mathbf{R}\cdot\mathbf{x})} = \sum_{\mathbf{k}\in\mathbb{Z}^2} \psi_{\mathbf{k}} e^{i(\mathbf{R}^{-1}\cdot\mathbf{k})\cdot\mathbf{x}} = \sum_{\mathbf{k}\in\mathbb{Z}^2} \psi_{\mathbf{R}\cdot\mathbf{k}} e^{i\mathbf{k}\cdot\mathbf{x}}; \tag{2-117}$$

therefore the rotation $\mathbf{x}\to\mathbf{R}\cdot\mathbf{x}$ corresponds to

$$\psi_{\mathbf{k}} \to \psi_{\mathbf{R}\cdot\mathbf{k}}. \tag{2-118}$$

A rotation preserves doubly periodic functions on a given lattice only if $\mathbf{R}$ preserves the $\mathbf{k}$ lattice. This is a major restriction. The rotations which preserve the five types of lattices, where $\mathbf{k}_1$ and $\mathbf{k}_2$ are chosen according to the classification of equations (2-104) through (2-108), are listed below.

Hexagonal lattice

$$\begin{aligned}(\mathbf{k}_1,\mathbf{k}_2)\to{}&(\mathbf{k}_1,\mathbf{k}_2),\ -(\mathbf{k}_1,\mathbf{k}_2),\ (\mathbf{k}_2,\mathbf{k}_1),\ -(\mathbf{k}_2,\mathbf{k}_1),\\ &(\mathbf{k}_1,-\mathbf{k}_1-\mathbf{k}_2),\ (-\mathbf{k}_1,\mathbf{k}_1+\mathbf{k}_2),\ (\mathbf{k}_2,-\mathbf{k}_1-\mathbf{k}_2),\ (-\mathbf{k}_2,\mathbf{k}_1+\mathbf{k}_2)\\ &(-\mathbf{k}_1-\mathbf{k}_2,\mathbf{k}_1),\ (\mathbf{k}_1+\mathbf{k}_2,-\mathbf{k}_1),\ (-\mathbf{k}_1-\mathbf{k}_2,\mathbf{k}_2),\ (\mathbf{k}_1+\mathbf{k}_2,-\mathbf{k}_2).\end{aligned} \tag{2-119}$$

Square lattice

$$\begin{aligned}(\mathbf{k}_1,\mathbf{k}_2)\to{}&(\mathbf{k}_1,\mathbf{k}_2),\ -(\mathbf{k}_1,\mathbf{k}_2),\ (\mathbf{k}_2,\mathbf{k}_1),\ -(\mathbf{k}_2,\mathbf{k}_1)\\ &(-\mathbf{k}_1,\mathbf{k}_2),\ (\mathbf{k}_1,-\mathbf{k}_2),\ (\mathbf{k}_2,-\mathbf{k}_1),\ (-\mathbf{k}_2,\mathbf{k}_1).\end{aligned} \tag{2-120}$$

Rhombic lattice

$$(\mathbf{k}_1,\mathbf{k}_2)\to(\mathbf{k}_1,\mathbf{k}_2),\ -(\mathbf{k}_1,\mathbf{k}_2),\ (\mathbf{k}_2,\mathbf{k}_1),\ -(\mathbf{k}_2,\mathbf{k}_1). \tag{2-121}$$

Rectangular lattice

$$(\mathbf{k}_1,\mathbf{k}_2)\to(\mathbf{k}_1,\mathbf{k}_2),\ -(\mathbf{k}_1,\mathbf{k}_2),\ (\mathbf{k}_1,-\mathbf{k}_2),\ (-\mathbf{k}_1,\mathbf{k}_2). \tag{2-122}$$

General lattice

$$(\mathbf{k}_1,\mathbf{k}_2)\to(\mathbf{k}_1,\mathbf{k}_2),\ -(\mathbf{k}_1,\mathbf{k}_2). \tag{2-123}$$

The hexagonal and square lattices are left invariant by the symmetries of the hexagon and square, respectively. Both of these include the symmetry of the rectangle as a subgroup, but neither is a subgroup of the other. The rhombic and rectangular lattices are preserved by the symmetries of the rectangle; two reflections across perpendicular lines, and the composition of these two which is a 180° rotation. The general lattice is preserved only by the 180° rotation and the identity transformation.

2.6.1. Irreducible representations

The irreducible representations are important for bifurcation problems, because if one member of an irreducible representation goes unstable, then they all do. Therefore the linear stability analysis need only be done for a single mode.

An irreducible representation is a linear space which is invariant under the symmetry, and which cannot be separated into two invariant spaces. For continuous symmetries the basis vectors of the linear space are functions.

A familiar example is provided by the irreducible representations of the rotation group in three dimensions, which are the sets of $Y_{l,m}$'s (for a given l). This means that any function on the sphere which is a linear combination of $Y_{l,m}$'s (for fixed l) remains such a linear combination when it is rotated.

The irreducible representations of the Euclidean group are generated by

$$\{e^{i\mathbf{k}\cdot\mathbf{x}} \mid |\mathbf{k}|^2 = const.\}. \qquad (2\text{-}124)$$

There is an infinite-dimensional irreducible representation for each nonzero value of $|\mathbf{k}|^2$.

The Euclidean group, restricted to doubly periodic functions, is a compact group; therefore the irreducible representations are finite dimensional. (This situation is similar to the rotation group and the $Y_{l,m}$'s.) The irreducible

representations of the Euclidean group, restricted to doubly periodic functions, are generated by

$$\{e^{i\mathbf{k}\cdot\mathbf{x}}, e^{i\mathbf{k}'\cdot\mathbf{x}}, \cdots, e^{i\mathbf{k}''\cdot\mathbf{x}}\}, \tag{2-125}$$

where the $\mathbf{k}$ vectors are the maximal sets which are taken into each other by the rotations which preserve the lattice. (The translations only mix $\mathbf{k}$ and $-\mathbf{k}$, so the rotations alone generate the invariant spaces.) The dimension of the irreducible representation is the number of $\mathbf{k}$ vectors in the set. From the list of allowed rotations in equations (2-119)-(2-23) it can be seen that the maximum dimension of the irreducible representations is 12 in the hexagonal lattice, 8 in the square lattice, etc. It is possible, however, that a $\mathbf{k}$ vector is invariant under one or more of the rotations, in which case the irreducible representation will have a smaller dimension. For instance, $\mathbf{k}=0$ always gives a one-dimensional representation.

The sets of $\mathbf{k}$ vectors can be indicated by the components in the canonical basis:

$$(l, m) \equiv l\,\mathbf{k}_1 + m\,\mathbf{k}_2. \tag{2-126}$$

The irreducible representations for the rhombic lattice are either 1, 2, or 4-dimensional.

$$\begin{array}{c} 1:\ (0,0) \\ 2:\ (l,l)\ (-l,-l),\quad l\neq 0 \\ 2:\ (l,-l)\ (-l,l),\quad l\neq 0 \\ 4:\ (l,m)\ (m,l)\ (-l,-m)\ (-m,-l),\quad l\neq m\ ,\ \text{but } m=0 \text{ is allowed.} \end{array} \tag{2-127}$$

For the square lattice, the irreducible representations are either 1, 4, or 8-dimensional:

$$\begin{array}{c} 1:\ (0,0) \\ 4:\ (l,0)\ (-l,0)\ (0,l)\ (0,-l), \\ 4:\ (l,l)\ (l,-l)\ (-l,l)\ (-l,-l), \\ 8:\ (l,m)\ (l,-m)\ (-l,m)\ (-l,-m)\ (m,l)\ (m,-l)\ (-m,l)\ (-m,-l), \end{array} \tag{2-128}$$

where $l\neq 0$, $m\neq 0$, and $l\neq m$ in all cases.

In a similar way, the irreducible representations for the hexagonal lattice are either 1, 6, or 12-dimensional.

Fig. 2-11 gives a graphical representation of various irreducible representations.

When $|\mathbf{k}_1|^2 = |\mathbf{k}_2|^2 = k_c^2$, the critical modes span a four (or six in the hexagonal lattice) dimensional irreducible representation which includes (1,0). More exotic possibilities include the 8 or 12-dimensional irreducible representations, as well as cases where two irreducible representations have the same $|\mathbf{k}|^2$. An example of this latter possibility is the (4+8)-dimensional (reducible) representation in the square lattice generated by all rotations of the following $\mathbf{k}$ vectors:

$$(5,0) \text{ and } (3,4). \tag{2-129}$$

These two irreducible representations go unstable at the same Rayleigh number since $|5\mathbf{k}_1|^2 = |3\mathbf{k}_1 + 4\mathbf{k}_2|^2$.

These higher dimensional representations may be important as a method for approximating the dislocations and imperfections of the doubly periodic patterns which are observed in the laboratory. The normal forms for these cases are high dimensional, and may have chaotic dynamics. This could correspond to the so-called phase turbulence, which sets in right at the critical Rayleigh number in large aspect ratio systems. This phase turbulence results when the pattern slowly shifts around, never annealing into perfect double periodicity (see Ahlers & Behringer 1978, Ahlers & Walden 1980). It should be mentioned that the system is extremely sensitive to external noise because of the translational invariance.

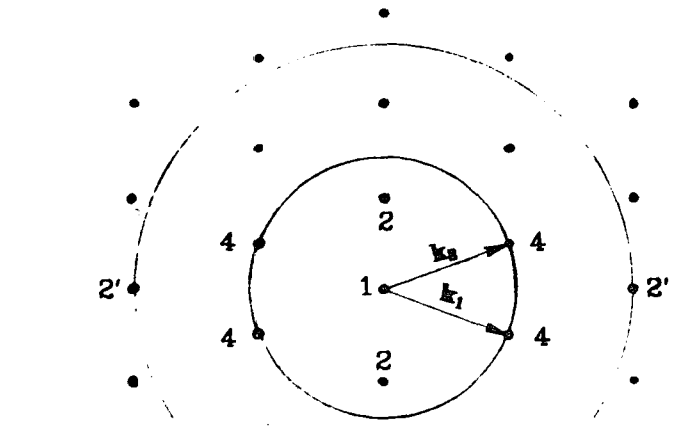

Rhombic lattice:
1 : (0, 0)
2: (1, −1)
4: (1, 0)
2′: (1, 1)

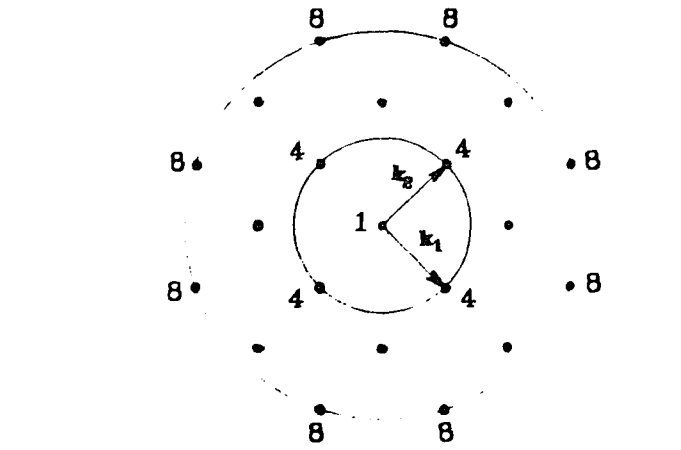

Square lattice:
1 : (0, 0)
4: (1, 0)
8: (2, 1)

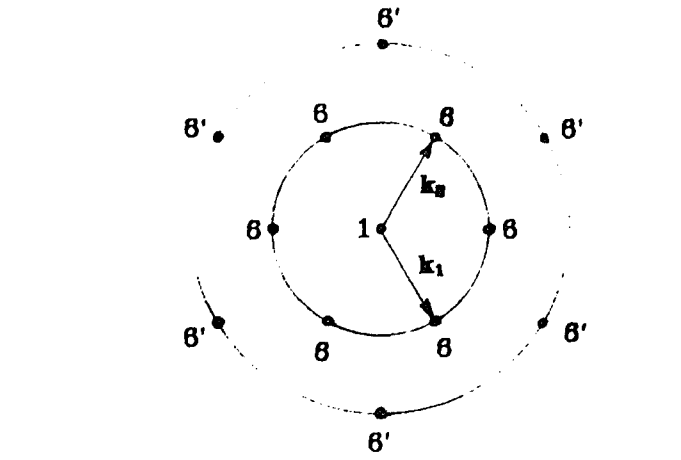

Hexagonal lattice:
1 : (0, 0)
6: (1, 0)
6′: (1, 1)

Fig. 2-11. Examples of irreducible representations of the group of translations and rotations of doubly periodic functions on the rhombic, square, and hexagonal lattices. The irreducible representations correspond to sets of $\mathbf{k}$ vectors which are connected by the symmetries listed in equations (2-119) through (2-123). The dimension of the irreducible representation is the number of $\mathbf{k}$ vectors which are connected in this way. The $\mathbf{k}$ vectors lie on a circle about the origin, as indicated. The dimension of the representation, (N), and one $\mathbf{k}$ vector in the set, $(l\,\mathbf{k}_1+m\,\mathbf{k}_2)$, are indicated by N:(l, m).

2.7. Convection on a Square or Rhombic Lattice

In convection, the critical eigenspace is the set of rolls which have the critical wavenumber. The normal form is an ordinary differential equation for the time dependent complex amplitudes of these critical rolls. In the rhombic and square lattice, when $\mathbf{k}_1$ and $\mathbf{k}_2$ are chosen to have the critical wavenumber, the phase space for the normal form is $\mathbb{C}^2$, the ordered pairs of two complex numbers. For instance, with stress-free boundary conditions in Bénard convection, the critical eigenspace is

$$w(\mathbf{x},z,t) = 3\sin(z)\left[z_1 e^{i\mathbf{k}_1\cdot\mathbf{x}} + \bar{z}_1 e^{-i\mathbf{k}_1\cdot\mathbf{x}} + z_2 e^{i\mathbf{k}_2\cdot\mathbf{x}} + \bar{z}_2 e^{-i\mathbf{k}_2\cdot\mathbf{x}}\right] \tag{2-130}$$

$$\vartheta(\mathbf{x},z,t) = \sin(z)\left[z_1 e^{i\mathbf{k}_1\cdot\mathbf{x}} + \bar{z}_1 e^{-i\mathbf{k}_1\cdot\mathbf{x}} + z_2 e^{i\mathbf{k}_2\cdot\mathbf{x}} + \bar{z}_2 e^{-i\mathbf{k}_2\cdot\mathbf{x}}\right] \tag{2-131}$$

where $(z_1,z_2) \in \mathbb{C}^2$. The normal form is then an ODE for $z_1(t)$ and $z_2(t)$.

The translations and rotations act on the critical eigenspace as follows: The translations are

$$(z_1,z_2) \to (e^{i\mathbf{k}_1\cdot\mathbf{d}} z_1, e^{i\mathbf{k}_2\cdot\mathbf{d}} z_2). \tag{2-132}$$

The 180° rotation is

$$(z_1,z_2) \to (\bar{z}_1,\bar{z}_2). \tag{2-133}$$

The reflection which interchanges $\mathbf{k}_1$ and $\mathbf{k}_2$ is

$$(z_1,z_2) \to (z_2,z_1). \tag{2-134}$$

The transformations listed above are relevant to all lattices. The square lattice also has the reflection across the $\mathbf{k}_1$ direction;

$$(z_1,z_2) \to (z_1,\bar{z}_2). \tag{2-135}$$

The hexagonal lattice will be discussed separately in section 2.9.

Not all of the symmetries have been listed here. The full symmetry group is made up of all compositions of the transformations (2-132), (2-133), (2-134), and if applicable, (2-135). The normal form is equivariant with respect to these transformations. The equivariance condition is the same as equation (2-39),

$$\gamma \mathbf{f}(\mathbf{a}) = \mathbf{f}(\gamma \mathbf{a}) \text{ for all } \gamma \in \Gamma, \tag{2-136}$$

except the symbols are now complex;

$$\mathbf{a} = (z_1, z_2) \in \mathbb{C}^2, \ \mathbf{f}: \mathbb{C}^2 \to \mathbb{C}^2, \text{ and } \gamma: \mathbb{C}^2 \to \mathbb{C}^2. \tag{2-137}$$

The equivariance condition for the translations, written in components, is

$$e^{i\mathbf{k}_1\cdot\mathbf{d}} \dot{z}_1(z_1, z_2) = \dot{z}_1(e^{i\mathbf{k}_1\cdot\mathbf{d}} z_1, e^{i\mathbf{k}_2\cdot\mathbf{d}} z_2) \tag{2-138}$$

$$e^{i\mathbf{k}_2\cdot\mathbf{d}} \dot{z}_2(z_1, z_2) = \dot{z}_2(e^{i\mathbf{k}_1\cdot\mathbf{d}} z_1, e^{i\mathbf{k}_2\cdot\mathbf{d}} z_2) \tag{2-139}$$

Without any symmetry considerations, a general term in the Taylor expansion of $\dot{z}_1$ is

$$\dot{z}_1 \sim {z_1}^{n_1} {\bar{z}_1}^{m_1} {z_2}^{n_2} {\bar{z}_2}^{m_2}. \tag{2-140}$$

When applied to this general term, the equivariance under translations implies that

$$e^{i\mathbf{k}_1\cdot\mathbf{d}} {z_1}^{n_1} {\bar{z}_1}^{m_1} {z_2}^{n_2} {\bar{z}_2}^{m_2} = \left(e^{i\mathbf{k}_1\cdot\mathbf{d}} z_1\right)^{n_1} \left(e^{-i\mathbf{k}_1\cdot\mathbf{d}} \bar{z}_1\right)^{m_1} \left(e^{i\mathbf{k}_2\cdot\mathbf{d}} z_2\right)^{n_2} \left(e^{-i\mathbf{k}_2\cdot\mathbf{d}} \bar{z}_2\right)^{m_2}, \tag{2-141}$$

which reduces to

$$e^{i\mathbf{k}_1\cdot\mathbf{d}} = e^{i(\mathbf{k}_1\cdot\mathbf{d})(n_1 - m_1)} e^{i(\mathbf{k}_2\cdot\mathbf{d})(n_2 - m_2)}. \tag{2-142}$$

This must be true for *all* translations $\mathbf{d}$; therefore

$$n_1 = m_1 + 1, \text{ and } n_2 = m_2, \tag{2-143}$$

and $\dot{z}_1$ is of the form

$$\dot{z}_1 = z_1 g(|z_1|^2, |z_2|^2), \tag{2-144}$$

where g is an arbitrary function.

As a consequence of the translational symmetry, the nonlinear interaction of two rolls with wavenumbers $\mathbf{k}$ and $\mathbf{k}'$ couples to the roll with wavenumber $\mathbf{k}+\mathbf{k}'$. This property is called *mode coupling*. The sum of the $\mathbf{k}$ vectors corresponding to the amplitudes on the right hand side of (2-140) must equal the $\mathbf{k}$ vector of the amplitude on the left hand side. (Note that $-\mathbf{k}_1$ is the $\mathbf{k}$ vector corresponding to $\bar{z}_1$.) In other words, the product of amplitudes transforms, under translations, with an effective $\mathbf{k}$ which is the sum of the individual $\mathbf{k}$ vectors.

When $\mathbf{d}$ is chosen so that $\mathbf{k}_1\cdot\mathbf{d} = \mathbf{k}_2\cdot\mathbf{d} = 0$, the translational symmetry is

$$(z_1, z_2) \to -(z_1, z_2). \tag{2-145}$$

This is the same as the symmetry which is forced by the Boussinesq approximation. Therefore, *the normal form for the square and rhombic lattices is the same in the Boussinesq and non-Boussinesq cases.* The symmetry of the higher order modes on the center manifold is different in the two cases, however. In the non-Boussinesq case the walls of the square pattern are distinguished from the centers, and the upward flow favors one or the other. In the Boussinesq case there is a symmetry between upward and downward flow.

The complex conjugation symmetry (2-133) forces the function g in equation (2-144) to be real. This is because the equivariance condition (2-136) requires that

$$\overline{\dot{z}_1(z_1, z_2)} = \dot{z}_1(\bar{z}_1, \bar{z}_2). \tag{2-146}$$

Applied to (2-144) this gives

$$\overline{z_1 g(|z_1|^2, |z_2|^2)} = \bar{z}_1 g(|z_1|^2, |z_2|^2). \tag{2-147}$$

Therefore g is a real valued function of two variables;

$$g : \mathbb{R}^2 \to \mathbb{R}. \tag{2-148}$$

The interchange symmetry of z_1 and z_2 allows the equation for $\dot{z}_2$ to be inferred from the ODE for $\dot{z}_1$;

$$\dot{z}_2(z_1, z_2) = \dot{z}_1(z_2, z_1). \tag{2-149}$$

Therefore, for convection on a rhombic lattice, the most general equivariant vector field can be written

$$\begin{aligned} \dot{z}_1(z_1, z_2) &= z_1 g(|z_1|^2, |z_2|^2) \\ \dot{z}_2(z_1, z_2) &= z_2 g(|z_2|^2, |z_1|^2). \end{aligned} \tag{2-150}$$

where g is an arbitrary real valued function of two variables.

In the square lattice, the additional symmetry

$$(z_1, z_2) \to (z_1, \bar{z}_2) \tag{2-151}$$

does not change the most general equivariant ODE. The difference between the square and rhombic lattices is not apparent in the normal form.

Truncating this ODE at third order gives the candidate for a normal form:

$$\begin{aligned} \dot{z}_1 &= \lambda z_1 + a z_1 |z_2|^2 + b z_1 (|z_1|^2 + |z_2|^2) \\ \dot{z}_2 &= \lambda z_2 + a z_2 |z_1|^2 + b z_2 (|z_1|^2 + |z_2|^2). \end{aligned} \tag{2-152}$$

where a and b are real. The bifurcation parameter λ is proportional to $R - R_c$.

2.7.1. The analysis of the normal form

Note the similarity of (2-152) to the normal form for bifurcations with the symmetry of the square in the real plane (2-51). The only difference is that in (2-152) the amplitudes are complex, rather than real. It turns out that the complex nature of the normal form for convection on a square or rhombic lattice does not change the results significantly; in particular the third order truncation (2-152) is a normal form and the bifurcation diagrams of fig. 2-8 are applicable to the complex normal form.

It is useful to use the polar coordinates for the complex amplitudes. Let

$$z_\alpha = x_\alpha e^{i\varphi_\alpha}, \tag{2-153}$$

where $\alpha = 1$ *or* 2, and x_α is real and nonnegative.

Using the technique of equations (2-30) and (2-31), the general equivariant ODE (2-150) becomes

$$\begin{aligned} \dot{x}_1 &= x_1 g(x_1^2, x_2^2) \\ \dot{x}_2 &= x_2 g(x_2^2, x_1^2) \\ \dot{\varphi}_1 &= 0 \\ \dot{\varphi}_2 &= 0. \end{aligned} \tag{2-154}$$

The first two equations above are identical to the normal form considered in section 2.3. The phases do not introduce any significant complications. If the initial phases are $\tilde{\varphi}_1$ and $\tilde{\varphi}_2$, the displacement $\mathbf{x} \to \mathbf{x} + \tilde{\mathbf{d}}$ transforms the phases to

zero, where

$$\tilde{\mathbf{d}}\cdot\mathbf{k}_1 = -\tilde{\varphi}_1 \ , \ \text{and} \ \tilde{\mathbf{d}}\cdot\mathbf{k}_2 = -\tilde{\varphi}_2 . \tag{2-155}$$

This is possible because there are two independent translations. (In the hexagonal lattice, the amplitudes cannot always be made real, because there are three phases and two translations.) Therefore the phases are unimportant, and many of the results of section 2.3 are applicable to the complex normal form.

There is a difference between the two systems in the linear stability analysis, however, since a solution in the complex system must have four eigenvalues. The analysis of the complex normal form follows, concentrating on the physics of solutions and the differences between the real and complex normal forms.

The analysis is similar to the analysis of the real normal form. The stationary solution types are found by cross multiplying the two equations:

$$z_1\dot{z}_2 - z_2\dot{z}_1 = bz_1z_2(|z_1|^2 - |z_2|^2) \tag{2-156}$$

Assuming $b \neq 0$, the only solution types are;

$$\text{conduction} : \ A^2 \equiv |z_1|^2 + |z_2|^2 = 0 \tag{2-157}$$

$$\text{rolls} : \ z_1z_2 = 0 , \ A^2 \neq 0 \tag{2-158}$$

$$\text{squares (or rectangles)} : \ |z_1|^2 = |z_2|^2 \neq 0 \tag{2-159}$$

Fig. 2-12 shows the ***planform***, or view from above, of these patterns. The cold regions, where the temperature perturbation is negative, are white and the hot regions are shaded. This corresponds to the shadowgraph technique of visualization, where the cold fluid has a higher index of refraction and acts like a converging lens.

The equal amplitude ($|z_1|^2 = |z_2|^2$) solutions are called ***squares*** in the square lattice and ***rectangles*** in the rhombic lattice. Note that the fundamental region (one "tile" in the tiling of the plane) for double periodicity on the rhombic lattice can be a rectangle as well as a rhombus. In the discussion

below, both the squares and rectangles are referred to as squares for simplicity.

The sum of the squares of the amplitudes (often called *the amplitude* of a solution),

$$A^2 = |z_1|^2 + |z_2|^2, \tag{2-160}$$

has an important physical interpretation; it is proportional to the convective heat transport. The vertical heat flux through the layer is measured non-dimensionally by the Nusselt number Nu, which is normalized so that $Nu = 1$ is the contribution of heat conduction. The heat transported across the layer due to convection is the average over the layer of

$$\left(\frac{\partial \vartheta}{\partial z} w \right)_{av.} \propto Nu - 1 \propto A^2 + O(A^4), \tag{2-161}$$

where w is the vertical velocity.

The amplitude as a function of the Rayleigh number (λ) for the two non-trivial solutions is easily found:

$$\text{rolls}: \quad A^2 = \frac{-\lambda}{b} \tag{2-162}$$

$$\text{squares}: \quad A^2 = \frac{-\lambda}{\frac{1}{2}a + b} \tag{2-163}$$

Convection Planforms

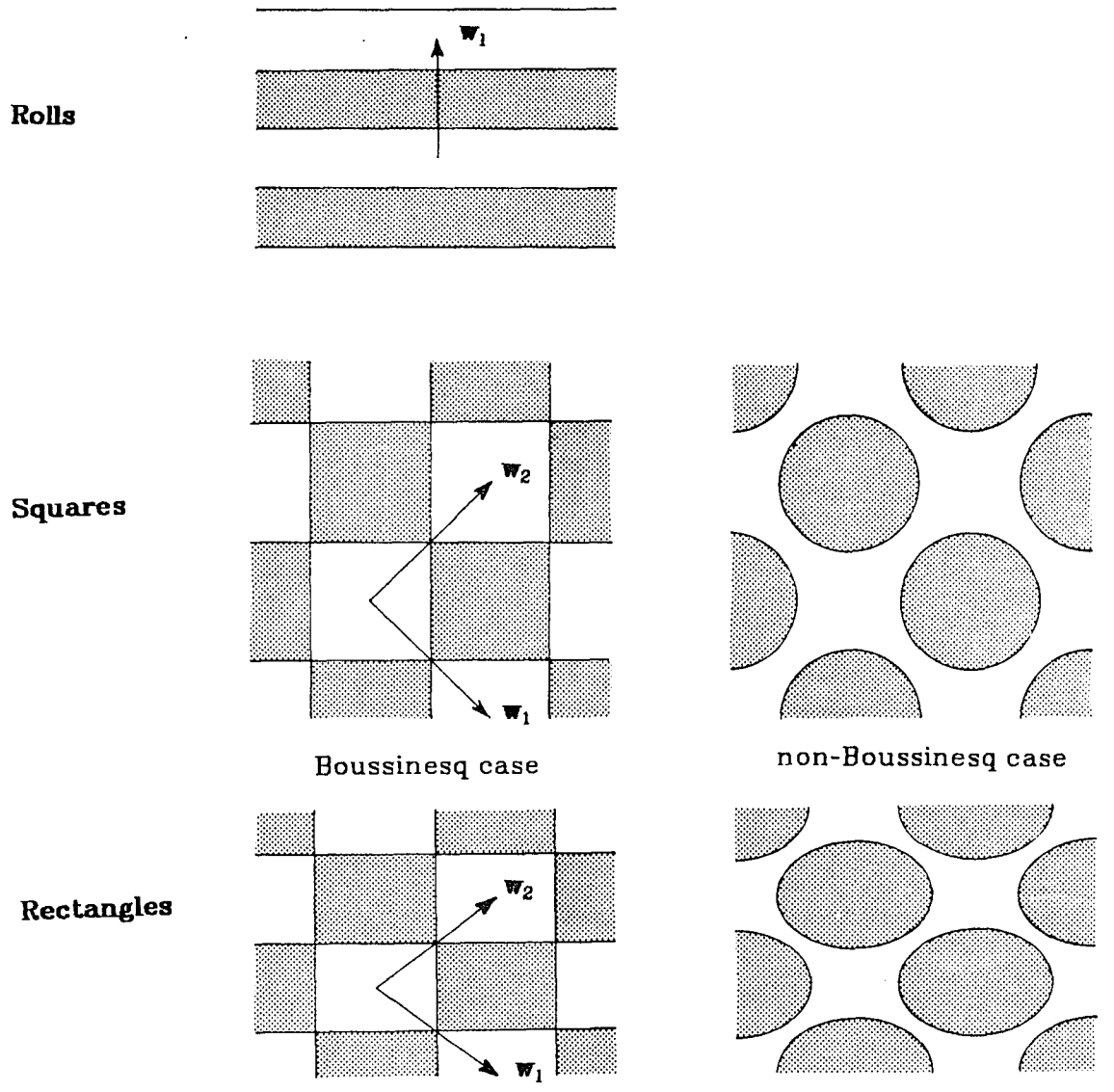

Fig. 2-12. Convection planforms with the double periodicity of the square or rhombic lattice. These figures schematically represent the convection planforms, as observed with the shadowgraph technique. Parallel light is shined through the fluid, in the $\hat{\mathbf{z}}$ direction, onto a screen. The cold regions act as a converging lens and are therefore brighter than the warm regions. The rolls are present on all the doubly periodic lattices. The squares and rectangles exist on the square and rhombic lattices, respectively. While the normal forms are the same for the Boussinesq and non-Boussinesq cases, the planforms differ as shown. In the non-Boussinesq case, second order modes with $\mathbf{k} = \mathbf{k}_1 \pm \mathbf{k}_2$, $n = 1$ are superposed with the critical modes ($\mathbf{k} = \mathbf{k}_1$ and $\mathbf{k} = \mathbf{k}_2$, $n = 1$). These second order modes with $n = 1$, which are forbidden by the Boussinesq symmetry, are responsible for the difference in the patterns.

The calculation of linear stability

The stability of the solutions is of paramount importance, since only the stable solutions are likely to be observed in the laboratory (unless the time scale of the instability is very long).

Because the continuous symmetry causes zero eigenvalues, the definition of structural stability in the presence of symmetry must be modified to say that all eigenvalues which are not forced to be zero by the symmetry should have a nonzero real part. Similarly, a stable solution has all negative eigenvalues, except those which are forced to be zero by the symmetry.

An explicit calculation of the eigenvalues follows. The purpose of this is to show that the stability can be calculated using the real system (2-45), (2-48), if the proper changes are made to take the symmetry into account.

The linear stability of a state (z_1,z_2) is the same as the linear stability of $\gamma(z_1,z_2)$, where γ is any element of the group of symmetries. All solutions can be put into a canonical form, where the amplitudes are real, and

$$|z_1| \geq |z_2| \geq 0. \tag{2-164}$$

Let an arbitrary perturbation of one of the steady states be

$$\begin{pmatrix} \delta z_1 \\ \delta \bar{z}_1 \\ \delta z_2 \\ \delta \bar{z}_2 \end{pmatrix} \tag{2-165}$$

The time evolution of the perturbation is given by

$$\frac{d}{dt}\begin{pmatrix} \delta z_1 \\ \delta \bar{z}_1 \\ \delta z_2 \\ \delta \bar{z}_2 \end{pmatrix} = \mathbf{J} \cdot \begin{pmatrix} \delta z_1 \\ \delta \bar{z}_1 \\ \delta z_2 \\ \delta \bar{z}_2 \end{pmatrix} \tag{2-166}$$

where

$$\mathbf{J} \equiv \mathbf{Df} = \begin{pmatrix} \frac{\partial \dot{z}_1}{\partial z_1} & \frac{\partial \dot{z}_1}{\partial \bar{z}_1} & \frac{\partial \dot{z}_1}{\partial z_2} & \frac{\partial \dot{z}_1}{\partial \bar{z}_2} \\ \frac{\partial \dot{\bar{z}}_1}{\partial z_1} & \frac{\partial \dot{\bar{z}}_1}{\partial \bar{z}_1} & \frac{\partial \dot{\bar{z}}_1}{\partial z_2} & \frac{\partial \dot{\bar{z}}_1}{\partial \bar{z}_2} \\ \frac{\partial \dot{z}_2}{\partial z_1} & \frac{\partial \dot{z}_2}{\partial \bar{z}_1} & \frac{\partial \dot{z}_2}{\partial z_2} & \frac{\partial \dot{z}_2}{\partial \bar{z}_2} \\ \frac{\partial \dot{\bar{z}}_2}{\partial z_1} & \frac{\partial \dot{\bar{z}}_2}{\partial \bar{z}_1} & \frac{\partial \dot{\bar{z}}_2}{\partial z_2} & \frac{\partial \dot{\bar{z}}_2}{\partial \bar{z}_2} \end{pmatrix}. \tag{2-167}$$

The first row of this Jacobian matrix contains all of the information, since the other rows can be obtained by the symmetries. However, it is simplest in this case to compute the matrix explicitly, rather than use the isotropy subgroups of the solutions, as was done in section 2.3.1. The Jacobian matrix is

$$\mathbf{J} = \begin{pmatrix} \begin{matrix}\lambda+2b|z_1|^2 \\ +(a+b)|z_2|^2\end{matrix} & bz_1^2 & (a+b)z_1\bar{z}_2 & (a+b)z_1z_2 \\ b\bar{z}_1^2 & \begin{matrix}\lambda+2b|z_1|^2 \\ +(a+b)|z_2|^2\end{matrix} & (a+b)\bar{z}_1\bar{z}_2 & (a+b)\bar{z}_1z_2 \\ (a+b)\bar{z}_1z_2 & (a+b)z_1z_2 & \begin{matrix}\lambda+2b|z_2|^2 \\ +(a+b)|z_1|^2\end{matrix} & bz_2^2 \\ (a+b)\bar{z}_1\bar{z}_2 & (a+b)z_1\bar{z}_2 & b\bar{z}_2^2 & \begin{matrix}\lambda+2b|z_2|^2 \\ +(a+b)|z_1|^2\end{matrix} \end{pmatrix}. \tag{2-168}$$

The Jacobian matrix must be evaluated at the solutions to determine their linear stability.

At the conduction solution ($z_1 = z_2 = 0$), the Jacobian matrix is

$$\mathbf{J}_C = \begin{pmatrix} \lambda & 0 & 0 & 0 \\ 0 & \lambda & 0 & 0 \\ 0 & 0 & \lambda & 0 \\ 0 & 0 & 0 & \lambda \end{pmatrix}, \tag{2-169}$$

and all four eigenvalues are λ.

The roll solution, in canonical form (2-164), is

$$(z_1 = \sqrt{A^2},\ z_2 = 0). \tag{2-170}$$

The Jacobian matrix for this roll solution is

$$J_R = A^2 \begin{bmatrix} b & b & 0 & 0 \\ b & b & 0 & 0 \\ 0 & 0 & a & 0 \\ 0 & 0 & 0 & a \end{bmatrix}. \tag{2-171}$$

The eigenvectors of this matrix are

$$\begin{bmatrix} 1 \\ 1 \\ 0 \\ 0 \end{bmatrix}, \begin{bmatrix} 0 \\ 0 \\ 1 \\ 0 \end{bmatrix}, \begin{bmatrix} 0 \\ 0 \\ 0 \\ 1 \end{bmatrix}, \text{ and } \begin{bmatrix} 1 \\ -1 \\ 0 \\ 0 \end{bmatrix}, \tag{2-172}$$

which give the eigenvalues $2bA^2$, aA^2, aA^2, and 0 respectively.

The last eigenvector corresponds to a translation of the whole pattern in the $\mathbf{k}_1$ direction (or equivalently, a φ_1 phase shift). When the amplitudes have general phase, the infinitesimal phase shift is

$$\frac{d}{d\varphi_1} \begin{bmatrix} z_1 \\ \bar{z}_1 \\ z_2 \\ \bar{z}_2 \end{bmatrix} \Bigg|_{z_2=0} = \begin{bmatrix} iz_1 \\ -i\bar{z}_1 \\ 0 \\ 0 \end{bmatrix}. \tag{2-173}$$

This is proportional to the null eigenvector listed above when z_1 is real.

It is easy to see why the translational symmetry forces the zero eigenvalue. If a stationary solution is perturbed in a way that corresponds to a translation, the new state is also a stationary solution. Therefore the perturbation will neither grow nor decay, and the eigenvalue corresponding to this perturbation is zero.

When the solution is unchanged by the translation, then there is a double eigenvalue rather than a zero eigenvalue. For instance the rolls (with $z_1 \neq 0$) are invariant under the translation in the $\mathbf{k}_2$ direction. The two linearly independent perturbations of z_2 and $\bar{z}_2$, or equivalently $\mathrm{Re}(z_2)$ and $\mathrm{Im}(z_2)$, each have the same eigenvalue.

The Jacobian matrix evaluated at the square solution, when the amplitudes are chosen to be real, is

$$\mathbf{J}_S = \frac{A^2}{2}\begin{bmatrix} b & b & (a+b) & (a+b) \\ b & b & (a+b) & (a+b) \\ (a+b) & (a+b) & b & b \\ (a+b) & (a+b) & b & b \end{bmatrix}. \tag{2-174}$$

The eigenvectors are

$$\begin{bmatrix} 1 \\ 1 \\ 1 \\ 1 \end{bmatrix}, \begin{bmatrix} 1 \\ 1 \\ -1 \\ -1 \end{bmatrix}, \begin{bmatrix} 0 \\ 0 \\ 1 \\ -1 \end{bmatrix}, \text{ and } \begin{bmatrix} 1 \\ -1 \\ 0 \\ 0 \end{bmatrix}. \tag{2-175}$$

These correspond to the eigenvalues $(a+2b)A^2$, aA^2, 0, and 0 respectively. The two zero eigenvectors are required because both translations change the square solution.

This completes the analysis of the non-degenerate normal form for the square and rhombic lattices. The following table summarizes the results.

name	definition	amplitude	eigenvalues
conduction	$z_1 = z_2 = 0$	$A^2 = 0$	$\lambda, \lambda, \lambda, \lambda$
rolls	$z_1 z_2 = 0,\ A^2 \neq 0$	$A^2 = \frac{-\lambda}{b}$	$2bA^2, aA^2, aA^2, 0$
squares	$\lvert z_1 \rvert^2 = \lvert z_2 \rvert^2 \neq 0$	$A^2 = \frac{-\lambda}{\frac{1}{2}a+b}$	$(a+2b)A^2, -aA^2, 0, 0$

Table 2-2. Solution data for equation (2-152). Note the similarity to table 2-1.

This table is the same as the table for bifurcation on the real plane with $\mathbf{D}_4$ symmetry. The additional eigenvalues in the complex system have no effect on the stability of the solutions. Therefore, convection on the square or rhombic lattice is equivalent to convection with the symmetry of the square in $\mathbb{R}^2$. The phase portraits and bifurcation diagrams have already been drawn for the equivalent real system so they are not repeated here.

The analysis of degenerate bifurcations in convection on the square or rhombic lattice that follows will therefore be done using the equivalent real

system. When the results are applied to the convection, multiple or zero eigenvalues are added on according to the symmetry of the solution. In the notation of section 2.3.1, the eigenvalues are:

$$\text{conduction}: \ \lambda, \lambda, \lambda, \lambda \tag{2-176}$$

$$\text{rolls}: \ \alpha, \beta, \beta, 0 \tag{2-177}$$

$$\text{squares}: \ \mu+\nu, \mu-\nu, 0, 0 \tag{2-178}$$

If there is a solution with $|z_1|^2 > |z_2|^2 > 0$, then it has two zero eigenvalues in addition to the eigenvalues of the two by two Jacobian.

2.8. Degenerate Bifurcations with D_4 Symmetry

The technique used in this dissertation, local bifurcation theory, has the disadvantage that the large amplitude behavior of the solutions cannot be studied. One alternative is to use computers to study the stability of the large amplitude solutions. Without resorting to numerical methods, the study of *degenerate bifurcations* allows the analysis of finite amplitude bifurcations using local methods. Technically, the bifurcations are at small amplitude, although the results are often qualitatively good at quite large amplitude.

In a degenerate bifurcation analysis, the parameters of the system are chosen so that two (or more) elementary bifurcations coalesce. The system, at this special setting of the parameters, is called the *organizing center*. An *unfolding* is the system obtained when the parameters are varied in a neighborhood of the organizing center. The *codimension* of a bifurcation is the number of different *unfolding parameters* needed to yield a structurally stable family of vector fields. The bifurcation parameter λ is an example of an unfolding parameter. Nondegenerate bifurcations have codimension-one; degenerate bifurcations have larger codimension.

There are two classes of degenerate bifurcations: first, the number of critical modes can be larger than one, and second, there can be degeneracies in the

higher order terms.

In the presence of symmetry, more than one mode are often forced to go unstable simultaneously. In convection, for example, all rolls with the critical wavenumber are unstable at the critical Rayleigh number. This is a degenerate bifurcation when the problem is considered in the context of vector fields without the symmetry. In this dissertation, however, the translational symmetry is always assumed to be valid. In this context, the bifurcations considered so far are nondegenerate.

The degenerate bifurcations considered in this section are the result of degeneracies in the cubic terms in the normal form (2-51) for bifurcations with $\mathbf{D}_4$ symmetry (the symmetry of the square). The results are directly applicable to convection on a square or rhombic lattice.

Recall that for this problem the normal is

$$\dot{x}_1 = x_1(\lambda + a x_2^2 + b A^2), \tag{2-179}$$

provided the following nondegeneracy conditions hold:

$$a \neq 0, \quad b \neq 0, \quad \text{and } a+2b \neq 0. \tag{2-180}$$

(see section 2.3.1.) When these conditions hold, the truncation of the normal form at third order is justified. This normal form describes a codimension-one bifurcation, defined by the condition:

$$\lambda = 0. \tag{2-181}$$

This section describes the behavior of the system in the neighborhood of the three degenerate cases. These are codimension-two bifurcations, and are defined by the conditions:

$$\lambda = 0, \quad b = 0 \tag{2-182}$$

in the first case,

$$\lambda = 0, \quad a+2b = 0 \tag{2-183}$$

in the second case, and

$$\lambda = 0, \quad a = 0 \tag{2-184}$$

in the final case. The bifurcations will be discussed in the order listed above.

When one of the nondegeneracy conditions does not hold, enough higher order terms must be added to the ODE to make it structurally stable. Then the offending terms, which caused the normal form to be degenerate in the first place, are reintroduced as unfolding parameters. This allows the local analysis to include secondary bifurcations of the solutions which bifurcated from the origin.

The fifth order terms are written here in two equivalent ways; this is done for convenience in the analysis. In the neighborhood of the first two degenerate bifurcations, (2-182) and (2-183), the following fifth order truncation is used:

$$\dot{x}_1 = x_1(\lambda + a{x_2}^2 + bA^2 + C{x_1}^2{x_2}^2 + D{x_1}^4 + E{x_2}^4). \tag{2-185}$$

For the $a \approx 0$ case the following is used:

$$\dot{x}_1 = x_1(\lambda + a{x_2}^2 + bA^2 + cA^4 + d{x_1}^4 + e{x_2}^4). \tag{2-186}$$

The relationship between the two versions of the quintic coefficients is

$$\begin{Bmatrix} C = 2c \\ D = d + c \\ E = e + c \end{Bmatrix}, \text{ or } \begin{Bmatrix} c = \frac{1}{2}C \\ d = D - \frac{1}{2}C \\ e = E - \frac{1}{2}C \end{Bmatrix}. \tag{2-187}$$

2.8.1. The case where $b \approx 0$

The degenerate bifurcation where $b = 0$ is the simplest of the three cases (2-182), (2-183), and (2-184). Note, from table 2-1, that $A^2 = -\lambda / b$ for the roll solutions, and that one of the eigenvalues is $2bA^2$. These results are not valid when $b = 0$, because the higher order terms which have been neglected become important. Although these results are valid for *any* nonzero b, the range of validity of the local analysis is $|\lambda| < O(b^2)$, which becomes very small when b is

small.

One approach to degenerate bifurcations, described in Guckenheimer & Holmes (1983), considers both λ and b to be unfolding parameters in the neighborhood of (2-182). The λ-b plane is divided into regions by curves of codimension-one bifurcations which meet at the codimension-two bifurcation at $\lambda = b = 0$. Within each of these regions, the qualitative nature of the system is unchanged as the unfolding parameters are varied. The phase portraits are drawn for each of the regions.

Another point of view, to be found in Golubitsky & Schaeffer (1984), treats λ as a *distinguished bifurcation parameter*, and b as the true unfolding parameter. Here the bifurcation diagrams, which plot the solutions as a function of λ are drawn for various values of the fixed unfolding parameter.

The approach used in this section follows Golubitsky & Schaeffer (1984). The first step is to set $b = 0$, and include enough higher order terms to make the λ-dependent family of vector fields structurally stable. Then, b is included as an unfolding parameter. The bifurcation diagrams for fixed (small) b are then drawn. These diagrams show a secondary saddle-node bifurcation of the rolls which occurs at finite amplitude.

When $b = 0$, the roll solutions grow without bound for $\lambda = 0^+$ in the third order truncation. The only fifth order term needed to break this degeneracy is $\dot{x}_1 = Dx_1^5$. The ODE is then

$$\dot{x}_1 = x_1\left[\lambda + ax_2^2 + Dx_1^4 + O(x_1^2x_2^2, x_2^4, x_2^6)\right] \qquad (2\text{-}188)$$

The other fifth order terms, $\dot{x}_1 \propto x_1x_1^2x_2^2$ and $x_1x_2^4$, do not change the amplitude vs. Rayleigh number, or the stability, of the rolls.

The equations for the amplitudes of the steady solutions are simple to derive. The results are in the table below.

The calculation of the stability involves the Jacobian matrix, which is

$$\mathbf{J}=\begin{bmatrix}\lambda+ax_2^2+5Dx_1^4 & 2ax_1x_2\\ 2ax_1x_2 & \lambda+ax_1^2+5Dx_2^4\end{bmatrix}. \tag{2-189}$$

When evaluated at the rolls, the Jacobian matrix is

$$\mathbf{J}_R=\begin{bmatrix}4DA^4 & 0\\ 0 & aA^2+O(A^4)\end{bmatrix}. \tag{2-190}$$

The radial eigenvalue,

$$\left.\frac{\partial \dot{x}_1}{\partial x_1}\right|_R = 4DA^4, \tag{2-191}$$

is negative when the rolls are supercritical, and positive when the rolls are subcritical. This is to be expected.

The Jacobian matrix for the squares is

$$\mathbf{J}_S=\begin{bmatrix}O(A^4) & aA^2\\ aA^2 & O(A^4)\end{bmatrix}. \tag{2-192}$$

The eigenvalues of these matrices, and other bifurcation data, are listed in the table below.

name	definition	amplitude	eigenvalues
rolls	$x_1x_2=0,\ A^2\neq 0$	$A^4=\frac{-\lambda}{D}$	$4DA^4,\ aA^2$
squares	$x_1^2=x_2^2\neq 0$	$A^2=\frac{-2\lambda}{a}$	$aA^2,\ -aA^2$

Table 2-3. Solution data for equation (2-188). Only the leading order in A^2 is shown. The conduction solution is not included because the definition and stability properties are unchanged from table 2-1.

The unfolding

When a nonzero b is added to (2-188), the resulting unfolding is

$$\dot{x}_1=x_1(\lambda+ax_2^2+bA^2+Dx_1^4)+\cdots, \tag{2-193}$$

where b is the unfolding parameter. (As mentioned before, λ can also be

considered an unfolding parameter.)

The equation for the rolls is

$$\lambda + b x_1^2 + D x_1^4 = 0, \tag{2-194}$$

which has the solution

$$A^2 = \frac{-b \pm \sqrt{b^2 - 4\lambda D}}{2D}, \tag{2-195}$$

where A^2 must be positive. If $-b/(2D)$ is positive, then the roll solution branch undergoes a saddle-node bifurcation as it "turns over" at

$$\lambda_{sn} = \frac{b^2}{4D}. \tag{2-196}$$

In contrast to the rolls, the amplitude of the squares is not changed significantly when b is added (see table 2-1).

For the most part, the stability results of table 2-1 are valid when b is small. The only eigenvalue which is modified significantly is the radial eigenvalue of the rolls, which is

$$\frac{\partial \dot{x}_1}{\partial x_1} = \lambda + a x_2^2 + 3 b x_1^2 + 5 D x_1^4. \tag{2-197}$$

When evaluated at the rolls, this is

$$2bA^2 + 4DA^4 = 4DA^2\left(\frac{b}{2D} + A^2\right). \tag{2-198}$$

The eigenvalue changes sign precisely where the branch turns over, and the eigenvalue has the same sign as D at the larger amplitude. This is a secondary saddle-node bifurcation.

The results are listed in the following table:

name	definition	amplitude	eigenvalues
rolls	$x_1 x_2 = 0,\ A^2 \neq 0$	$A^2 = \frac{-b \pm \sqrt{b^2 - 4\lambda D}}{2D}$	$4DA^2\left(\frac{b}{2D} + A^2\right),\ aA^2$
squares	$x_1^2 = x_2^2 \neq 0$	$A^2 = \frac{-2\lambda}{a}$	$aA^2,\ -aA^2$

Table 2-4: Bifurcation data for equation (2-193).

The bifurcation diagrams, for fixed b, are drawn in fig. 2-13 for the case where $a < 0$. This degenerate bifurcation can also be described by two unfolding parameters, as in fig. 2-14.

If b is not small the branch will turn over at such a large amplitude that the fifth order truncation is non-rigorous. The analysis can predict qualitatively incorrect results when b is not small; the seventh order terms become important, and modes which have been neglected become important at large amplitude. However, one often knows from the physics that trajectories of the system cannot go to infinity. This is true in convection, where the energy is bounded (Joseph 1976). If the third order analysis predicts a subcritical bifurcation in these cases, one can argue that the branch must "turn over" at some larger amplitude. However, this branch might not be stable as shown in fig. 2-13.

$$\dot{x}_1 = x_1(\lambda + ax_2^2 + bA^2 + Dx_1|x_1|^4)$$

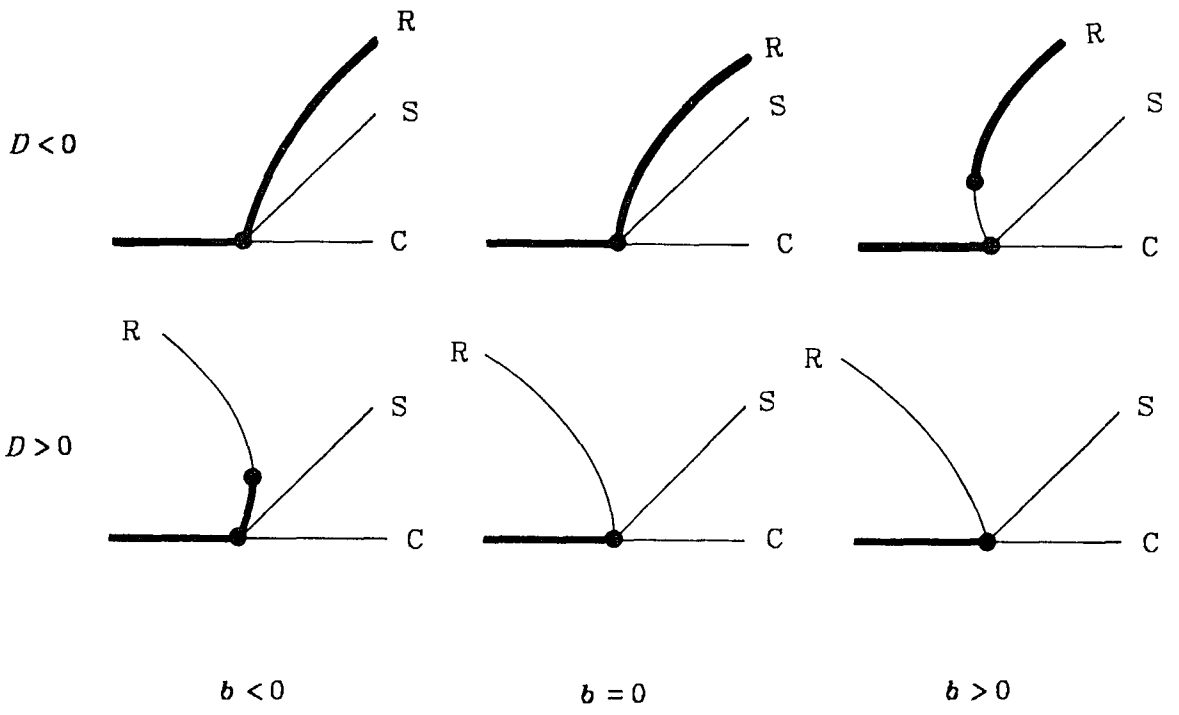

Fig. 2-13. The organizing center ($b = 0$) and the unfolding ($b \neq 0$, but small) in the two cases where $a < 0$: $D < 0$ (upper row), and $D > 0$ (lower row). These cases are chosen because there are no stable solutions predicted by the local analysis when $a > 0$.

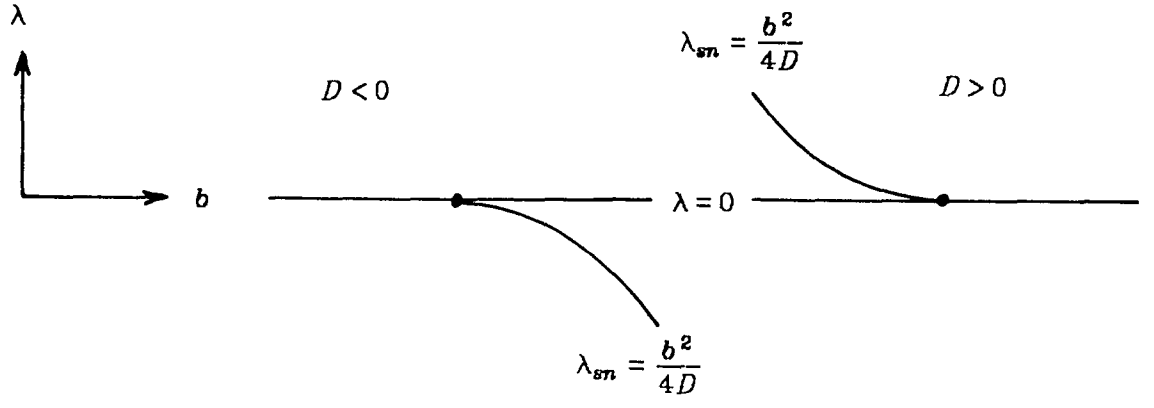

Fig. 2-14. The 2 parameter (λ, b) unfolding space of the codimension-two bifurcation at $\lambda = b = 0$. The ODE is structurally stable in the open regions. The dividing lines are codimension-one bifurcations, which coalesce at $\lambda = b = 0$ in a codimension-two bifurcation. There is a saddle-node bifurcation at λ_{sn}; at $\lambda = 0$ there is the nondegenerate bifurcation ($b \neq 0$) described in the previous section.

2.8.2. The case where $a+2b \approx 0$

This case is almost identical to the degenerate bifurcation near $b=0$. The difference is that, when $a+2b=0$, the squares rather than the rolls bifurcate vertically. The analysis is entirely analogous to the previous case, so only the results are given, by way of table 2-5. For compactness, the unfolding parameter is defined as

$$\varepsilon \equiv \tfrac{1}{2}a+b\,. \tag{2-199}$$

name	definition	amplitude	eigenvalues
rolls	$x_1x_2=0,\ A^2\neq 0$	$A^2=\dfrac{-\lambda}{b}$	$2bA^2,\ aA^2$
squares	$x_1^2=x_2^2\neq 0$	$A^2=\dfrac{-\varepsilon\pm\sqrt{\varepsilon^2-\lambda(C+D+E)}}{\frac{1}{2}(C+D+E)}$	$2\varepsilon A^2+(C+D+E)A^4,$ $-aA^2$

Table 2-5. Solution data for equation (2-185) in the neighborhood of $\varepsilon=\frac{1}{2}a+b=0$. The conduction solution is unchanged from table 2-1.

The bifurcation diagrams near $a+2b=0$ are identical to those in the neighborhood of $b=0$ (fig. 2-13), where D is replaced by $C+D+E$, b is replaced by ε, and the rolls and squares are interchanged.

2.8.3. The case where $a \approx 0$

Recall that when $a=0$ the third order ODE has a whole circle of solutions. All of the fifth order terms have an effect here. The degenerate fifth order normal form is

$$\dot{x}_1 = x_1(\lambda+bA^2+cA^4+dx_1^4+ex_2^4)\,; \tag{2-200}$$

and the unfolding is

$$\dot{x}_1 = x_1(\lambda+ax_2^2+bA^2+cA^4+dx_1^4+ex_2^4)\,, \tag{2-201}$$

where a and λ are both small.

In this section, the two unfolding parameters, λ and a, are treated equally; therefore the system with both parameters (2-201) is analyzed from the start.

The behavior of (2-200) is obtained in the limit of $a \to 0$.

The roll solutions have an amplitude given by

$$0 = \lambda + bA^2 + (c+d)A^4, \tag{2-202}$$

and the squares satisfy

$$0 = \lambda + (\tfrac{1}{2}a + b)A^2 + cA^4 + \frac{(d+e)}{4}A^4. \tag{2-203}$$

Since $b \neq 0$, both of these solutions approximately satisfy

$$A^2 = \frac{-\lambda}{b} + O(A^4, aA^2), \tag{2-204}$$

and the solution branch does not turn over. (In other words, A^2 is monotonic in λ.)

When $a \neq 0$, a new stationary solution is possible. To see this, use the same procedure which showed before that no small amplitude solutions are possible when $a = O(1)$. A stationary solution satisfies

$$\begin{aligned} 0 = x_2\dot{x}_1 - x_1\dot{x}_2 &= x_1x_2\left[a(x_2^2 - x_1^2) + (d-e)(x_1^4 - x_2^4)\right] \\ &= x_1x_2(x_1^2 - x_2^2)\left[-a + (d-e)(x_1^2 + x_2^2)\right]. \end{aligned} \tag{2-205}$$

Thus, there are solutions with $x_1^2 \neq x_2^2$ and $x_1x_2 \neq 0$. These new solutions satisfy

$$A^2 = \frac{a}{d-e}, \tag{2-206}$$

and they only exist if A^2 is positive. The amplitude is independent of λ, but the solutions only exist in a small λ interval, near $\lambda = -A^2b$.

These new solutions are called *general solutions*, since they have no symmetry. The amplitude of the general solutions can be inserted into equation (2-202) for A^2 vs. λ of the rolls, and (2-204) for the squares, to find the limits of the λ interval in which the general solutions exist. The general solutions intersect the rolls at

$$\lambda_R = -a\frac{b}{(d-e)} - a^2\frac{(c+d)}{(d-e)^2}. \tag{2-207}$$

The general solutions intersect the squares at

$$\begin{aligned}\lambda_S &= -\frac{a}{(d-e)}\left(\tfrac{1}{2}a+b\right)-\left(\frac{(d+e)}{4}+c\right)\frac{a^2}{(d-e)^2} \\ &= -a\frac{b}{(d-e)}-a^2\frac{\left[4(c+d)-(d+e)\right]}{4(d-e)^2}.\end{aligned} \tag{2-208}$$

The difference in the two λ values is

$$\lambda_S-\lambda_R=\frac{a^2}{4}\frac{(d+e)}{(d-e)^2}. \tag{2-209}$$

The equations for λ_S and λ_R define two curves in the a-λ plane. These two curves are quadratically tangent at the origin; the general solutions exist in the horn-shaped region between the curves.

Now the stability of the various solutions is computed. The Jacobian matrix is

$$\begin{bmatrix} \lambda+(a+b)x_2^2+bx_1^2+cA^4+dx_1^4+ex_2^4 \\ \quad +2x_1^2(b+2cA^2+2dx_1^2) & 2x_1x_2(a+b+2cA^2+2ex_1^2) \\ 2x_1x_2(a+b+2cA^2+2ex_2^2) & \lambda+(a+b)x_1^2+bx_2^2+cA^4+dx_2^4+ex_1^4 \\ & \quad +2x_2^2(b+2cA^2+2dx_2^2) \end{bmatrix}. \tag{2-210}$$

Evaluated at the rolls, the Jacobian matrix is

$$\mathbf{J}_R=\begin{bmatrix} 2A^2\left[b+2(c+d)A^2\right] & 0 \\ 0 & A^2\left[a-(d-e)A^2\right] \end{bmatrix}. \tag{2-211}$$

The eigenvalues of the rolls are therefore

$$2bA^2+O(A^2),\ \text{and}\ A^2\left[a-(d-e)A^2\right]. \tag{2-212}$$

Evaluated at the squares,

$$\mathbf{J}_S=\begin{bmatrix} A^2(b+2cA^2+dA^2) & A^2(a+b+2cA^2+eA^2) \\ A^2(a+b+2cA^2+eA^2) & A^2(b+2cA^2+dA^2) \end{bmatrix}. \tag{2-213}$$

The eigenvalues of the squares are therefore

$$2bA^2+O(aA^2,A^4),\ \text{and}\ A^2\left[(d-e)A^2-a\right]. \tag{2-214}$$

The eigenvalues (2-12) and (2-14) are listed so that the first is the radial eigenvalue and the second is the tangential eigenvalue. Observe that the tangential eigenvalues of the rolls and squares are equal and opposite, and that they

change sign when (and if)

$$A^2 = \frac{a}{d-e} > 0. \tag{2-215}$$

This is at precisely the amplitude of the general solutions. The stability of the rolls (and squares) changes when they undergo a secondary pitchfork bifurcation, which creates or annihilates a branch of general solutions. The two pitchfork bifurcations effectively transfer the stability between the rolls and squares.

The next step is to find the stability of the general solutions. The Jacobian matrix, evaluated at the general solutions, is

$$\mathbf{J_G} = \begin{bmatrix} 2x_1^2(b+2cA^2+2dx_1^2) & x_1x_2\left[2(a+b)+4cA^2+4ex_1^2\right] \\ x_1x_2\left[2(a+b)+4cA^2+4ex_2^2\right] & 2x_2^2(b+2cA^2+2dx_2^2) \end{bmatrix}. \tag{2-216}$$

The exact eigenvalues of this matrix are not easily found, except in terms of messy square roots which are difficult to interpret. Fortunately, the eigenvalues can be calculated by a perturbative technique because the radial eigenvalue is much larger than the tangential one. This relationship of the eigenvalues implies that

$$|\operatorname{Det}\mathbf{J_G}| \ll (\operatorname{Tr}\mathbf{J_G})^2. \tag{2-217}$$

Thus, the eigenvalues of the two by two matrix (2-216) are

$$\begin{aligned} &\operatorname{Tr}\mathbf{J_G} + O\left(\frac{\operatorname{Det}\mathbf{J_G}}{\operatorname{Tr}\mathbf{J_G}}\right), \text{ and} \\ &\frac{\operatorname{Det}\mathbf{J_G}}{\operatorname{Tr}\mathbf{J_G}} + O\left(\frac{(\operatorname{Det}\mathbf{J_G})^2}{(\operatorname{Tr}\mathbf{J_G})^3}\right). \end{aligned} \tag{2-218}$$

The trace of $\mathbf{J_G}$ is

$$\operatorname{Tr}\mathbf{J_G} = 2bA^2+4cA^4+4d(x_1^4+x_2^4) = 2bA^2+O(A^4). \tag{2-219}$$

The calculation of the determinant is somewhat more involved. When a is eliminated in favor of $(d-e)A^2$, the determinant of $\mathbf{J_G}$ is

$$\text{Det}\, J_G = 4(e-d)(e+d)x_1^2x_2^2(x_1^2-x_2^2)^2. \tag{2-220}$$

The inequality (2-217) can now be verified explicitly. From equation (2-218), the eigenvalues of J_G are

$$\begin{gathered} 2bA^2+O(A^4), \text{ and} \\ \frac{-2(d-e)(d+e)}{b}\frac{x_1^2x_2^2(x_1^2-x_2^2)^2}{A^2}+O(A^8). \end{gathered} \tag{2-221}$$

Note that the tangential eigenvalue of the general solutions does not change sign as a and λ are varied. Information on the solutions is summarized here.

name	definition	amplitude	signs of eigenvalues
rolls	$x_1x_2=0,\ A^2\neq 0$	$A^2=\frac{-\lambda+O(\lambda^2)}{b}$	$b,\ a-(d-e)A^2$
squares	$x_1^2=x_2^2\neq 0$	$A^2=\frac{-\lambda+O(\lambda^2)}{\left(\frac{1}{2}a+b\right)}$	$b,\ -a+(d-e)A^2$
general	$0\neq x_1^2\neq x_2^2\neq 0$	$A^2=\frac{a}{d-e}$	$b,\ \frac{(d-e)(d+e)}{-b}$

Table 2-6. Solution data for equation (2-201).

This completes the calculations needed to draw the phase portraits in the various regions of the a-λ plane. The plane is divided into regions by the three curves:

$$\lambda=0,\ \lambda=\lambda_R, \text{ and } \lambda=\lambda_S, \tag{2-222}$$

where the curves λ_R and λ_S are given in equations (2-207) and (2-208). These two curves define the horn shaped region where the general solutions exist; this region extends into only one quadrant of the λ-a plane because of the restriction

$$A^2\approx\frac{-\lambda}{b}>0, \tag{2-223}$$

which implies that

$$\text{sgn}(\lambda)=-\text{sgn}(b). \tag{2-224}$$

Fig. 2-15 shows the a-λ plane for certain cases of the other relevant

parameters:

$$b\,,\ (d-e)\,,\ \text{and}\ (d+e)\,. \tag{2-225}$$

When any of these combinations of parameters is zero, the system is degenerate, and yet higher order terms are needed. The coefficient c is not important here because it contributes the same curvature to the λ_S and λ_R curves. Fig. 2-16 shows the phase portraits in the x_1-x_2 plane.

Fig. 2-15, with $(d+e)<0$, is similar to the results of Frick & Busse (1983) for convection in a highly non-Boussinesq fluid. The ratio of the viscosity at the top and bottom boundaries measures how non-Boussinesq the system is. They find that the preferred solution changes from rolls to squares as the viscosity ratio exceeds a critical value. In other words, $a=0$ at the critical viscosity ratio. Near this critical value, the departure from the critical viscosity ratio is proportional to a, and the Rayleigh number is proportional to λ. Frick & Busse find that rolls and squares are both stable in a wedge shaped region, as in fig. 2-15 with $(d+e)<0$.

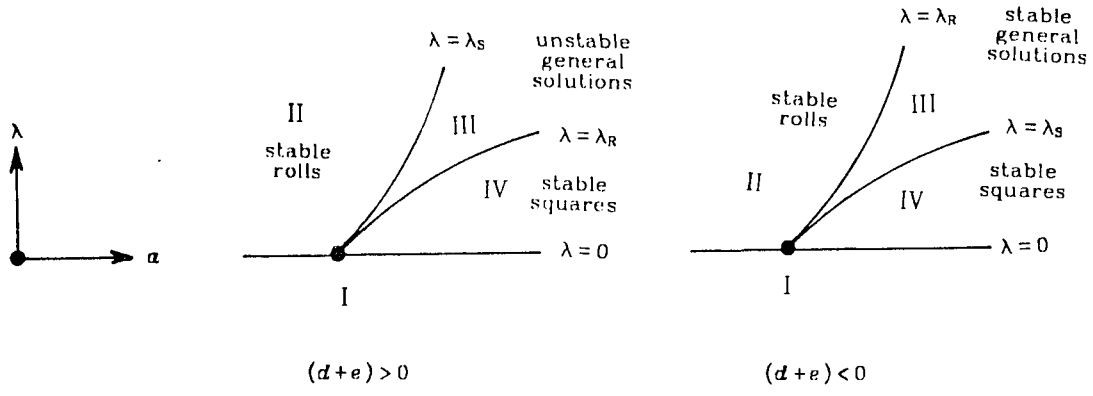

Fig. 2-15. The division of the a-λ plane for equation (2-200), with the parameters b, c, d, and e fixed: $b < 0$ and $(d-e) < 0$. In the left figure, $(d+e) > 0$, and the general solutions are unstable in the horn-shaped region. In the right figure, $(d+e) < 0$, and the general solutions are stable. The parameter c has no qualitative effect on the phase portraits. The general solutions only exist inside the horn-shaped region. The rolls and squares undergo a pitchfork bifurcation, creating a branch of general solutions, at $\lambda = \lambda_R$ and $\lambda = \lambda_S$, respectively.

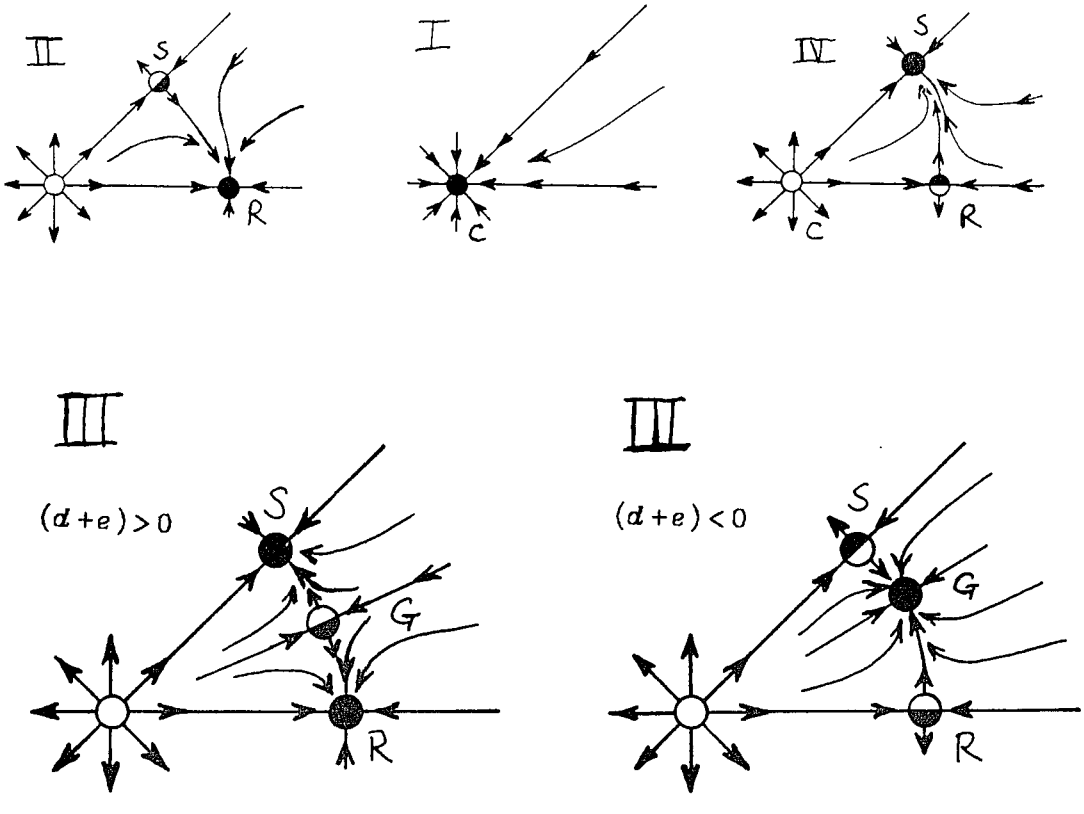

Fig. 2-16. The phase portraits in the x_1-x_2 plane, corresponding to the regions in the a-λ plane shown if fig. 2-15 above. The only difference in the two cases, $(d+e) > 0$ and $(d+e) < 0$, is the stability of the general solution in region III. The solution types are: conduction (C), rolls (R), squares (S), and general (G).

The bifurcation diagrams

The bifurcation diagrams plot A^2 as a function of a single parameter. This parameter can be thought of as the knob that the experimentalist turns. As the parameter is varied, the coefficients λ, a, b, etc. will change in general. When the system is near $\lambda = a = 0$, the variations in b and the higher order terms are insignificant, as long the nondegeneracy conditions below hold:

$$b \neq 0, \quad d+e \neq 0, \quad \text{and } d-e \neq 0. \tag{2-226}$$

As the experimental parameter (e.g. $R-R_c$) is varied, the system follows a ***path*** in a-λ space. It is assumed that λ increases monotonically with the experimental parameter, so that the experimental parameter can be rescaled (with a shift of origin) to be precisely λ.

The path through λ-a space is therefore

$$a = a_0 + \lambda a_1 + \cdots \tag{2-227}$$

The bifurcation diagrams plot A^2 vs. λ for this path. Thus, λ is the distinguished bifurcation parameter, and a_0 is the unfolding parameter; in this way, the two dimensional unfolding space is broken up into a series of lines.

For a fixed set of parameters b, d, and e, the bifurcation diagrams are qualitatively different in the two cases:

$$\begin{aligned} &(i) \quad a_1 > \frac{d-e}{-b}, \text{ and} \\ &(ii) \quad a_1 < \frac{d-e}{-b}. \end{aligned} \tag{2-228}$$

This difference is because a_1 is the slope of the path in a-λ space, and $(d-e)/b$ is the asymptotic slope of the horn in which the general solutions exist (see fig. 2-17).

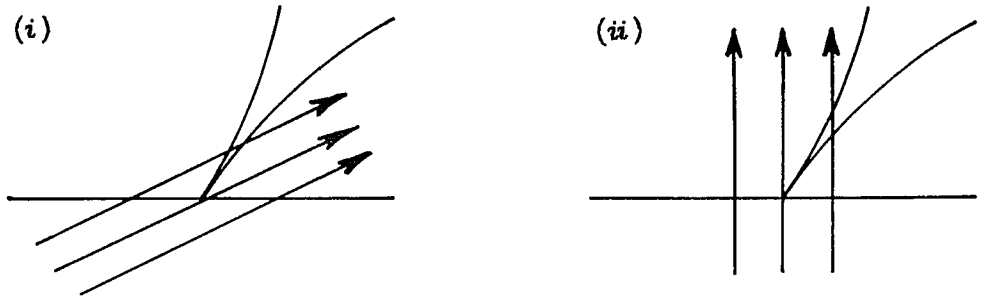

Fig. 2-17. One-parameter families of paths through a-λ space, near $a=\lambda=0$. The horn-shaped regions are those of fig. 2-15. The arrows indicate paths, defined by $a=a_0+\lambda a_1$, where λ is varied and a_0 and a_1 are fixed. The parameter which labels the path is a_0. The bifurcation diagrams plot the solutions as a function of λ for these paths. As far as the bifurcation diagrams are concerned, all that matters is the slope of the paths (a_1), relative to the opening slope of the horn-shaped region, $\left(\frac{(d-e)}{-b}\right)$. The two cases of equation (2-228) are indicated, for $(d-e)>0$ and $b<0$.

When the slope of the path in a-λ space is not vertical (i.e. $a_1 \neq 0$) the general solutions do not exist at a unique amplitude. Equation (2-206) is replaced by

$$A^2 = \frac{a_0}{d-e+a_1 b} + O(\lambda^2). \tag{2-229}$$

The significance of $d-e+a_1 b$ is clear from equation (2-228).

Following the sloped paths, the difference in the endpoints of the λ interval where the general solutions exist is

$$\lambda_S - \lambda_R = \frac{{a_0}^2}{4(d-e+a_1 b)^2} \frac{(d+e)(d-e)}{(d-e+a_1 b)} + O({a_0}^3). \tag{2-230}$$

Comparing equations (2-206) and (2-209) with equations (2-229) and (2-230), respectively, one finds that the following two ODEs have qualitatively the same bifurcation diagrams:

$$\dot{x}_1 = x_1\left[\lambda+(a_0+\lambda a_1){x_2}^2+bA^2+cA^4+d{x_1}^4+e{x_2}^4\right], \tag{2-231}$$

and

$$\dot{x}_1 = x_1(\lambda+a_0{x_2}^2+bA^2+\tilde{d}{x_1}^4+\tilde{e}{x_2}^4), \tag{2-232}$$

where

$$\begin{aligned}\tilde{d}-\tilde{e} &= d-e+a_1 b \\ \tilde{d}+\tilde{e} &= (d+e)\frac{(d-e)}{(d-e+a_1 b)}.\end{aligned} \tag{2-233}$$

Thus, all of the possible bifurcation diagrams can be obtained by considering paths in a-λ space where a is a constant.

Singularity theory gives a technique for showing that two systems, such as (2-231) and (2-232), are equivalent as far as the bifurcation diagrams are concerned. While such a proof has not been done here, the above analysis suggests that (2-231) may be a singularity theory normal form, provided

$$\tilde{d}-\tilde{e}\neq 0,\ \ \tilde{d}+\tilde{e}\neq 0,\ \text{ and } b\neq 0. \tag{2-234}$$

Note that $(d+e)(d-e)=(\tilde{d}+\tilde{e})(\tilde{d}-\tilde{e})$; as a result the stability of the general solution is the same for the two systems (2-231) and (2-232). This is of course necessary because the path through a-λ space cannot effect the stability of the solutions.

The result of this section is that the original normal form (2-201) can be used to generate all of the bifurcation diagrams, where a, d, and e represent a_0, $\tilde{d}$, and $\tilde{e}$; this is done in figs. 2-18 and 2-19. Fig. 2-18 shows how the d-e plane is divided into four regions by what could be called the super nondegeneracy conditions: $d+e\neq 0$ and $d-e\neq 0$. The bifurcation diagrams are drawn in fig. 2-19 for various fixed values of the parameters.

In addition to the nondegeneracy conditions listed above, a further division of the d-e plane is needed to distinguish between the cases where the rolls have larger amplitude than the squares, and vise verse. To see this, consider the case where $a=0$: The difference in amplitude of the two branches, at a fixed value of λ, is

$$(A^2)_S-(A^2)_R=\frac{(3d-e)}{4b}A^4+O(A^6). \tag{2-235}$$

When $a\neq 0$, the relative amplitude of the rolls and squares is given, at small

amplitude, by the initial slope of A^2 vs. λ. The two branches have the same amplitude when

$$A^2 = \frac{2a}{(3d-e)}, \tag{2-236}$$

if this expression is positive. This result is found by eliminating λ from equations (2-202) and (2-203). For amplitudes larger than $O(a)$, the relative amplitude agrees with the $a = 0$ case, given by equation (2-235).

The difference in the bifurcation diagrams, depending on the sign of $(3d-e)$, is not independent of coordinates. Therefore one should *not* include $(3d-e)$ as a nondegeneracy condition. To see this, consider the following near identity change of variables:

$$\begin{aligned} x_1 &\to x_1 + a x_1 x_2^2 \\ x_2 &\to x_2 + a x_2 x_1^2, \end{aligned} \tag{2-237}$$

which implies

$$A^2 \to A^2 + 2a x_1^2 x_2^2. \tag{2-238}$$

This change of variables preserves the symmetry and yet can change the relative amplitude of the squares and rolls; it adds an $O(A^4)$ correction to the squares, but leaves the rolls unchanged, since

$$\begin{aligned} &(A^2)_R \to (A^2)_R, \text{ and} \\ &(A^2)_S \to (A^2)_S + \tfrac{1}{2}a(A^4)_S. \end{aligned} \tag{2-239}$$

The initial slope of A^2 vs. λ is not changed by this, or any other, near identity change of coordinates which preserves the symmetry of the vector field. In the nondegenerate bifurcations considered here, the solutions all have different slopes; therefore the relative amplitude (at small enough amplitude) is invariant under coordinate changes which preserve the symmetry.

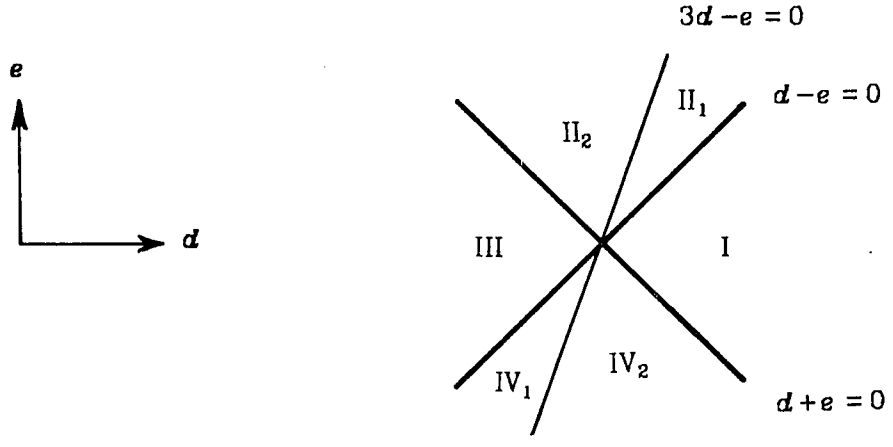

Fig. 2-18. The bifurcation diagrams of the normal form (2-201) depend on the coefficients a (which is considered the unfolding parameter), b, d, and e. This figure shows how the d-e plane is divided into four regions by two of the nondegeneracy conditions: $(d+e)\neq 0$, and $(d-e)\neq 0$. The relative amplitude of the roll and square solutions also depends on the combination $(3d-e)$; thus regions II and IV are subdivided. The normal form is not degenerate, however, when $(3d-e)=0$.

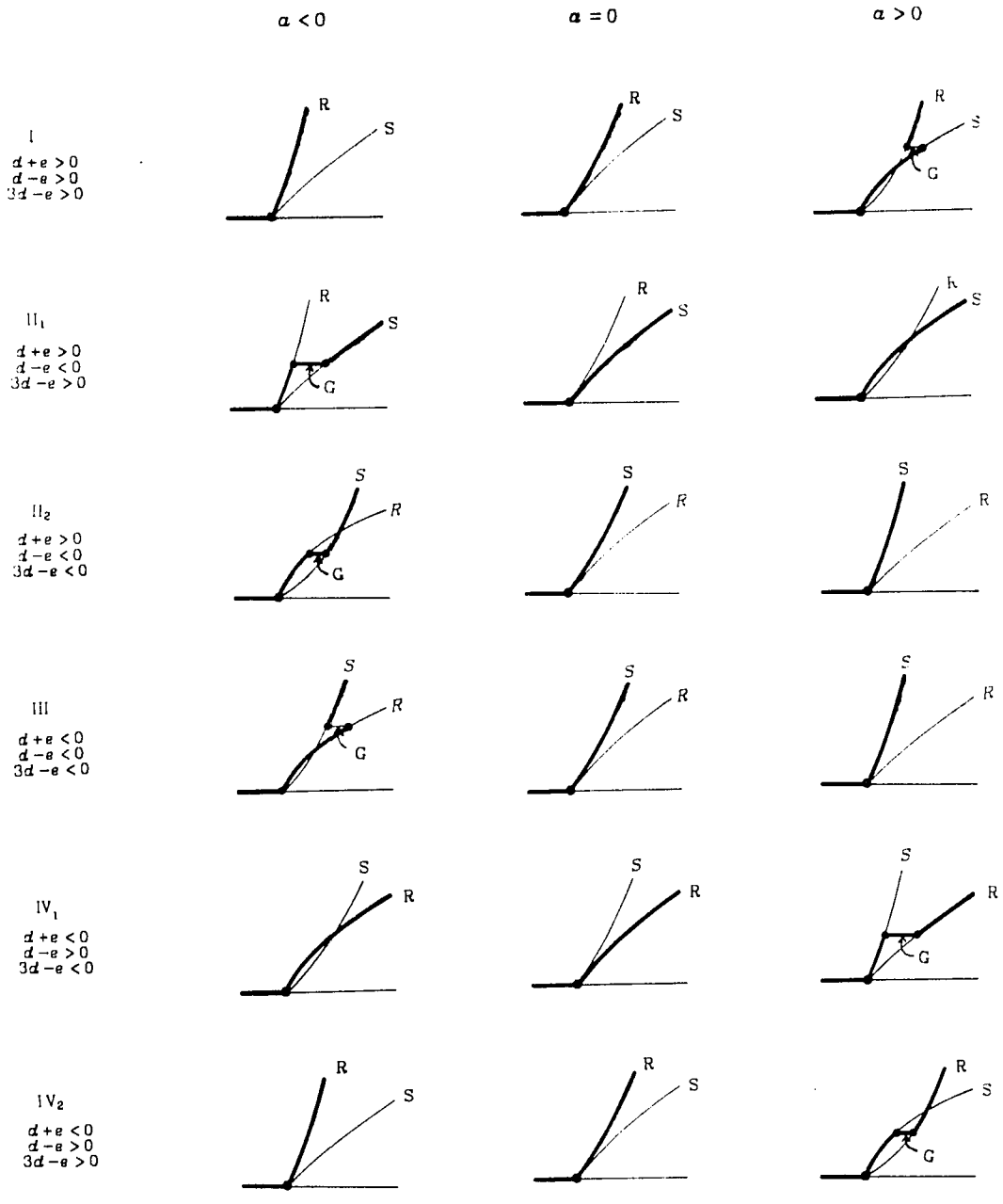

Fig. 2-19. The bifurcation diagrams (A^2 vs. $\lambda \propto R - R_c$) for the normal form (2-201). In each row, the coefficients d and e in the normal form correspond to the six regions of fig. 2-18, and $b < 0$ in all the diagrams. The three columns are for $a < 0$ (but small), $a = 0$, and $a > 0$, respectively. The general solutions (G) connect the rolls (R) and squares (S). The zero amplitude solution is conduction. As usual, the thicker lines indicate stable solutions. The difference between the diagrams of regions II_1 and II_2 only concerns the relative amplitudes of the roll and square solutions. This difference is not invariant under near identity coordinate transformations.

2.9. Convection on the Hexagonal Lattice

The hexagonal lattice is different than the other lattices because there is a third critical amplitude; the normal forms are ODEs in *three* complex variables. The most convenient choice for the third critical $\mathbf{k}$ vector is $\mathbf{k}_3 = -(\mathbf{k}_1+\mathbf{k}_2)$.

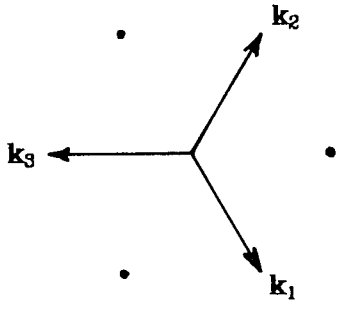

The third amplitude will be called z_3, so that a typical field is

$$\psi(\mathbf{x}) = \left(z_1 e^{i\mathbf{k}_1\cdot\mathbf{x}} + z_2 e^{i\mathbf{k}_2\cdot\mathbf{x}} + z_3 e^{i\mathbf{k}_3\cdot\mathbf{x}} + c.c.\right), \tag{2-240}$$

where the *c.c.* represents the complex conjugate of the proceeding terms.

The translations cause a phase shift of the amplitudes

$$(z_1, z_2, z_3) \to \left(e^{i\mathbf{k}_1\cdot\mathbf{d}} z_1, e^{i\mathbf{k}_2\cdot\mathbf{d}} z_2, e^{i\mathbf{k}_3\cdot\mathbf{d}} z_3\right). \tag{2-241}$$

All of the rotations (2-119) can be obtained by composing one or more of the following: a reflection across the $\mathbf{k}_1$ direction,

$$(z_1, z_2, z_3) \to (z_1, z_3, z_2), \tag{2-242}$$

the 180° rotation,

$$(z_1, z_2, z_3) \to (\bar{z}_1, \bar{z}_2, \bar{z}_3), \tag{2-243}$$

and a 120° rotation,

$$(z_1, z_2, z_3) \to (z_2, z_3, z_1). \tag{2-244}$$

When the Boussinesq approximation holds and the boundary conditions are symmetric, the partial differential equations have the symmetry (1-159)-(1-161). The critical amplitudes reverse sign under this transformation, and therefore the normal form has the symmetry

$$(z_1, z_2, z_3) \to -(z_1, z_2, z_3) \tag{2-245}$$

in the Boussinesq case. If it holds, this symmetry forbids of all even order terms in the normal form.

The symmetry group formed by all compositions of (2-242), (2-243) and (2-244) is called Γ_n, the "nonsymmetric" symmetry group. When the Boussinesq symmetry (2-245) is added, the symmetry group is called Γ_s, the "symmetric" symmetry group.

The determination of the most general equivariant ODE proceeds as in the square or rhombic lattice. The general term in the Taylor expansion can be written as

$$\dot{z}_1 \sim {z_1}^{n_1} {\bar{z}_1}^{m_1} {z_2}^{n_2} {\bar{z}_2}^{m_2} {z_3}^{n_3} {\bar{z}_3}^{m_3}. \tag{2-246}$$

It is helpful to separate the largest possible factors of $|z_1|^2$, $|z_2|^2$, and $|z_3|^2$ from the other terms, since they are invariant under translations. The Taylor expansion involves only positive powers; however, using the convention

$$z^{-|n|} \equiv \bar{z}^{|n|}, \tag{2-247}$$

one can write

$${z_1}^{n_1} {\bar{z}_1}^{m_1} \equiv {z_1}^{(n_1-m_1)} (|z_1|^2)^{\max(n_1, m_1)}. \tag{2-248}$$

Therefore, in place of equation (2-246), the general term in the Taylor series becomes

$$\dot{z}_1 \sim {z_1}^{n_1} {z_2}^{n_2} {z_3}^{n_3} f(|z_1|^2, |z_2|^2, |z_3|^2), \tag{2-249}$$

where n_1 replaces $n_1 - m_1$.

It must be remembered that n_1 can be negative in equation (2-249), and that a negative exponent is interpreted as the positive power of the complex conjugate. For instance,

$${z_1}^{-3} (|z_1|^2)^2 \equiv {z_1}^2 {\bar{z}_1}^5. \tag{2-250}$$

The equivariance under translations for the general term (2-249) gives

$$e^{i\mathbf{k}_1\cdot\mathbf{d}} = e^{i(n_1\mathbf{k}_1\cdot\mathbf{d}+n_2\mathbf{k}_2\cdot\mathbf{d}+n_3\mathbf{k}_3\cdot\mathbf{d})}. \tag{2-251}$$

One of the $\mathbf{k}$ vectors can be eliminated using $\mathbf{k}_3 = -\mathbf{k}_1 - \mathbf{k}_2$:

$$e^{i\mathbf{k}_1\cdot\mathbf{d}} = e^{i\left[(n_1-n_3)\mathbf{k}_1\cdot\mathbf{d}+(n_2-n_3)\mathbf{k}_2\cdot\mathbf{d}\right]}. \tag{2-252}$$

This is true for all $\mathbf{d}$, which implies that

$$\begin{aligned} 1 &= n_1 - n_3 \\ 0 &= n_2 - n_3 . \end{aligned} \tag{2-253}$$

This is a system of two equations for three integers, so there is a one parameter family of solutions:

$$\begin{aligned} n_1 &= n \\ n_2 &= n_3 = n-1 . \end{aligned} \tag{2-254}$$

Thus the most general Γ_n-equivariant vector field can be written as

$$\dot{z}_1 = \sum_{n=-\infty}^{\infty} z_1{}^n (z_2 z_3)^{n-1} f_n(|z_1|^2, |z_2|^2, |z_3|^2), \tag{2-255}$$

and the most general Γ_s-equivariant vector field as

$$\dot{z}_1 = \sum_{\substack{n=-\infty \\ n \text{ odd}}}^{\infty} z_1{}^n (z_2 z_3)^{n-1} f_n(|z_1|^2, |z_2|^2, |z_3|^2), \tag{2-256}$$

where the functions f_n are real-valued due to the complex conjugation symmetry (2-243), and symmetric under interchange of z_2 and z_3:

$$f_n : \mathbb{R}^3 \to \mathbb{R};\ f_n(|z_1|^2, |z_2|^2, |z_3|^2) = f_n(|z_1|^2, |z_3|^2, |z_2|^2). \tag{2-257}$$

The equations for $\dot{z}_2$ and $\dot{z}_3$ follow from the permutation symmetry (2-244).

Using the convention (2-247), the prefactors of f_n are

$$z_1{}^n (z_2 z_3)^{n-1} = \begin{cases} z_1 (z_1 z_2 z_3)^{n-1} & \text{for } n \geq 1 . \\ \bar{z}_2 \bar{z}_3 (\bar{z}_1 \bar{z}_2 \bar{z}_3)^{|n|} & \text{for } n \leq 0 . \end{cases} \tag{2-258}$$

In Buzano & Golubitsky (1983) and Golubitsky *et al.* (1984) the equivariant vector fields were written in a different, but equivalent, way. They wrote the general equivariant vector field as a module over the ring of invariant functions, so that singularity theory could be used. The present approach does not

require this special form of the equivariant ODEs, however. Nevertheless, it is convenient to define

$$q \equiv z_1 z_2 z_3 + \bar{z}_1 \bar{z}_2 \bar{z}_3 . \tag{2-259}$$

Note that q is invariant under all of the symmetries in Γ_n. Buzano & Golubitsky (1983) showed that the most general equivariant vector field is

$$\dot{z}_1 = z_1 g(q, |z_1|^2, |z_2|^2, |z_3|^2) + \bar{z}_2 \bar{z}_3 h(q, |z_1|^2, |z_2|^2, |z_3|^2), \tag{2-260}$$

where the functions g and h are real valued and symmetric under the interchange of z_2 and z_3. As before, $\dot{z}_2$ and $\dot{z}_3$ follow from the cyclic permutation symmetry (2-244).

When the Boussinesq symmetry holds, only odd power terms are allowed in the Γ_s-equivariant ODE, which can be written as

$$\dot{z}_1 = z_1 \tilde{g}(q^2, |z_1|^2, |z_2|^2, |z_3|^2) + \bar{z}_2 \bar{z}_3 q \, \tilde{h}(q^2, |z_1|^2, |z_2|^2, |z_3|^2). \tag{2-261}$$

The complex nature of the amplitudes is essential in the hexagonal lattice, unlike the square or rhombic lattices. The important function is the sum of the phases,

$$\Phi \equiv \varphi_1 + \varphi_2 + \varphi_3 , \tag{2-262}$$

where

$$z_\alpha = x_\alpha e^{i\varphi_\alpha}, \quad \alpha = 1, 2, 3. \tag{2-263}$$

This combination of the phases is invariant under translations, since

$$\varphi_\alpha \to \varphi_\alpha + \mathbf{k}_\alpha \cdot \mathbf{d} \tag{2-264}$$

$$\Phi \to \Phi + (\mathbf{k}_1 + \mathbf{k}_2 + \mathbf{k}_3) \cdot \mathbf{d} = \Phi . \tag{2-265}$$

There are three phases and two independent translations, so there is only one invariant function of the phases, namely Φ.

If at least one of the amplitudes is zero, then the remaining amplitudes can be made real by a suitable choice of the displacement **d**. In this case the phase Φ is undefined.

In the first form of the equivariant ODEs (2-255), all the terms with $n \neq 1$ cause a nonzero time derivative of the phase. The second form, (2-260) or (2-261), has the advantage that only the h term effects the phase;

$$\dot{\varphi}_1 = \frac{1}{2i|z_1|^2}(\bar{z}_1\bar{z}_2\bar{z}_3 - z_1 z_2 z_3)h \tag{2-266}$$

in the non-symmetric case (Γ_n), and

$$\dot{\varphi}_1 = \frac{1}{2i|z_1|^2}(\bar{z}_1\bar{z}_2\bar{z}_3 - z_1 z_2 z_3)q\,\tilde{h} \tag{2-267}$$

in the symmetric case (Γ_s).

2.9.1. Truncations of the ODEs

There are three different truncations of the most general equivariant ODE which are applicable in different cases. When writing the truncations it is convenient to use

$$A^2 \equiv |z_1|^2 + |z_2|^2 + |z_3|^2, \quad A^4 \equiv (A^2)^2. \tag{2-268}$$

As in the square and rhombic lattice cases, A^2 is proportional to the convective heat transport.

(1) Truncating the general ODE at third order gives

$$\dot{z}_1 = z_1\left[\lambda + a(|z_2|^2 + |z_3|^2) + bA^2\right] + \varepsilon\bar{z}_2\bar{z}_3, \tag{2-269}$$

where a, b, and ε are real. Note that when one of the amplitudes is zero, say z_3, this is identical to the normal form for convection on the rhombic lattice.

The results of Buzano & Golubitsky (1983) imply that this truncation is structurally stable provided

$$\varepsilon \neq 0, \text{ and } b \neq 0. \tag{2-270}$$

However, in this case there are no stable solutions in the neighborhood of the origin. There are stable solutions at $A^2 = O(\varepsilon^2)$, but these are outside the range of validity of the truncation. The higher order terms which have been neglected are important at this larger amplitude.

(2) When ε is perturbed from zero, stable solutions are captured by the local analysis. In other words, the stable solutions exist for small enough ε. Busse (1962, 1967) analyzed this system for the parameters relevant to Bénard convection ($a < 0, b < 0$). Although Busse's analysis correctly identified all of the stable solutions in this case, Buzano & Golubitsky (1983) found that this third order system must be modified to include fourth and fifth order terms when ε is in the neighborhood of zero. The important higher order terms are those which effect the phase. Adding these gives

$$\dot{z}_1 = z_1\left[\lambda+a(|z_2|^2+|z_3|^2)+bA^2\right]+\bar{z}_2\bar{z}_3\left[\varepsilon+d(|z_2|^2+|z_3|^2)+eA^2+c\,q\right]. \quad (2\text{-}271)$$

This is a normal form of the *degenerate bifurcation* (with codimension-two) in the neighborhood of $\lambda=0$, $\varepsilon=0$, provided the following nondegeneracy conditions hold:

$$\begin{array}{c} a\neq 0,\ b\neq 0,\ a+2b\neq 0,\ 2a+3b\neq 0,\ c\neq 0, \\ a+3b\neq 0,\ a+6b\neq 0,\ d\neq 0,\ \text{and } 2d+3e\neq 0. \end{array} \quad (2\text{-}272)$$

The normal form found by Buzano & Golubitsky (1983) includes another fifth order term,

$$\dot{z}_1 \sim z_1 A^4, \quad (2\text{-}273)$$

although this term has no effect on the qualitative behavior of the solutions. furthermore it is *not* required that the coefficient of this term in nonzero. Buzano & Golubitsky (1983) used singularity theory, and showed that *all* the higher order terms can be transformed away, using a more general transformation of the domain (z_a) and range ($\dot{z}_a$) than that used here. From the structural stability point of view this term is not necessary.

The nondegeneracy condition $2d+3e\neq 0$ requires that the fourth order terms are nonzero. Therefore the normal form (2-271) with the nondegeneracy conditions (2-272) is *not* applicable when the Boussinesq symmetry (2-245) holds. There are physical circumstances, however, where it is natural for the second order terms to vanish, even though the fourth order terms are nonzero.

The most notable such case is when the boundary conditions are different on the upper and lower boundaries, although the Boussinesq approximation is valid. In general, when the linear problem is selfadjoint the quadratic terms vanish, even without the vertical symmetry. According to Busse (1962), this was shown by Lortz in his dissertation.

The previous paragraph points out that the Boussinesq *approximation* does not necessarily imply the Boussinesq *symmetry* (2-245). The boundary conditions must be symmetric as well. There are many ways in which the Boussinesq symmetry can be broken, some of which are listed in Golubitsky *et al.* (1984).

(3) When all of the symmetry breaking terms are small, the bifurcation has codimension-three, and the normal form is equation (2-271) in the neighborhood of

$$\lambda = 0, \ \varepsilon = 0, \ \text{and} \ 2d+3e = 0. \tag{2-274}$$

The nondegeneracy conditions are

$$a \neq 0, \ b \neq 0, \ a+2b \neq 0, \ 2a+3b \neq 0, \ \text{and} \ c \neq 0. \tag{2-275}$$

Note that the nondegeneracy conditions only require that odd terms are nonzero. The Boussinesq symmetry can hold at the organizing center, where $\varepsilon = 2d+3e = 0$. Thus, the normal form (2-271) allows the study of symmetry breaking, where the unfolding parameters ε and $2d+3e$ are the symmetry breaking terms. This normal form was found using structural stability arguments in Golubitsky *et al.* (1984), but the singularity theory analysis has not been performed for this case.

In the Boussinesq case, only odd power terms are allowed in the normal form. The first term which effects the phase Φ is fifth order, so the simplest candidate for a normal form is

$$\dot{z}_1 = z_1\left[\lambda+a(|z_2|^2+|z_3|^2)+bA^2\right]+c\bar{z}_2\bar{z}_3 q\,. \tag{2-276}$$

This is indeed a normal form, based on structural stability considerations (Golubitsky *et al.*, 1984). The nondegeneracy conditions are

$$a\neq 0,\ b\neq 0,\ a+2b\neq 0,\ 2a+3b\neq 0,\ \text{and}\ c\neq 0. \tag{2-277}$$

The scaled normal forms used in Golubitsky *et al.* (1984), are

$$\dot{z}_1 = z_1(-\lambda_G+a_G A^2+|z_1|^2)+\bar{z}_2\bar{z}_3(-\varepsilon_G+b_G A^2+|z_1|^2+c_G q)\,, \tag{2-278}$$

in the nonsymmetric case, and

$$\dot{z}_1 = z_1(-\lambda_G+a_G A^2+|z_1|^2)+c_G\bar{z}_2\bar{z}_3 q\,, \tag{2-279}$$

in the symmetric case.

To arrive at the normal form (2-279), Golubitsky *et al.* used the fact that $a\neq 0$, which is one of the nondegeneracy conditions, to set $a=-1$ by scaling the variables. In going from the unscaled equation (2-276) to the scaled version, first the direction of time is reversed if $a>0$, and then the amplitudes are scaled by

$$z_a \to \frac{z_a}{\sqrt{|a|}}. \tag{2-280}$$

The ODE is then in the form (2-279), with

$$\begin{aligned} \lambda_G &= -\mathrm{sgn}(a)\lambda \\ a_G &= -\left(\frac{a+b}{a}\right) \\ c_G &= \frac{-c}{a}. \end{aligned} \tag{2-281}$$

The time can then be scaled (with a positive scale factor) to set $c_G=\pm 1$, but this is not pursued here. The details are in Golubitsky *et al.* (1984, p. 264).

In the non-Boussinesq case, Buzano & Golubitsky (1983) used the two scalings (z and t) to set $a=-1$ and $d=-1$. The coefficients of the scaled normal form are obtained from the unscaled normal form as follows:

$$
\begin{aligned}
a_G &= -\left(\frac{a+b}{a}\right) \\
b_G &= -\left(\frac{d+e}{d}\right) \\
\mathrm{sgn}(\lambda_G) &= -\mathrm{sgn}(a\,\lambda) \\
\mathrm{sgn}(\varepsilon_G) &= -\mathrm{sgn}(d\,\varepsilon) \\
\mathrm{sgn}(c_G) &= \mathrm{sgn}(a\,c)\,.
\end{aligned}
\tag{2-282}
$$

The results of the analysis in the present notation can be applied to the normal forms in the notation of Golubitsky *et al.* by letting

$$
\begin{aligned}
\lambda &= -\lambda_G \\
\varepsilon &= -\varepsilon_G \\
a &= -1 \\
b &= a_G + 1 \\
c &= c_G \\
d &= -1 \\
e &= b_G + 1\,.
\end{aligned}
\tag{2-283}
$$

The notation used here is chosen because it directly conforms to the results of the calculations of Chapter Four. When the coefficients of the normal forms are calculated, it is preferable *not* to use the scaled version of the normal form for comparison.

2.9.2. The subspace of equal amplitudes

The three complex amplitudes in the ODEs can be quite cumbersome. The analysis is simplified by the restriction of the ODEs to two invariant subspaces: the *equal amplitude subspace* and the *real subspace*. The equal amplitude subspace is discussed in this section and the real subspace is discussed in the next section. One can show that all of the small amplitude solutions of the normal forms are in one (or both) of these invariant subspaces.

The equal amplitude subspace is defined by

$$
|z_1|^2 = |z_2|^2 = |z_3|^2. \tag{2-284}
$$

It is convenient to choose the origin of the fluid layer so that all of the phases are equal;

$$z_1 = z_2 = z_3 \equiv z = re^{i\varphi}, \tag{2-285}$$

$$\Phi = 3\varphi, \tag{2-286}$$

where Φ has been defined in equation (2-262). Thus, the equal amplitude subspace can be identified with a single complex number, z. With these phases it is trivial to verify that the subspace of equal amplitudes is invariant:

$$\dot{z}_1\big|_{(z_1=z_2=z_3)} = \dot{z}_2\big|_{(z_1=z_2=z_3)} = \dot{z}_3\big|_{(z_1=z_2=z_3)}. \tag{2-287}$$

A solution of the ODEs which is in this subspace is called an *equal amplitude solution*. The possible equal amplitude solutions are listed below:

- Hexagons ($H^{\pm}$)

$$|z_1|^2 = |z_2|^2 = |z_3|^2, \quad \begin{Bmatrix} \Phi = 0 & (H^+) \\ \Phi = \pi & (H^-) \end{Bmatrix} \tag{2-288}$$

- Triangles (T)

$$|z_1|^2 = |z_2|^2 = |z_3|^2, \quad \Phi \neq 0, \Phi \neq \pi \tag{2-289}$$

- Regular Triangles (RT)

$$|z_1|^2 = |z_2|^2 = |z_3|^2, \quad \Phi = \pm \frac{\pi}{2}. \tag{2-290}$$

The *hexagons* come in two types; the flow can be upward (H^+, $\Phi = 0$), or downward (H^-, $\Phi = \pi$), in the centers of the hexagonal cells. The other patterns are called *triangles*, following Buzano and Golubitsky (1983), due to their symmetry. In the Boussinesq case the *regular triangles*, defined by $\Phi = \pm \pi/2$, have more symmetry than the other triangles.

The flow pattern and temperature distributions of the equal amplitude solutions are shown in fig. 2-20. The shadowgraph visualization used is the same as that used in fig. 2-12.

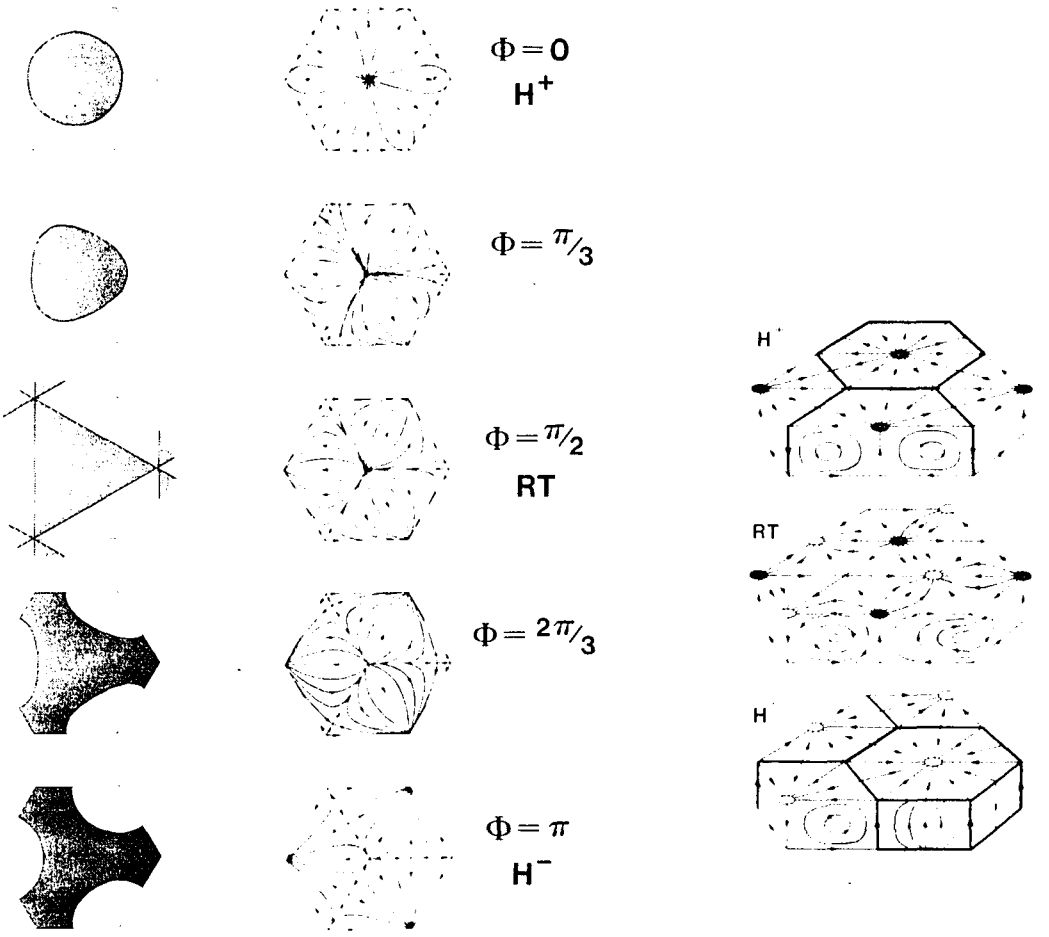

Fig. 2-20. The equal amplitude solutions: the hexagons, regular triangles, and triangles. The solutions are parametrized by the angle Φ (see equations (2-285) and (2-286)). Three different methods of visualization are used. The leftmost column shows the hot and cold regions, using the shadowgraph technique used in fig. 2-12. The center column shows the paths of the fluid particles on the upper (free boundary) surface. The right column shows a perspective drawing of the pattern of the hexagons and regular triangles, where the dark circles represent upwelling and the open circles represent downwelling fluid.

Often, the Boussinesq approximation is not valid because the viscosity depends on temperature. In this case, the hexagonal pattern with the larger viscosity in the centers of each cell is stable. In liquids, the viscosity tends to increase with temperature, and in gases, the viscosity decreases with temperature as a rule. For this reason, Busse (1962) has named the two types of hexagons, H^+ and H^-, l- and g-hexagons, respectively. The +/ − nomenclature comes from the sign of the amplitudes when they are chosen to be real:

$$z_1 = z_2 = z_3 = x\,, \quad \left\{ \begin{array}{l} x > 0 \text{ for } H^+. \\ x < 0 \text{ for } H^-. \end{array} \right\} \tag{2-291}$$

The most general Γ_n-equivariant ODE (2-260), restricted to the equal amplitude subspace, is

$$\dot{z} = z\, g(q\,, |z|^2) + \bar{z}^2 h(q\,, |z|^2)\,, \tag{2-292}$$

and the most general Γ_s-equivariant ODE (2-261), restricted to the equal amplitude subspace, is

$$\dot{z} = z\, \tilde{g}(q^2, |z|^2) + \bar{z}^2 q\, \tilde{h}(q^2, |z|^2)\,. \tag{2-293}$$

The symmetry of (2-260) is the 6 element group $\mathbf{D}_3$, generated by

$$\begin{array}{l} z \to e^{i2\pi/3} z\,, \text{ and} \\ z \to \bar{z}\,. \end{array} \tag{2-294}$$

This is the symmetry of an equilateral triangle in the plane. The symmetry of (2-261) is the 12 element group $\mathbf{D}_6$, generated by the above transformations and

$$z \to -z\,. \tag{2-295}$$

This is the symmetry group of a regular hexagon in the plane. It is worth noting that the two types of hexagons are identified by the symmetry $z \to -z$ in the Boussinesq case. Therefore, if hexagons are preferred in a symmetric system, then the initial conditions determine whether H^+ or H^- are observed. There would most likely be many defects in such a pattern.

One-dimensional invariant subspaces are important because the solutions are defined by a single equation. It is much simpler to solve a single nonlinear

equation than six coupled nonlinear equations. The lines of reflectional symmetry in the complex plane are one-dimensional invariant subspaces of the full phase space. In the non-Boussinesq ($\mathbf{D}_3$) case the lines

$$\varphi = 0,\ \pm\frac{\pi}{3},\ \pm\frac{2\pi}{3},\ \left[\text{i.e. } \sin\Phi = 0\right], \tag{2-296}$$

contain the hexagons. In the Boussinesq ($\mathbf{D}_6$) case there are additional lines of reflectional symmetry,

$$\varphi = \pm\frac{\pi}{6},\ \pm\frac{\pi}{2},\ \pm\frac{5\pi}{6},\ \left[\text{i.e. } \cos\Phi = 0\right], \tag{2-297}$$

which contain the regular triangles.

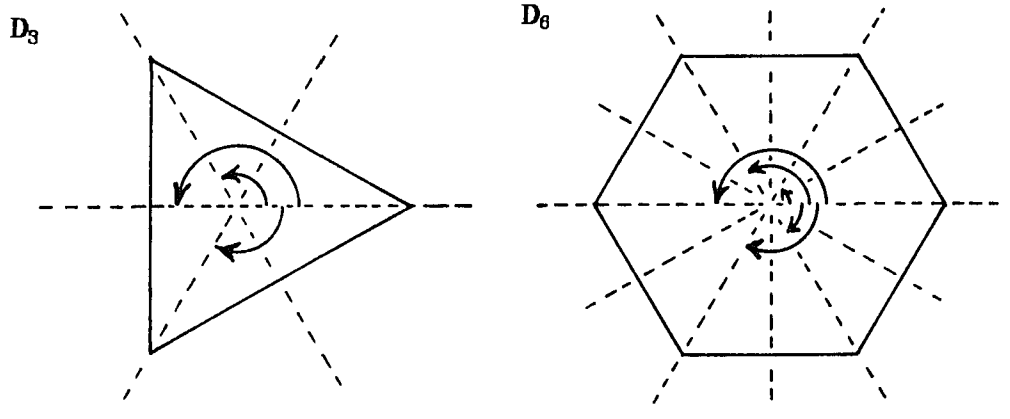

Fig. 2-21. The symmetries of the triangle ($\mathbf{D}_3$) and hexagon ($\mathbf{D}_6$) in the plane. The dotted lines represent lines of reflection, and the curved arrows indicate proper rotations.

2.9.3. The real subspace

An important invariant subspace of $\mathbb{C}^3$ is the real subspace, defined by

$$\sin\Phi = 0 \text{ if } z_1 z_2 z_3 \neq 0, \text{ or} \tag{2-298}$$

$$z_1 z_2 z_3 = 0. \tag{2-299}$$

The reason for the name is that all three complex amplitudes can be made real by some translation ($\mathbf{x} \to \mathbf{x}+\mathbf{d}$). The proof consists of two parts: (1) If all of the amplitudes are nonzero, then Φ is defined. Two of the phases can be made zero by a choice of the origin, therefore the third phase is Φ. If $\Phi = 0$ or π, then all of

the amplitudes are real. (2) If $z_1 z_2 z_3 = 0$ then at least one of the amplitudes is zero, and the remaining amplitudes can be made real by a translation.

The real solutions are an invariant subspace. When $z_1 z_2 z_3 \neq 0$, the general equivariant ODE (2-260) implies

$$\dot{\Phi} = -\sin\Phi\,|z_1|\,|z_2|\,|z_3|\left(\frac{h_1}{|z_1|^2}+\frac{h_2}{|z_2|^2}+\frac{h_3}{|z_3|^2}\right), \tag{2-300}$$

where $h_1 \equiv h(q^2, |z_1|^2, |z_2|^2, |z_3|^2)$, $h_2 \equiv h(q^2, |z_2|^2, |z_3|^2, |z_1|^2)$, etc.

When $z_1 z_2 z_3 = 0$ the above argument breaks down. If exactly one of the amplitudes, say z_3, is zero at $t = 0$, then the ODE is

$$\begin{aligned} \dot{z}_1 &= z_1 g_1 \\ \dot{z}_2 &= z_2 g_2 \\ \dot{z}_3 &= \bar{z}_2 \bar{z}_3 h_3 . \end{aligned} \tag{2-301}$$

However, if z_2 and z_3 are real, then $\dot{z}_3$ (and thus z_3) are real and nonzero for $t = 0^+$, unless $h = 0$. In any case the solution remains on the real subspace.

There are some one-dimensional invariant subspaces which are real. The most important is the space of rolls, where only one amplitude is nonzero. The rolls can be put in the following canonical form:

- Rolls (R)

$$z_1 \in \mathbb{R},\ z_2 = z_2 = 0 . \tag{2-302}$$

- Hexagons ($H^{\pm}$)

$$z_1 = z_2 = z_3 \in \mathbb{R} . \tag{2-303}$$

In the Boussinesq case another one dimensional subspace is defined by the (Boussinesq) rectangles, or patchwork quilt solutions, which can be put in the form

- Boussinesq Rectangles (RA)

$$z_1 = z_2 \in \mathbb{R},\ z_3 = 0 . \tag{2-304}$$

(When the Boussinesq symmetry holds, and $z_1 z_2 z_3 = 0$, then $h_3 = q\tilde{h}_3 = 0$ in equa-

tion (2-301).)

In the non-Boussinesq case there are small amplitude solutions in a two-dimensional invariant subspace which can be put in the form:

- Non-Boussinesq Rectangles (RA)

$$z_1 = z_2 \neq z_3, \quad \Phi = 0 \text{ or } \pi. \tag{2-305}$$

Fig. 2-22 shows the planforms of the different non-Boussinesq rectangles. Note that all of the previously mentioned real solutions, the rolls, hexagons and Boussinesq rectangles, are special cases of the non-Boussinesq rectangles.

When $|z_3| < |z_1| = |z_2|$, the non-Boussinesq rectangles on the hexagonal lattice are very similar to the non-Boussinesq rectangles on the rhombic lattices (see fig. 2-12).

The symmetries of the ODEs, restricted to the real subspace, are discussed in Swift (1984) (Appendix B).

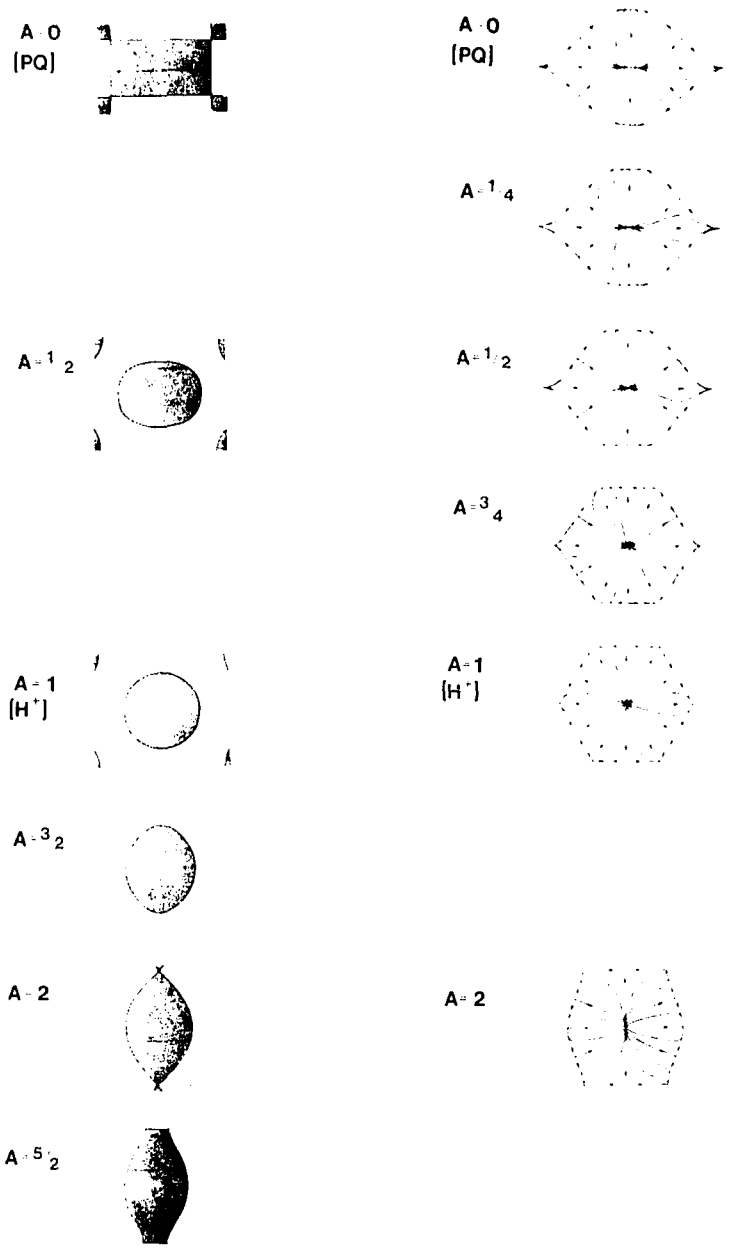

Fig. 2-22. The real solutions on the hexagonal lattice. The methods of visualization are the same as those of the first two columns of fig. 2-20. The real solutions are parametrized by the ratio of amplitudes,

$$\mathbf{A} \equiv \frac{x_1}{x_2}, \text{ where } x_2 = x_3.$$

2.9.4. The analysis of the Boussinesq normal form

The Boussinesq normal form is simpler to analyze than the other cases, so it is done first.

The analysis of the Boussinesq normal form is done in two steps; first the invariant subspace of equal amplitudes is analyzed, and then the invariant subspace of real amplitudes is analyzed.

The equal amplitude subspace (D_6 symmetry)

The ODE for the equal amplitude solutions is obtained from equation (2-276). In terms of polar coordinates, this is

$$\dot{r} = r\left[\lambda+(2a+3b)r^2\right]+c\,r^5\cos^2(3\varphi)\,. \tag{2-306}$$

$$\dot{\varphi} = -cr^4\sin(6\varphi) \tag{2-307}$$

Therefore, there are only two types of solutions; the hexagons ($6\varphi = 0$, mod 2π) and regular triangles ($6\varphi = \pi$, mod 2π). The other triangles cannot be stationary solutions except at larger amplitudes, where the seventh order terms dominate the fifth order term.

The amplitude (r^2) of the hexagons or regular triangles is determined by $\dot{r} = 0$, which implies

$$\lambda+(2a+3b)r^2+2c\,r^2\cos^2(3\varphi) = 0\,. \tag{2-308}$$

When $(2a+3b)\neq 0$, the amplitude is

$$r^2 = \frac{-\lambda}{(2a+3b)} - \frac{\lambda^2}{(2a+3b)^3}2c\cos^2(3\varphi), \tag{2-309}$$

where

$$\cos^2(3\varphi) = \begin{cases} 1 \text{ for hexagons.} \\ 0 \text{ for regular triangles.} \end{cases} \tag{2-310}$$

The stability of the solutions is determined by the eigenvalues of

$$\mathbf{J} = \begin{pmatrix} \frac{\partial \dot{r}}{\partial r} & \frac{\partial \dot{r}}{\partial \varphi} \\ \frac{\partial \dot{\varphi}}{\partial r} & \frac{\partial \dot{\varphi}}{\partial \varphi} \end{pmatrix}. \tag{2-311}$$

A computation shows that the off-diagonal elements of $\mathbf{J}$ are proportional to $\sin(6\varphi)$. The hexagons and triangles are on the lines of reflectional symmetry, where $\sin(6\varphi) = 0$; therefore $\mathbf{J}$ is a diagonal matrix when evaluated at the stationary solutions. As a consequence, the two eigenvectors are in the radial and tangential directions. The radial eigenvalue is

$$\frac{\partial \dot{r}}{\partial r} = \lambda + (2a + 3b)3r^2 + O(r^4) \tag{2-312}$$

$$= 2(2a + 3b)r^2 + O(r^4). \tag{2-313}$$

The last step follows when the expression is evaluated at the solution. The phase eigenvalues for these solutions are

$$\frac{\partial \dot{\varphi}}{\partial \varphi} = -2cr^2\cos(6\varphi) = \begin{cases} -2cr^2 \text{ for hexagons.} \\ 2cr^2 \text{ for regular triangles.} \end{cases} \tag{2-314}$$

Note that when the equal amplitude solutions are supercritical (i.e. $(2a + 3b) < 0$), then the one with the larger amplitude has the negative (stable) phase eigenvalue. This completes the analysis of the $\mathbf{D}_6$ normal form.

The real and imaginary subspaces

In the Boussinesq case, the *imaginary subspace*, defined by

$$\Phi = \pm \frac{\pi}{2} \text{ if } z_1 z_2 z_3 = 0, \text{ or} \tag{2-315}$$

$$z_1 z_2 z_3 = 0 \tag{2-316}$$

is invariant, as well as the real subspace. Thus, there are *two* different three-dimensional invariant subspaces. The hexagons are in the real subspace, and the regular triangles are in the imaginary subspace.

The only differences between the hexagons and regular triangles are due to the fifth order term which has been analyzed in the equal amplitude

subspace. In the analysis of the real subspace, it is sufficient to truncate the normal form (2-276) at third order. The imaginary subspace yields the same third order truncation. There is no difference between the hexagons and regular triangles at third order.

The analysis of the invariant subspace of real solutions begins by setting $z_\alpha = x_\alpha$ to accentuate the fact that the amplitudes are real. The ODE (2-276), evaluated at the real subspace, and truncated to third order, is

$$\dot{x}_1 = x_1\left[\lambda + a\left(x_2^2 + x_3^2\right) + bA^2\right]. \tag{2-317}$$

The fifth order term is unimportant here.

The two types of real solutions present at small amplitude in the Boussinesq case are:

- Rolls (R)

$$A^2 = \frac{-\lambda}{b}, \tag{2-318}$$

- Boussinesq Rectangles (RA)

$$A^2 = \frac{-\lambda}{\frac{1}{2}a + b}, \text{ and} \tag{2-319}$$

- Equal amplitude solutions ($H^{\pm}$, T)

$$A^2 = \frac{-\lambda}{\frac{3}{2}a + b}. \tag{2-320}$$

Three of the eigenvalues of these solutions can be calculated using the third order truncation in the real subspace. In going from the real system to the complex system, three eigenvalues must be added. The phase eigenvalue of the equal amplitude solutions has already been calculated for the $\mathbf{D}_6$ system. All of the other eigenvalues can be calculated on the real subspace. After the calculation, zero eigenvalue(s) must be added and some eigenvalues have multiplicity two due to the continuous symmetry. The technique for doing this has been discussed in section 2.7.1.

The Jacobian matrix of the real system (2-317) is

$$\mathbf{J} \equiv \mathrm{D}f = \begin{pmatrix} \frac{\partial \dot{x}_1}{\partial x_1} & \frac{\partial \dot{x}_1}{\partial x_2} & \frac{\partial \dot{x}_1}{\partial x_3} \\ \frac{\partial \dot{x}_2}{\partial x_1} & \frac{\partial \dot{x}_2}{\partial x_2} & \frac{\partial \dot{x}_2}{\partial x_3} \\ \frac{\partial \dot{x}_3}{\partial x_1} & \frac{\partial \dot{x}_3}{\partial x_2} & \frac{\partial \dot{x}_3}{\partial x_3} \end{pmatrix}, \tag{2-321}$$

where the x_i are real.

The fifth order term has been neglected because it only causes an $O(A^4)$ correction to the eigenvalues. Evaluating the derivatives, the Jacobian matrix is

$$\mathbf{J} = \begin{pmatrix} \begin{pmatrix} \lambda+3bx_1^2 \\ +(a+b)(x_2^2+x_3^2) \end{pmatrix} & 2(a+b)x_1x_2 & 2(a+b)x_1x_3 \\ 2(a+b)x_1x_2 & \begin{pmatrix} \lambda+3bx_2^2 \\ +(a+b)(x_1^2+x_3^2) \end{pmatrix} & 2(a+b)x_2x_3 \\ 2(a+b)x_1x_3 & 2(a+b)x_2x_3 & \begin{pmatrix} \lambda+3bx_3^2 \\ +(a+b)(x_1^2+x_2^2) \end{pmatrix} \end{pmatrix} + O(A^4). \tag{2-322}$$

Note that this matrix is symmetric. (This is true only because the fifth order terms have been neglected.)

- The Jacobian matrix, evaluated at the rolls, is

$$\mathbf{J}_R = A^2 \begin{pmatrix} 2b & 0 & 0 \\ 0 & a & 0 \\ 0 & 0 & a \end{pmatrix} + O(A^4). \tag{2-323}$$

The eigenvalues for the x_2 and x_3 perturbations (A^2a) are the same, by symmetry. Both are double eigenvalues since the translation which leaves z_1 unchanged causes a phase shift of z_2 and z_3. There is also a null eigenvector corresponding to the z_1 phase shift. Therefore, the eigenvalues of the roll solutions are

$$2bA^2, \ (aA^2)\times 4, \ \text{and } 0, \tag{2-324}$$

where the notation $(\mu)\times N$ means that the eigenvalue μ has multiplicity N.

• The Jacobian matrix, evaluated at the hexagons or regular triangles, is

$$\mathbf{J}_{\mathrm{H}} = \tfrac{2}{3}A^2\begin{bmatrix} b & (a+b) & (a+b) \\ (a+b) & b & (a+b) \\ (a+b) & (a+b) & b \end{bmatrix} + O(A^4), \tag{2-325}$$

where only the matrix of order A^4 is different for the two equal amplitude solutions. The eigenvectors of this matrix are

$$\begin{bmatrix} 1 \\ 1 \\ 1 \end{bmatrix}, \begin{bmatrix} 1 \\ -1 \\ 0 \end{bmatrix}, \text{ and } \begin{bmatrix} 1 \\ 0 \\ -1 \end{bmatrix}, \tag{2-326}$$

and the corresponding eigenvalues are

$$\tfrac{2}{3}A^2(2a+3b), \; -\tfrac{2}{3}A^2a, \text{ and } -\tfrac{2}{3}A^2a. \tag{2-327}$$

There are also two null eigenvalues corresponding to the translations. The sixth and final eigenvalue determines the stability in the "phase" direction: see equation (2-314).

• The Jacobian matrix, evaluated at the rectangles, is

$$\mathbf{J}_{\mathrm{RA}} = A^2\begin{bmatrix} b & (a+b) & 0 \\ (a+b) & b & 0 \\ 0 & 0 & \frac{1}{2}a \end{bmatrix}. \tag{2-328}$$

The eigenvectors are

$$\begin{bmatrix} 1 \\ 1 \\ 0 \end{bmatrix}, \begin{bmatrix} 1 \\ -1 \\ 0 \end{bmatrix}, \text{ and } \begin{bmatrix} 0 \\ 0 \\ 1 \end{bmatrix}, \tag{2-329}$$

with eigenvalues

$$A^2(a+2b), \; -A^2a, \text{ and } \tfrac{1}{2}A^2a. \tag{2-330}$$

The third eigenvalue has multiplicity two, since the z_3 perturbation can be real or imaginary. Finally, there are two zero eigenvalues corresponding to the translations.

The nondegeneracy conditions, listed in equation (2-277), ensure that all the eigenvalues in the table are non-zero (except where forced by the symmetry), and that none of the branches bifurcate vertically. Golubitsky, *et al.*

(1984) show that there are no other small amplitude solutions when the nondegeneracy conditions hold.

This completes the analysis of the Boussinesq normal form (2-276). The results are summarized in the following table.

name	definition	amplitude	eigenvalues
conduction (C)	$z_1 = z_2 = z_3 = 0$	$A^2 = 0$	$(\lambda)\times 6$
rolls (R)	$\lvert z_1\rvert^2 = A^2 \neq 0$ $z_2 = z_3 = 0$	$A^2 = \frac{-\lambda}{b}$	$2bA^2,\ (aA^2)\times 4,\ 0$
hexagons ($H^{\pm}$)	$\lvert z_1\rvert^2 = \lvert z_2\rvert^2 = \lvert z_3\rvert^2$ $\Phi = 0$ or π, $A^2 \neq 0$	$A^2 = \frac{-\lambda + O(\lambda^2)}{\frac{2}{3}a + b}$	$\frac{2}{3}A^2(2a+3b),\ -\frac{2}{3}cA^4,$ $(-\frac{2}{3}aA^2)\times 2,\ (0)\times 2$
regular triangles (RT)	$\lvert z_1\rvert^2 = \lvert z_2\rvert^2 = \lvert z_3\rvert^2$ $\Phi = \pm\frac{\pi}{2}$, $A^2 \neq 0$	$A^2 = \frac{-\lambda}{\frac{2}{3}a + b}$	$\frac{2}{3}A^2(2a+3b),\ \frac{2}{3}cA^4,$ $\left(-\frac{2}{3}aA^2\right)\times 2,\ (0)\times 2$
rectangles (RA)	$\lvert z_1\rvert^2 = \lvert z_2\rvert^2 \neq 0$ $z_3 = 0$	$A^2 = \frac{-\lambda}{\frac{1}{2}a + b}$	$A^2(a+2b),\ -A^2a,$ $\left(\frac{1}{2}A^2a\right)\times 2,\ (0)\times 2$

Table 2-7. Solution data for equation (2-276). Eigenvalues with multiplicity N are denoted by $(\mu)\times N$.

Fig. 2-23 shows how the parameter space is divided by the nondegeneracy conditions, and fig. 2-24 shows the bifurcation diagrams in the eight regions. Note that, if the equal amplitude solutions are ignored, the results are similar to those of the rhombic lattice. The most important difference is that the rectangle solution is unstable to the hexagon and regular triangle solutions in region II_1.

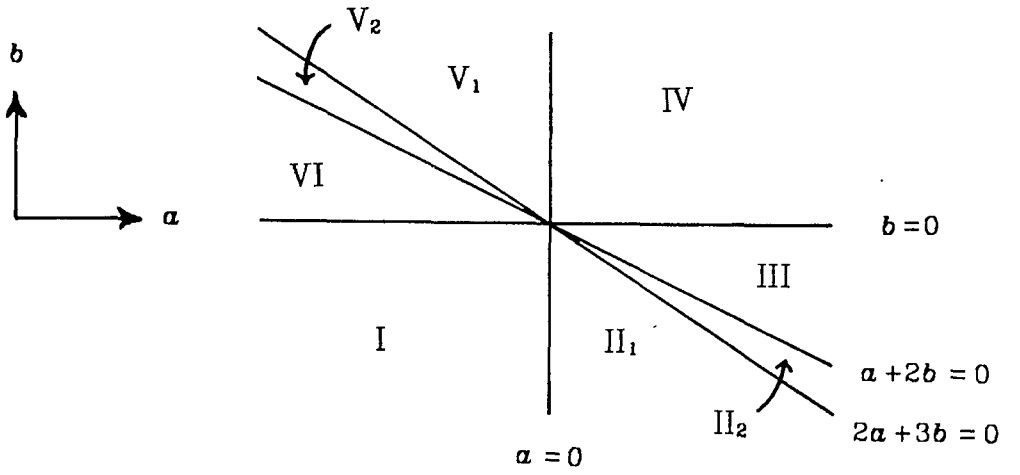

Fig. 2-23. The space of coefficients of the Boussinesq normal form (2-276) for convection on the hexagonal lattice. The a-b plane is divided into eight regions by the nondegeneracy conditions (2-277). The Roman numerals are chosen to correspond to the square and rhombic lattice cases (fig. 2-7); regions II and IV are divided by the extra nondegeneracy condition which is present on the hexagonal lattice: $2a+3b \neq 0$.

Bifurcation Diagrams for Boussinesq Convection on a Hexagonal Lattice

$$\dot{z}_1 = z_1\left[\lambda + a(|z_2|^2+|z_3|^2)+bA^2\right]+c\bar{z}_2\bar{z}_3 q$$
$$A^2 \equiv |z_1|^2+|z_2|^2+|z_3|^2, \quad q \equiv z_1 z_2 z_3+\bar{z}_1\bar{z}_2\bar{z}_3$$

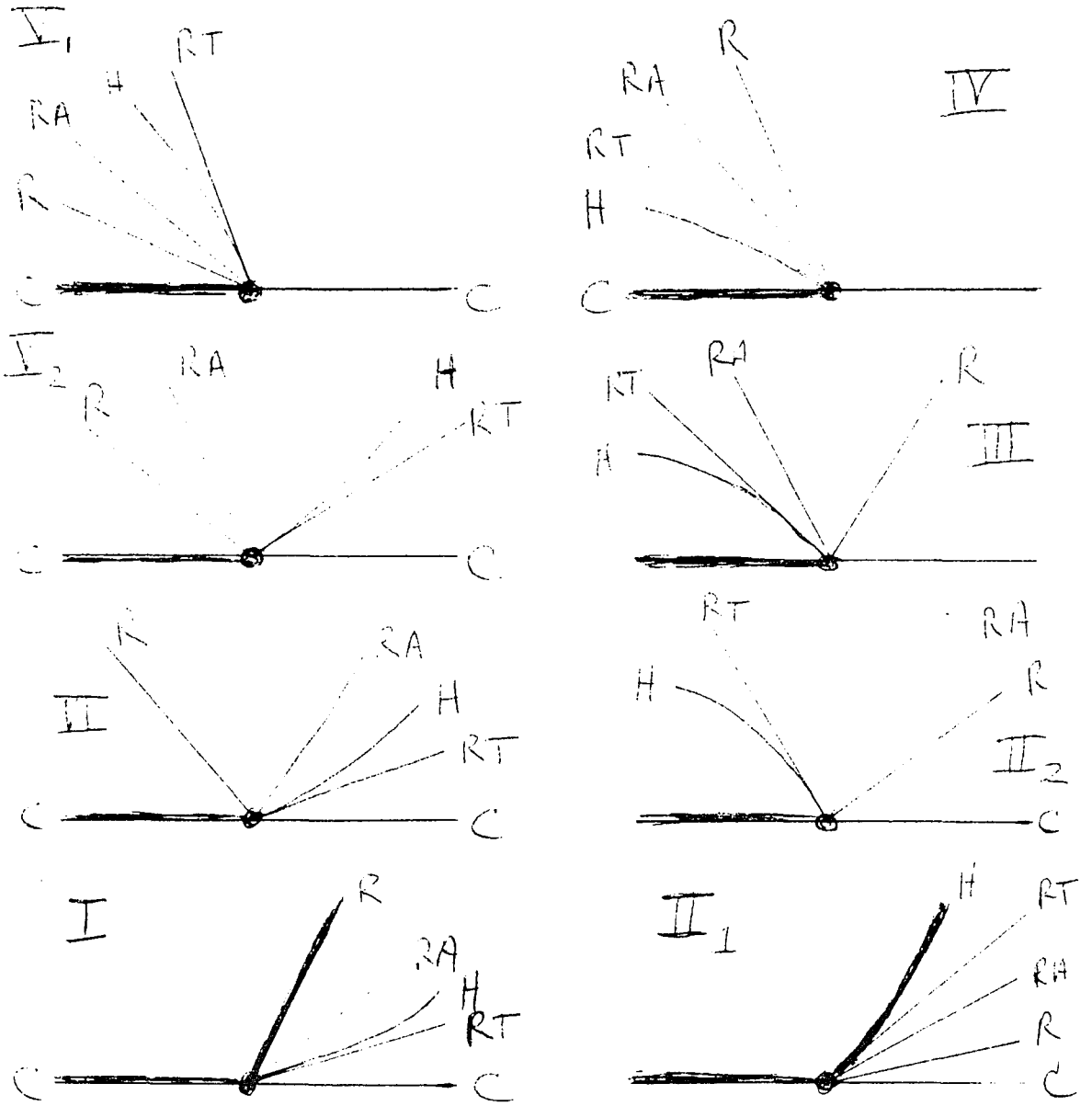

C: Conduction R: Rolls H: Hexagons RT: RegularTriangles RA: Rectangles

Fig. 2-24. The possible bifurcation diagrams for Boussinesq convection on a hexagonal lattice when $c > 0$. The Roman numerals indicate the regions in the a-b plane of fig 2-23. When $c < 0$ the hexagons and regular triangles are interchanged. For example, in region II_1 the regular triangles are stable when $c < 0$.

2.9.5. The analysis of the non-Boussinesq normal forms

In the non-Boussinesq case of hexagonal convection, degenerate bifurcations must be studied in order to find stable solutions in the small amplitude analysis. Much of the complexity of the hexagonal case is present in the problem of bifurcation in the plane with the symmetry of the triangle. The remainder of the problem can be analyzed on the subspace where the amplitudes are real.

The equal amplitude subspace (D_3 symmetry)

As with the Boussinesq case, it is easiest to start the analysis with the equal amplitude solutions, the hexagons and triangles. The restriction of the normal form to the equal amplitude subspace gives an ODE with the symmetry of the triangle in the plane (D_3).

Three cases are discussed here. First all of the cases are defined, and then the normal forms are analyzed for each separately. Which normal form is relevant depends on the degree to which the Boussinesq approximation is violated.

(1) The simplest case is when

$$\lambda \approx 0, \quad \varepsilon \neq 0. \tag{2-331}$$

This is a transcritical bifurcation with D_3 symmetry. As usual, the condition $\varepsilon \neq 0$ means that ε is not *near* zero. The second order truncation is sufficient here:

$$\dot{z} = \lambda z + \varepsilon \bar{z}^2. \tag{2-332}$$

(2) The next case is when

$$\lambda \approx 0, \quad \varepsilon \approx 0. \tag{2-333}$$

The cubic truncation is not sufficient in this case, because when $\varepsilon = 0$ there is a degeneracy between hexagons and regular triangles (see the discussion of the Boussinesq case). The fourth order terms, and the fifth order term which was

present in the Boussinesq normal form are needed:

$$\dot{z} = z\left[\lambda+(2a+3b)|z|^2+fq\right]+\bar{z}^2\left[\varepsilon+(2d+3e)|z|^2+\tilde{c}q\right]. \qquad (2\text{-}334)$$

The nondegeneracy conditions are

$$(2a+3b)\neq 0,\ \ (2d+3e)\neq 0,\ \text{and}\ (2a+3b)\tilde{c}-(2d+3e)f\neq 0. \qquad (2\text{-}335)$$

Note that the fourth order term, fzq, is included here even though it has no counterpart in the normal forms of the $\mathbb{C}^3$ system (2-271). The explanation is as follows: The analysis below shows that the qualitative behavior of the ODE (3-334) does not depend on $\tilde{c}$ and f separately, but rather on the combination $(2a+3b)\tilde{c}-(2d+3e)f$. Therefore, the term proportional to f can be removed if c is repaced by

$$c \equiv \tilde{c}-\frac{(2d+3e)f}{(2a+3b)}. \qquad (2\text{-}336)$$

In other words, equation (3-334) is equivalent to

$$\dot{z} = z\left[\lambda+(2a+3b)|z|^2\right]+\bar{z}^2\left[\varepsilon+(2d+3e)|z|^2+cq\right]. \qquad (2\text{-}337)$$

Buzano and Golubitsky (1983) eliminated the corresponding fourth order term of the $\mathbb{C}^3$ system, $\dot{z}_1 \propto z_1 q$, in exactly this way to obtain the normal form (2-271).

(3) The final case considered here is when all of the non-Boussinesq terms are small:

$$\lambda\approx 0,\ \ \varepsilon\approx 0,\ \ (2d+3e)\approx 0,\ \text{and}\ f\approx 0. \qquad (2\text{-}338)$$

This corresponds to breaking the Boussinesq symmetry. This case of of major importance because the Boussinesq approximation is often used although it is never exactly valid. The study of symmetry breaking tells what behavior one is likely to find when the symmetry is approximate. Case (2) is not appropriate when the symmetry breaking terms are small, because the nondegeneracy conditions (3-335) require that the fourth order terms $(2d+3e)$ are nonzero, (i.e. not small).

The truncation (3-337) is structurally stable when the non-Boussinesq terms are small, provided the following nondegeneracy conditions hold:

$$(2a+3b)\neq 0,\ \ \tilde{c}\neq 0. \tag{2-339}$$

Note that the organizing center for this case (when $\varepsilon=(2d+3e)=f=0$) is exactly the Boussinesq normal form (2-306)-(2-307). When f is small and $\tilde{c}\neq 0$, the value of c is very close to $\tilde{c}$, so the term proportional to f can be ignored entirely. Therefore, symmetry breaking is described by a codimension-three bifurcation, defined by

$$\lambda=0,\ \ \varepsilon=0,\ \text{ and } (2d+3e)=0. \tag{2-340}$$

Case (1):

The normal form of the transcritical $\mathbf{D}_3$ bifurcation (2-332), written in polar coordinates, $z=re^{i\varphi}$, is

$$\begin{aligned}\dot{r}&=\lambda r+\varepsilon r^2\cos\Phi\\ \dot{\Phi}&=-3\varepsilon r\sin\Phi.\end{aligned} \tag{2-341}$$

(Either φ or $\Phi=3\varphi$ can be used here.)

The solutions are easily found; the Φ equation implies that $\sin\Phi=0$, so that hexagons are the only solutions other than conduction ($z=0$). For the hexagon solutions it is convenient to define

$$x\equiv r\cos\Phi, \tag{2-342}$$

so that

$$x=\begin{cases} r>0 \text{ for } H^+, \text{ and}\\ -r<0 \text{ for } H^-.\end{cases} \tag{2-343}$$

In terms of x, the radial equation is

$$\dot{x}=\lambda x+\varepsilon x^2. \tag{2-344}$$

This is the same as the normal form (2-33) for the transcritical bifurcation. The stationary solutions are

$$x = \frac{-\lambda}{\varepsilon}. \tag{2-345}$$

The stability of the solutions is determined the Jacobian matrix,

$$\mathbf{J} = \begin{pmatrix} \frac{\partial \dot{r}}{\partial r} & \frac{\partial \dot{r}}{\partial \Phi} \\ \frac{\partial \dot{\Phi}}{\partial r} & \frac{\partial \dot{\Phi}}{\partial \Phi} \end{pmatrix}. \tag{2-346}$$

Because the hexagons are invariant under the transformation

$$z \to \bar{z}, \tag{2-347}$$

which is equivalent to

$$\begin{aligned} r &\to r \\ \Phi &\to -\Phi, \end{aligned} \tag{2-348}$$

thus the matrix $\mathbf{J}_H$ commutes with

$$\begin{pmatrix} 1 & 0 \\ 0 & -1 \end{pmatrix}. \tag{2-349}$$

Therefore the eigenvalues of the hexagons are always

$$\left.\frac{\partial \dot{r}}{\partial r}\right|_H, \text{ and } \left.\frac{\partial \dot{\Phi}}{\partial \Phi}\right|_H. \tag{2-350}$$

If the symmetry argument seems too abstract, observe that the off-diagonal elements of $\mathbf{J}$ are proportional to $\sin\Phi$ for the most general $\mathbf{D}_3$-equivariant ODE (2-292). This is zero when evaluated at the hexagons.

For the quadratic truncation (2-341), the eigenvalues of the hexagons are

$$\left.\frac{\partial \dot{r}}{\partial r}\right|_H = \lambda + 2\varepsilon r\cos\Phi = \varepsilon x, \tag{2-351}$$

and

$$\left.\frac{\partial \dot{\Phi}}{\partial \Phi}\right|_H = -3\varepsilon r\cos\Phi = -3\varepsilon x. \tag{2-352}$$

The two eigenvalues have opposite sign, therefore *the hexagons are always unstable at small amplitude.* While the radial part of the system is the same as the one-dimensional transcritical bifurcation of section 2.1, the phase eigenvalue prevents the hexagon solution from being stable. The phase portraits and

$$x = \frac{-\lambda}{\varepsilon}. \tag{2-345}$$

The stability of the solutions is determined the Jacobian matrix,

$$\mathbf{J} = \begin{pmatrix} \frac{\partial \dot{r}}{\partial r} & \frac{\partial \dot{r}}{\partial \Phi} \\ \frac{\partial \dot{\Phi}}{\partial r} & \frac{\partial \dot{\Phi}}{\partial \Phi} \end{pmatrix}. \tag{2-346}$$

Because the hexagons are invariant under the transformation

$$z \to \bar{z}, \tag{2-347}$$

which is equivalent to

$$\begin{aligned} r &\to r \\ \Phi &\to -\Phi, \end{aligned} \tag{2-348}$$

thus the matrix $\mathbf{J}_H$ commutes with

$$\begin{pmatrix} 1 & 0 \\ 0 & -1 \end{pmatrix}. \tag{2-349}$$

Therefore the eigenvalues of the hexagons are always

$$\left.\frac{\partial \dot{r}}{\partial r}\right|_H, \text{ and } \left.\frac{\partial \dot{\Phi}}{\partial \Phi}\right|_H. \tag{2-350}$$

If the symmetry argument seems too abstract, observe that the off-diagonal elements of $\mathbf{J}$ are proportional to $\sin\Phi$ for the most general $\mathbf{D}_3$-equivariant ODE (2-292). This is zero when evaluated at the hexagons.

For the quadratic truncation (2-341), the eigenvalues of the hexagons are

$$\left.\frac{\partial \dot{r}}{\partial r}\right|_H = \lambda + 2\varepsilon r\cos\Phi = \varepsilon x, \tag{2-351}$$

and

$$\left.\frac{\partial \dot{\Phi}}{\partial \Phi}\right|_H = -3\varepsilon r\cos\Phi = -3\varepsilon x. \tag{2-352}$$

The two eigenvalues have opposite sign, therefore *the hexagons are always unstable at small amplitude.* While the radial part of the system is the same as the one-dimensional transcritical bifurcation of section 2.1, the phase eigenvalue prevents the hexagon solution from being stable. The phase portraits and

bifurcation diagrams for (2-341) are drawn in fig. 2-25.

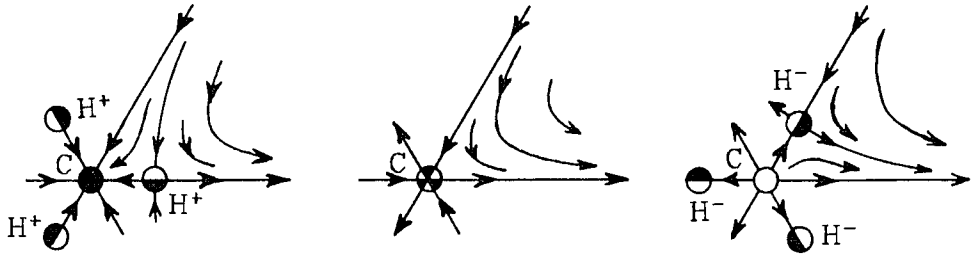

$\lambda<0$ $\varepsilon>0$ | $\lambda=0$ $\varepsilon>0$ | $\lambda>0$ $\varepsilon>0$

Fig. 2-25. Phase portraits of the transcritical $\mathbf{D_3}$ bifurcation (equation (2-341)). Only one sixth of the phase space is shown; the rest of the plane follows from the symmetries (see fig. 2-21). Three hexagons pass through the conduction solution at $\lambda=0$. These hexagons are unstable for λ positive and negative.

Case (2):

Recalling that $q=z^3+\bar{z}^3=2r^3\cos\Phi$, equation (2-337) can be written in polar coordinates;

$$\dot{r}=r\left[\lambda+(2a+b)r^2+f\,2r^3\cos\Phi\right]+r^2\cos\Phi\left[\varepsilon+(2d+3e)r^2+2\tilde{c}r^3\cos\Phi\right] \quad (2\text{-}353)$$

$$\dot{\Phi}=3\dot{\varphi}=-3r\sin\Phi\left[\varepsilon+(2d+3e)r^2+2\tilde{c}r^3\cos\Phi\right]. \quad (2\text{-}354)$$

The solutions are:

- Hexagons ($H^{\pm}$)

$$\lambda+(2a+3b)r^2+r\cos\Phi\left[\varepsilon+(2d+3e+2f)r^2+2\tilde{c}r^3\cos\Phi\right]=0, \quad (2\text{-}355)$$

$$\cos\Phi=\pm 1. \quad (2\text{-}356)$$

- Triangles (T)

$$\lambda+(2a+3b)r^2+2fr^3\cos\Phi=0, \quad (2\text{-}357)$$

$$\varepsilon+(2d+3e)r^2+2\tilde{c}r^3\cos\Phi=0. \quad (2\text{-}358)$$

In terms of $x=r\cos\Phi$ the radial equation for the hexagons becomes

$$\lambda+\varepsilon x+(2a+3b)x^2+(2d+3e+2f)x^3+2\tilde{c}x^4=0. \quad (2\text{-}359)$$

Ignoring the terms of third order and higher, this has the solution

$$x = \frac{-\varepsilon \pm \sqrt{\varepsilon^2 - 4\lambda(2a+3b)}}{2(2a+3b)}. \tag{2-360}$$

There is a saddle-node bifurcation when the hexagon branch "turns around", at

$$\begin{aligned} \lambda_{sn} &= \frac{\varepsilon^2}{4(2a+3b)} + O(\varepsilon^3), \\ x_{sn} &= \frac{-\varepsilon}{2(2a+3b)} + O(\varepsilon^2). \end{aligned} \tag{2-361}$$

As usual, the stability is determined by the Jacobian matrix (2-346), where

$$\frac{\partial \dot{r}}{\partial r} = \lambda + 2\varepsilon r\cos\Phi + 3(2a+3b)r^2 + 4(2d+3e+2f)\cos\Phi\, r^3 + 10\tilde{c}\cos^2\Phi\, r^4, \tag{2-362}$$

$$\frac{\partial \dot{r}}{\partial \Phi} = r^2(-\sin\Phi)\left[\varepsilon + (2d+3e+2f)r^2 + 4\tilde{c}r^3\cos\Phi\right], \tag{2-363}$$

$$\frac{\partial \dot{\Phi}}{\partial r} = -3\sin\Phi\left[\varepsilon + 3(2d+3e)r^2 + 8\tilde{c}r^3\cos\Phi\right], \text{ and} \tag{2-364}$$

$$\frac{\partial \dot{\Phi}}{\partial \Phi} = -3r\cos\Phi\left[\varepsilon + (2d+3e)r^2 + 2\tilde{c}r^3\cos\Phi\right] + 6\tilde{c}r^4\sin^2\Phi. \tag{2-365}$$

The stability of the hexagons is easy to calculate in polar coordinates. The eigenvalues of $\mathbf{J}_H$ are

$$\left.\frac{\partial \dot{r}}{\partial r}\right|_H = x\left[\varepsilon + 2(2a+3b)x\right] + O(x^3), \text{ and} \tag{2-366}$$

$$\left.\frac{\partial \dot{\Phi}}{\partial \Phi}\right|_H = -3x\left[\varepsilon + (2d+3e)x^2 + 2\tilde{c}x^3\right]. \tag{2-367}$$

The radial eigenvalue changes sign at x_{sn}, where the saddle-node bifurcation occurs. Outside the interval between $x = 0$ and x_{sn}, the radial eigenvalue has the same sign as $2a+3b$. Inside this interval, the sign of the radial eigenvalue is the same as the sign of εx.

The phase eigenvalue (2-367) is more subtle. When $\varepsilon = 0$, and $2d+3e \neq 0$, the hexagons are the only small amplitude solution, and the phase eigenvalue is

$$-3x(2d+3e) + O(x^4) \tag{2-368}$$

When $\varepsilon \neq 0$ and the sign of ε is opposite the sign of $2d+3e$, the phase eigenvalue changes sign at

$$x^2 = \frac{-\varepsilon}{2d+3e} + O(\varepsilon^{3/2}), \tag{2-369}$$

where the correction term is different for the two types of hexagons. When the phase eigenvalue of the hexagons passes through zero there is a saddle node bifurcation, and a branch of triangles is created. The conditions for this pitchfork are therefore the same as the conditions that a triangle exists with $\cos\Phi = \pm 1$ (see equations (2-357) and (2-358)):

$$\lambda + (2a+3b)x^2 + 2fx^3 = 0 \tag{2-370}$$

$$\varepsilon + (2d+3e)x^2 + 2\tilde{c}x^3 = 0. \tag{2-371}$$

When the bifurcation diagrams are drawn, ε is thought of as a fixed parameter while λ is varied, so it is advantageous to find $\lambda_\pm$ as a function of ε, where λ_+ and λ_- are the λ values where the triangles collide with the H^+ and H^- branches, respectively. When $(2d+3e)$ is not near zero, one can solve (2-371) for x^2 and x^3:

$$x^2 = \frac{-\varepsilon}{(2d+3e)} - \frac{2\tilde{c}x^3}{(2d+3e)}. \tag{2-372}$$

$$x^3 = \pm\left(\frac{-\varepsilon}{(2d+3e)}\right)^{\frac{3}{2}} + \cdots, \tag{2-373}$$

This can then be inserted into (2-370) to find

$$\begin{aligned}\lambda &= -(2a+3b)\left(\frac{-\varepsilon}{(2d+3e)} - \frac{2\tilde{c}x^3}{(2d+3e)}\right) - 2fx^3 \\ &= \frac{(2a+3b)}{(2d+3e)}\varepsilon + \left(\frac{(2a+3b)\tilde{c}}{(2d+3e)} - f\right)2x^3.\end{aligned} \tag{2-374}$$

The result is

$$\lambda_\pm = \frac{(2a+3b)}{(2d+3e)}\left(\varepsilon \pm 2c\left(\frac{-\varepsilon}{(2d+3e)}\right)^{\frac{3}{2}}\right), \tag{2-375}$$

where c is defined in equation (2-336). The two curves, λ_+ and λ_-, are tangent at the origin of the λ-ε plane, and they open up to a horn-shaped region as shown in fig. 2-26. When $(2d+3e) \approx 0$, the above argument breaks down. Assum-

ing $(2a+3b)$ is not near zero, a similar procedure leads to

$$\varepsilon_{\pm} = \frac{(2d+3e)}{(2a+3b)}\lambda \pm (-2c)\left[\frac{-\lambda}{(2a+3b)}\right]^{\frac{3}{2}}. \tag{2-376}$$

This version of the lines defining the horn is valid even when $(2d+3e)=0$. Note that the combination $(2a+3b)\tilde{c}-(2d+3e)f$ is proportional to the width of the horn.

Next, the stability of the triangles is computed. The Jacobian matrix, evaluated at the triangle solutions, is not diagonal because $\sin\Phi \neq 0$. The elements of the Jacobian matrix are

$$\left.\frac{\partial \dot{r}}{\partial r}\right|_{T} = 2(2a+3b)r^2 + O(r^3), \tag{2-377}$$

$$\left.\frac{\partial \dot{r}}{\partial \Phi}\right|_{T} = -2r^4\sin\Phi(f+\tilde{c}r\cos\Phi), \tag{2-378}$$

$$\left.\frac{\partial \dot{\Phi}}{\partial r}\right|_{T} = -6r^2\sin\Phi\left[(2d+3e)+3r\cos\Phi\right], \text{ and} \tag{2-379}$$

$$\left.\frac{\partial \dot{\Phi}}{\partial \Phi}\right|_{T} = 6\tilde{c}r^4\sin^2\Phi, \tag{2-380}$$

The phase eigenvalue is much smaller than the radial eigenvalue, so the technique described in section 2.8.3 works here: The trace of $\mathbf{J}_T$ is

$$\mathrm{Tr}\,\mathbf{J}_T = 2(2a+3b)r^2 + O(r^3), \tag{2-381}$$

and the determinant is

$$\mathrm{Det}\,\mathbf{J}_T = 12r^6\sin^2\Phi\left[(2a+3b)\tilde{c}-(2d+3e)f\right] + O(r^7). \tag{2-382}$$

The matrix satisfies the inequality $|\mathrm{Det}\,\mathbf{J}_T| \ll (\mathrm{Tr}\,\mathbf{J}_T)^2$; therefore the eigenvalues are approximately

$$\mathrm{Tr}\,\mathbf{J}_T, \text{ and } \frac{\mathrm{Det}\,\mathbf{J}_T}{\mathrm{Tr}\,\mathbf{J}_T} = 6r^4c\sin^2\Phi + O(r^5). \tag{2-383}$$

This completes the analysis of case (2). The phase portraits for the various regions of fig. 2-26 are drawn in fig. 2-27, and the bifurcation diagrams are drawn in fig. 2-28.

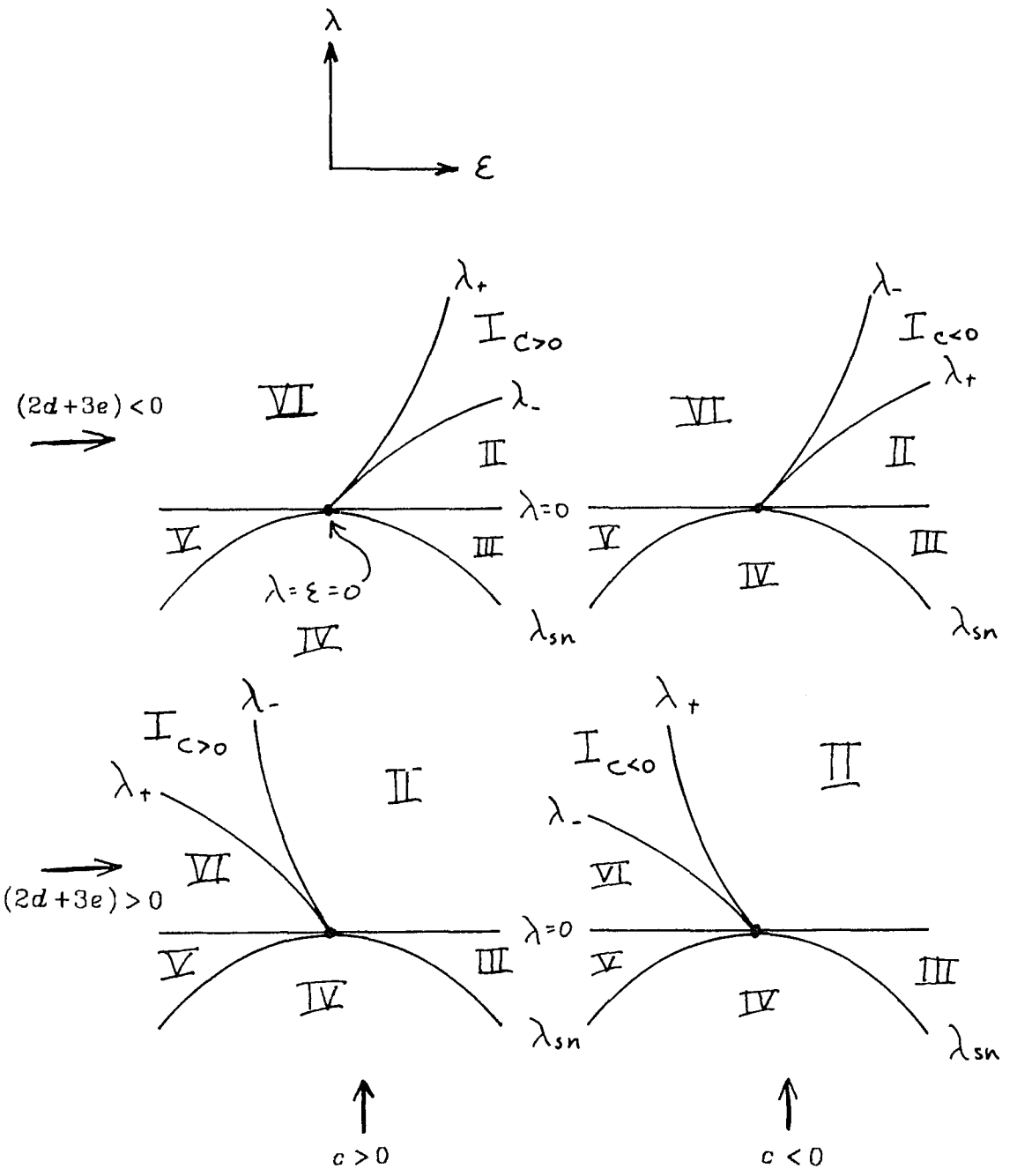

Fig. 2-26. The unfolding space of the codimension-two $\mathbf{D}_3$-symmetric bifurcation (2-334) at $\lambda = \varepsilon = 0$. The coefficients, $2a+3b$, $\tilde{c}$, f, and $2d+3e$ are fixed, and $(2a+3b) < 0$ in all cases. Note that the coefficient c, rather than $\tilde{c}$ and f, is important (see equation (2-336).)

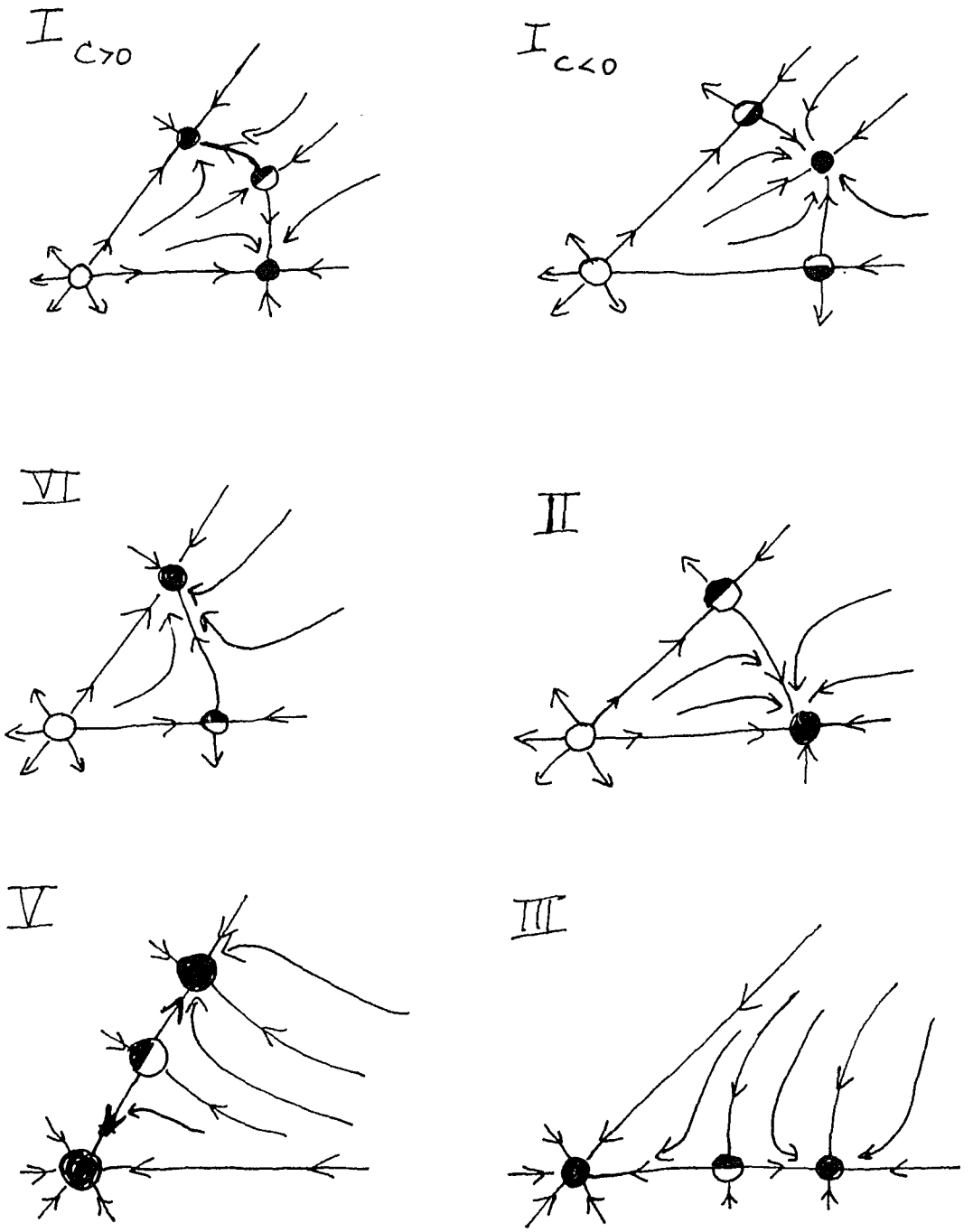

Fig. 2-27. The phase portraits of equation (2-334) corresponding to the regions in fig. 2-26. The phase portrait in region IV is not drawn because it is trivial: all the trajectories approach the conduction solution at $z = 0$.

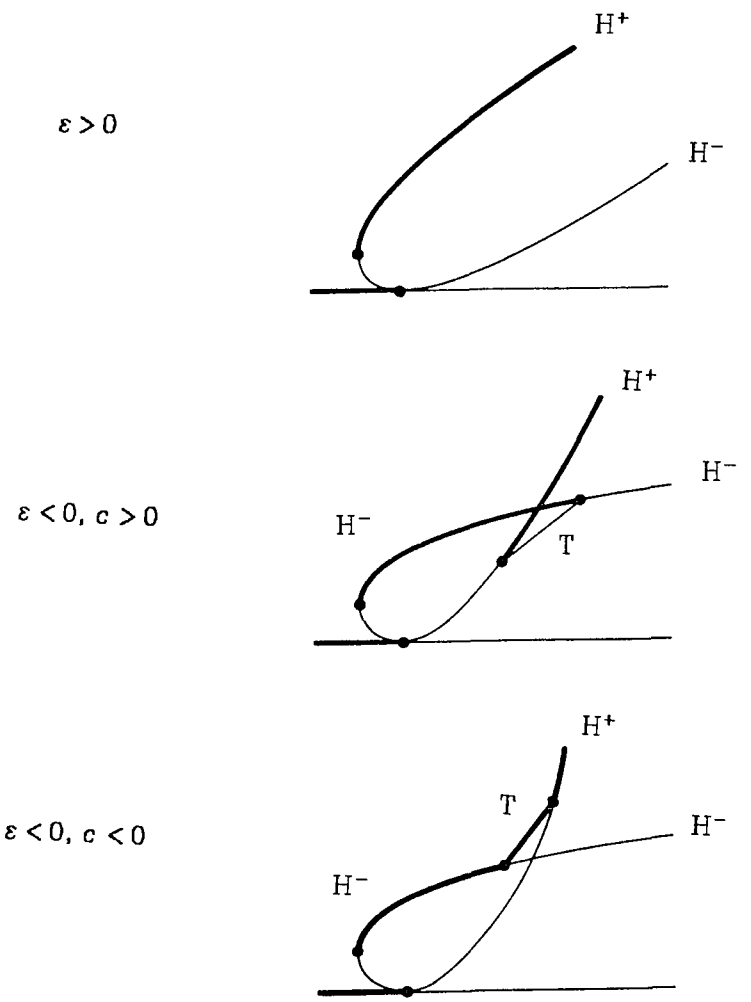

Fig. 2-28. The bifurcation diagrams, which plot A^2 vs. λ, of equation (2-334). In all cases, $(2a+3b)>0$ so that the solutions are generally supercritical, and $(2d+3e)>0$ so that H^+ is the stable solution at "large" amplitude. These diagrams are drawn for the case where $f=0$, thus $c=\tilde{c}$. The slope of the triangle branch depends on f and $\tilde{c}$, although the stability of the solution and the ordering of the bifurcations only depends on c (defined in equation (2-336).) The diagram for $\varepsilon=0$, which is not shown, has the two hexagon solutions bifurcating with the same slope at the origin, and H^+ is always stable.

Case (3):

The previous discussion was general enough to apply to the final case, where all of the even order terms are small. When $(2d+3e)$ is small, the horn-shaped region opens almost vertical in the ε-λ diagrams, as shown in fig. 2-29. This causes no further degeneracies, however.

Note that the coefficient f was only important through the combination

$$(2a+3b)\tilde{c}-(2d+3e)f\ . \tag{2-384}$$

In the present case both $(2d+3e)$ and f are small, therefore f does not effect the qualitative results. In the following analysis, no distinction is made between c and $\tilde{c}$.

When $\varepsilon = 0$ there is a branch of triangle solutions which is created at

$$x = \frac{-(2d+3e)}{2c}. \tag{2-385}$$

In case (2), this branch was not present in the analysis because it was at too large an amplitude. When $(2d+3d)$ is in the neighborhood of zero, this branch is captured by the local analysis. In other words, one boundary of the horn-shaped region, $\varepsilon = \varepsilon_{\pm}$ in the λ-ε plane, intersects the $\varepsilon = 0$ line at small λ. Therefore, when the bifurcation diagrams are drawn for fixed $\varepsilon \approx 0$, the paths always go into the horn shaped region at small λ, and the bifurcation diagrams always contain triangle solutions.

An alternative way of displaying the results is to plot the regions in the ε-$(2d+3e)$ plane where the bifurcation diagrams are qualitatively similar. The sign of ε is obviously important. Another curve in the ε-$(2d+3e)$ plane is determined by the parameter values where two pitchfork bifurcation of the phase eigenvalue coalesce. This corresponds to the paths in ε-λ space which are tangent to the $\varepsilon_{\pm}$ curves, as shown in fig. 2-29. This happens at the value of ε where there is a double root of the cubic equation which determines the phase eigenvalue:

$$\varepsilon+(2d+3e)x^2+2cx^3=0. \tag{2-386}$$

The double root is determined by the simultaneous vanishing of (2-386) and its derivative,

$$(2d+3e)2x+6cx^2=0. \tag{2-387}$$

This last equation has two roots,

$$x=0, \text{ and } x=\frac{-1}{3}\frac{(2d+3e)}{c}. \tag{2-388}$$

When $x=0$ is inserted into equation (2-386), one finds that this double root only occurs when $\varepsilon=0$. This is just the tip of the horn. When the nontrivial root is inserted into equation (2-386) one finds that

$$\varepsilon+\frac{1}{27}\frac{(2d+3e)^3}{c^2}=0. \tag{2-389}$$

Therefore the ε-$(2d+3e)$ plane is divided into four regions, as shown in fig. 2-30. The bifurcation diagrams, for each of these regions, are shown in fig. 2-31.

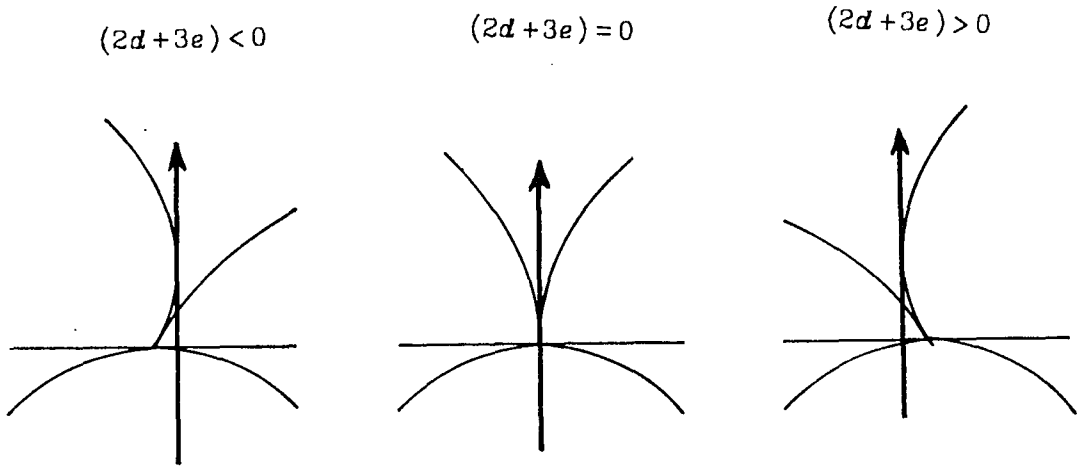

Fig. 2-29. The λ-ε unfolding space of equation (2-334) when $(2d+3e)$ is small. (Compare to fig. 2-26.) The other parameters are $(2a+3b)<0$ and $c<0$. The horn-shaped region, where the triangle solutions exist, opens vertically when $(2d+3e)=0$. The arrows indicate paths which are tangent to the λ_+ or λ_- curve. These tangencies occur at $\varepsilon = \frac{-1}{27}\frac{(d+e)^3}{c^2}$. These paths correspond to the boundaries between regions 1 and 2, or regions 3 and 4, in fig. 2-30. The bifurcation diagrams for these paths are shown in fig. 2-31.

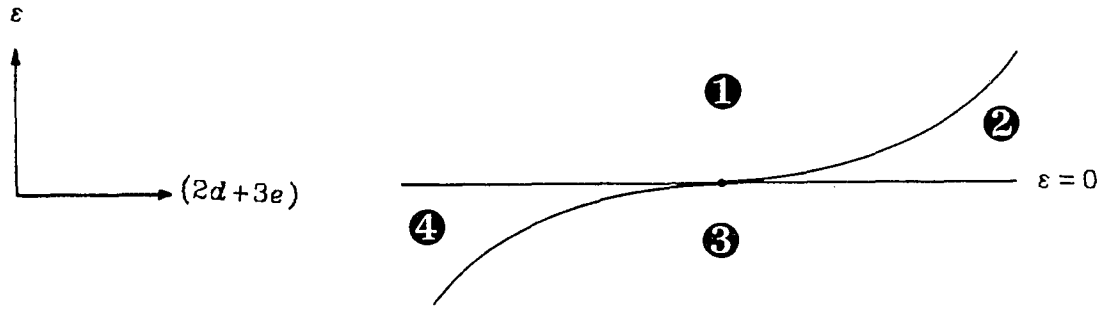

$$\varepsilon = \frac{-1}{27}\frac{(2d+3e)^3}{c^2}$$

Fig. 2-30. The unfolding space for the bifurcation diagrams of equation (2-334) when the Boussinesq symmetry is slightly broken. In the thin regions, 2 and 4, the fourth order terms dominate the quadratic terms.

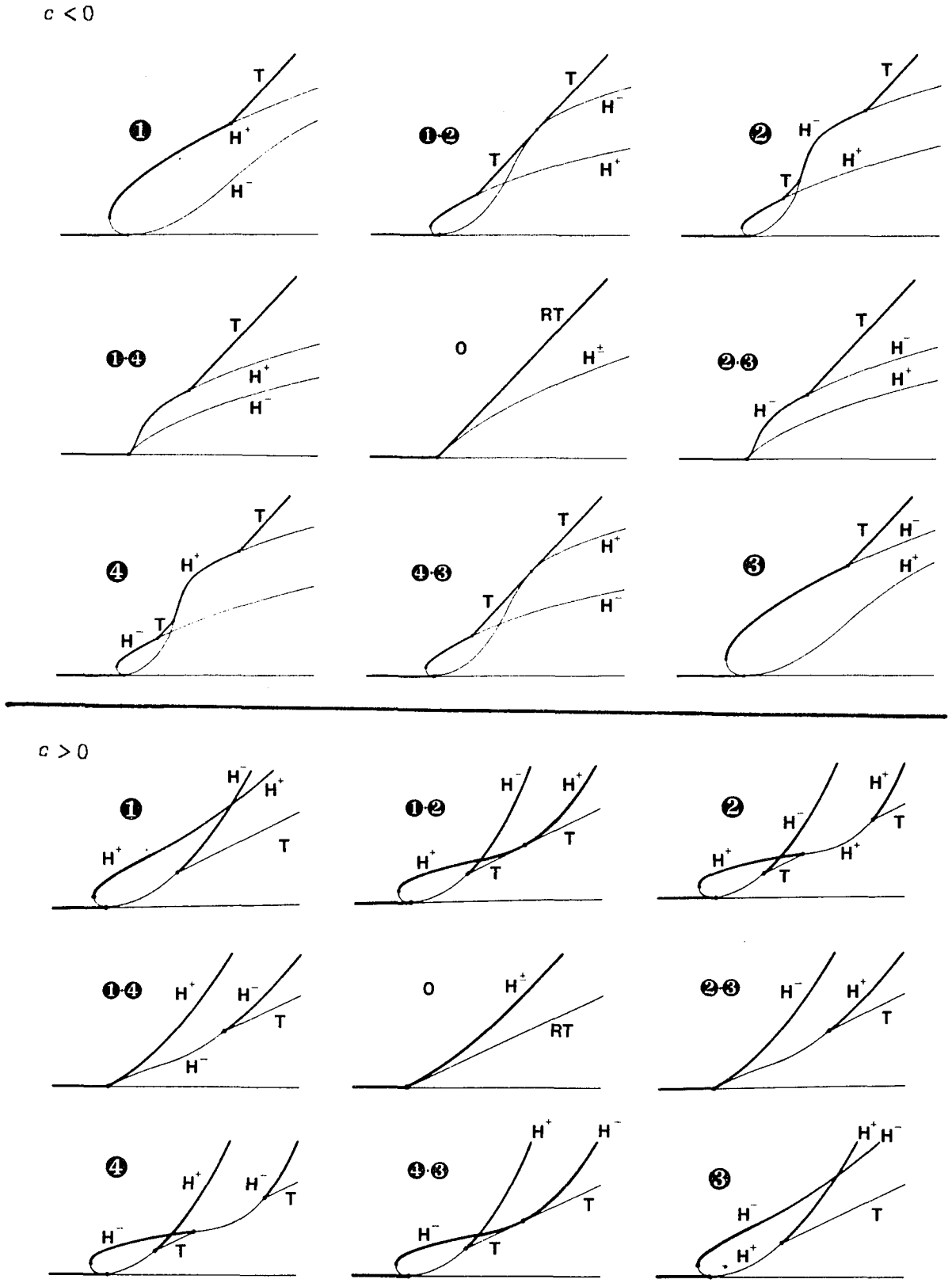

Fig. 2-31. The bifurcation diagrams (A^2 vs. λ) for equation (2-334), with $(2b+3b)<0$ and all of the even order coefficients small. The coefficients ε and $(2d+3e)$ are indicated by the numbered regions of fig. 2-30.

The real subspace

The remainder of the analysis is for the real subspace. The truncation of the ODE (2-271) to third order is sufficient here; the fourth and fifth order terms are only needed to capture the subtleties of the phase. All the solutions which exist for $A^2 \leq O(\varepsilon^2)$ can be made real by a suitable choice of the origin using $\mathbf{x} \to \mathbf{x}+\mathbf{d}$. The hexagons of both types are present in the real subspace, and the effect of the quadratic term on the hexagons is faithfully carried over by letting

$$\dot{z}_1 = \varepsilon \bar{z}_2 \bar{z}_3 \to \dot{x}_1 = \varepsilon x_2 x_3 . \tag{2-390}$$

The third order truncation of (2-271), restricted to the real subspace, is

$$\dot{x}_1 = x_1\left[\lambda + a(x_2^2 + x_3^2) + bA^2\right] + \varepsilon x_2 x_3 . \tag{2-391}$$

The equations for $\dot{x}_2$ and $\dot{x}_3$ follow from the permutation symmetry. The real equations have the symmetry of the tetrahedron when $\varepsilon \neq 0$, and the symmetry of the cube when $\varepsilon = 0$. See Appendix B for a discussion of this symmetry, as well as the symmetry of the real subspace in the case of rotating Boussinesq and non-Boussinesq convection on the hexagonal lattice.

The solutions of the third order system are listed here in canonical form:

- Conduction (C)

$$A^2 = 0 \tag{2-392}$$

- Rolls (R)

$$x_1^2 = A^2, \quad x_2^2 = x_3^2 = 0 \tag{2-393}$$

$$A^2 = \frac{-\lambda}{b} \tag{2-394}$$

- Hexagons ($H^{\pm}$)

$$x_1^2 = x_2^2 = x_3^2 = \tfrac{1}{3}A^2 \tag{2-395}$$

$$x_1 = x_2 = x_3 \equiv x \quad \begin{cases} x > 0 \text{ for } H^+ \\ x < 0 \text{ for } H^- \end{cases} \tag{2-396}$$

$$x = \frac{-\varepsilon \pm \sqrt{\varepsilon^2 - 4\lambda(2a+3b)}}{2(2a+3b)} \tag{2-397}$$

• Rectangles (RA)

$$x_1 \neq x_2 = x_3, \quad A^2 = x_1^2 + 2x_2^2. \tag{2-398}$$

The calculation of the amplitude of the rectangles is difficult enough that it is done here. Two equations are needed for the rectangles;

$$\dot{x}_1 = x_1(\lambda + 2ax_2^2 + bA^2) + \varepsilon x_2^2 \tag{2-399}$$

$$\dot{x}_2 = x_2\left(\lambda + \varepsilon x_1 + a(x_1^2 + x_2^2) + bA^2\right). \tag{2-400}$$

Cross multiplying, one finds

$$0 = x_1\dot{x}_2 - x_2\dot{x}_1 = (x_1^2 - x_2^2)x_2(\varepsilon + ax_1). \tag{2-401}$$

If $x_1^2 = x_2^2$ then this is a hexagon solution. If $x_2 = 0$ then this is a roll solution. Therefore, the rectangles have

$$x_1 = \frac{-\varepsilon}{a}. \tag{2-402}$$

Now x_1 can be inserted into equation (2-399) to find

$$x_2^2 = \frac{-(\lambda - \lambda_p)}{a+2b}, \tag{2-403}$$

where

$$\lambda_p = \frac{-b\,\varepsilon^2}{a^2}. \tag{2-404}$$

The rectangles are created when the rolls undergo a pitchfork bifurcation at $\lambda = \lambda_p$. This is discussed below after the stability of the rolls is determined. The amplitude of the rectangles is linear in λ:

$$A^2 = \frac{\varepsilon^2}{a^2} + \frac{\lambda_p - \lambda}{\frac{1}{2}a + b} > \frac{\varepsilon^2}{a^2}. \tag{2-405}$$

These rectangles are different than the rectangles on the rhombic lattice since there are three nonzero amplitudes. On the rhombic lattice, however, there are second-order modes, with vertical "quantum number " $n = 1$, which are similar to the third critical amplitude on the hexagonal lattice.

The stability of the solutions is given by the eigenvalues of the Jacobian matrix,

$$\mathbf{J}=\begin{bmatrix} \begin{matrix}\lambda+a(x_2^2+x_3^2)+bA^2\\ +2bx_1^2\end{matrix} & 2(a+b)x_1x_2+\varepsilon x_3 & 2(a+b)x_1x_3+\varepsilon x_2 \\ * & \begin{matrix}\lambda+a(x_1^2+x_3^2)+bA^2\\ +2bx_2^2\end{matrix} & 2(a+b)x_2x_3+\varepsilon x_1 \\ * & * & \begin{matrix}\lambda+a(x_1^2+x_2^2)+bA^2\\ +2bx_3^2\end{matrix} \end{bmatrix}, \quad (2\text{-}406)$$

where the matrix is symmetric, so the terms below the diagonal are not written. The symmetry of the matrix is a consequence of the truncation. When higher order terms (for instance $\dot{x}_1 = x_1x_2^4$) are added, $\mathbf{J}$ is not a symmetric matrix.

- When evaluated at the conduction solution, the Jacobian matrix is

$$\mathbf{J}_C=\begin{bmatrix}\lambda & 0 & 0\\ 0 & \lambda & 0\\ 0 & 0 & \lambda\end{bmatrix}. \quad (2\text{-}407)$$

The eigenvalues of the real system are $(\lambda)\times 3$, i.e. λ has multiplicity 3. For the complex system the multiplicity of the eigenvalue is six.

- The Jacobian matrix, evaluated at the rolls, is

$$\mathbf{J}_R=\begin{bmatrix}2bx_1^2 & 0 & 0\\ 0 & ax_1^2 & \varepsilon x_1\\ 0 & \varepsilon x_1 & ax_1^2\end{bmatrix}. \quad (2\text{-}408)$$

The eigenvectors are

$$\begin{bmatrix}1\\0\\0\end{bmatrix}, \begin{bmatrix}0\\1\\1\end{bmatrix}, \text{ and } \begin{bmatrix}0\\-1\\1\end{bmatrix}. \quad (2\text{-}409)$$

The corresponding eigenvalues of the real system are

$$2bA^2, \ ax_1^2+\varepsilon x_1, \text{ and } ax_1^2-\varepsilon x_1. \quad (2\text{-}410)$$

In the complex system, the eigenvalues are

$$2bA^2, \ \left(aA^2+\varepsilon\sqrt{A^2}\right)\times 2, \left(aA^2-\varepsilon\sqrt{A^2}\right)\times 2, \text{ and } 0. \quad (2\text{-}411)$$

It is clear that the x_1 roll must treat the real and imaginary parts of z_2 and z_3 equivalently; this gives the double eigenvalues. The zero eigenvalue comes from

the translation in the $\mathbf{k}_1$ direction.

One of the eigenvalues of $\mathbf{J}_R$ changes sign when

$$\lambda = \lambda_p\,, \quad A^2 = (A^2)_p = \left(\frac{\varepsilon}{a}\right)^2. \tag{2-412}$$

At this bifurcation the rectangles are created (see equation (2-404)). In the real system this is a pitchfork bifurcation, and in the complex system this is a pitchfork of revolution. The normal form of a pitchfork of revolution is

$$\dot{z} = \lambda z \pm z\,|\,z\,|^2. \tag{2-413}$$

This normal form has $O(2)$ symmetry in the plane, generated by

$$z \to \bar{z}\,, \tag{2-414}$$

and

$$z \to e^{i\varphi} z \tag{2-415}$$

for *any* angle φ. In the present problem, any phase of z_2 is possible when the rectangles bifurcate off the z_1 rolls. The phase of z_3 is then determined by the condition

$$\cos\Phi = -\mathrm{sgn}(a)\,. \tag{2-416}$$

- The Jacobian matrix for the hexagons is

$$\mathbf{J}_H = \begin{bmatrix} A & B & B \\ B & A & B \\ B & B & A \end{bmatrix}, \tag{2-417}$$

where

$$A = 2bx^2 - \varepsilon x\,, \text{ and} \tag{2-418}$$

$$B = 2(a+b)x^2 + \varepsilon x\,. \tag{2-419}$$

The eigenvectors of this matrix are

$$\begin{bmatrix} 1 \\ 1 \\ 1 \end{bmatrix}, \begin{bmatrix} -1 \\ 1 \\ 0 \end{bmatrix}, \text{ and } \begin{bmatrix} 0 \\ -1 \\ 1 \end{bmatrix}. \tag{2-420}$$

The corresponding eigenvalues are

$$A + 2B = \left[2(2a+3b)x^2 + \varepsilon x\right], \tag{2-421}$$

and a double eigenvalue:

$$A-B=-2(ax^2+\varepsilon x). \tag{2-422}$$

The radial eigenvalue (2-421) has been discussed in the section on the equal amplitude solutions. The double eigenvalue (2-422) changes sign at

$$\lambda_t=\frac{-(a+3b)}{a^2}\varepsilon^2,\quad x_t=\frac{-\varepsilon}{a}. \tag{2-423}$$

At this amplitude the three rectangles collide with the each hexagon in a $\mathbf{D}_3$ transcritical bifurcation. Here the $\mathbf{D}_3$ symmetry is generated by

$$\begin{aligned}&(x_1,x_2,x_3)\to(x_2,x_3,x_1),\text{ and}\\&(x_1,x_2,x_3)\to(x_1,x_3,x_2).\end{aligned} \tag{2-424}$$

This is the same type of bifurcation as the one in which the three hexagons collide with the conduction solution in the $\mathbf{D}_3$ transcritical bifurcation (2-332). This equivalence is discussed further after the stability of the rectangles is computed.

In the complex system, there are two zero eigenvalues corresponding to the two translations. The sixth and final eigenvector is from the phase, see equation (2-367). Therefore the eigenvalues of the hexagons are

$$\begin{aligned}&2\left[(2a+3b)x^2+\varepsilon x\right],\ \left[-2(ax^2+\varepsilon x)\right]\times 2,\\&-3x\left[\varepsilon+(2d+3e)x^2+2\tilde{c}x^3\right],\text{ and }(0)\times 2.\end{aligned} \tag{2-425}$$

• The Jacobian matrix, evaluated at the rectangles with $x_1=-\varepsilon/a$, is

$$\mathbf{J}_{RA}=\begin{bmatrix}A & B & B\\ B & C & D\\ B & D & C\end{bmatrix}, \tag{2-426}$$

where

$$\begin{aligned}A&=\frac{2b\varepsilon^2}{a^2}+ax_2{}^2,\\ B&=\left[\frac{-(a+2b)}{a}\right]\varepsilon x_2,\\ C&=\frac{\varepsilon^2}{a}+2bx_2{}^2,\text{ and}\\ D&=2(a+b)x_2{}^2-\frac{\varepsilon^2}{a}.\end{aligned} \tag{2-427}$$

The eigenvectors of this matrix are not obvious, with the exception of

$$\begin{bmatrix} 0 \\ 1 \\ -1 \end{bmatrix}. \tag{2-428}$$

Since the matrix is symmetric, the eigenvalues are real, and the eigenvectors are orthogonal. The problem can be reduced to finding the eigenvalues of a two by two matrix in this plane as follows. The eigenvalues of $\mathbf{J}$ are invariant under a similarity transformation

$$\mathbf{J} \rightarrow \mathbf{S}^{-1} \cdot \mathbf{J} \cdot \mathbf{S}. \tag{2-429}$$

In order to isolate the known eigenvalue, the first column of $\mathbf{S}$ is chosen to be the known eigenvector. The other columns are chosen to make $\mathbf{S}$ the orthogonal matrix which diagonalizes $\mathbf{J}$ when $B = 0$.

$$\mathbf{S} = \frac{1}{\sqrt{2}} \begin{bmatrix} 0 & \sqrt{2} & 0 \\ 1 & 0 & 1 \\ -1 & 0 & 1 \end{bmatrix} \tag{2-430}$$

The inverse is

$$\mathbf{S}^{-1} = \frac{1}{\sqrt{2}} \begin{bmatrix} 0 & 1 & -1 \\ \sqrt{2} & 0 & 0 \\ 0 & 1 & 1 \end{bmatrix}, \tag{2-431}$$

and the result of the similarity transformation is

$$\mathbf{S}^{-1} \cdot \mathbf{J}_{RA} \cdot \mathbf{S} = \begin{bmatrix} (C-D) & 0 & 0 \\ 0 & A & \sqrt{2}B \\ 0 & \sqrt{2}B & C+D \end{bmatrix}. \tag{2-432}$$

The obvious eigenvalue is

$$C - D = \frac{2}{a}\left[\varepsilon^2 - (ax_2)^2\right]. \tag{2-433}$$

This eigenvalue changes sign once, precisely where the rectangle solutions collide with the hexagons.

The eigenvalues of the two by two block,

$$\begin{bmatrix} A & \sqrt{2}B \\ \sqrt{2}B & C+D \end{bmatrix}, \tag{2-434}$$

can be found by taking its determinant and trace. The trace of (2-434) is

$$\mathrm{Tr} \equiv A+C+D = (3a+4b)x_2^2 + \frac{b\varepsilon^2}{a^2}, \tag{2-435}$$

and the determinant is

$$\mathrm{Det} \equiv A(C+D)-2B^2 = \frac{2}{a}(a+2b)x_2^2\left[(ax_2)^2-\varepsilon^2\right]. \tag{2-436}$$

The eigenvalues of the two by two block are

$$\tfrac{1}{2}\mathrm{Tr} \pm \left[(\tfrac{1}{2}\mathrm{Tr})^2-\mathrm{Det}\right]^{\frac{1}{2}}. \tag{2-437}$$

This form of the eigenvalues is not very convenient. All that is really important are the signs of the eigenvalues, and the following observations allow the signs to be determined.

The eigenvalues can be thought of as functions of x_2^2. As x_2^2 ranges from 0 to greater than of order ε^2 the determinant changes sign exactly once. When the rectangles first bifurcate off the rolls, $x_2^2 \ll \varepsilon^2 \ll 1$, and $|\mathrm{Det}| \ll (\mathrm{Tr})^2$. As a consequence, the eigenvalues are approximately

$$\begin{aligned} C-D &\approx \frac{2\varepsilon^2}{a} \\ \mathrm{Tr} &\approx \frac{b\varepsilon^2}{a^2}, \text{ and} \\ \frac{\mathrm{Det}}{\mathrm{Tr}} &\approx \frac{-2a(a+2b)x_2^2}{b}. \end{aligned} \tag{2-438}$$

On the other hand, when $\varepsilon^2 \ll x_2^2 \ll 1$, the matrix is almost diagonal, and the eigenvalues are

$$\begin{aligned} C-D &\approx -2ax_2^2 \\ A &\approx ax_2^2, \text{ and} \\ C+D &= 2(a+2b)x_2^2. \end{aligned} \tag{2-439}$$

The determinant is zero when the rectangles collide with the hexagons, at which point the eigenvalues are

$$\begin{aligned} C-D &= 0, \\ \mathrm{Det} &= 0, \text{ and} \\ \mathrm{Tr} &= 2(a+2b)\frac{\varepsilon^2}{a^2}. \end{aligned} \tag{2-440}$$

The result is simple. In both cases (2-438) and (2-439) the signs of the eigenvalues of the rectangles are

$$+1, -1, \text{ and } \operatorname{sgn}(a+2b). \tag{2-441}$$

The only time an eigenvalue can go through through zero is when the determinant vanishes. This happens when three rectangle solutions collide with a hexagon solution in a transcritical bifurcation with $\mathbf{D}_3$ symmetry. This bifurcation was studied for case (1) above (see fig. 2-25). In the present context, the symmetry comes from the permutation group of z_1, z_2, and z_3. The hexagons in fig. 2-25 correspond to the rectangles here, and the conduction solution in fig. 2-25 corresponds to the hexagon. Note that, in the present context, the number of positive and negative eigenvalues of the rectangles is the same before and after the bifurcation, while two eigenvalues of the hexagons change sign. At the bifurcation, the eigenvalues of the rectangles are given by (2-440); for all other parameter values the results of equation (2-441) hold.

In the complex system, the phase Φ of the rectangles is defined since all three amplitudes are nonzero. As a consequence there are two zero eigenvalues corresponding to the two translations, and there is a phase eigenvalue. In order to calculate the phase eigenvalue, first note that the rectangles are real solutions, meaning that $\sin\Phi = 0$, so that

$$\left.\frac{\partial \dot{r}_\alpha}{\partial \Phi}\right|_{\sin\Phi=0} = \left.\frac{\partial \dot{\Phi}}{\partial r_\alpha}\right|_{\sin\Phi=0} = 0 \tag{2-442}$$

for $\alpha = 1$, 2, and 3. Therefore the phase eigenvalue is

$$\frac{\partial \dot{\Phi}}{\partial \Phi} \tag{2-443}$$

Assuming $|z_2|^2 = |z_3|^2$, equation (2-266) for $\dot{\varphi}_1$ and the implied equation for $\dot{\varphi}_2$ are

$$\dot{\varphi}_1 = \frac{1}{2i|z_1|^2}(\bar{z}_1\bar{z}_2\bar{z}_3 - z_1z_2z_3)\left[\varepsilon + O(A^2)\right] \tag{2-444}$$

$$= \frac{-\sin\Phi\,|z_1|\,|z_2|^2}{|z_1|^2}\varepsilon\cdots, \tag{2-445}$$

$$\dot{\varphi}_2 = \frac{1}{2i\,|z_2|^2}(\bar{z}_1\bar{z}_2\bar{z}_3 - z_1z_2z_3)\left[\varepsilon + O(A^2)\right]. \tag{2-446}$$

$$= -\sin\Phi\,|z_1|\,\varepsilon + \cdots. \tag{2-447}$$

Therefore,

$$\dot{\Phi} = \dot{\varphi}_1 + 2\dot{\varphi}_2 = -\sin\Phi\,\varepsilon\left(\frac{|a|}{|\varepsilon|}|z_2|^2 + 2\frac{|\varepsilon|}{|a|}\right), \tag{2-448}$$

and the phase eigenvalue is

$$-\cos\Phi\,\varepsilon\left(\frac{|a|}{|\varepsilon|}|z_2|^2 + 2\frac{|\varepsilon|}{|a|}\right). \tag{2-449}$$

Note that a requirement for a stationary solution is that $\sin\Phi = 0$, so that $\cos\Phi = \pm 1$. Only one of these corresponds to the rectangles, however. From equations (2-398) and (2-402), the rectangles satisfy

$$\mathrm{sgn}(x_1x_2x_3) = \mathrm{sgn}\left(\frac{-\varepsilon}{a}\right), \tag{2-450}$$

when the amplitudes are real. This implies in general that

$$\cos(\Phi) = -\mathrm{sgn}\left(\frac{\varepsilon}{a}\right) \tag{2-451}$$

for the rectangles, so the phase eigenvalue is

$$a\,|z_2|^2 + 2\frac{\varepsilon^2}{a}. \tag{2-452}$$

The sign of the phase eigenvalue is $\mathrm{sgn}(a)$. This agrees with the phase eigenvalue implicitly given by Buzano & Golubitsky (1983, p. 635).

In the limit that $\varepsilon \to 0$, all of the eigenvalues of the rectangles are of order $|z_2|^2$, and they agree with the the results of table 2-7 for the Boussinesq rectangles. Therefore, in the degenerate case where $\varepsilon = 0$, but the Boussinesq symmetry does not hold, the fourth (and higher) order terms do not change the signs of the eigenvalues of the rectangles. (The fourth order terms contribute to the eigenvalues at order three.) This concludes the calculation of the

eigenvalues of the rectangles.

Two eigenvalues of the triangles remain to be calculated. The radial and the phase eigenvalues were calculated in the previous section, and two eigenvalues are zero due to the translational symmetry. In the Boussinesq case, the remaining two eigenvalues are

$$-\tfrac{2}{3}aA^2, \tag{2-453}$$

and the eigenvectors are in the the plane which is perpendicular to the radial eigenvector in the three-dimensional imaginary subspace. A calculation shows that these eigenvalues are not changed significantly in the non-Boussinesq case. The eigenvalues of the triangles are

$$\tfrac{2}{3}(2a+b)A^2+O(r^3),\ \tfrac{2}{3}cA^2\sin^2\Phi+O(r^5),\ \left[-\tfrac{2}{3}aA^2+O(\varepsilon r)\right]\times 2,\ \text{and } (0)\times 2. \tag{2-454}$$

The results of the analysis of this section are summarized in two tables and two diagrams. Table 2-8 lists the data on the amplitude and stability of the solutions, and table 2-9 gives the locations of the various bifurcations on the λ-ε plane.

name	amplitude	eigenvalues
conduction (C)	$A^2 = 0$	$(\lambda)\times 6$
rolls (R)	$A^2 = \frac{-\lambda}{b}$ $z_1 = x\,,\ z_2 = z_3 = 0$	$2bA^2,\ (ax^2+\varepsilon x)\times 2,$ $(ax^2-\varepsilon x)\times 2,\ 0$
hexagons ($H^{\pm}$)	$x = \frac{-\varepsilon \pm \sqrt{\varepsilon^2 - 4\lambda(2a+3b)}}{2(2a+3b)}$ $z_1 = z_2 = z_3 = x$	$\left[2(2a+3b)x^2+\varepsilon x\right],$ $\left[-2(ax^2+\varepsilon x)\right]\times 2,$ $-3x\left[\varepsilon+(2d+3e)x^2+2cx^3\right],$ $(0)\times 2$
triangles (T)	$\lvert z_1\rvert^2 = \lvert z_2\rvert^2 = \lvert z_3\rvert^2$ $\cos\Phi \neq \pm 1$ see equation (nnn)	$\frac{2}{3}(2a+b)A^2,\ \frac{2}{3}cA^2\sin^2\Phi,$ $\left[-\frac{2}{3}aA^2\right]\times 2,\ (0)\times 2$
rectangles (RA)	$x_1 = \frac{-\varepsilon}{a},\ x_2 = x_3$ $x_2^2 = \frac{-(\lambda-\lambda_p)}{\left(\frac{1}{2}a+b\right)},\ \lambda_p = -bx_1^2$	(signs of eigenvalues) $1,\ -1,\ \mathrm{sgn}(a+2b),$ $\mathrm{sgn}(a),\ (0)\times 2$

Table 2-8. Solution data for equation (2-271).

primary bifurcation	$\lambda = 0$
saddle-node $H^{\pm}$	$\lambda_{sn} = \frac{\varepsilon^2}{4(2a+3b)},\ x_{sn} = \frac{-\varepsilon}{2(2a+3b)}$
pitchfork $H^{\pm}\cdot T$	$\lambda_{\pm} = \frac{(2a+3b)}{(2d+3e)}\left(\varepsilon \pm 2c\left(\frac{-\varepsilon}{(2d+3e)}\right)^{\frac{3}{2}}\right)$
pitchfork of revolution $R\cdot RA$	$\lambda_p = \frac{-b\varepsilon^2}{a^2},\ (A^2)_p = \left(\frac{\varepsilon}{a}\right)^2$
transcritical, $\mathbf{D_3}$ symmetry $RA\cdot H^{\pm}$	$\lambda_t = \frac{-(a+3b)\varepsilon^2}{a^2},\ x_t = \frac{-\varepsilon}{a}$

Table 2-9. Secondary bifurcation data for equation (2-271).

In addition to the nondegeneracy conditions discussed previously, there are nondegeneracy conditions which ensure that the secondary bifurcations occur at different λ values. The degeneracies where two bifurcations occur simultaneously are listed in the following table.

degeneracy	condition
$\lambda_{sn} = \lambda_p$	$(a+6b)(a+2b)=0$
$\lambda_{sn} = \lambda_t$	$(a+2b)=0$
$\lambda_p = \lambda_t$	$(a+2b)=0$
$\lambda_p = 0$	$b=0$
$\lambda_t = 0$	$(a+3b)=0$
$\lvert\lambda_p\rvert, \lvert\lambda_t\rvert \to \infty$	$a=0$
$\lambda_+ = \lambda_-$	$c=0$
$\lvert\lambda_+\rvert, \lvert\lambda_-\rvert \to \infty$	$(2d+3e)=0$

Table 2-10. Degenerate parameter values due to simultaneous secondary bifurcations.

Note that this table implies two nondegeneracy conditions involving a and b,

$$(a+6b)\neq 0, \quad \text{and } (a+3b)\neq 0, \tag{2-455}$$

which are not present for the Boussinesq normal form. Fig. 2-32 shows the nondegenerate regions in the a-b plane form the non-Boussinesq normal form. Within each of these regions the order of the bifurcations, as λ is increased for fixed ε, is the same. Fig. 2-32 shows the λ-ε plane for half of the regions in fig. 2-33, along with the corresponding bifurcation diagrams. The other cases can be obtained by reversing the direction of time. Regions I and II_1 of fig. 2-32 are the most interesting, because there are no solutions which are subcritical (except for the hexagons, which turn over at small amplitude). For these cases, the local bifurcation analysis gives a possible description of the *global* bifurcation behavior. While region I is predicted for Bénard convection with small

non-Boussinesq effects, the bifurcation sequence of region II_1 is observed for highly non-Boussinesq fluids (White, 1983). In other words, the hexagons remain the stable solution at large Rayleigh numbers.

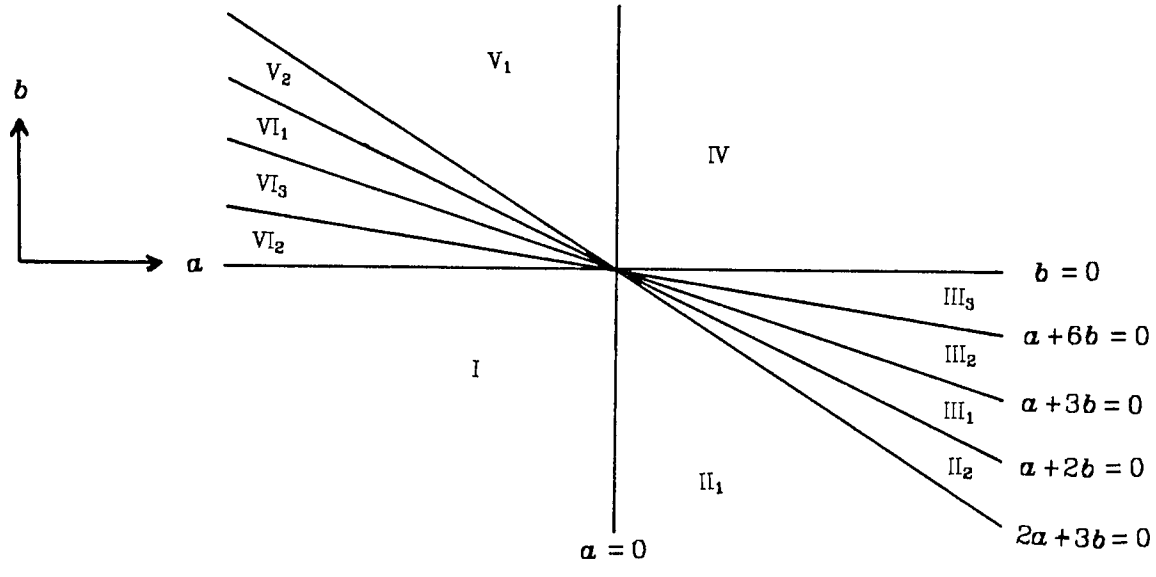

Fig. 2-32. The nondegeneracy conditions (2-272) of the normal form (2-271) divide the a-b plane into 12 regions, as shown. The labeling of the regions is chosen to correspond to figs. 2-7 and 2-23. Region III of fig. 2-23, which applies to the Boussinesq case, is divided into three regions here by the new nondegeneracy conditions which are needed in the non-Boussinesq case (2-455).

I

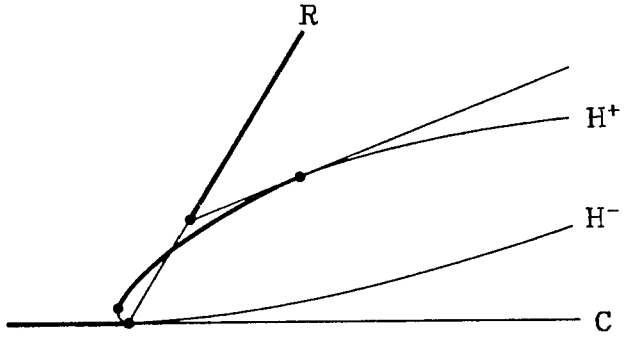

II_1

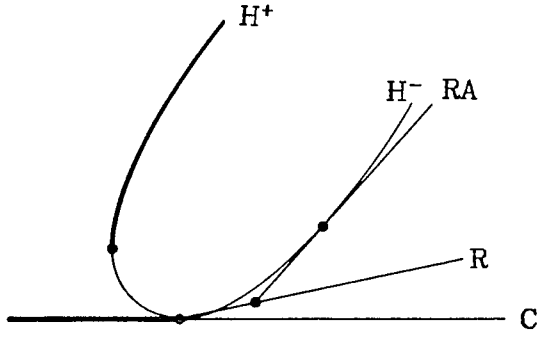

II_2

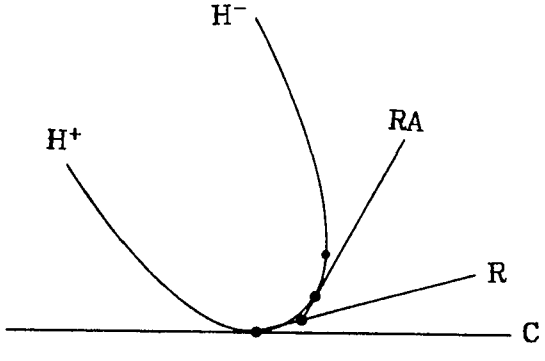

Fig. 2-33.

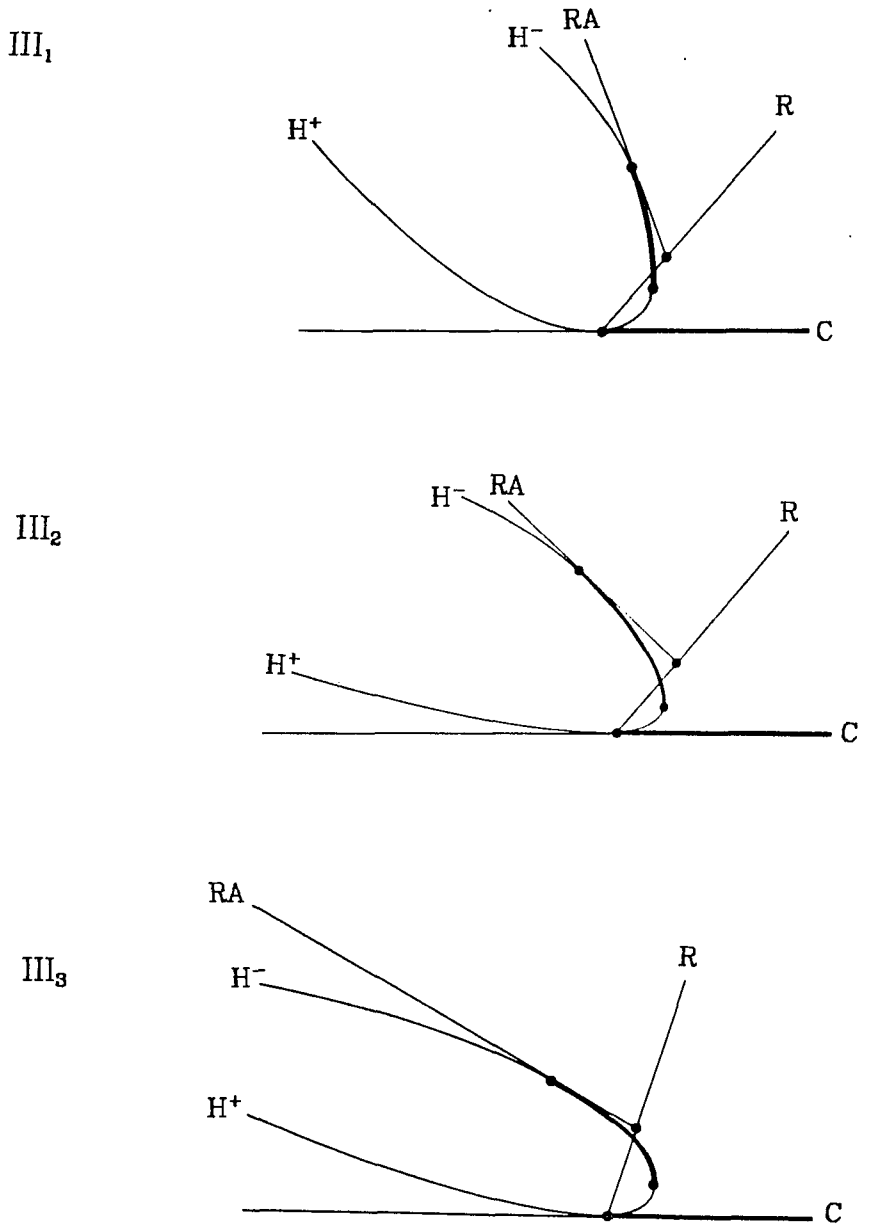

Fig. 2-33. The bifurcation diagrams for equation (2-271), for the coefficients a and b in the regions numbered in fig. 2-32. (Only the regions with $b<0$ are shown.) The other coefficients are $\varepsilon>0$, and $(2d+3e)>0$. This combination is chosed so that there are no bifurcations involving the triangle solutions. The differences between the three bifurcation diagrams for regions III_1, III_2, and III_3 only involves the ordering of the secondary bifurcations.

2.10. The Lattice Function

For certain examples of convection, a and b can be calculated. The parameter a depends on the angle between $\mathbf{k}_1$ and $\mathbf{k}_2$. Furthermore, because of the reflection symmetry which interchanges $\mathbf{k}_1$ and $\mathbf{k}_2$, a must be an even function of this angle. Following Schlüter, Lortz & Busse (1965), define φ as the *cosine* of the angle between $\mathbf{k}_1$ and $\mathbf{k}_2$:

$\varphi \equiv \cos(\alpha)$

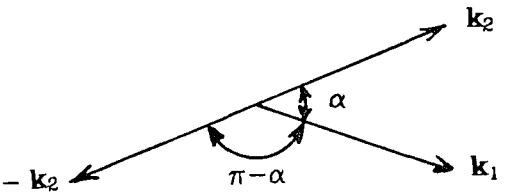

There are contributions to the a term in $\dot{z}_1$ from rolls at the angles α and $\pi-\alpha$. Therefore the function for a has the form

$$a = a_{\varphi^2} = \hat{a}(\varphi)+\hat{a}(-\varphi)\,. \tag{2-456}$$

Sattinger (1979) calls a_{φ^2} the *lattice function*. He proves that

$$b = \lim_{\varphi^2 \to 1} a_{\varphi^2}\,, \tag{2-457}$$

which gives the normal form

$$\dot{z}_1 = z_1\left[\lambda+b\,(2|z_2|^2+|z_1|^2)\right] \tag{2-458}$$

in the limit $\alpha \to 0$.

This result is implicit in the results of Schlüter *et al.* (1965). It follows from continuity, since as $\mathbf{k}_1$ and $\mathbf{k}_2$ approach each other they become indistinguishable. The factor of two in equation (2-458) follows from a combinatoric argument found in Sattinger (1979).

As mentioned above, the equal amplitude solutions in the rhombic lattice are traditionally called rectangles. The *limiting rectangles* live on the rhombic lattice where the angle between the two $\mathbf{k}$ vectors approaches zero. Equation (2-457) shows that $a = b$ for the limiting rectangles, so they are never stable.

The value of a in the hexagonal lattice normal form is

$$a_H \equiv a_{\varphi^2=\frac{1}{4}}. \tag{2-459}$$

In other words, the same calculation which determines a for the rectangles can be used for the coefficient a in the hexagonal lattice normal form. The rectangle solutions on the hexagonal lattice are continuous with the rectangles in the nearby rhombic lattices.

The value of a in the square lattice normal form is

$$a_S \equiv a_{\varphi^2=0}. \tag{2-460}$$

In the usual approach (such as Malkus & Veronis, 1958), one calculates R_2 to determine if the pattern is subcritical or supercritical, where

$$R = R_c + R_2 A^2 + \cdots . \tag{2-661}$$

In terms of the coefficients a and b, R_2 can be expressed as

$$R_2 \propto \begin{cases} -b \text{ for rolls.} \\ -\left(\frac{1}{2}a_{\varphi^2}+b\right) \text{ for rectangles.} \\ -\left(\frac{2}{3}a_{\varphi^2=0}+b\right) \text{ for squares.} \\ -\left(\frac{2}{3}a_{\varphi^2=\frac{1}{4}}+b\right) \text{ for hexagons.} \end{cases} \tag{2-662}$$

(The constant of proportionality is positive definite, and it is the same for all of the patterns.)

Note that the only possible *unique* stable pattern is the rolls. Many different rectangle patterns are stable in the cases where the lattice function predicts that three-dimensional patterns are stable in a symmetric system. In this case it is not obvious what would happen in a physical fluid layer, where double periodicity is not imposed. There is no rigorous way to test stability of a pattern on one lattice when perturbed by a pattern in another lattice. However, since the pattern with the greatest heat transport is stable within a given lattice, it seems reasonable that the pattern with the greatest heat transport among all the lattices would be the most stable. If the lattice function is linear,

and all the patterns are supercritical, then either the squares or the rolls have the greatest heat transport in the Boussinesq case.

There are at least two cases where calculations have shown that three dimensional patterns are stable at the onset of convection.

- Busse and Riahi (1980) have shown that squares are stable when the conductivity of the boundaries is very small. They found that the lattice function is linear, and that $a_H = 0$, in the limit where the conductivity goes to zero (see fig. 2-34). This is the first known example where three-dimensional patterns are stable in a system with the Boussinesq symmetry. Riahi (1983) has shown that the effect persists whether or not the vertical symmetry of the boundary conditions is preserved. He has also calculated the regions, in the space of conductivity of the top and bottom boundary, where squares and rolls are preferred.
- Frick & Busse (1983) have calculated the a parameter for squares in highly non-Boussinesq convection, where the viscosity depends on temperature. They find that squares are stable for a sufficiently non-Boussinesq system. There is a mathematical advantage to using the square lattice for highly non-Boussinesq systems, because stable solutions can be found at small amplitude. By contrast, the hexagons bifurcate transcritically and are always unstable near the origin in non-Boussinesq systems.

For a given realization of the lattice function, the bifurcation diagrams for the various special lattices can be superimposed. Some examples are shown in fig. 2-34.

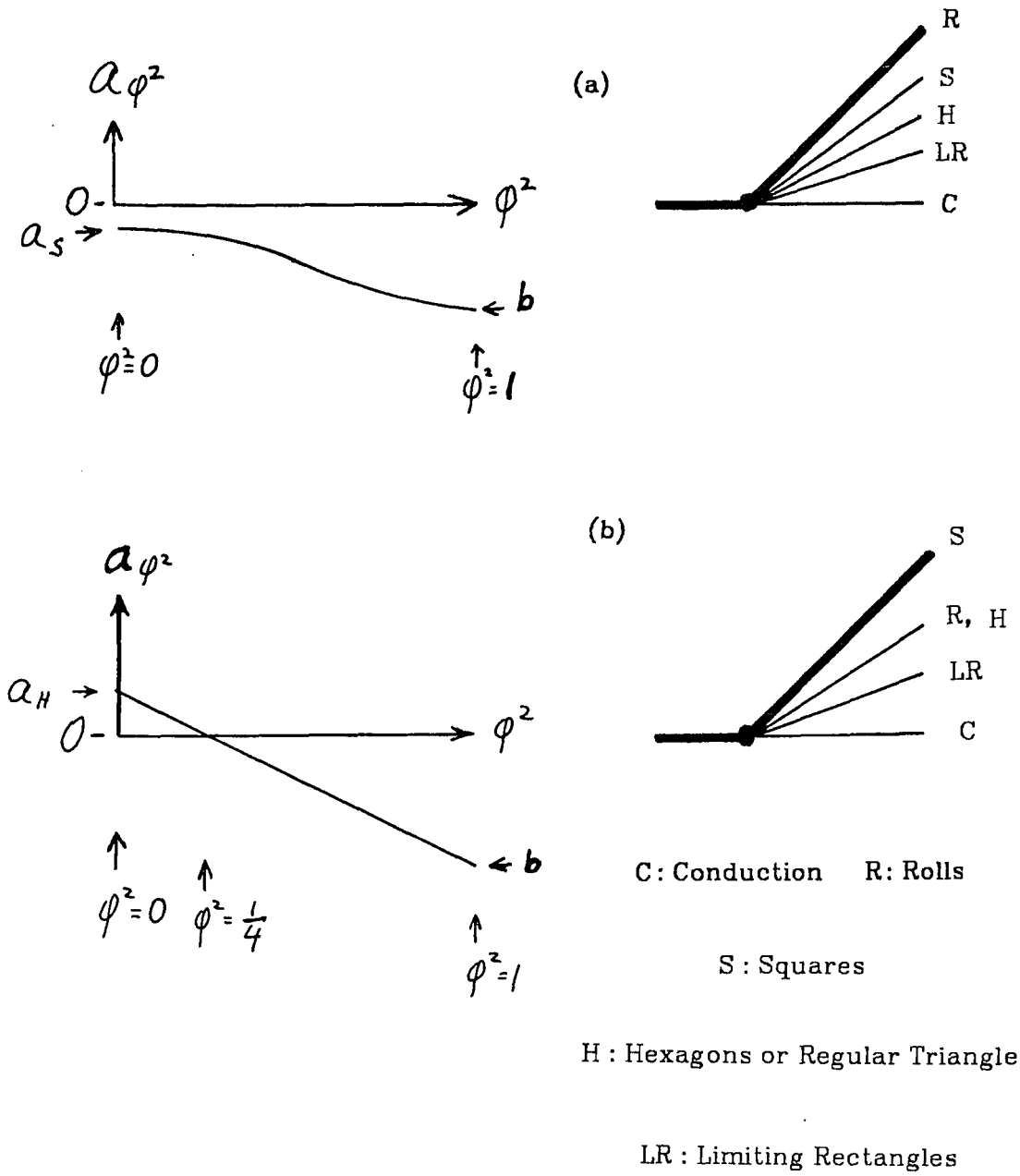

Fig. 2-34. The bifurcation diagrams corresponding to two lattice functions. Fig. (a) shows the lattice function typical of Bénard convection, where $a < 0$ for all lattices. Fig. (b) shows the linear lattice function found by Busse and Riahi (1980) for convection with nearly insulating boundaries. The rolls are the only stable solution for the upper lattice function (a). For the lattice function (b), all rectangles are supercritical, and rectangles with $\varphi^2 < \frac{1}{4}$ are stable to perturbations within their own lattice. In this lower case the squares have the largest heat transport, and $a_H = 0$, so that the rolls and hexagons have the same heat transport.

Experimentally, Whitehead & Parsons (1978) observed that there is a tendency for squares to be stable at large Rayleigh numbers in large Prandtl number Boussinesq convection. The effects of the side walls eventually destroy the stability of the squares; this has been studied quantitatively by Whitehead (1983). In an infinite fluid layer, perhaps the squares gain stability in a secondary bifurcation similar to fig. 2-19, (region II or III, $a < 0$). Frick, Busse, & Clever (1983) have calculated numerically (for infinite Prandtl number) that the squares have larger heat transport than the rolls at large Rayleigh numbers. They discuss the possibility that the squares gain stability at even larger Rayleigh numbers.

White (1983) has observed a tendency toward square pattern convection in highly non-Boussinesq fluids, which are used to simulate convection in the earth's mantle. White set up the initial convection pattern by heating certain places, using the technique of Busse & Whitehead (1971). The interaction between squares and hexagons is quite interesting and complicated in these experiments, and there are large regions in parameter space where both are stable.

One of White's most interesting observations is of a pattern which he calls triangles, for obvious reasons (see fig. 2-35). (These are *not* what are called triangles here.) These triangles were initiated by heating points on a hexagonal grid. In the experiments the triangles lasted for up to 10 hours before the effects from the sidewalls destroyed the pattern. The pattern was more stable at larger Rayleigh numbers. White predicts that this pattern would be stable at very large Rayleigh numbers, in the absence of sidewalls. Observation of fig. 2-35 shows that these triangles are in fact hexagons of the "wrong" sign, H^-. In other words, these are g-hexagons in a liquid. The distinctive triangular grid of white lines that White observes are perhaps due to the l-hexagons of

wavenumber $\sqrt{3}k_c$ which are superposed on the g-hexagons of wavenumber k_c.

Recall that one of the bifurcation diagrams, fig. 2-31 ($c > 0$), shows exactly what one would expect from White's experiments. At small Rayleigh number only H^+ is stable, but at larger Rayleigh number the H^- branch gains stability. While these bifurcation diagrams are technically only good for very small non-Boussinesq effects and small amplitude, they seem to work in this case. This often happens; the secondary bifurcations which are present in the degenerate bifurcations capture behavior that typically occurs at quite large amplitude.

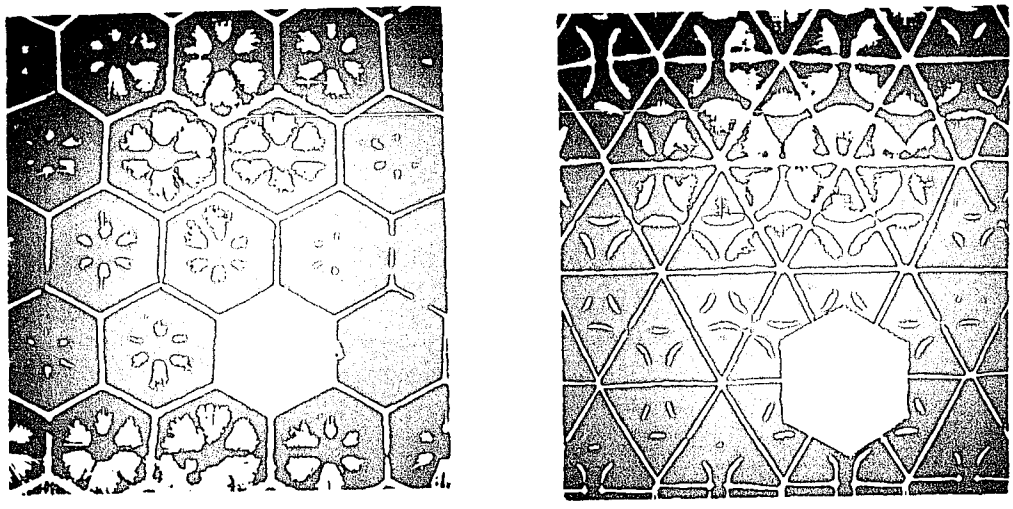

H^+ H^-

Fig. 2-35. Convection planforms observed by D. White (1983) in highly non-Boussinesq syrup. These patterns were induced by shining light through a grid pattern onto the fluid layer, thus causing "hot spots". Then the grid is removed and the Rayleigh number is increased greatly. One unit cell in each pattern is remoded to aid the identification of the pattern. The pattern on the left is the usual H^+ pattern observed in fluids. Note the center of each hexagonal unit cell is dark, warmer, rising fluid. The pattern on the right is the H^- pattern, which White calls triangles. These are not the triangles discussed here, however. White finds that the triangles seem to gain stability at large Rayleigh numbers. This is consistent with the results of the upper figures of fig. 2-31. These pictures were kindly supplied by David White.

Chapter Three

Normal Forms for Hopf Bifurcations

In doubly diffusive convection and rotating convection, as well as magneto-convection, the convective instability can take the form of growing oscillations. In the linear stability analysis, a complex conjugate pair of eigenvalues crosses into the right-half plane. This is often called overstability in the fluid mechanics literature, since a perturbed system is attracted back to the origin with such force that it overshoots and gains energy with each oscillation.

The exponential growth of the oscillations, predicted by linear theory, is of course modified by the nonlinear terms. If the cubic terms are attracting, then there is a stable branch of oscillatory solutions, called *limit cycles*, which grows as the bifurcations parameter exceeds the critical value. This is called a supercritical Hopf bifurcation. A subcritical Hopf bifurcation is analogous: an unstable branch of limit cycles is swallowed up by the origin at the critical parameter value.

The Hopf bifurcation of a roll pattern leads to wave solutions, since the fields oscillate in both space and time. In two-dimensional convection, the limit cycles can correspond to two different physical solutions: standing waves and traveling waves. In three-dimensional convection, standing and traveling squares and other exotic patterns are possible.

The pattern selection between standing and traveling waves is described by a normal form which is essentially the same as the normal form for bifurcations in the two-dimensional plane with square symmetry. Recall that normal convection in a square or rhombic lattice can also be reduced to this case. Therefore, the results of the previous chapter apply to oscillatory convection, where rolls are replaced by traveling waves, and squares are replaced by standing waves.

3.1. Hopf Bifurcations in the Plane

If the two-dimensional plane is described by a complex number z, then the linearization of an ODE near a Hopf bifurcation at the origin is

$$\dot{z} = (\lambda + i\omega)z \tag{3-1}$$

$$\dot{\bar{z}} = (\lambda - i\omega)\bar{z}\,. \tag{3-2}$$

where λ and ω are real. The ODE for $\bar{z}$ is just the complex conjugate of the equation for $\dot{z}$, and can be ignored.

In this section it is shown that the normal form for a Hopf bifurcation in the plane is

$$\dot{z} = z\left[(\lambda + i\omega) + a\,|z|^2\right]. \tag{3-3}$$

Adding the most general quadratic and cubic terms to the linear ODE in the neighborhood of a Hopf bifurcation gives

$$\dot{z} = (\lambda + i\omega)z + q_1 z^2 + q_2 z\bar{z} + q_3 \bar{z}^2 + c_1 z^3 + c_2 z^2\bar{z} + c_3 z\bar{z}^2 + c_4 \bar{z}^3, \tag{3-4}$$

where q_α and c_α are complex.

If the ODE has the symmetry

$$z \to -z\,, \tag{3-5}$$

then the quadratic coefficients are all zero. This is the case with Boussinesq convection.

When $\lambda = 0$, and the q_α are zero, a near identity change of coordinates can get rid of all of the cubic terms except c_2. The general near identity change of coordinates which preserves the $z \to -z$ symmetry of the ODE is

$$\zeta = z + a_1 z^3 + a_2 z^2\bar{z} + a_3 z\bar{z}^2 + a_4 \bar{z}^3 + O(|z|^5), \tag{3-6}$$

where the a_α are complex. The ODE for the new coordinate is

$$\dot{\zeta} = \dot{z} + 3i\omega a_1 z^3 + i\omega a_2 z^2\bar{z} - i\omega a_3 z\bar{z}^2 - 3i\omega a_4 \bar{z}^3 + O(|\zeta|^5). \tag{3-7}$$

When $\dot{z}$ in the above formula is replaced by

$$\dot{z} = i\omega\left[\zeta - a_1 z^3 - a_2 z^2\bar{z} - a_3 z\bar{z}^2 - a_4 \bar{z}^3\right] + c_1 z^3 + c_2 z^2\bar{z} + c_3 z\bar{z}^2 + c_4 \bar{z}^3 + O(|\zeta|^5), \tag{3-8}$$

the ODE becomes

$$\dot{\zeta} = i\omega\zeta + (c_1 - 2i\omega a_1)z^3 + c_2 z^2\bar{z} + (c_3 + 2i\omega a_3)z\bar{z}^2 + (c_4 + 4i\omega a_4)\bar{z}^3 + O(|z|^5). \quad (3\text{-}9)$$

By a judicious choice of the a_α coefficients, all of the terms except c_2 can be eliminated. (Note that a_2 can be anything.) The z's in the third order terms can be replaced by ζ's to obtain the normal form for the Hopf bifurcation,

$$\dot{\zeta} = i\omega\zeta + c_2\zeta|\zeta|^2 + O(|\zeta|^5). \quad (3\text{-}10)$$

Knowing this result, it is now easier to find the normal form for the general cubic system (3-4), including the quadratic terms. All of the quadratic terms can be eliminated by a near identity change of variables,

$$\zeta = z + b_1 z^2 + b_2 z\bar{z} + b_3\bar{z}^2, \quad (3\text{-}11)$$

but at the expense of introducing new cubic coefficients. Only the induced coefficient of $z^2\bar{z}$ is needed for the normal form, since the change of variables (3-6) can then be used to eliminate all other cubic term.

Differentiating (3-11) gives

$$\begin{aligned}\dot{\zeta} &= \dot{z} + 2b_1 z\dot{z} + b_2(z\dot{\bar{z}} + \dot{z}\bar{z}) + 2b_3\bar{z}\dot{\bar{z}} + O(z^3, z\bar{z}^2, \bar{z}^3) + O(|z|^4) \\ &= \dot{z} + 2b_1(i\omega z^2 + q_2 z|z|^2) + b_2(\bar{q}_2 + q_1)z|z|^2 + 2b_3(-i\omega\bar{z}^2 + \bar{q}_3 z|z|^2) \\ &\quad + O(z^3, z\bar{z}^2, \bar{z}^3) + O(|z|^4).\end{aligned} \quad (3\text{-}12)$$

Since only the coefficient of $z|z|^2$ is important, the other cubic coefficients are ignored. In the above equation, $\dot{z}$ should be replaced by

$$\begin{aligned}\dot{z} &= i\omega(\zeta - b_1 z^2 - b_2 z\bar{z} - b_3\bar{z}^2) + q_1 z^2 + q_2 z\bar{z} + q_3\bar{z}^2 + c_2 z|z|^2 \\ &\quad + O(z^3, z\bar{z}^2, \bar{z}^3) \\ &= i\omega\zeta + (q_1 - i\omega b_1)z^2 + (q_2 - i\omega b_2)z\bar{z} + (q_3 - i\omega b_3)\bar{z}^2 + c_2 z|z|^2 \\ &\quad + O(z^3, z\bar{z}^2, \bar{z}^3).\end{aligned} \quad (3\text{-}13)$$

Inserting the last equation into (3-12) gives

$$\begin{aligned}\dot{\zeta} &= i\omega\zeta + (q_1 + i\omega b_1)z^2 + (q_2 - i\omega b_2)z\bar{z} + (q_3 - 3i\omega b_3)\bar{z}^2 \\ &\quad + \left[c_2 + 2b_1 q_2 + b_2(\bar{q}_2 + q_1) + 2b_3\bar{q}_3\right]z|z|^2 \\ &\quad + O(z^3, z\bar{z}^2, \bar{z}^3) + O(|z|^4).\end{aligned} \quad (3\text{-}14)$$

The choice of the b_α coefficients which eliminates the quadratic terms is

$$b_1 = \frac{-q_1}{i\omega}, \quad b_2 = \frac{q_2}{i\omega}, \quad \text{and } b_3 = \frac{q_3}{3i\omega}. \tag{3-15}$$

These values of b_a are inserted into the coefficient of $z|z|^2$ in equation (3-14), and z can be replaced by ζ at third order to give

$$\dot{\zeta} = i\omega\zeta + \left[c_2 + \frac{1}{i\omega}(-q_1q_2 + q_2\bar{q}_2 + \frac{2}{3}q_3\bar{q}_3)\right]\zeta|\zeta|^2 + O(\zeta^3, \zeta\bar{\zeta}^2, \bar{\zeta}^3) + O(|\zeta|^4). \tag{3-16}$$

At this point, the near identity transformation with cubic terms (3-6) can be used to eliminate the cubic terms other than $\zeta|\zeta|^2$. Relabeling ζ as z, the normal form corresponding to the general ODE (3-4) is

$$\dot{z} = i\omega z + \left[c_2 + \frac{1}{i\omega}(-q_1q_2 + q_2\bar{q}_2 + \frac{2}{3}q_3\bar{q}_3)\right]z|z|^2 + O(|z|^5) \tag{3-17}$$

This formula is derived in Hassard, Kazarinoff, and Wan (1981).

The error term listed above is order 5 because the order 4 terms can be eliminated by yet another near identity change of variables. The general result is that the normal form is

$$\dot{z} = z\,f(|z|^2) \tag{3-18}$$

to all orders in the Taylor expansion. Therefore the normal form is equivariant under rotations in the complex plane:

$$z \to e^{i\varphi_t}z\,. \tag{3-19}$$

(There is also an exponentially flat "tail" which does not have this symmetry, but this is a technicality which is not important here.)

The symmetry (3-19) will be called the *time translation* symmetry. Note its similarity to the space translation symmetry (2-132) in a periodic spatial domain. There is a difference between these two symmetries. The convection equations are equivariant under translations, and therefore so is the normal form. On the other hand, the time translation symmetry is not present in the original equation (3-4).

3.2. Traveling and Standing Waves

When the Hopf bifurcation is in the space of roll amplitudes, the symmetries are different than they are in the planar example. The critical modes are the eigenfunctions with eigenvalues $\pm i\omega$. The normalization can be chosen so that

$$\begin{aligned} \psi_{i\omega} &= Cf(\hat{\mathbf{z}}\cdot\mathbf{x})e^{i\mathbf{k}\cdot\mathbf{x}}, \text{ and} \\ \psi_{-i\omega} &= \bar{C}f(\hat{\mathbf{z}}\cdot\mathbf{x})e^{i\mathbf{k}\cdot\mathbf{x}}, \end{aligned} \tag{3-20}$$

where $f(\hat{\mathbf{z}}\cdot\mathbf{x})$ is the vertical eigenfunction. (The vertical coordinate z is referred to as $\hat{\mathbf{z}}\cdot\mathbf{x}$ to avoid confusion with the amplitude z.) When the system is on the critical eigenspace, a typical field is of the form

$$\psi(\mathbf{x},t) = f(\hat{\mathbf{z}}\cdot\mathbf{x})\left[(C\,z+\bar{C}\,w)e^{i\mathbf{k}\cdot\mathbf{x}}+(\bar{C}\,\bar{z}+C\,\bar{w})e^{-i\mathbf{k}\cdot\mathbf{x}}\right]. \tag{3-21}$$

The time-dependent amplitudes, z and w, satisfy

$$\dot{z} = i\omega z + \cdots \tag{3-22}$$

$$\dot{w} = -i\omega w + \cdots \tag{3-23}$$

at the critical Rayleigh number. Note that this equation is similar to the linearized equation at a Hopf bifurcation in the real plane ((3-1) and (3-2), with $\lambda = 0$), except that w replaces $\bar{z}$. The fact that w is not constrained to equal $\bar{z}$ is responsible for the possibility of both traveling waves and standing waves.

As can be observed from equation (3-21), the symmetry corresponding to $\mathbf{k} \to -\mathbf{k}$ is

$$(z, w) \to (\bar{w}, \bar{z}). \tag{3-24}$$

When $|z|^2 = |w|^2$, it is possible to choose a translation, $\mathbf{x} \to \mathbf{x}+\mathbf{d}$, such that

$$z = \bar{w}. \tag{3-25}$$

(This relationship is preserved under the dynamics because $\dot{z} = \dot{\bar{w}}$.) In this case the solution is a standing wave:

$$\psi(\mathbf{x}, t) \propto f(\hat{\mathbf{z}}\cdot\mathbf{x})\cos(\omega t+\delta)\cos(\mathbf{k}\cdot\mathbf{x}). \tag{3-26}$$

When $z = 0$ or $w = 0$ it is possible to put the solution in the form $w = 0$, using the

symmetry (3-24) if necessary. The solution is a traveling wave:

$$\psi(\mathbf{x},t) \propto f(\mathbf{x}\cdot\hat{\mathbf{z}})\cos(\omega t+\mathbf{k}\cdot\mathbf{x}). \tag{3-27}$$

As with the normal Hopf bifurcation, the normal form has the time translation symmetry,

$$(z,w)\to(e^{i\varphi_t}z, e^{-i\varphi_t}w), \tag{3-28}$$

and the space translation symmetry,

$$(z,w)\to e^{i\mathbf{k}\cdot\mathbf{d}}(z,w). \tag{3-29}$$

It is advantageous to combine the two translation symmetries into space-time translation symmetries which follow the left and right going traveling waves. Choose the displacement so that $\mathbf{k}\cdot\mathbf{d}=\pm\varphi_t$ to give

$$(z,w)\to(z, e^{i2\varphi_t}w), \tag{3-30}$$

and

$$(z,w)\to(e^{i2\varphi_t}z, w). \tag{3-31}$$

The equivariant vector fields with this symmetry are

$$\dot{z} = z\, g(|z|^2, |w|^2) \tag{3-32}$$

$$\dot{w} = w\, \bar{g}(|w|^2, |z|^2) \tag{3-33}$$

where g is an arbitrary complex function of two real arguments, i.e.

$$g:\mathbb{R}^2\to\mathbb{C}. \tag{3-34}$$

The first nontrivial truncation of this general ODE is

$$\dot{z} = z\left[(\lambda+i\omega)+a|w|^2+b(|z|^2+|w|^2)\right] \tag{3-35}$$

$$\dot{w} = w\left[(\lambda-i\omega)+\bar{a}|z|^2+\bar{b}(|z|^2+|w|^2)\right], \tag{3-36}$$

where λ and ω are real, and a and b are complex.

The behavior of this system is most easily analyzed by looking at the magnitudes of z and w. These amplitudes can be written in polar coordinate as follows:

$$z \equiv x_1 e^{i\varphi_1} \tag{3-37}$$

$$w \equiv x_2 e^{i\varphi_2}. \tag{3-38}$$

The overall amplitude is

$$A^2 \equiv |z|^2 + |w|^2 = x_1^2 + x_2^2. \tag{3-39}$$

In terms of the polar coordinates, equations (3-40) and (3-41) are

$$\dot{x}_1 = x_1\left[\lambda + \mathrm{Re}(a)x_2^2 + \mathrm{Re}(b)A^2\right], \tag{3-40}$$

$$\dot{x}_2 = x_2\left[\lambda + \mathrm{Re}(a)x_1^2 + \mathrm{Re}(b)A^2\right], \tag{3-41}$$

$$\dot{\varphi}_1 = \omega + \mathrm{Im}(a)x_2^2 + \mathrm{Im}(b)A^2, \tag{3-42}$$

$$\dot{\varphi}_2 = -\omega - \mathrm{Im}(a)x_1^2 - \mathrm{Im}(b)A^2. \tag{3-43}$$

The coordinates x_1 and x_2 satisfy the normal form for bifurcation with $\mathbf{D_4}$ symmetry, equation (2-51). The coefficients a and b in equation (2-51) are replaced by $\mathrm{Re}(a)$ and $\mathrm{Re}(b)$ in equations (3-40) and (3-41). The behavior of the phase is not important for the qualitative behavior of the solutions; the oscillatory solutions have an angular frequency of approximately ω.

Therefore, *the bifurcations of two-dimensional oscillatory convection have similar behavior to the bifurcations in the real plane with the symmetry of the square which in turn have similar behavior to the bifurcations in three-dimensional stationary convection.* The standing waves in the oscillatory system corresponding to the squares in three-dimensional convection, and the traveling waves corresponding to the rolls.

The reason that the three problems are similar is that they all have an underlying $\mathbf{D_4}$ symmetry.

This bifurcation has been studied by many workers, including Bajaj (1982) and Golubitsky & Stuart (1984). They find that the stability of the standing and traveling wave solutions agrees with the results of the real system (2-51).

The linear stability of a periodic orbit is typically found by calculating the Floquet exponents, which describe how the perturbations grow or decay. One of the Floquet exponents is always zero because displacements along the flow

direction on the limit cycle neither grow nor decay. The stability analysis of Bajaj (1982) and Golubitsky & Stuart (1984) confirms the behavior of (3-35) and (3-36) is qualitatively similar to the behavior of (2-51).

3.3. Three-Dimensional Oscillatory Convection

In this section the most general equivariant ODEs for oscillatory convection on a rhombic, square, or hexagonal lattice is found. The analysis of the truncations has not been done completely enough to determine the normal forms for these cases. There are two important results in this section. The equivariant vector fields for oscillatory convection in a square lattice are different than those for a general rhombic lattice, and the normal forms for the hexagonal lattice are the same in the Boussinesq and non-Boussinesq case.

For three-dimensional oscillatory convection on a square or rhombic lattice, the critical eigenspace is described by four complex numbers:

$$\psi(\mathbf{x},t) = f(\mathbf{x}\cdot\hat{\mathbf{z}})\left[(C z_1+\bar{C} w_1)e^{i\mathbf{k}_1\cdot\mathbf{x}}+(C z_2+\bar{C} w_2)e^{i\mathbf{k}_2\cdot\mathbf{x}}+c.c.\right], \tag{3-44}$$

where the linear ODE for the amplitudes is

$$\dot{z}_\alpha = i\omega z_\alpha \tag{3-45}$$

$$\dot{w}_\alpha = -i\omega w_\alpha, \tag{3-46}$$

and α ranges over 1 and 2. In the hexagonal lattice a third pair of amplitudes is added, z_3 and w_3, an α ranges from 1 to 3 in the following discussion.

As with two-dimensional oscillatory convection, the normal form is equivariant under the time translation symmetry:

$$(z_\alpha, w_\alpha) \to (e^{i\varphi_t} z_\alpha, e^{-i\varphi_t} w_\alpha), \tag{3-47}$$

and the space translation symmetry:

$$(z_\alpha, w_\alpha) \to e^{i\mathbf{k}_\alpha\cdot\mathbf{d}}(z_\alpha, w_\alpha). \tag{3-48}$$

In addition, all the lattices have the 180° rotation symmetry,

$$(z_a, w_a) \to (\bar{w}_a, \bar{z}_a), \tag{3-49}$$

and the reflection which interchanges $\mathbf{k}_1$ and $\mathbf{k}_2$,

$$z_1 \leftrightarrow z_2 \text{ and } w_1 \leftrightarrow w_2 \tag{3-50}$$

(In the hexagonal lattice z_3 and w_3 are unchanged).

In the square lattice, there is an additional symmetry corresponding to the reflection which takes

$$\mathbf{k}_1 \to \mathbf{k}_1, \text{ and } \mathbf{k}_2 \to -\mathbf{k}_2. \tag{3-51}$$

This gives the transformation on the amplitudes,

$$(z_1, w_1) \to (z_1, w_1), \text{ and } (z_2, w_2) \to (\bar{w}_2, \bar{x}_2). \tag{3-52}$$

This symmetry causes the normal form to be different in the square and rhombic lattices.

3.3.1. The square and rhombic lattices

The equivariant vector fields are highly constrained by the translations. First, the effect of the translations will be computed, after which the discrete symmetries will be added in. The complex notation used here makes the computation simple. A general term in the ODE for $\dot{z}_1$ is

$$\dot{z}_1 = z_1^{n_1} z_2^{n_2} w_1^{m_1} w_2^{m_2} f(|z_1|^2, |z_2|^2, |w_1|^2, |w_2|^2), \tag{3-53}$$

where n_a is positive or negative; when n_1 is negative

$$z_1^{-|n_1|} \equiv \bar{z}_1^{|n_1|} \tag{3-54}$$

by definition (see (2-247)).

The equivariance condition for the time translations, applied to equation (3-53), implies

$$e^{i\varphi_t}\dot{z}_1 = (e^{i\varphi_t} z_1)^{n_1} (e^{i\varphi_t} z_2)^{n_2} (e^{-i\varphi_t} w_1)^{m_1} (e^{-i\varphi_t} w_2)^{m_2} f \,. \tag{3-55}$$

$$= e^{i(n_1+n_2-m_1-m_2)\varphi_t} z_1^{n_1} z_2^{n_2} w_1^{m_1} w_2^{m_2} f \,. \tag{3-56}$$

Therefore,

$$e^{i\varphi_t} = e^{i(n_1+n_2-m_1-m_2)\varphi_t} \tag{3-57}$$

for *all* φ_t. This equation has the simple interpretation that $\dot{z}_1$ transforms like z_1 under the time translation symmetry. The only way equation (3-57) can be satisfied for all φ_t is if

$$1 = n_1+n_2-m_1-m_2. \tag{3-58}$$

Similarly, the equivariance under space translations leads to the condition,

$$e^{i\mathbf{k}_1\cdot\mathbf{d}} = e^{i\left[(\mathbf{k}_1\cdot\mathbf{d})(n_1+m_1)+(\mathbf{k}_2\cdot\mathbf{d})(n_2+m_2)\right]}. \tag{3-59}$$

Since $\mathbf{k}_1$ and $\mathbf{k}_2$ are linearly independent, this is true for all translations $\mathbf{d}$ if and only if

$$1 = n_1+m_1\ , \text{ and } 0 = n_2+m_2. \tag{3-60}$$

The three equations, (3-58) and (3-60), for the four integers can be solved so that only one integer is arbitrary and the others are given as a function of the first. It is reasonable to choose n_1 as the independent integer, in which case the other integers are given by

$$n_2 = 1-n_1 \tag{3-61}$$

$$m_1 = 1-n_1 \tag{3-62}$$

$$m_2 = n_1-1. \tag{3-63}$$

This means that the ODE which is equivariant under the space and time translations is of the form

$$\dot{z}_1 = \sum_{n_1=-\infty}^{\infty} z_1{}^{n_1}(z_2 w_1 \overline{w}_2)^{1-n_1} f_{n_1}(|z_1|^2, |z_2|^2, |w_1|^2, |w_2|^2). \tag{3-64}$$

It must be remembered that a negative exponent is to be interpreted as the complex conjugate of the quantity to a positive power. The prefactors of f_{n_1}, written explicitly for a few n_1, are

$$\begin{aligned} n_1 &= 1 \quad & z_1 \\ n_1 &= 0 \quad & z_2 w_1 \bar{w}_2 \\ n_1 &= 2 \quad & z_1(z_1 \bar{z}_2 \bar{w}_1 w_2) \\ n_1 &= -1 \quad & z_2 w_1 \bar{w}_2 (z_1 \bar{z}_2 \bar{w}_1 w_2). \end{aligned} \tag{3-65}$$

It is clear from this table that the most general ODE (3-64) can be written as

$$\begin{aligned} \dot{z}_1 = z_1 \, g(Q, |z_1|^2, |z_2|^2, |w_1|^2, |w_2|^2) \\ + z_2 w_1 \bar{w}_2 \, h(Q, |z_1|^2, |z_2|^2, |w_1|^2, |w_2|^2), \end{aligned} \tag{3-66}$$

where

$$Q \equiv z_1 \bar{z}_2 \bar{w}_1 w_2, \tag{3-67}$$

and g and h are complex valued functions. Note that the term with $n_1 = 2$ is obtained from $g = Q, h = 0$, and the term with $n_1 = -1$ is obtained from $g = 0, h = \bar{Q}$.

The function Q is invariant under all of the symmetries. It is the analog of q in the hexagonal lattice (see section 2.9). The difference is that Q is complex, whereas q is real.

The invariant function of the phases is related to Q. There are three translational symmetries, the two space translations and the time translation, and there are four phases. Therefore there is one combination of the phases which is invariant under the translations:

$$\Phi \equiv \varphi_{z_1} - \varphi_{z_2} - \varphi_{w_1} + \varphi_{w_2}. \tag{3-68}$$

The context should prevent this Φ from being confused with the Φ defined for stationary convection on the hexagonal lattice.

In the rhombic lattice, the most general equivariant ODE, truncated at third order, is

$$\dot{z}_1 = z_1 \left[(\lambda + i\omega) + a_1 |z_1|^2 + a_2 |z_2|^2 + b_1 |w_1|^2 + b_2 |w_2|^2 \right] + c \, z_2 w_1 \bar{w}_2, \tag{3-69}$$

where the coefficients a_α, b_α, and c are complex. Be warned that the coefficients are *not* chosen to correspond to the a and b of the previous section. The other equations can be found from the discrete symmetries, but they

are listed here for completeness:

$$\dot{z}_2 = z_2\left[(\lambda+i\omega)+a_1|z_2|^2+a_2|z_1|^2+b_1|w_2|^2+b_2|w_1|^2\right]+c\,z_1 w_2 \bar{w}_1 \quad (3\text{-}70)$$

$$\dot{w}_1 = w_1\left[(\lambda-i\omega)+\bar{a}_1|w_1|^2+\bar{a}_2|w_2|^2+\bar{b}_1|z_1|^2+\bar{b}_2|z_2|^2\right]+\bar{c}\,w_2 z_1 \bar{z}_2 \quad (3\text{-}71)$$

$$\dot{w}_2 = w_2\left[(\lambda-i\omega)+\bar{a}_1|w_2|^2+\bar{a}_2|w_1|^2+\bar{b}_1|z_2|^2+\bar{b}_2|z_1|^2\right]+\bar{c}\,w_1 z_2 \bar{z}_1 . \quad (3\text{-}72)$$

In the square lattice, the symmetry (3-52) leaves z_1 unchanged, but interchanges z_2 and $\bar{w}_2$. The effect of this symmetry is most easily seen in the $\dot{z}_1$ equation. The result is that

$$a_2 = b_2 \quad (3\text{-}73)$$

in the square lattice.

The analysis of this equivariant ODE is quite difficult, and it has not been completed. Some solutions are known, but the possibility of other solutions cannot be ruled out. These known solutions are listed below:

- Traveling waves

$$|z_1|^2 \neq 0, \text{ all others zero (AOZ)} \quad (3\text{-}74)$$

$$A^2 = \frac{-\lambda}{\mathrm{Re}(a_1)} \quad (3\text{-}75)$$

- Standing waves

$$z_1 = \bar{w}_1, \text{ AOZ} \quad (3\text{-}76)$$

$$A^2 = \frac{-2\lambda}{\mathrm{Re}(a_1+b_1)} \quad (3\text{-}77)$$

- Traveling squares

$$z_1 = z_2, \text{ AOZ} \quad (3\text{-}78)$$

$$A^2 = \frac{-2\lambda}{\mathrm{Re}(a_1+a_2)} \quad (3\text{-}79)$$

- Standing squares I

$$z_1 = \bar{w}_1 = z_2 = \bar{w}_2 \quad (3\text{-}80)$$

$$A^2 = \frac{-4\lambda}{\mathrm{Re}(a_1+a_2+b_1+b_2+c)} \quad (3\text{-}81)$$

• Standing squares II

$$z_1 = \bar{w}_1 = iz_2 = -i\bar{w}_2 \tag{3-82}$$

$$A^2 = \frac{-4\lambda}{\mathrm{Re}(a_1+a_2+b_1+b_2-c)} \tag{3-83}$$

In the rectangular lattice there are two types of traveling rectangles since the pattern can move in the direction of the long side or the short side of the rectangle. These r ce the traveling squares listed above. The standing rectangles are the s . as the standing squares.

• Traveling rectangles I

$$z_1 = z_2, \ \mathrm{AOZ} \tag{3-84}$$

$$A^2 = \frac{-2\lambda}{\mathrm{Re}(a_1+a_2)} \tag{3-85}$$

• Traveling rectangles II

$$z_1 = \bar{w}_2, \ \mathrm{AOZ} \tag{3-86}$$

$$A^2 = \frac{-2\lambda}{\mathrm{Re}(a_1+b_2)} \tag{3-87}$$

With the exception of the standing squares, it is trivial to prove that the above solution types exist. The exotic term, proportional to c, is zero for all of the solutions listed except the standing squares. In all of these cases, the solution is defined by a single equation, of the form

$$\dot{z}_1 = z_1\left[(\lambda+i\omega)+(constant)\,|z_1|^2\right], \tag{3-88}$$

so that the solution has

$$|z_1|^2 = \frac{-\lambda}{\mathrm{Re}(constant)} \tag{3-89}$$

The general equal amplitude solution, ($|z_1|^2 = |z_2|^2 = |w_1|^2 = |w_2|^2$), can be written as

$$\begin{aligned} z_1 &= z \\ w_2 &= \bar{z} \\ z_2 &= e^{-i\Phi/2} z \\ w_2 &= e^{i\Phi/2} \bar{z} \,. \end{aligned} \tag{3-90}$$

The system is written in this way because Φ is the invariant phase defined in equation (3-68). When these amplitudes are introduced into the equation for $\dot{z}_1$, it becomes

$$\dot{z}_1 = z_1 \left[(\lambda + i\omega) + (a_1 + a_2 + b_1 + b_2 + c e^{-i\Phi}) |z|^2 \right], \tag{3-91}$$

and the derivative of the phase of z_1 is

$$\dot{\varphi}_{z_1} = \omega + \mathrm{Im}(a_1 + a_2 + b_1 + b_2 + c e^{-i\Phi}) |z|^2 . \tag{3-92}$$

A similar calculation shows

$$\begin{aligned} \dot{\varphi}_{z_2} &= \omega + \mathrm{Im}(a_1 + a_2 + b_1 + b_2 + c e^{i\Phi}) |z|^2 , \\ \dot{\varphi}_{w_1} &= -\omega - \mathrm{Im}(a_1 + a_2 + b_1 + b_2 - c e^{-i\Phi}) |z|^2 , \\ \dot{\varphi}_{w_2} &= -\omega - \mathrm{Im}(a_1 + a_2 + b_1 + b_2 - c e^{i\Phi}) |z|^2 . \end{aligned} \tag{3-93}$$

These equations imply that

$$\dot{\Phi} = \dot{\varphi}_{z_1} - \dot{\varphi}_{z_2} - \dot{\varphi}_{w_1} + \dot{\varphi}_{w_2} = 2\,\mathrm{Im}\left[c (e^{-i\Phi} - e^{i\Phi}) \right] |z|^2 = -4\,\mathrm{Re}(c \sin\Phi) . \tag{3-94}$$

Therefore, assuming that $\mathrm{Re}(c) \neq 0$, there are two solutions: $\Phi = 0$ (standing squares I), or $\Phi = \pi$ (standing squares II).

There are other solutions of the type

$$z_1 = \bar{w}_1 , \;\; z_2 = \bar{w}_2 , \;\; |z_1|^2 \neq |z_2|^2 , \tag{3-95}$$

but these satisfy a complicated pair of equations. Furthermore, it is difficult to prove that there are not other small amplitude solutions to the cubic truncation (3-69). Therefore it is not possible at this time to determine if the cubic truncation is a normal form.

3.3.2. The hexagonal lattice

The situation on the hexagonal lattice is even more complicated than the rectangular or square lattice. One result, however, is immediate; because of the

time translation symmetry (3-48), there is always the symmetry

$$(z_a, w_a) \to -(z_a, w_a) \tag{3-96}$$

which corresponds to $\varphi_t = \pi$. This is the symmetry which follows from the Boussinesq approximation. As a result, the normal form is the same in the Boussinesq and non-Boussinesq case. There can be no preference for upward flow in the center of each hexagon because half a period later the flow has reversed direction.

The equivariant vector fields on a hexagonal lattice are quite different from equivariant vector fields on a square or rhombic lattice. An important symmetry for the $\dot{z}_1$ equation is the reflection which leaves $\mathbf{k}_1$ unchanged:

$$(z_1, w_1) \to (z_1, w_1) \tag{3-97}$$

$$(z_2, w_2) \leftrightarrow (z_3, w_3). \tag{3-98}$$

This forces $\dot{z}_1$ to be symmetric under an interchange of 2 and 3, so that a typical term is

$$\dot{z}_1 = \left({z_1}^{n_1} {z_2}^{n_2} {z_3}^{n_3} {w_1}^{m_1} {w_2}^{m_2} {w_3}^{n_3} f + [2 \leftrightarrow 3] \right), \tag{3-99}$$

where f is an arbitrary function of $|z_1|^2$, $|z_2|^2$, $|z_3|^2$, $|w_1|^2$, $|w_2|^2$, and $|w_3|^2$:

$$f : \mathbb{R}^6 \to \mathbb{C}, \tag{3-100}$$

and $[2 \leftrightarrow 3]$ is a shorthand for the interchange (3-81)-(3-82).

The equivariance of (3-99) under the time translations gives

$$e^{i\varphi_t} = e^{i(n_1+n_2+n_3-m_1-m_2-m_3)\varphi_t}, \tag{3-101}$$

therefore

$$1 = n_1+n_2+n_3-m_1-m_2-m_3. \tag{3-102}$$

The equivariance under space translations gives

$$e^{i\mathbf{k}_1\cdot\mathbf{d}} = e^{i(\mathbf{k}_1\cdot\mathbf{d})(n_1+m_1)} e^{i(\mathbf{k}_2\cdot\mathbf{d})(n_2+m_2)} e^{i(\mathbf{k}_3\cdot\mathbf{d})(n_3+m_3)}. \tag{3-103}$$

When $\mathbf{k}_3$ is replaced by $-(\mathbf{k}_1+\mathbf{k}_2)$, the above equation implies

$$e^{i\mathbf{k}_1\cdot\mathbf{d}} = e^{i(\mathbf{k}_1\cdot\mathbf{d})(n_1+m_1-n_3-m_3)} + e^{i(\mathbf{k}_2\cdot\mathbf{d})(n_2+m_2-n_3-m_3)} \tag{3-104}$$

for all displacements $\mathbf{d}$, and therefore

$$1 = n_1 + m_1 - n_3 - m_3 \tag{3-105}$$

$$0 = n_2 + m_2 - n_2 - m_3 . \tag{3-106}$$

One must solve a system of three equations, (3-102), (3-105) and (3-106), for six variable integers. There is a three parameter family of solutions. It is a nontrivial condition that all of the variables are indeed integers. For instance, arbitrarily choosing $n_1 = n_2 = n_3 = 0$ leads to the solution $m_1 = \frac{1}{3}$, $m_2 = m_3 = -\frac{2}{3}$, which is not an integer solution.

The integer solutions of the system (3-102), (3-105) and (3-106) are given by

$$\begin{aligned} n_1 &= 1 + p - q - r \\ n_2 &= p + q \\ n_3 &= p + r \\ m_1 &= p + q + r \\ m_2 &= p - q \\ m_3 &= p - r \end{aligned} \tag{3-107}$$

where p, q, and r range over all the integers. Those who wish can skip the proof and go to the table of results below.

To find the integer solutions of the system, first solve for n_1 and m_1. This can be done by taking the combinations (3-102) $\pm$ (3-105) $-\frac{1}{2}$ (3-106):

$$n_1 = 1 - \tfrac{1}{4}\left[(n_2 + n_3) - 3(m_2 + m_3)\right] \tag{3-108}$$

$$m_1 = \tfrac{1}{4}\left[3(n_2 + n_3) - (m_2 + m_3)\right]. \tag{3-109}$$

For the moment, let

$$n_2 + n_3 \equiv \sigma \text{ , and } m_2 + m_3 \equiv \tau . \tag{3-110}$$

In order for n_1 and m_1 to be integers, it is necessary that

$$\sigma - 3\tau = 0 \pmod 4 \text{ , and } 3\sigma - \tau = 0 \pmod 4 . \tag{3-111}$$

Since $-3 = 1 \pmod 4$, these are both the same condition:

$$\sigma + \tau = 0 \pmod 4 . \tag{3-112}$$

All such pairs σ and τ can be written as

$$\sigma = 2p + l \text{ , and } \tau = 2p - l \tag{3-113}$$

for some unique pair of integers p and l. Obviously, all integers p and l yield an integer solution for σ and τ. The system of equations is now

$$n_2 + n_3 = 2p + l \tag{3-114}$$

$$m_2 + m_3 = 2p - l \tag{3-115}$$

$$0 = n_2 - n_3 + m_2 - m_3 . \tag{3-116}$$

This is a system of three equations for six variables, so there is a three parameter family of solutions. In terms of the integer parameters p, q, and r, the solutions are

$$p = p \text{ , } l = q + r \text{ , } \tag{3-117}$$

$$n_2 = p + q \text{ , } n_3 = p + r \text{ , } m_2 = p - q \text{ , } m_3 = p - r \text{ . } \tag{3-118}$$

These values are then substituted into (3-108) and (3-109) to obtain the solutions listed above, (3-107). This ends the proof.

The following table shows the terms of order five or less. When $q \neq r$ there is another term with $[2 \leftrightarrow 3]$, which comes about when q and r switched.

p	q	r	n_1	n_2	m_3	m_1	m_2	m_3	$\dot{z}_1 \propto$
0	0	0	1	0	0	0	0	0	z_1
0	1	0	0	1	0	1	−1	0	$z_2 w_1 \bar{w}_2$
−1	0	0	0	−1	−1	−1	−1	−1	$\bar{z}_2 \bar{z}_3 \bar{w}_1 \bar{w}_2 \bar{w}_3$
0	−1	0	2	−1	0	−1	1	0	$z_1^2 \bar{z}_2 \bar{w}_1 w_2$
−1	1	−1	0	0	−2	1	−2	0	$\bar{z}_3^2 w_1 \bar{w}_2^2$

Table 3-1. Equivariant terms for oscillatory convection on a hexagonal lattice.

The vector fields which are equivariant under the symmetries appropriate to normal forms for oscillatory convection in a hexagonal lattice can be written as

$$\dot{z}_1 = \sum_{p,q,r=-\infty}^{\infty} \left[z_1^{(1+p-q-r)} z_2^{(p+q)} z_3^{(p+r)} w_1^{(p+q+r)} w_2^{(p-q)} w_3^{(p-r)} f_{p,q,r} \right. \\ \left. +[2 \leftrightarrow 3] \right], \tag{3-119}$$

where $f_{p,q,r}$ are arbitrary complex valued functions of $|z_1|^2$, $|z_2|^2$, $|z_3|^2$, $|w_1|^2$, $|w_2|^2$, and $|w_3|^2$:

$$f_{p,q,r}: \mathbb{R}^6 \to \mathbb{C}. \tag{3-120}$$

The equations for the five other complex amplitudes follow from the discrete symmetries: the 180° rotation,

$$z_\alpha \leftrightarrow \bar{w}_\alpha, \quad \alpha = 1, 2 \text{ and } 3, \tag{3-121}$$

and the 120° rotation, or cyclic permutation symmetry,

$$\left\{ \begin{array}{l} (z_1, w_1) \to (z_2, w_2) \\ (z_2, w_2) \to (z_3, w_3) \\ (z_3, w_3) \to (z_1, w_1). \end{array} \right\} \tag{3-122}$$

Truncating the normal form to third order gives

$$\dot{z}_1 = z_1 \left[(\lambda + i\omega) + a_1 |z_1|^2 + a_2 (|z_2|^2 + |z_3|^2) + b_1 |w_1|^2 + b_2 (|w_2|^2 + |w_3|^2) \right] \\ + c\,(z_2 w_1 \bar{w}_2 + z_3 w_1 \bar{w}_3). \tag{3-123}$$

where the coefficients a_α, b_α, and c are complex.

In addition to the solutions present on the rectangular lattice there are hexagonal solutions to the cubic truncation:

- Traveling hexagons I

$$z_1 = z_2 = z_3, \quad \text{AOZ} \tag{3-124}$$

$$A^2 = \frac{-3\lambda}{\mathrm{Re}(a_1 + 2a_2)} \tag{3-125}$$

- Standing hexagons I

$$z_1 = \bar{w}_1 = z_2 = \bar{w}_2 = z_3 = \bar{w}_3 \tag{3-126}$$

$$A^2 = \frac{-6\lambda}{\mathrm{Re}(a_1 + 2a_2 + b_1 + 2b_2 + 2c)}. \tag{3-127}$$

- Standing regular triangles I

$$z_1 = -\overline{w}_1 = z_2 = -\overline{w}_2 = z_3 = -\overline{w}_3 \tag{3-128}$$

$$A^2 = \frac{-6\lambda}{\mathrm{Re}(a_1+2a_2+b_1+2b_2+2c)}. \tag{3-129}$$

Note that the "traveling hexagons" are similar to the stationary triangles (see section 2.9.2), except that Φ increases linearly with time. The standing hexagons and regular triangles are have the same planform as the corresponding stationary patterns, except that the amplitude varies like $\sin(\omega t)$.

There are undoubtedly more types of traveling and standing hexagons, but the dynamics of the phases is quite complicated. A full analysis has not been attempted. There are six phases and three translational symmetries, so there are three invariant functions of the phases. It is evident that the cubic truncation is not sufficient, however, because the standing hexagons and standing regular triangles have the same amplitude squared (3-127) and (3-129). The fifth order terms listed in table 2-1 with $p = -1$ cause the amplitudes of these two solutions to be different, since they involve odd powers of w_α. Although the normal form for this example is not known, the solutions listed here, (3-74)ff and (3-124)ff, are sure to survive when the higher order terms are added, because of their symmetry.

Chapter Four

Calculational Techniques

This chapter describes how to generate the nonlinear terms in the infinite set of ODEs corresponding to the partial differential equations (PDEs) of convection. In addition, the coefficients of the normal form for doubly diffusive convection are calculated using the center manifold reduction of the infinite dimensional set of ODEs.

4.1. Nonlinear couplings

In Chapter One the linear ODEs for any $(\mathbf{k},n)$ spatial mode are presented for the simplest boundary conditions. In this section, the linear terms are dropped to accentuate the nonlinear terms. All of the special cases of convection can be treated together, since the nonlinear terms are the same. The ODEs of interest are

$$\hat{\mathbf{z}}\cdot\nabla\times\nabla\times\dot{\mathbf{u}} = lin. -\hat{\mathbf{z}}\cdot\nabla\times\nabla\times[(\mathbf{u}\cdot\nabla)\mathbf{u}] \tag{4-1}$$

$$\hat{\mathbf{z}}\cdot\nabla\times\dot{\mathbf{u}} = lin. -\hat{\mathbf{z}}\cdot\nabla\times[(\mathbf{u}\cdot\nabla)\mathbf{u}] \tag{4-2}$$

$$\dot{\vartheta} = lin. -\mathbf{u}\cdot\nabla\vartheta \tag{4-3}$$

$$\dot{\xi} = lin. -\mathbf{u}\cdot\nabla\xi\,. \tag{4-4}$$

where the overdot represents the partial time derivative, and "*lin.*" replaces the linear terms. The fields are represented as sums of the complex plane waves

$$e_{\mathbf{k},n} \equiv e^{i(\mathbf{k}\cdot\mathbf{x}+nz)}. \tag{4-5}$$

The velocity field is

$$\mathbf{u} = \sum_{\substack{\mathbf{k}\in\mathbb{Z}^2 \\ \mathbf{k}\cdot\hat{\mathbf{z}}=0}} \sum_{n=-\infty}^{\infty} [w_{\mathbf{k},n}\mathbf{W}_{\mathbf{k},n} + \zeta_{\mathbf{k},n}\mathbf{Z}_{\mathbf{k},n}] \equiv \sum_{\mathbf{k}}\sum_{n}\mathbf{u}_{\mathbf{k},n}, \text{ where} \tag{4-6}$$

$$\mathbf{W}_{\mathbf{k},n} = (-\mathbf{k}n + |\mathbf{k}|^2\hat{\mathbf{z}})e_{\mathbf{k},n} \text{ are the vertical velocity modes,} \tag{4-7}$$

$$\mathbf{Z}_{\mathbf{k},n} = (\hat{\mathbf{z}}\times\mathbf{k})e_{\mathbf{k},n} \text{ are the vertical vorticity modes,} \tag{4-8}$$

and $w_{\mathbf{k},n}$ and $\zeta_{\mathbf{k},n}$ are time-dependent complex amplitudes. In the sums, $\mathbf{k}$ ranges over a lattice in the plane, so all fields are doubly periodic, and n goes from $-\infty$ to ∞. The temperature and solute variations relative to a linear profile are

$$\vartheta = \sum_{\mathbf{k}}\sum_{n}(\vartheta_{\mathbf{k},n}\, e_{\mathbf{k},n}), \text{ and} \tag{4-9}$$

$$\xi = \sum_{\mathbf{k}}\sum_{n}(\xi_{\mathbf{k},n}\, e_{\mathbf{k},n}). \tag{4-10}$$

The pure exponential notation has many advantages over sines and cosines. Two modes, $(\mathbf{k},n)$ and $(\mathbf{k}',n')$, only couple to one mode, $(\mathbf{k}+\mathbf{k}',n+n')$, whereas the product of two sine functions involves the sum and difference of the two arguments. In addition, the curl and divergence operators are simpler in the pure exponential notation because "∇" is replaced by "$i(\mathbf{k}+n\hat{\mathbf{z}})$."

Starting with the simplest nonlinear terms, the ϑ equation is

$$\sum_{\mathbf{k}}\sum_{n}(\dot{\vartheta}_{\mathbf{k},n}\, e_{\mathbf{k},n}) = lin. - \sum_{\mathbf{k}'}\sum_{n'}\sum_{\mathbf{k}''}\sum_{n''}\mathbf{u}_{\mathbf{k}',n'}\cdot\nabla(\vartheta_{\mathbf{k}'',n''}\, e_{\mathbf{k}'',n''}). \tag{4-11}$$

Due to the mode coupling property of exponential waves, only $\mathbf{k}'' = \mathbf{k}-\mathbf{k}'$ and $n'' = n-n'$ contribute to the $(\mathbf{k},n)$ term on the left hand side. Each such term can be written separately:

$$\dot{\vartheta}_{\mathbf{k},n}\, e_{\mathbf{k},n} = lin. - \sum_{\mathbf{k}'}\sum_{n'}\mathbf{u}_{\mathbf{k}',n'}\cdot\nabla(\vartheta_{\mathbf{k}-\mathbf{k}',n-n'}\, e_{\mathbf{k}-\mathbf{k}',n-n'}). \tag{4-12}$$

The amplitude $\vartheta_{\mathbf{k},n}$ has no spatial dependence, therefore the gradient does not affect it. The nonlinear coupling needed for both the temperature and solute equations is

$$\mathbf{u}_{\mathbf{k}',n'}\cdot\nabla e_{\mathbf{k}-\mathbf{k}',n-n'} = \left[w_{\mathbf{k}',n'}\mathbf{W}_{\mathbf{k}',n'} + \zeta_{\mathbf{k}',n'}\mathbf{Z}_{\mathbf{k}',n'}\right]\cdot i\left[\mathbf{k}-\mathbf{k}'+(n-n')\hat{\mathbf{z}}\right]e_{\mathbf{k}-\mathbf{k}',n-n'} \tag{4-13}$$

$$= i[(n\,|\mathbf{k}'|^2 - n'\mathbf{k}\cdot\mathbf{k}')w_{\mathbf{k}',n'} + (\hat{\mathbf{z}}\cdot\mathbf{k}'\times\mathbf{k})\xi_{\mathbf{k}',n'}]e_{\mathbf{k},n}. \tag{4-14}$$

Therefore, the nonlinear equations for the temperature and solute variations

are

$$\dot{\vartheta}_{\mathbf{k},n} = lin. -i\sum_{\mathbf{k}'}\sum_{n'}[(n\,|\,\mathbf{k}'\,|^2 - n'\mathbf{k}\cdot\mathbf{k}')w_{\mathbf{k}',n'} + (\hat{\mathbf{z}}\cdot\mathbf{k}'\times\mathbf{k})\xi_{\mathbf{k}',n'}]\vartheta_{\mathbf{k}-\mathbf{k}',n-n'}, \qquad (4\text{-}15)$$

$$\dot{\xi}_{\mathbf{k},n} = lin. -i\sum_{\mathbf{k}'}\sum_{n'}[(n\,|\,\mathbf{k}'\,|^2 - n'\mathbf{k}\cdot\mathbf{k}')w_{\mathbf{k}',n'} + (\hat{\mathbf{z}}\cdot\mathbf{k}'\times\mathbf{k})\xi_{\mathbf{k}',n'}]\xi_{\mathbf{k}-\mathbf{k}',n-n'}. \qquad (4\text{-}16)$$

A similar procedure works for the velocity. Recall that repeated curls are used to eliminate the pressure term and separate the vertical velocity and vertical vorticity fields:

$$\hat{\mathbf{z}}\cdot\nabla\times\nabla\times\dot{\mathbf{u}}_{\mathbf{k},n} = |\,\mathbf{k}\,|^2(|\,\mathbf{k}\,|^2+n^2)\dot{w}_{\mathbf{k},n}e_{\mathbf{k},n} = lin. -\sum_{\mathbf{k}'}\sum_{n'}\hat{\mathbf{z}}\cdot\nabla\times\nabla\times[(\mathbf{u}_{\mathbf{k}',n'}\cdot\nabla)\mathbf{u}_{\mathbf{k}-\mathbf{k}',n-n'}] \quad (4\text{-}17)$$

$$\hat{\mathbf{z}}\cdot\nabla\times\dot{\mathbf{u}}_{\mathbf{k},n} = i\,|\,\mathbf{k}\,|^2\dot{\zeta}_{\mathbf{k},n}e_{\mathbf{k},n} = lin. -\sum_{\mathbf{k}'}\sum_{n'}\hat{\mathbf{z}}\cdot\nabla\times[(\mathbf{u}_{\mathbf{k}',n'}\cdot\nabla)\mathbf{u}_{\mathbf{k}-\mathbf{k}',n-n'}]. \qquad (4\text{-}18)$$

Expanding the nonlinear terms and isolating the time derivatives of the amplitudes, this implies

$$\dot{w}_{\mathbf{k},n} = lin. -\frac{e_{-\mathbf{k},-n}}{|\,\mathbf{k}\,|^2(|\,\mathbf{k}\,|^2+n^2)}\hat{\mathbf{z}}\cdot\nabla\times\nabla\times\sum_{\mathbf{k}'}\sum_{n'}\begin{bmatrix} w_{\mathbf{k}',n'}w_{\mathbf{k}-\mathbf{k}',n-n'}\left[(\mathbf{W}_{\mathbf{k}',n'}\cdot\nabla)\mathbf{W}_{\mathbf{k}-\mathbf{k}',n-n'}\right] \\ +w_{\mathbf{k}',n'}\zeta_{\mathbf{k}-\mathbf{k}',n-n'}\begin{bmatrix}(\mathbf{W}_{\mathbf{k}',n'}\cdot\nabla)\mathbf{Z}_{\mathbf{k}-\mathbf{k}',n-n'} \\ +(\mathbf{Z}_{\mathbf{k}-\mathbf{k}',n-n'}\cdot\nabla)\mathbf{W}_{\mathbf{k}',n'}\end{bmatrix} \\ +\zeta_{\mathbf{k}',n'}\zeta_{\mathbf{k}-\mathbf{k}',n-n'}\left[(\mathbf{Z}_{\mathbf{k}',n'}\cdot\nabla)\mathbf{Z}_{\mathbf{k}-\mathbf{k}',n-n'}\right] \end{bmatrix} \quad (4\text{-}19)$$

and

$$\dot{\zeta}_{\mathbf{k},n} = lin. -\frac{e_{-\mathbf{k},-n}}{i\,|\,\mathbf{k}\,|^2}\hat{\mathbf{z}}\cdot\nabla\times\sum_{\mathbf{k}'}\sum_{n'}\begin{bmatrix} w_{\mathbf{k}',n'}w_{\mathbf{k}-\mathbf{k}',n-n'}\left[(\mathbf{W}_{\mathbf{k}',n'}\cdot\nabla)\mathbf{W}_{\mathbf{k}-\mathbf{k}',n-n'}\right] \\ +w_{\mathbf{k}',n'}\zeta_{\mathbf{k}-\mathbf{k}',n-n'}\begin{bmatrix}(\mathbf{W}_{\mathbf{k}',n'}\cdot\nabla)\mathbf{Z}_{\mathbf{k}-\mathbf{k}',n-n'} \\ +(\mathbf{Z}_{\mathbf{k}-\mathbf{k}',n-n'}\cdot\nabla)\mathbf{W}_{\mathbf{k}',n'}\end{bmatrix} \\ +\zeta_{\mathbf{k}',n'}\zeta_{\mathbf{k}-\mathbf{k}',n-n'}\left[(\mathbf{Z}_{\mathbf{k}',n'}\cdot\nabla)\mathbf{Z}_{\mathbf{k}-\mathbf{k}',n-n'}\right] \end{bmatrix}. \quad (4\text{-}20)$$

In the sums over $\mathbf{k}'$ and n', every pair of modes adding up to $(\mathbf{k},n)$ is counted twice. The $\mathbf{WW}$ and $\mathbf{ZZ}$ terms on the right hand side of equations (4-19) and (4-20) can be symmetrized,

$$(\mathbf{W}_{\mathbf{k},n}\cdot\nabla)\mathbf{W}_{\mathbf{k}',n'} \to \tfrac{1}{2}\left[(\mathbf{W}_{\mathbf{k},n}\cdot\nabla)\mathbf{W}_{\mathbf{k}',n'} + (\mathbf{W}_{\mathbf{k}',n'}\cdot\nabla)\mathbf{W}_{\mathbf{k},n}\right] \qquad (4\text{-}21)$$

$$(\mathbf{Z}_{\mathbf{k},n}\cdot\nabla)\mathbf{Z}_{\mathbf{k}',n'} \to \tfrac{1}{2}\left[(\mathbf{Z}_{\mathbf{k},n}\cdot\nabla)\mathbf{Z}_{\mathbf{k}',n'} + (\mathbf{Z}_{\mathbf{k}',n'}\cdot\nabla)\mathbf{Z}_{\mathbf{k},n}\right]. \qquad (4\text{-}22)$$

If each $(\mathbf{k},n)$, $(\mathbf{k}',n')$ pair is counted only once the factor of one half can be dropped for these terms. Each pair must be counted twice for the $\mathbf{ZW}$ term, however.

It is useful to have a notation for the nonlinear couplings. Let

$$N^{w:ww}_{\mathbf{k}',n';\mathbf{k}-\mathbf{k}',n-n'} = \frac{e_{-\mathbf{k},-n}}{|\mathbf{k}|^2(|\mathbf{k}|^2+n^2)}\hat{\mathbf{z}}\cdot\nabla\times\nabla\times\tfrac{1}{2}\begin{pmatrix}(\mathbf{W}_{\mathbf{k}',n'}\cdot\nabla)\mathbf{W}_{\mathbf{k}-\mathbf{k}',n-n'}\\+(\mathbf{W}_{\mathbf{k}-\mathbf{k}',n-n'}\cdot\nabla)\mathbf{W}_{\mathbf{k}',n'}\end{pmatrix} \tag{4-23}$$

$$N^{w:w\zeta}_{\mathbf{k}',n';\mathbf{k}-\mathbf{k}',n-n'} = \frac{e_{-\mathbf{k},-n}}{|\mathbf{k}|^2(|\mathbf{k}|^2+n^2)}\hat{\mathbf{z}}\cdot\nabla\times\nabla\times\begin{pmatrix}(\mathbf{W}_{\mathbf{k}',n'}\cdot\nabla)\mathbf{Z}_{\mathbf{k}-\mathbf{k}',n-n'}\\+(\mathbf{Z}_{\mathbf{k}-\mathbf{k}',n-n'}\cdot\nabla)\mathbf{W}_{\mathbf{k}',n'}\end{pmatrix} \tag{4-24}$$

$$N^{w:\zeta\zeta}_{\mathbf{k}',n';\mathbf{k}-\mathbf{k}',n-n'} = \frac{e_{-\mathbf{k},-n}}{|\mathbf{k}|^2(|\mathbf{k}|^2+n^2)}\hat{\mathbf{z}}\cdot\nabla\times\nabla\times\tfrac{1}{2}\begin{pmatrix}(\mathbf{Z}_{\mathbf{k}',n'}\cdot\nabla)\mathbf{Z}_{\mathbf{k}-\mathbf{k}',n-n'}\\+(\mathbf{Z}_{\mathbf{k}-\mathbf{k}',n-n'}\cdot\nabla)\mathbf{Z}_{\mathbf{k}',n'}\end{pmatrix} \tag{4-25}$$

$$N^{\zeta:ww}_{\mathbf{k}',n';\mathbf{k}-\mathbf{k}',n-n'} = \frac{e_{-\mathbf{k},-n}}{i|\mathbf{k}|^2}\hat{\mathbf{z}}\cdot\nabla\times\tfrac{1}{2}\left[(\mathbf{W}_{\mathbf{k}',n'}\cdot\nabla)\mathbf{W}_{\mathbf{k}-\mathbf{k}',n-n'}+(\mathbf{W}_{\mathbf{k}-\mathbf{k}',n-n'}\cdot\nabla)\mathbf{W}_{\mathbf{k}',n'}\right] \tag{4-26}$$

$$N^{\zeta:w\zeta}_{\mathbf{k}',n';\mathbf{k}-\mathbf{k}',n-n'} = \frac{e_{-\mathbf{k},-n}}{i|\mathbf{k}|^2}\hat{\mathbf{z}}\cdot\nabla\times\left[(\mathbf{W}_{\mathbf{k}',n'}\cdot\nabla)\mathbf{Z}_{\mathbf{k}-\mathbf{k}',n-n'}+(\mathbf{Z}_{\mathbf{k}-\mathbf{k}',n-n'}\cdot\nabla)\mathbf{W}_{\mathbf{k}',n'}\right] \tag{4-27}$$

$$N^{\zeta:\zeta\zeta}_{\mathbf{k}',n';\mathbf{k}-\mathbf{k}',n-n'} = \frac{e_{-\mathbf{k},-n}}{i|\mathbf{k}|^2}\hat{\mathbf{z}}\cdot\nabla\times\tfrac{1}{2}\left[(\mathbf{Z}_{\mathbf{k}',n'}\cdot\nabla)\mathbf{Z}_{\mathbf{k}-\mathbf{k}',n-n'}+(\mathbf{Z}_{\mathbf{k}-\mathbf{k}',n-n'}\cdot\nabla)\mathbf{Z}_{\mathbf{k}',n'}\right] \tag{4-28}$$

$$N^{e:we}_{\mathbf{k}',n';\mathbf{k}-\mathbf{k}',n-n'} = (e_{-\mathbf{k},-n})\mathbf{W}_{\mathbf{k},n}\cdot\nabla e_{\mathbf{k}-\mathbf{k}',n-n'} \tag{4-29}$$

$$N^{e:\zeta e}_{\mathbf{k}',n';\mathbf{k}-\mathbf{k}',n-n'} = (e_{-\mathbf{k},-n})\mathbf{Z}_{\mathbf{k},n}\cdot\nabla e_{\mathbf{k}-\mathbf{k}',n-n'}. \tag{4-30}$$

Using these definitions, the ODEs can be written

$$\dot{w}_{\mathbf{k},n} = lin. -\sum_{\mathbf{k}'}\sum_{n'}\begin{pmatrix}N^{w:ww}_{\mathbf{k}',n';\mathbf{k}-\mathbf{k}',n-n'}(w_{\mathbf{k}',n'})(w_{\mathbf{k}-\mathbf{k}',n-n'})\\+N^{w:w\zeta}_{\mathbf{k}',n';\mathbf{k}-\mathbf{k}',n-n'}(w_{\mathbf{k}',n'})(\zeta_{\mathbf{k}-\mathbf{k}',n-n'})\\+N^{w:\zeta\zeta}_{\mathbf{k}',n';\mathbf{k}-\mathbf{k}',n-n'}(\zeta_{\mathbf{k}',n'})(\zeta_{\mathbf{k}-\mathbf{k}',n-n'})\end{pmatrix} \tag{4-31}$$

$$\dot{\zeta}_{\mathbf{k},n} = lin. -\sum_{\mathbf{k}'}\sum_{n'}\begin{pmatrix}N^{\zeta:ww}_{\mathbf{k}',n';\mathbf{k}-\mathbf{k}',n-n'}(w_{\mathbf{k}',n'})(w_{\mathbf{k}-\mathbf{k}',n-n'})\\+N^{\zeta:w\zeta}_{\mathbf{k}',n';\mathbf{k}-\mathbf{k}',n-n'}(w_{\mathbf{k}',n'})(\zeta_{\mathbf{k}-\mathbf{k}',n-n'})\\+N^{\zeta:\zeta\zeta}_{\mathbf{k}',n';\mathbf{k}-\mathbf{k}',n-n'}(\zeta_{\mathbf{k}',n'})(\zeta_{\mathbf{k}-\mathbf{k}',n-n'})\end{pmatrix} \tag{4-32}$$

$$\dot{\vartheta}_{\mathbf{k},n} = lin. -\sum_{\mathbf{k}'}\sum_{n'}\begin{pmatrix}N^{e:we}_{\mathbf{k}',n';\mathbf{k}-\mathbf{k}',n-n'}(w_{\mathbf{k}',n'})(\vartheta_{\mathbf{k}-\mathbf{k}',n-n'})\\+N^{e:\zeta e}_{\mathbf{k}',n';\mathbf{k}-\mathbf{k}',n-n'}(\zeta_{\mathbf{k}',n'})(\vartheta_{\mathbf{k}-\mathbf{k}',n-n'})\end{pmatrix} \tag{4-33}$$

$$\dot{\xi}_{\mathbf{k},n} = lin. -\sum_{\mathbf{k}'}\sum_{n'}\begin{Bmatrix} N^{e:we}_{\mathbf{k}',n';\mathbf{k}-\mathbf{k}',n-n'}(w_{\mathbf{k}',n'})(\xi_{\mathbf{k}-\mathbf{k}',n-n'}) \\ +N^{e:\zeta e}_{\mathbf{k}',n';\mathbf{k}-\mathbf{k}',n-n'}(\zeta_{\mathbf{k}',n'})(\xi_{\mathbf{k}-\mathbf{k}',n-n'}) \end{Bmatrix}. \tag{4-34}$$

The velocity couplings can be computed with the help of the identities

$$\hat{\mathbf{z}}\cdot\nabla\times\nabla\times(\mathbf{A}e_{\mathbf{k},n}) = (-\mathbf{k}n + |\mathbf{k}|^2\hat{\mathbf{z}})\cdot\mathbf{A}e_{\mathbf{k},n} \tag{4-35}$$

$$\hat{\mathbf{z}}\cdot\nabla\times(\mathbf{A}e_{\mathbf{k},n}) = i\hat{\mathbf{z}}\cdot\mathbf{k}\times\mathbf{A}e_{\mathbf{k},n}, \tag{4-36}$$

where **A** is a constant vector. The result of a few pages of straightforward calculation is:

$$N^{w:ww}_{\mathbf{k},n;\mathbf{k}',n'} = \frac{1}{2}C_w\begin{Bmatrix} (n+n')\begin{Bmatrix}\mathbf{k}\cdot\mathbf{k}'(n'^2|\mathbf{k}|^2+n^2|\mathbf{k}'|^2-nn'|\mathbf{k}+\mathbf{k}'|^2)\\ +(n^2+n'^2)|\mathbf{k}|^2|\mathbf{k}'|^2\end{Bmatrix} \\ +|\mathbf{k}+\mathbf{k}'|^2\begin{Bmatrix}(n+n')|\mathbf{k}|^2|\mathbf{k}'|^2\\ -\mathbf{k}\cdot\mathbf{k}'(n|\mathbf{k}'|^2+n'|\mathbf{k}|^2)\end{Bmatrix}\end{Bmatrix} \tag{4-37}$$

$$N^{w:w\zeta}_{\mathbf{k},n;\mathbf{k}',n'} = C_w(\hat{\mathbf{z}}\cdot\mathbf{k}\times\mathbf{k}')\begin{Bmatrix}(n+n')[-2n\,\mathbf{k}\cdot\mathbf{k}'+(n'-n)|\mathbf{k}|^2]\\ -|\mathbf{k}|^2|\mathbf{k}+\mathbf{k}'|^2\end{Bmatrix} \tag{4-38}$$

$$N^{w:\zeta\zeta}_{\mathbf{k},n;\mathbf{k}',n'} = \frac{1}{2}C_w(\hat{\mathbf{z}}\cdot\mathbf{k}\times\mathbf{k}')^2\,2(n+n') \tag{4-39}$$

$$N^{\zeta:ww}_{\mathbf{k},n;\mathbf{k}',n'} = \frac{1}{2i|\mathbf{k}+\mathbf{k}'|^2}(\hat{\mathbf{z}}\cdot\mathbf{k}\times\mathbf{k}')(n'^2|\mathbf{k}|^2-n^2|\mathbf{k}'|^2) \tag{4-40}$$

$$N^{\zeta:w\zeta}_{\mathbf{k},n;\mathbf{k}',n'} = \frac{1}{i|\mathbf{k}+\mathbf{k}'|^2}\left[(|\mathbf{k}'|^2+\mathbf{k}\cdot\mathbf{k}')(n\,\mathbf{k}\cdot\mathbf{k}'-n'|\mathbf{k}|^2)+n(\hat{\mathbf{z}}\cdot\mathbf{k}\times\mathbf{k}')^2\right] \tag{4-41}$$

$$N^{\zeta:\zeta\zeta}_{\mathbf{k},n;\mathbf{k}',n'} = \frac{1}{2i|\mathbf{k}+\mathbf{k}'|^2} = (\hat{\mathbf{z}}\cdot\mathbf{k}\times\mathbf{k}')(|\mathbf{k}|^2-|\mathbf{k}'|^2) \tag{4-42}$$

$$N^{e:we}_{\mathbf{k},n;\mathbf{k}',n'} = i(-n\,\mathbf{k}\cdot\mathbf{k}'+n'|\mathbf{k}|^2), \text{ and} \tag{4-43}$$

$$N^{e:\zeta e}_{\mathbf{k},n;\mathbf{k}',n'} = i(\hat{\mathbf{z}}\cdot\mathbf{k}\times\mathbf{k}'). \tag{4-44}$$

The first three expressions above use the temporary notation:

$$C_w \equiv \frac{i}{|\mathbf{k}+\mathbf{k}'|^2\left[|\mathbf{k}+\mathbf{k}'|^2+(n+n')^2\right]}. \tag{4-45}$$

These nonlinear couplings can be inserted into equations (4-31), (4-32) and (4-33) to give the full infinite dimensional ODE. The last two equations are included for completeness, although the nonlinear equations for ϑ and ξ have already been written ((4-15) and (4-16)). Note the difference between equation (4-13) and (4-43). In the first, the modes are chosen so that they couple to $(\mathbf{k},n)$. This is desirable for writing the full equations symbolically, such as equation (4-15). In equation (4-43), $\mathbf{k}$ and $\mathbf{k}'$ are only dummy indices. This representation is easier to use when the truncated ODEs are generated by hand.

Although the nonlinear couplings (4-37)-(4-44) may seem complicated, they are quite compact. Ken Rimey and John Salmon used the vaxima computer algebra program to compute these nonlinear couplings. They used sines and cosines rather than pure exponentials and it took approximately 3 pages to display the results.

4.2. Symmetries of the ODEs

In this section the symmetries of the infinite dimensional ODEs are discussed. Some of the symmetries are associated with the constraints, such as boundary conditions. For these symmetries, the system must remain invariant under the symmetry transformation. Other, more general symmetries are also discussed.

The ODEs can be written symbolically as

$$\dot{\mathbf{a}} = \mathbf{f}(\mathbf{a}) \tag{4-46}$$

where $\mathbf{a}$ is an infinite dimensional vector of amplitudes. The symmetries discussed here are *linear* transformations of the amplitudes,

$$\mathbf{a} \to \gamma\mathbf{a}, \tag{4-47}$$

which commute with the function $\mathbf{f}$:

$$\mathbf{f}(\gamma\mathbf{a}) = \gamma\mathbf{f}(\mathbf{a}), \quad \text{or} \quad \mathbf{f}\circ\gamma = \gamma\circ\mathbf{f}. \tag{4-48}$$

This says that $\mathbf{f}$ is *equivariant* under the symmetry, or that γ is a symmetry of

the ODE.

4.2.1. Constraints

There is no *a priori* guarantee that the nonlinear terms preserve the stress free boundary conditions. If the boundary conditions are not preserved then Lagrange multipliers are needed, and the problem become intractable using a "pencil and paper" approach (See the discussion in Chapter One). The boundary conditions are satisfied if

$$\begin{aligned} w_{\mathbf{k},n} + w_{\mathbf{k},-n} &= 0 \\ \zeta_{\mathbf{k},n} - \zeta_{\mathbf{k},-n} &= 0 \\ \vartheta_{\mathbf{k},n} + \vartheta_{\mathbf{k},-n} &= 0 \\ \xi_{\mathbf{k},n} + \xi_{\mathbf{k},-n} &= 0 . \end{aligned} \tag{4-49}$$

These constraints are stronger than the free boundary conditions, but they are necessary for the modal techniques used here.

It will be shown that the boundary conditions *are* preserved since the nonlinear terms are equivariant under the $\mathbb{Z}_2$ symmetry

$$\begin{aligned} w_{\mathbf{k},n} &\to -w_{\mathbf{k},-n} \\ \zeta_{\mathbf{k},n} &\to +\zeta_{\mathbf{k},-n} \\ \vartheta_{\mathbf{k},n} &\to -\vartheta_{\mathbf{k},-n} \\ \xi_{\mathbf{k},n} &\to -\xi_{\mathbf{k},-n} . \end{aligned} \tag{4-50}$$

The equivariance follows from the symmetry of the couplings:

$$\mathrm{N}^{w:ww}, \mathrm{N}^{w:\zeta\zeta}, \mathrm{N}^{\zeta:w\zeta}, \text{ and } \mathrm{N}^{\vartheta:w\vartheta} \text{ are odd, and} \tag{4-51}$$

$$\mathrm{N}^{w:w\zeta}, \mathrm{N}^{\zeta:ww}, \mathrm{N}^{\zeta:\zeta\zeta}, \text{ and } \mathrm{N}^{\vartheta:\zeta\vartheta} \text{ are even,} \tag{4-52}$$

under the interchange $(n,n') \to (-n,-n')$. For example,

$$\mathrm{N}^{w:ww}_{\mathbf{k},n;\mathbf{k}',n'} = -\mathrm{N}^{w:ww}_{\mathbf{k},-n;\mathbf{k}',-n'} \tag{4-53}$$

$$\mathrm{N}^{w:w\zeta}_{\mathbf{k},n;\mathbf{k}',n'} = \mathrm{N}^{w:w\zeta}_{\mathbf{k},-n;\mathbf{k}',-n'}, \text{ etc.} \tag{4-54}$$

To see how this symmetry works, consider a typical set of terms:

$$\dot{w}_{\mathbf{k},n} = \cdots - \sum_{\mathbf{k}'} \sum_{n'} \mathrm{N}^{w:w\zeta}_{\mathbf{k}',n';\mathbf{k}-\mathbf{k}',n-n'} (w_{\mathbf{k}',n'})(\zeta_{\mathbf{k}-\mathbf{k}',n-n'}) + \cdots . \tag{4-55}$$

The left hand side of the equivariance condition (4-48) is

$$\dot{w}_{\mathbf{k},n}(\gamma\mathbf{a}) = \cdots - \sum_{\mathbf{k}'}\sum_{n'} N^{w:w\zeta}_{\mathbf{k}',n';\mathbf{k}-\mathbf{k}',n-n'}(-w_{\mathbf{k}',-n'})(\zeta_{\mathbf{k}-\mathbf{k}',-n+n'}) + \cdots, \tag{4-56}$$

$$= \cdots (-)^2 \sum_{\mathbf{k}'}\sum_{n'} N^{w:w\zeta}_{\mathbf{k}',n';\mathbf{k}-\mathbf{k}',n-n'}(w_{\mathbf{k}',-n'})(\zeta_{\mathbf{k}-\mathbf{k}',-n+n'}) + \cdots. \tag{4-57}$$

On the right hand side,

$$\gamma\dot{w}_{\mathbf{k},n}(\mathbf{a}) = -\dot{w}_{\mathbf{k},-n} \tag{4-58}$$

$$= \cdots (-1)^2 \sum_{\mathbf{k}'}\sum_{n'} N^{w:w\zeta}_{\mathbf{k}',-n';\mathbf{k}-\mathbf{k}',-n+n'}(w_{\mathbf{k}',-n'})(\zeta_{\mathbf{k}-\mathbf{k}',-n+n'}) + \cdots, \tag{4-59}$$

Since $N^{w:w\zeta}$ is even under the interchange, the equivariance holds. It is fairly easy to verify that all of the nonlinear terms are equivariant.

As a consequence of the equivariance, the fixed point set,

$$\Delta_\gamma = \{\text{all } \mathbf{a} \text{ such that } \mathbf{a} - \gamma\mathbf{a} = 0\}, \tag{4-60}$$

is invariant under the dynamics. The proof is simple:

$$\frac{d}{dt}(\mathbf{a} - \gamma\mathbf{a}) = \mathbf{f}(\mathbf{a}) - \gamma\mathbf{f}(\mathbf{a}) = \mathbf{f}(\mathbf{a}) - \mathbf{f}(\gamma\mathbf{a}) \tag{4-61}$$

$$= 0 \text{ when restricted to } \mathbf{a} \in \Delta_\gamma. \tag{4-62}$$

Thus, if the initial condition is on Δ_γ, then the trajectory stays on Δ_γ for all time, and Δ_γ is invariant. The boundary conditions (4-50) imply that the system is constrained to the fixed point set. Due to the symmetry, the boundary conditions are automatically preserved by the dynamics. It is worth noting that, when the rotation vector is not vertical, the linear ODE is not equivariant under this symmetry and the strong form of the boundary conditions (4-50) cannot be used (see Chapter One).

The fields in the original PDEs are real. This implies another constraint on the amplitudes:

$$\begin{aligned} w_{\mathbf{k},n} - \overline{w}_{-\mathbf{k},-n} &= 0 \\ \zeta_{\mathbf{k},n} + \overline{\zeta}_{-\mathbf{k},-n} &= 0 \\ \vartheta_{\mathbf{k},n} - \overline{\vartheta}_{-\mathbf{k},-n} &= 0 \\ \xi_{\mathbf{k},n} - \overline{\xi}_{-\mathbf{k},-n} &= 0. \end{aligned} \tag{4-63}$$

As with the boundary conditions, this constraint is built into the equations

by a $\mathbb{Z}_2$ symmetry. The equations (4-31) through (4-34) are equivariant under

$$\begin{aligned} w_{\mathbf{k},n} &\to \overline{w}_{-\mathbf{k},-n} \\ \zeta_{\mathbf{k},n} &\to -\overline{\zeta}_{-\mathbf{k},-n} \\ \vartheta_{\mathbf{k},n} &\to \overline{\vartheta}_{-\mathbf{k},-n} \\ \xi_{\mathbf{k},n} &\to \overline{\xi}_{-\mathbf{k},-n}. \end{aligned} \tag{4-64}$$

The requirement that the physical fields are real constrains the system to be on the fixed point set of this symmetry. The equivariance follows from the following symmetry properties of the nonlinear couplings under the interchange $\mathbf{k} \to -\mathbf{k}$, $n \to -n$, and complex conjugation,

$$\mathrm{N}^{w:ww}, \mathrm{N}^{w:\zeta\zeta}, \mathrm{N}^{\zeta:w\zeta}, \text{ and } \mathrm{N}^{\vartheta:w\vartheta} \text{ are even, and} \tag{4-65}$$

$$\mathrm{N}^{w:w\zeta}, \mathrm{N}^{\zeta:ww}, \mathrm{N}^{\zeta:\zeta\zeta}, \text{ and } \mathrm{N}^{\vartheta:\zeta\vartheta} \text{ are odd.} \tag{4-66}$$

It can be explicitly verified that

$$\mathrm{N}^{w:ww}_{\mathbf{k},n;\mathbf{k}',n'} = \overline{\mathrm{N}}^{w:ww}_{-\mathbf{k},-n;-\mathbf{k}',-n'}, \text{ etc.} \tag{4-67}$$

The proof of equivariance, for a typical term, proceed as follows:

The left hand side of equation (4-48) is

$$\dot{\zeta}_{\mathbf{k},n}(\gamma\mathbf{a}) = \cdots - \sum_{\mathbf{k}'}\sum_{n'} \mathrm{N}^{\zeta:\zeta\zeta}_{\mathbf{k}',n';\mathbf{k}-\mathbf{k}',n-n'} (-\overline{\zeta}_{-\mathbf{k},-n})(-\overline{\zeta}_{-\mathbf{k}+\mathbf{k}',-n+n'}) + \cdots \tag{4-68}$$

$$= \cdots - \sum_{\mathbf{k}'}\sum_{n'} \mathrm{N}^{\zeta:\zeta\zeta}_{\mathbf{k}',n';\mathbf{k}-\mathbf{k}',n-n'} (\overline{\zeta}_{-\mathbf{k},-n})(\overline{\zeta}_{-\mathbf{k}+\mathbf{k}',-n+n'}) + \cdots. \tag{4-69}$$

The right hand side of the equivariance condition is

$$\gamma\dot{\zeta}_{\mathbf{k},n} = -\dot{\overline{\zeta}}_{-\mathbf{k},-n} \tag{4-70}$$

$$= \cdots (-1)^2 \sum_{\mathbf{k}'}\sum_{n'} \overline{\mathrm{N}}^{\zeta:\zeta\zeta}_{-\mathbf{k}',-n';-\mathbf{k}+\mathbf{k}',-n+n'} (\overline{\zeta}_{-\mathbf{k}',-n'})(\overline{\zeta}_{-\mathbf{k}+\mathbf{k}',-n+n'}) + \cdots \tag{4-71}$$

The equality follows since $\mathrm{N}^{\zeta:\zeta\zeta}$ changes sign under the symmetry. Note that the number of ζ's in the nonlinear coupling determines the parity under (4-64), with an extra minus sign added for the complex conjugation.

All of the fields are real in the initial condition, so the system is in the fixed point set of (4-64) at $t = 0$. The equivariance guarantees that the fields will stay real at all later times.

4.2.2. Other symmetries

There are other symmetries of the equations which do not correspond to constraints, and consequently the system is not necessarily on the fixed point sets of these symmetries. Note that all of the $\mathrm{N}^{x:xx}$ terms are pure imaginary, where x is one element of the set $\{w,\zeta,e\}$. This implies the symmetry

$$\mathbf{a}_{\mathbf{k},n} \to -\bar{\mathbf{a}}_{\mathbf{k},n}\ , \text{ where} \tag{4-72}$$

$$\mathbf{a}_{\mathbf{k},n} \equiv \begin{pmatrix} w_{\mathbf{k},n} \\ \zeta_{\mathbf{k},n} \\ \vartheta_{\mathbf{k},n} \\ \xi_{\mathbf{k},n} \end{pmatrix}. \tag{4-73}$$

Note that $\mathbf{a}_{\mathbf{k},n}$ is a four-dimensional vector, while $\mathbf{a}$ in equation (4-64) is an infinite dimensional vector. The amplitudes are not all pure imaginary for an arbitrary initial condition, although the origin of the coordinate system can be chosen so that two amplitudes are pure imaginary (see Chapter Two).

Another symmetry is related to the Boussinesq approximation. The Boussinesq symmetry (1-161) transforms the amplitudes as follows:

$$\mathbf{a}_{\mathbf{k},n} \to (-1)^n \mathbf{a}_{\mathbf{k},n} \tag{4-74}$$

The equivariance follows since $(\mathbf{k},n)$ and $(\mathbf{k}',n')$ couple to $(\mathbf{k}+\mathbf{k}',n+n')$:

$$\dot{w}_{\mathbf{k},n}(\gamma\mathbf{a}) = lin. - \sum_{\mathbf{k}'}\sum_{n'} \mathrm{N}^{w:ww}_{\mathbf{k}',n';\mathbf{k}-\mathbf{k}',n-n'} (-1)^{n'} w_{\mathbf{k}',n'} (-1)^{n-n'} w_{\mathbf{k}-\mathbf{k}',n-n'} + \cdots \tag{4-75}$$

$$= (-1)^n \dot{w}_{\mathbf{k},n} = \gamma \dot{w}_{\mathbf{k},n}. \tag{4-76}$$

Since the critical modes all have $n = 1$, this symmetry guarantees that the normal forms are equivariant under $(x_1, x_2) \to -(x_1, x_2)$, where (x_1, x_2) is the complex vector of critical roll amplitudes. This is called the Boussinesq symmetry in this dissertation. When the Boussinesq approximation is not valid, the critical eigenfunctions are not odd under the symmetry (4-74). (Typically the symmetry (4-74) does not hold for the linear terms, and the coefficients in the PDEs are not constant.)

The PDEs are equivariant under the Euclidean group in the horizontal plane. The translations in the plane,

$$\mathbf{x} \to \mathbf{x}+\mathbf{d}, \tag{4-77}$$

correspond to the phase shift

$$\mathbf{a}_{\mathbf{k},n} \to e^{i\mathbf{k}\cdot\mathbf{d}}\mathbf{a}_{\mathbf{k},n}. \tag{4-78}$$

It is simple to prove equivariance under this symmetry since the subscripts $(\mathbf{k}, n)$ do not change:

$$\dot{\mathbf{a}}_{\mathbf{k},n}(\gamma\mathbf{a}) = lin. + \sum_{\mathbf{k}'}\sum_{n'}\mathbf{N}(e^{i\mathbf{k}'\cdot\mathbf{d}}\mathbf{a}_{\mathbf{k}',n'})(e^{i(\mathbf{k}-\mathbf{k}')\cdot\mathbf{d}}\mathbf{a}_{\mathbf{k}-\mathbf{k}',n-n'}) = e^{i\mathbf{k}\cdot\mathbf{d}}\dot{\mathbf{a}}_{\mathbf{k},n} = \gamma\dot{\mathbf{a}}_{\mathbf{k},n}, \tag{4-79}$$

where $\mathbf{N}$ represents the coefficients.

In the doubly periodic spatial domain implied by the lattice of $\mathbf{k}$ vectors, only those rotations which take the lattice into itself are allowed. The 180° rotation always takes the lattice into itself. This is $\mathbf{x} \to -\mathbf{x}$, or equivalently $\mathbf{k} \to -\mathbf{k}$, which corresponds to

$$\mathbf{a}_{\mathbf{k},n} \to \mathbf{a}_{-\mathbf{k},n}. \tag{4-80}$$

It is easy to verify the equivariance under this symmetry since $\mathrm{N}^{x:xx}$ are all unchanged by $\mathbf{k} \to -\mathbf{k}$ and $\mathbf{k}' \to -\mathbf{k}'$. This symmetry is redundant, however, since it is the composition of (4-50), (4-64), and (4-72).

An explicit representation of the lattice of $\mathbf{k}$ vectors is needed in order to discuss the symmetry of the ODEs further. Chapter Two includes a discussion of double periodicity in the horizontal plane. The important results are repeated here: Doubly periodic functions in the plane can be represented by a Fourier series,

$$\psi(\mathbf{x}) = \sum_{\mathbf{k}}\psi_{\mathbf{k}}e^{i\mathbf{k}\cdot\mathbf{x}}, \tag{4-81}$$

where the sum over $\mathbf{k}$ includes all vectors in a lattice,

$$\mathbf{k} = \to l\,\mathbf{k}_1 + m\,\mathbf{k}_2. \tag{4-82}$$

The sum over $\mathbf{k}$ is therefore a sum over two integers,

$$\sum_{\mathbf{k}} \rightarrow \sum_{l=-\infty}^{\infty} \sum_{m=-\infty}^{\infty} . \tag{4-83}$$

As a result, the amplitudes and nonlinear couplings can be labeled by 3 integers rather than $(\mathbf{k}, n)$:

$$\mathbf{a}_{\mathbf{k},n} \rightarrow \mathbf{a}_{l,m,n} \text{, and} \tag{4-84}$$

$$N^{x:xx}_{\mathbf{k},n;\mathbf{k}',n'} \rightarrow N^{x:xx}_{l,m,n;l',m',n''} \tag{4-85}$$

The generators of the lattice, $\mathbf{k}_1$ and $\mathbf{k}_2$ are not uniquely determined. For the square, rhombic, and hexagonal lattice one can choose the two generators so that $|\mathbf{k}_1|^2 = |\mathbf{k}_2|^2$. This is why these lattices are important for pattern selection: both $\mathbf{k}_1$ and $\mathbf{k}_2$ can have the critical wavenumber. Therefore, assume that

$$|\mathbf{k}_1|^2 = |\mathbf{k}_2|^2 = k_c^2. \tag{4-86}$$

(The rectangular lattice, where $\mathbf{k}_1 \cdot \mathbf{k}_2 = 0$ and $|\mathbf{k}_1|^2 \neq |\mathbf{k}_2|^2$, is important for many of the finite amplitude instabilities discussed by Busse, although numerical techniques are needed to analyze these instabilities.)

The different lattices are distinguished by φ, the cosine of the angle between the two $\mathbf{k}$ vectors,

$$\mathbf{k}_1 \cdot \mathbf{k}_2 = \varphi k_c^2, \tag{4-87}$$

and ψ, defined by

$$\hat{\mathbf{z}} \cdot \mathbf{k}_1 \times \mathbf{k}_2 = \psi k_c^2. \tag{4-88}$$

These definitions are used by Schlüter *et al.*. Although these lattice parameters are clearly related by $\varphi^2 + \psi^2 = 1$, the sign of ψ is not determined by φ. (In rotating convection the sign of ψ is important.) The square lattice has $\varphi = 0$ and the hexagonal lattice has $\varphi = \pm \frac{1}{2}$. All other angles give rhombic lattices, with the exception of $\varphi = \pm 1$, which is excluded since in this case there is only one independent $\mathbf{k}$ vector.

It is now possible to discuss more of the symmetries of the infinite dimensional ODEs.

For any lattice, the ODEs have a useful discrete symmetry when the displacement $\mathbf{d}$ in equation (4-78) is either

$$\mathbf{d} = \frac{\mathbf{w}_1}{2}, \text{ or } \mathbf{d} = \frac{\mathbf{w}_2}{2}, \tag{4-89}$$

where $\mathbf{k}_\alpha \cdot \mathbf{w}_\beta = 2\pi \delta_{\alpha,\beta}$. Recall from equation (2-99) that $\mathbf{w}_1$ and $\mathbf{w}_2$ are the two real space lattice vectors that define the double periodicity in the plane. The symmetries corresponding to the two translations are

$$\mathbf{a}_{l,m,n} \to (-1)^l \mathbf{a}_{l,m,n}, \text{ and} \tag{4-90}$$

$$\mathbf{a}_{l,m,n} \to (-1)^m \mathbf{a}_{l,m,n} \tag{4-91}$$

respectively. These symmetries can be combined with (4-74) to yield

$$\mathbf{a}_{l,m,n} \to (-1)^{l+m+n} \mathbf{a}_{l,m,n}. \tag{4-92}$$

Although this last symmetry is not independent of the others, it has the advantage that in the rhombic and square lattices the critical modes are $\mathbf{a}_{1,0,1}$ and $\mathbf{a}_{0,1,1}$, which are on the fixed point set of (4-92). Note that on the hexagonal lattice $\mathbf{a}_{-1,-1,1}$ is also a critical mode, so the critical modes are not on the fixed point set.

There are no *proper* rotations, other than the 180° rotation, which leave the rhombic lattice invariant. A reflection in the horizontal plane through the line bisecting $\mathbf{k}_1$ and $\mathbf{k}_2$ does preserve the lattice, since it is equivalent to

$$\mathbf{k}_1 \leftrightarrow \mathbf{k}_2. \tag{4-93}$$

(Remember that $|\mathbf{k}_1|^2 = |\mathbf{k}_2|^2$.) In the nonrotating layer the PDEs are equivariant under reflections, and the ODEs have the symmetry

$$\begin{aligned} w_{l,m,n} &\to w_{m,l,n} \\ \zeta_{l,m,n} &\to -\zeta_{m,l,n} \\ \vartheta_{l,m,n} &\to \vartheta_{m,l,n} \\ \xi_{l,m,n} &\to \xi_{m,l,n}. \end{aligned} \tag{4-94}$$

The equivariance is due to the symmetry of the nonlinear couplings:

$$N^{w:ww}, N^{w:\zeta\zeta}, N^{\zeta:w\zeta}, \text{ and } N^{\vartheta:w\vartheta} \text{ are even, and} \tag{4-95}$$

$$N^{w:w\zeta}, N^{\zeta:ww}, N^{\zeta:\zeta\zeta}, \text{ and } N^{\vartheta:\zeta\vartheta} \text{ are odd,} \tag{4-96}$$

under $l \leftrightarrow m$ and $l' \leftrightarrow m'$. In other words,

$$N^{w:ww}_{l,m,n;l',m',n'} = N^{w:ww}_{m,l,n:m',l',n'} \text{ , etc.} \tag{4-97}$$

There is another reflection symmetry through the vertical plane perpendicular to that of equation (4-93). This is obtained by composing (4-94) with $\mathbf{a}_{\mathbf{k},n} \to \mathbf{a}_{-\mathbf{k},n}$:

$$\begin{aligned} w_{l,m,n} &\to w_{-m,-l,n} \\ \zeta_{l,m,n} &\to -\zeta_{-m,-l,n} \\ \vartheta_{l,m,n} &\to \vartheta_{-m,-l,n} \\ \xi_{l,m,n} &\to \xi_{-m,-l,n} \,. \end{aligned} \tag{4-98}$$

When the layer is rotating about the vertical axis the reflection (4-94) or (4-98) combined with $\Omega\cdot\hat{\mathbf{z}} \to -\Omega\cdot\hat{\mathbf{z}}$ leaves the ODEs unchanged. This is not a true symmetry, however, because a parameter in the equations is changed, not just the time dependent variables. This is called a *pseudo –symmetry* of the ODEs in this dissertation. A pseudo-symmetry relates one physical system to another. (In this case the two systems are rotating in opposite directions.)

A related pseudo-symmetry comes about from interchanging the labels of $\mathbf{k}_1$ and $\mathbf{k}_2$, Here the pseudo-symmetry relates two different $\mathbf{k}$ space lattices, with different lattice parameter ψ, whereas the reflection symmetry (4-94) is a transformation of the amplitudes on a single lattice. The new definitions of $\mathbf{k}_1$ and $\mathbf{k}_2$ define a pseudo-symmetry transformation:

$$\begin{aligned} &\mathbf{a}_{l,m,n} \to \mathbf{a}_{m,l,n} \\ &[\varphi \to \varphi] \\ &[\psi \to -\psi]. \end{aligned} \tag{4-99}$$

The square brackets indicate changes in the parameters of the system. The ODEs are equivariant under the pseudo-symmetry. An important point is that $\psi \to -\psi$ only on the left hand side of the equivariance condition:

$$\dot{w}_{l,m,n}\left(\mathbf{a}_{m,l,n\,[\psi\to-\psi]}\right)=\sum_{l',m',n'}\mathrm{N}^{w:w\zeta}_{l',m',n';l-l',m-m',n-n'[-\psi]}(w_{m',l',n'})(\zeta_{m-m',l-l',n-n'})+\cdots. \tag{4-100}$$

The right hand side of the equivariance condition is

$$\dot{w}_{m,l,n}=\sum_{l',m',n'}\mathrm{N}^{w:w\zeta}_{m',l',n';m-m',l-l',n-n'}(w_{m',l',n'})(\zeta_{m-m',l-l',n-n'})+\cdots. \tag{4-101}$$

The pseudo-equivariance follows since all of the nonlinear couplings satisfy

$$\mathrm{N}^{x:xx}_{l,m,n;l',m',n'[\psi]}=\mathrm{N}^{x:xx}_{m,l,n;m',l',n'[-\psi]}. \tag{4-102}$$

This in turn follows since $\mathbf{k}\cdot\mathbf{k}'$ and $\hat{\mathbf{z}}\cdot\mathbf{k}\times\mathbf{k}'$ are unchanged under

$$\begin{aligned}&\mathbf{k}=(l\,\mathbf{k}_1+m\,\mathbf{k}_2)\to(l\,\mathbf{k}_2+m\,\mathbf{k}_1)\\&\mathbf{k}'=(l'\mathbf{k}_1+m'\mathbf{k}_2)\to(l'\mathbf{k}_2+m'\mathbf{k}_1)\\&\mathbf{k}_1\cdot\mathbf{k}_2\to\mathbf{k}_2\cdot\mathbf{k}_1\\&\mathbf{k}_1\times\mathbf{k}_2\to\mathbf{k}_2\times\mathbf{k}_1.\end{aligned} \tag{4-103}$$

Note finally that the nonlinear couplings also satisfy the relation

$$\mathrm{N}^{x:xx}_{l,m,n;l',m',n'[\varphi,\psi]}=\mathrm{N}^{x:xx}_{-l,m,n;-l',m',n'[-\varphi,-\psi]}. \tag{4-104}$$

Therefore the ODEs have the pseudo-symmetry which comes from relabeling $\mathbf{k}_1$ as $-\mathbf{k}_1$:

$$\begin{aligned}&\mathbf{a}_{l,m,n}\to\mathbf{a}_{-l,m,n}\\&[\varphi\to-\varphi]\\&[\psi\to-\psi].\end{aligned} \tag{4-105}$$

For future reference, the symmetries of the ODEs for the rhombic lattice, along with the equation numbers which identify them, are listed in table 4-1.

Symmetries of the ODEs which preserve constraints		
equation:	(4-50)	(4-64)
$w_{\mathbf{k},n} \rightarrow$	$-w_{\mathbf{k},-n}$	$\overline{w}_{-\mathbf{k},-n}$
$\zeta_{\mathbf{k},n} \rightarrow$	$\zeta_{\mathbf{k},-n}$	$-\overline{\zeta}_{-\mathbf{k},-n}$
$\vartheta_{\mathbf{k},n} \rightarrow$	$-\vartheta_{\mathbf{k},-n}$	$\overline{\vartheta}_{-\mathbf{k},-n}$
$\xi_{\mathbf{k},n} \rightarrow$	$-\xi_{\mathbf{k},-n}$	$\overline{\xi}_{-\mathbf{k},-n}$

Symmetries of the ODEs II				
equation:	(4-72)	(4-74)	(4-78)	(4-80)
$\mathbf{a}_{\mathbf{k},n} \rightarrow$	$-\bar{\mathbf{a}}_{\mathbf{k},n}$	$(-1)^n \mathbf{a}_{\mathbf{k},n}$	$e^{i\mathbf{k}\cdot\mathbf{d}} \mathbf{a}_{\mathbf{k},n}$	$\mathbf{a}_{-\mathbf{k},n}$

Symmetries [and pseudo-symmetries] of the ODEs III			$[\varphi \rightarrow \varphi]$ $[\psi \rightarrow -\psi]$	$[\varphi \rightarrow -\varphi]$ $[\psi \rightarrow -\psi]$
equation:	(4-90)	(4-92)	(4-99)	(4-105)
$\mathbf{a}_{l,m,n} \rightarrow$	$(-1)^m \mathbf{a}_{l,m,n}$	$(-1)^{l+m+n} \mathbf{a}_{l,m,n}$	$\mathbf{a}_{m,l,n}$	$\mathbf{a}_{-l,m,n}$

Symmetries of the ODEs in a nonrotating layer (In a rotating layer include $[\Omega\cdot\hat{\mathbf{z}} \rightarrow -\Omega\cdot\hat{\mathbf{z}}]$)		
equation:	(4-94)	(4-98)
$w_{l,m,n} \rightarrow$	$w_{m,l,n}$	$w_{-m,-l,n}$
$\zeta_{l,m,n} \rightarrow$	$-\zeta_{m,l,n}$	$-\zeta_{-m,-l,n}$
$\vartheta_{l,m,n} \rightarrow$	$\vartheta_{m,l,n}$	$\vartheta_{-m,-l,n}$
$\xi_{l,m,n} \rightarrow$	$\xi_{m,l,n}$	$\xi_{-m,-l,n}$

Table 4-1. The symmetries of the infinite-dimensional modal convection equations, equations (4-31) through (4-34).

4.2.3. Special symmetries of the square and hexagonal lattices

There are proper rotations of the plane that leave the square and hexagonal lattices invariant.

For the square lattice the 90° rotation about the vertical axis is a true symmetry. This is

$$\mathbf{a}_{l,m,n} \to \mathbf{a}_{-m,l,n}. \tag{4-106}$$

The hexagonal lattice is preserved by 60° and 120° rotations. (The 60° rotation is the same as a 120° rotation followed by a 180° rotation.) When the $\mathbf{k}$ vectors are chosen such that $\varphi = -\frac{1}{2}$, the 120° rotation corresponds to

$$\begin{aligned} \mathbf{k}_1 &\to \mathbf{k}_2 \\ \mathbf{k}_2 &\to -(\mathbf{k}_1+\mathbf{k}_2), \end{aligned} \tag{4-107}$$

which implies the symmetry of the ODEs under

$$\mathbf{a}_{l,m,n} \to \mathbf{a}_{-m,l-m,n}. \tag{4-108}$$

The above symmetry corresponds to (4-107) since

$$\mathbf{a}_{1,0,1} \to \mathbf{a}_{0,1,1}, \text{ and } \mathbf{a}_{0,1,1} \to \mathbf{a}_{-1,-1,1}. \tag{4-109}$$

To prove that the transformation (4-108) is truly a 120° rotation, note that it preserves the length of the $\mathbf{k}$ vectors,

$$|l\,\mathbf{k}_1+m\,\mathbf{k}_2|^2 = |-m\,\mathbf{k}_1+(l-m)\mathbf{k}_2|^2 \tag{4-110}$$

and that three applications of this symmetry gives the identity,

$$\begin{bmatrix} l \\ m \end{bmatrix} \to \begin{bmatrix} -m \\ l-m \end{bmatrix} \to \begin{bmatrix} -l+m \\ -l \end{bmatrix} \to \begin{bmatrix} l \\ m \end{bmatrix}. \tag{4-111}$$

The equivariance under the rotations follows since the couplings $\mathrm{N}^{x:xx}$ depend only on the dot product and cross product of the two $\mathbf{k}$ vectors.

This ends the discussion of the symmetries of the infinite dimensional set of ODEs. (There is no way to prove that *all* of the symmetries have been exhibited, however.)

4.3. Modal truncations

In this section the infinite dimensional ODEs for doubly diffusive convection are truncated, keeping all modes which contribute to the normal form at third order. The symmetry of the critical eigenspace is used to predict what modes are needed in the truncation.

The results of Chapter Two show that for stationary convection on the square or rhombic lattice the normal form is cubic in the critical amplitudes. For Boussinesq convection on a hexagonal lattice, the normal form also has fifth order terms, but the third order terms determine if rolls or equal amplitude solutions (hexagons and regular triangles) are stable.

If the critical amplitudes are $O(\varepsilon)$, then only the modes with an amplitude of $O(\varepsilon)$ and $O(\varepsilon^2)$ are needed to compute the normal form to third order. (The product of $O(\varepsilon)$ and $O(\varepsilon^3)$ is $O(\varepsilon^4)$, which can be ignored.) All possible couplings of two critical modes generate the $O(\varepsilon^2)$ modes. For Bénard convection (and doubly diffusive convection) the critical modes are

$$w_{\mathbf{k}n},\ \vartheta_{\mathbf{k}n},\ (\text{ and } \xi_{\mathbf{k}n}), \tag{4-112}$$

$$\text{where } |\mathbf{k}|^2 = \tfrac{1}{2} \text{ and } n = \pm 1. \tag{4-113}$$

The following discussion will concentrate on doubly diffusive convection; Bénard convection can be obtained as a limiting case.

Convection in a rotating layer is more complicated since the $\zeta_{\mathbf{k}n}$ mode is also critical, and $|\mathbf{k}|^2 \neq \frac{1}{2}$ at the onset of convection. The normal forms for the rotating layer are also different; this case is discussed in Appendix B.

Let $\mathbf{k}_1$ and $\mathbf{k}_2$ be two critical vectors which generate the $\mathbb{Z}^2$ lattice in the plane:

$$|\mathbf{k}_1|^2 = |\mathbf{k}_2|^2 = \tfrac{1}{2} \tag{4-114}$$

The vertical vorticity mode is not in the critical eigenspace; therefore the

following notation is convenient: Let

$$\mathbf{c}_{\mathbf{k},n} \equiv \begin{pmatrix} w_{\mathbf{k},n} \\ \vartheta_{\mathbf{k},n} \\ \xi_{\mathbf{k},n} \end{pmatrix}, \text{ and } \mathbf{c}_{l,m,n} \equiv \begin{pmatrix} w_{l,m,n} \\ \vartheta_{l,m,n} \\ \xi_{l,m,n} \end{pmatrix}. \tag{4-115}$$

In this notation the critical modes of doubly diffusive convection are are $\mathbf{c}_{1,0,1}$ and $\mathbf{c}_{0,1,1}$. With this notation, the constraints on $\mathbf{c}_{l,m,n}$ can be written concisely, since the ζ mode is eliminated. They are

$$\mathbf{c}_{\mathbf{k},n} = -\mathbf{c}_{\mathbf{k},-n} = -\bar{\mathbf{c}}_{-\mathbf{k},-n} = \mathbf{c}_{-\mathbf{k},n}\,. \tag{4-116}$$

Using the mode coupling property of the nonlinear terms, the second order modes which can be generated from $\mathbf{c}_{1,0,1}$ and $\mathbf{c}_{0,1,1}$ are

$$\mathbf{a}_{2,0,2},\ \mathbf{a}_{0,2,2},\ \mathbf{a}_{1,1,2},\ \mathbf{a}_{1,-1,2},\ \mathbf{a}_{0,0,2} \tag{4-117}$$

$$\mathbf{a}_{2,0,0},\ \mathbf{a}_{0,2,0},\ \mathbf{a}_{1,1,0},\ \mathbf{a}_{1,-1,0},\ \mathbf{a}_{0,0,0}, \tag{4-118}$$

and the other modes which follow from the constraints.

The critical modes do not couple to $\mathbf{a}_{2,0,2}$ and $\mathbf{a}_{0,2,2}$ because the velocity field is divergence-free:

$$(\mathbf{u}_{\mathbf{k},n}\cdot\nabla)\mathbf{u}_{\mathbf{k},n} = \left[\mathbf{u}_{\mathbf{k},n}\cdot(\mathbf{k}+n\,\hat{\mathbf{z}})\right]\mathbf{u}_{\mathbf{k},n} = 0 \tag{4-119}$$

$$(\mathbf{u}_{\mathbf{k},n}\cdot\nabla)e_{\mathbf{k},n} = \left[\mathbf{u}_{\mathbf{k},n}\cdot(\mathbf{k}+n\,\hat{\mathbf{z}})\right]e_{\mathbf{k},n} = 0. \tag{4-120}$$

The $\mathbf{c}_{\mathbf{k},0}$ modes are all zero due to the constraint $\mathbf{c}_{\mathbf{k},n} = -\mathbf{c}_{\mathbf{k},-n}$. Note, however, that the vertical vorticity modes with $n = 0$ *do* exist with the free boundary conditions. Furthermore, the $\mathbf{W}_{\mathbf{k},n}$ and $\mathbf{Z}_{\mathbf{k},n}$ fields vanish when $\mathbf{k} = 0$.

From the above considerations, the possible second order modes are

$$\mathbf{a}_{1,1,2},\ \mathbf{a}_{1,-1,2},\ \vartheta_{0,0,2},\ \xi_{0,0,2} \tag{4-121}$$

$$\zeta_{2,0,0},\ \zeta_{0,2,0},\ \zeta_{1,1,0},\ \text{and}\ \zeta_{1,-1,0}. \tag{4-122}$$

It turns out that the ζ modes do not enter at second order. One can verify this by computing the quadratic couplings directly from equations (4-40)-(4-42), but the same result follows from symmetry considerations. The next sections give a theoretical discussion of the center manifold calculation in the

presence of symmetry.

4.3.1. The center eigenspace and center manifold

It is important to realize the distinction between the critical modes (4-112), and the critical eigenspace, or *center eigenspace* (E_c). The null eigenvectors of the linear problem span the center eigenspace. Let $\mathbf{X}_0^r$ be the null eigenvector of $\mathbf{L}_{1,0,1}$ and $\mathbf{L}_{0,1,1}$.

$$\mathbf{L}_{1,0,1}\mathbf{X}_0^r = 0, \text{ and } \mathbf{L}_{0,1,1}\mathbf{X}_0^r = 0. \tag{4-123}$$

The "r" denotes the right eigenvector. Choose $\mathbf{X}_0^r$ to be real (this is always possible). The amplitudes of the two critical modes are complex numbers z_1 and z_2. Therefore E_c can be identified with the space $\mathbb{C}^2$:

$$E_c \sim (z_1, z_2), \tag{4-124}$$

where

$$\mathbf{c}_{1,0,1} = z_1\mathbf{X}_0^r, \quad \mathbf{c}_{0,1,1} = z_2\mathbf{X}_0^r, \tag{4-125}$$

and all other amplitudes are zero, except those related by constraints.

The *center manifold* (W_c), introduced in section 2.1, is the invariant set (under the dynamics) which is tangent to E_c at 0. There is a mapping from the critical eigenspace to the space of amplitudes,

$$\mathbf{g}: E_c \to \{\mathbf{a}\}, \tag{4-126}$$

such that the center manifold is the image of the center eigenspace

$$W_c = \mathbf{g}(E_c). \tag{4-127}$$

This is because the dynamics on the center manifold are so slow that all of the perpendicular directions collapse down to W_c on a much faster time scale.

The function $\mathbf{g}(z_1, z_2)$, called the *center manifold function*, has the components

$$
\begin{aligned}
&\mathbf{c}_{1,0,1}(z_1,z_2) = z_1\mathbf{X}_0^T + O(z_1|z_1|^2, z_1|z_2|^2)\\
&\mathbf{c}_{0,1,1}(z_1,z_2) = z_2\mathbf{X}_0^T + O(z_2|z_1|^2, z_2|z_2|^2)\\
&\mathbf{a}_{1,1,2}(z_1,z_2) = O(z_1 z_2)\\
&\mathbf{a}_{1,-1,2}(z_1,z_2) = O(z_1\bar{z}_2)\\
&\mathbf{a}_{0,0,2}(z_1,z_2) = O(|z_1|^2, |z_2|^2)\\
&\text{etc.}
\end{aligned}
\tag{4-128}
$$

The Taylor expansion of $\mathbf{g}$ to second order is sufficient for the calculation of the normal form at third order.

4.3.2. The symmetries of the center manifold

If the ODE is equivariant under a linear transformation γ, then so is $\mathbf{g}$:

$$\mathbf{g}\circ\gamma = \gamma\circ\mathbf{g}. \tag{4-129}$$

In addition, the center eigenspace is always invariant under the symmetry γ:

$$E_c = \gamma E_c\ , \tag{4-130}$$

since if $\mathbf{a}$ is a null eigenvector, then $\gamma\mathbf{a}$ is also a null eigenvector. As a consequence of (4-129) and (4-130), the center manifold is invariant under γ:

$$W_c = \mathbf{g}(E_c) = \mathbf{g}(\gamma E_c) = \gamma\mathbf{g}(E_c) = \gamma W_c. \tag{4-131}$$

For some symmetries the center eigenspace is in the fixed point set,

$$E_c \subset \Delta_\gamma, \tag{4-132}$$

i.e. if $\mathbf{a}\in E_c$, then $\mathbf{a}=\gamma\mathbf{a}$. In this case W_c is also in the fixed point set of γ:

$$\mathbf{g}(\mathbf{a}) = \mathbf{g}(\gamma\mathbf{a}) = \gamma\mathbf{g}(\mathbf{a}). \tag{4-133}$$

Therefore

$$W_c \subset \Delta_\gamma. \tag{4-134}$$

The main results on the symmetries of the center manifold are summarized in the box below:

Let $\dot{\mathbf{a}} = \mathbf{f}(\mathbf{a})$.

If $\mathbf{f} \circ \gamma = \gamma \circ \mathbf{f}$, then $W_c = \gamma W_c$.

If, in addition, $E_c \subset \Delta_\gamma$, then $W_c \subset \Delta_\gamma$.

The above discussion does not constitute a proof, and from a mathematical point of view the boxed statements are not strictly true, because of a technicality. The problem is that the center manifold is not uniquely defined. However, from a practical point of view it is not a problem that $\mathbf{g}$ is not uniquely defined, since all possible $\mathbf{g}$'s have the same Taylor expansion to all orders (see Marsden and McCracken 1976). The following example illustrates the problem: Consider the ODE in the plane $(x,y) \in \mathbb{R}^2$.

$$\begin{aligned} \dot{x} &= -x^3 \\ \dot{y} &= -y \,. \end{aligned} \tag{4-135}$$

This ODE has two reflection symmetries,

$$\begin{aligned} x &\to -x \\ y &\to y \,, \end{aligned} \tag{4-136}$$

and

$$\begin{aligned} x &\to x \\ y &\to -y \,. \end{aligned} \tag{4-137}$$

The solutions can be easily found,

$$\begin{aligned} x(t) &= \frac{1}{\sqrt{2(t-t_o)}}, \text{ or } x(t) = 0 \,, \\ y(t) &= Ae^{-t} \,, \end{aligned} \tag{4-138}$$

where t_o and A are arbitrary constants. The time can be eliminated, giving the equation for the trajectories,

$$y = Ae^{-2/x^2}, \text{ or } x = 0 \,. \tag{4-139}$$

The line $x = 0$ is the stable manifold of 0, while *any* of the other trajectories is half of a possible center manifold. Equation (4-139) is the classic example of a nonzero function with a Taylor expansion which is zero to all orders. The Taylor expansion of any of the center manifolds yields the line $y = 0$, which satisfies

the boxed symmetry properties listed above.

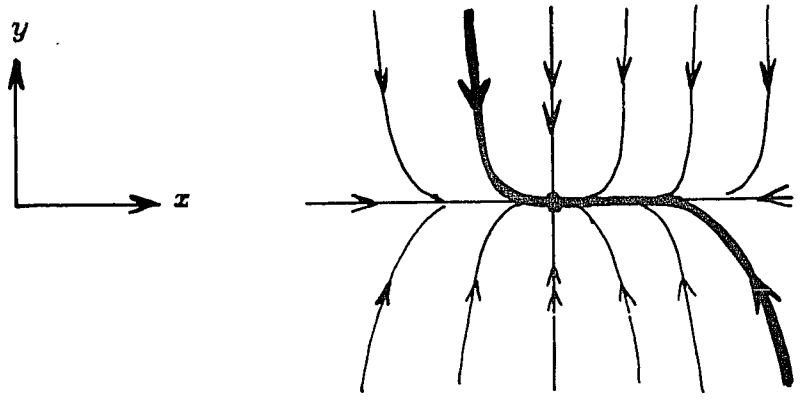

Fig. 4-1. The phase portrait of system (4-135). One of the possible center manifolds is indicated by the bold lines. Note that this choice of W_c is not invariant under (4-136), and it is not in the fixed point set of (4-137). The canonical choice for W_c is the x axis, which *does* have these symmetry properties.

For doubly diffusive convection on a square or rhombic lattice, where the critical modes are $\mathbf{c}_{\pm 1,0,+-1}$ and $\mathbf{c}_{0,\pm 1,+-1}$, the center eigenspace is in the fixed point set of

$$\mathbf{a}_{l,m,n} \to (-1)^{l+m+n}\,\mathbf{a}_{l,m,n} \tag{4-140}$$

as well as the two symmetries, (4-50) and (4-64), associated with the constraints. In addition, the two critical amplitudes can be made pure imaginary by a suitable displacement of the origin (symmetry (4-78)). This puts the center eigenspace on the fixed point set of

$$\mathbf{a}_{\mathbf{k},n} \to -\bar{\mathbf{a}}_{\mathbf{k},n}\,. \tag{4-141}$$

Using symmetry considerations, one can show that the ζ amplitudes do not enter at second order. On the center manifold, the amplitude $\zeta_{1,1,2}$ is given by one component of the center manifold function of z_1 and z_2,

$$\zeta_{1,1,2} = \zeta_{1,1,2}(z_1, z_2)\,. \tag{4-142}$$

The symmetry

$$\begin{aligned} \mathbf{c}_{l,m,n} &\to \mathbf{c}_{m,l,n} \\ \zeta_{l,m,n} &\to -\zeta_{m,l,n} \end{aligned} \tag{4-143}$$

acts on the center eigenspace by

$$(z_1,z_2) \to (z_2,z_1). \tag{4-144}$$

Therefore, by the equivariance of $\mathbf{g}$,

$$\zeta_{1,1,2}(z_2,z_1) = -\zeta_{1,1,2}(z_1,z_2) \tag{4-145}$$

Due to mode coupling, or equivalently the symmetry (4-78),

$$\zeta_{1,1,2}(z_1,z_2) = \zeta_{1,1,2}(z_1 z_2,\ z_1|z_1|^2,\ z_1|z_2|^2,\ \cdots). \tag{4-146}$$

Combining the two symmetries, one finds

$$\zeta_{1,1,2}(z_1,z_2) = O(z_1 z_2(|z_1|^2 - |z_2|^2)). \tag{4-147}$$

The coefficient of $z_1 z_2(|z_1|^2 - |z_2|^2)$ is nonzero, due to the following terms in the ODE:

$$\dot{\zeta}_{1,1,2} \propto (w_{2,1,3} w_{-1,0,-1} - w_{1,2,3} w_{0,-1,-1}). \tag{4-148}$$

Note that $w_{2,1,3} = O(z_1^2 z_2)$, and $w_{-1,0,-1} = -\bar{z}_1 + \cdots$.

By the same argument as that leading to (4-147),

$$\zeta_{1,1,0} = O(z_1 z_2(|z_1|^2 - |z_2|^2)). \tag{4-149}$$

A similar argument, using the symmetry (4-98), shows that

$$\zeta_{1,-1,2} \text{ and } \zeta_{1,-1,0} = O(z_1 \bar{z}_2(|z_1|^2 - |z_2|^2)). \tag{4-150}$$

The amplitudes $\zeta_{2,0,0}$ and $\zeta_{0,0,2}$ are also of fourth order in the critical amplitudes. By mode coupling, the $\zeta_{2,0,0}$ component of the $\mathbf{g}$ function is

$$\zeta_{2,0,0} = \zeta_{2,0,0}(z_1^2,\ z_1^2|z_1|^2,\ z_1^2|z_2|^2,\ \cdots), \tag{4-151}$$

and the equation for $\zeta_{0,0,2}$ has a similar structure. However, the lowest order nonzero term in the center manifold function is $\zeta_{2,0,0} \propto z_1^2|z_2|^2$. Thus this mode does not contribute to the cubic coefficient of the normal form. The proof is as follows: The terms which are present when $z_2 = 0$ ($\zeta_{2,0,0} \propto z_1^2(|z_1|^2)^n$) can be calculated when the fluid flow is two-dimensional, and z_1 is the only nonzero critical amplitude. In the two-dimensional problem all the $\mathbf{k}$ vectors are of the form $l\mathbf{k}_1$, and the ODE has the symmetry

$$\begin{aligned} w_{l,n} &\to w_{l,n} \\ \zeta_{l,n} &\to -\zeta_{l,n} \\ \vartheta_{l,n} &\to \vartheta_{l,n} \\ \xi_{l,n} &\to \xi_{l,n} \end{aligned} \tag{4-152}$$

corresponding to the reflection which leaves $\mathbf{k}_1$ and $\hat{\mathbf{z}}$ invariant. By the equivariance of $\mathbf{g}$ under this symmetry,

$$\zeta_{l,n}(z_1) = -\zeta_{l,n}(z_1). \tag{4-153}$$

Therefore, in the two-dimensional problem the vertical vorticity is identically zero on the center manifold.

Eliminating the vertical vorticity modes from the list of candidates (4-121) and (4-122), the remaining second order modes are

$$\mathbf{c}_{1,1,2},\ \mathbf{c}_{1,-1,2},\ \vartheta_{0,0,2},\ \text{and}\ \xi_{0,0,2}. \tag{4-154}$$

At this point the nonlinear couplings have to be calculated by hand from equations (4-23) and (4-29). The modal equations for doubly diffusive convection, including $O(\varepsilon)$ and $O(\varepsilon^2)$ modes, are

$$\begin{aligned} \dot{w}_{1,0,1} = &-\tfrac{3}{2}w_{1,0,1} + \tfrac{2}{3}[R_T\vartheta_{1,0,1} + R_S\xi_{1,0,1}] \\ &-i(1-\varphi)(1+\varphi)(w_{1,1,2}w_{0,-1,-1} + w_{1,-1,2}w_{0,1,-1}) \end{aligned} \tag{4-155}$$

$$\begin{aligned} \dot{\vartheta}_{1,0,1} = &\frac{1}{2\sigma_T}w_{1,0,1} - \frac{3}{2\sigma_T}\vartheta_{1,0,1} \\ &-\tfrac{1}{2}i\left[(1-\varphi)w_{0,-1,-1}\vartheta_{1,1,2} + (1+\varphi)w_{0,1,-1}\vartheta_{1,-1,2}\right] - iw_{1,0,-1}\vartheta_{0,0,2} \end{aligned} \tag{4-156}$$

$$\begin{aligned} \dot{\xi}_{1,0,1} = &\frac{1}{2\sigma_T}w_{1,0,1} - \frac{3}{2\sigma_T}\xi_{1,0,1} \\ &-\tfrac{1}{2}i\left[(1-\varphi)w_{0,-1,-1}\xi_{1,1,2} + (1+\varphi)w_{0,1,-1}\xi_{1,-1,2}\right] - iw_{1,0,-1}\xi_{0,0,2} \end{aligned} \tag{4-157}$$

$$\dot{w}_{1,1,2} = -(5+\varphi)w_{1,1,2} + \frac{1}{(5+\varphi)}[R_T\vartheta_{1,1,2} + R_S\xi_{1,1,2}] - \frac{3i}{2}\frac{(1-\varphi)}{(5+\varphi)}w_{1,0,1}w_{0,1,1} \tag{4-158}$$

$$\dot{\vartheta}_{1,1,2} = \frac{(1+\varphi)}{\sigma_T}w_{1,1,2} - \frac{1}{\sigma_T}(5+\varphi)\vartheta_{1,1,2} - \tfrac{1}{2}i(1-\varphi)(w_{1,0,1}\vartheta_{0,1,1} + w_{0,1,1}\vartheta_{1,0,1}) \tag{4-159}$$

$$\dot{\xi}_{1,1,2} = \frac{(1+\varphi)}{\sigma_S}w_{1,1,2} - \frac{1}{\sigma_S}(5+\varphi)\xi_{1,1,2} - \tfrac{1}{2}i(1-\varphi)(w_{1,0,1}\xi_{0,1,1} + w_{0,1,1}\xi_{1,0,1}) \tag{4-160}$$

$$\dot{\vartheta}_{0,0,2} = \frac{-4}{\sigma_T}\vartheta_{0,0,2} - i(w_{1,0,1}\vartheta_{-1,0,1} + w_{-1,0,1}\vartheta_{1,0,1} + w_{0,1,1}\vartheta_{0,-1,1} + w_{0,-1,1}\vartheta_{0,1,1}) \tag{4-161}$$

$$\dot{\xi}_{0,0,2} = \frac{-4}{\sigma_S}\xi_{0,0,2} - i(w_{1,0,1}\xi_{-1,0,1} + w_{-1,0,1}\xi_{1,0,1} + w_{0,1,1}\xi_{0,-1,1} + w_{0,-1,1}\xi_{0,1,1}) \tag{4-162}$$

The ODEs for $\dot{w}_{0,1,1}$, $\dot{\vartheta}_{0,1,1}$, and $\dot{\xi}_{0,1,1}$ can be obtained using the symmetry

$$\mathbf{c}_{l,m,n} \to \mathbf{c}_{m,l,n}\,. \tag{4-163}$$

The ODEs for $w_{1,-1,2}$, $\vartheta_{1,-1,2}$, and $\xi_{1,-1,2}$ can be obtained using the pseudo-symmetry

$$\begin{array}{l} \mathbf{a}_{l,m,n} \to \mathbf{a}_{l,-m,n} \\ [\varphi \to -\varphi] \\ [\,\psi \to -\psi]. \end{array} \tag{4-164}$$

For convenience, the $\dot{\xi}$ equations have been included, although they could have been inferred from $\dot{\vartheta}$, using the pseudo-symmetry

$$\begin{array}{l} \vartheta_{l,m,n} \leftrightarrow \xi_{l,m,n} \\ [R_T \leftrightarrow R_S] \\ [\sigma_T \leftrightarrow \sigma_S]\,. \end{array} \tag{4-165}$$

4.4. The pitchfork bifurcation in doubly diffusive convection

The first step in the calculation of the normal form is a linear change of variables. The new coordinates, z_1 and z_2, are the complex amplitudes of the critical rolls with wavevectors $\mathbf{k}_1$ and $\mathbf{k}_2$, respectively.

For doubly diffusive convection the linear problem is

$$\dot{\mathbf{c}}_{l,m,n} = \mathbf{L}_{l,m,n}\,\mathbf{c}_{l,m,n} \tag{4-166}$$

where $\mathbf{c}_{l,m,n}$ is a 3 element column vector and $\mathbf{L}_{l,m,n}$ is a 3×3 matrix, for l, m, and n fixed.

Both the left and right critical eigenvectors of the matrix $\mathbf{L}_{1,0,1}$,

$$\mathbf{X}_0^l \text{ and } \mathbf{X}_0^r \tag{4-167}$$

respectively, are needed. The right critical eigenvector of the matrix $\mathbf{L}_{1,0,1}$ determines the critical eigenspace $\mathrm{E_c}$.

The eigenvectors satisfy the conditions

$$\mathbf{X}_0^l \cdot \mathbf{L}_{1,0,1} = 0 \text{ and } \mathbf{L}_{1,0,1} \cdot \mathbf{X}_0^r = 0, \tag{4-168}$$

where $\mathbf{X}_0^l$ is a 3 element row vector, $\mathbf{X}_0^r$ is a 3 element column vector, and

$$\mathbf{L}_{1,0,1} = \begin{pmatrix} -\frac{3}{2} & \frac{2}{3}R_T & \frac{2}{3}R_S \\ \frac{1}{2\sigma_T} & -\frac{3}{2\sigma_T} & 0 \\ \frac{1}{2\sigma_S} & 0 & -\frac{3}{2\sigma_S} \end{pmatrix}. \tag{4-169}$$

The critical eigenvectors are

$$\mathbf{X}_0^l = (\tfrac{3}{2}\ ,\ \tfrac{2}{3}R_T\sigma_T\ ,\ \tfrac{2}{3}R_S\sigma_S), \text{ and } \mathbf{X}_0^r = \begin{pmatrix} 3 \\ 1 \\ 1 \end{pmatrix}. \tag{4-170}$$

In this entire calculation it is implicitly assumed that the pitchfork condition holds:

$$R_S + R_T = \tfrac{27}{4} \tag{4-171}$$

(see section 1.7.2). Usually, R_S is thought of as a fixed parameter, while R_T is the control parameter. In order to exhibit the pseudo-symmetry between S and T, however, R_T will not be eliminated in favor of R_S until the final results have been obtained.

The critical eigenspace can now be given the coordinates $(z_1, z_2) \in \mathbb{C}^2$, where

$$\begin{pmatrix} w_{1,0,1} \\ \vartheta_{1,0,1} \\ \xi_{1,0,1} \end{pmatrix} = z_1 \begin{pmatrix} 3 \\ 1 \\ 1 \end{pmatrix}, \text{ and } \begin{pmatrix} w_{0,1,1} \\ \vartheta_{0,1,1} \\ \xi_{0,1,1} \end{pmatrix} = z_2 \begin{pmatrix} 3 \\ 1 \\ 1 \end{pmatrix}, \tag{4-172}$$

and the other amplitudes, such as $w_{1,0,-1}$, are given by the constraints (4-50) and (4-64).

Equation (4-172) is part of a linear change of coordinates,

$$\begin{pmatrix} w_{1,0,1} \\ \vartheta_{1,0,1} \\ \xi_{1,0,1} \end{pmatrix} = \begin{pmatrix} 3 & * & * \\ 1 & * & * \\ 1 & * & * \end{pmatrix} \begin{pmatrix} z_1 \\ * \\ * \end{pmatrix} \equiv \mathbf{S} \begin{pmatrix} z_1 \\ * \\ * \end{pmatrix} \tag{4-173}$$

(and a similar equation for $\mathbf{c}_{1,0,1}$). The stars (*) in the 3×3 matrix $\mathbf{S}$ represent

unimportant elements. For instance, if the new coordinates replacing $\mathbf{c}_{1,0,1}$ are

$$\begin{pmatrix} z_1 \\ p \\ q \end{pmatrix}, \tag{4-174}$$

then p and q are at least order $O(3)$, and therefore they do not contribute to the normal form at third order.

In the new coordinates, the ODE is

$$\begin{pmatrix} \dot{z}_1 \\ * \\ * \end{pmatrix} = \mathbf{S}^{-1}\mathbf{L}_{1,0,1}\mathbf{S}\begin{pmatrix} z_1 \\ * \\ * \end{pmatrix} + \mathbf{S}^{-1}\begin{pmatrix} N_w \\ N_\vartheta \\ N_\xi \end{pmatrix}, \tag{4-175}$$

where

$$N_w = -i(1+\varphi)(1-\varphi)[w_{1,1,2}w_{0,-1,-1} + w_{1,-1,2}w_{0,1,-1}], \tag{4-176}$$

$$N_\vartheta = -\tfrac{1}{2}i[(1-\varphi)w_{0,-1,-1}\vartheta_{1,1,2} + (1+\varphi)w_{0,1,-1}\vartheta_{1,-1,2}] - iw_{1,0,-1}\vartheta_{0,0,2}, \tag{4-177}$$

and N_ξ follows from the pseudo-symmetry relating T and S.

The reason the left eigenvector is needed is that it allows one to find the important elements of $\mathbf{S}^{-1}$:

$$\mathbf{S}^{-1} = \frac{1}{\mathbf{X}_0^l \cdot \mathbf{X}_0^r}\begin{pmatrix} \frac{3}{2} & \frac{2}{3}R_T\sigma_T & \frac{2}{3}R_S\sigma_S \\ * & * & * \\ * & * & * \end{pmatrix}. \tag{4-178}$$

The transformation becomes singular when $\mathbf{X}_0^l \cdot \mathbf{X}_0^r = 0$. This is precisely at the codimension-two bifurcation, when the Hopf and Pitchfork bifurcations coalesce. To see this, note that the condition found in Chapter One (equation (1-122), with $\omega = 0$) for the codimension-two bifurcation is

$$\mathbf{X}_0^l \cdot \mathbf{X}_0^r = \tfrac{2}{3}(\tfrac{27}{4} + R_T\sigma_T + R_S\sigma_S) = \tfrac{2}{3}[\tfrac{27}{4}(1+\sigma_T) + R_S(\sigma_S - \sigma_T)] = 0. \tag{4-179}$$

The conduction solution loses stability via a pitchfork bifurcation only if $\mathbf{X}_0^l \cdot \mathbf{X}_0^r > 0$. If the inequality is reversed, the instability occurs via a Hopf bifurcation.

By construction, $\mathbf{S}$ partially diagonalizes $\mathbf{L}_{1,0,1}$.

$$\mathbf{S}^{-1}\mathbf{L}_{1,0,1}\mathbf{S}=\begin{bmatrix}0 & 0 & 0\\ 0 & * & *\\ 0 & * & *\end{bmatrix}, \tag{4-180}$$

and the ODE for z_1, evaluated at $R_T+R_S=\frac{27}{4}$, is

$$\dot{z}_1=\frac{1}{\mathbf{X}_0^l\cdot\mathbf{X}_0^r}\mathbf{X}_0^l\cdot\begin{bmatrix}N_w\\ N_\vartheta\\ N_\xi\end{bmatrix}+O(\varepsilon^5)=\frac{1}{\mathbf{X}_0^l\cdot\mathbf{X}_0^r}\left(\tfrac{3}{2}N_w+\tfrac{2}{3}R_T\sigma_T N_\vartheta+\tfrac{2}{3}R_S\sigma_S N_\xi\right)+O(\varepsilon^5). \tag{4-181}$$

Two tasks remain, one is to write N_w, N_ϑ, and N_ξ in terms of z_1 and z_2, the other is to calculate the linear terms when $R_S+R_T\approx\frac{27}{4}$.

4.4.1. The linear ODEs near the bifurcation

Near the bifurcation, the linear ODE for z_1 is

$$\dot{z}_1=(\text{coeff.})(R_T+R_S-\tfrac{27}{4})z_1+O\left((R_T+R_S-\tfrac{27}{4})^2 z_1\right). \tag{4-182}$$

The above coefficient is determined in this section.

The critical value of (R_S, R_T) is found by solving the characteristic equation,

$$\text{Det}\,(\mathbf{L}_{1,0,1}-\lambda\mathbf{I})=0, \tag{4-183}$$

and demanding that one of the eigenvalues is 0. In general, if λ_1, λ_2, and λ_3 are the three solution of the characteristic equation, then

$$\begin{aligned}\text{Det}\,(\mathbf{L}_{1,0,1}-\lambda\mathbf{I}) &= (\lambda_1-\lambda)(\lambda_2-\lambda)(\lambda_3-\lambda)\\ &= -\lambda^3+(\lambda_1+\lambda_2+\lambda_3)\lambda^2-(\lambda_1\lambda_2+\lambda_2\lambda_3+\lambda_3\lambda_1)\lambda+\lambda_1\lambda_2\lambda_3.\end{aligned} \tag{4-184}$$

Assume that λ_1 is the only eigenvalue near zero:

$$0\approx|\lambda_1|\ll|\lambda_2|,\ |\lambda_3| \tag{4-185}$$

(This assumption breaks down near the codimension-two bifurcation.) From equation (1-114), the characteristic equation, when $|\mathbf{k}|^2=\frac{1}{2}$ and $n^2=1$, is

$$0 = -\lambda^3 - \frac{3}{2}\left(1+\frac{1}{\sigma_T}+\frac{1}{\sigma_S}\right)\lambda^2 - \left(\frac{9}{4}\left(\frac{1}{\sigma_T}+\frac{1}{\sigma_S}+\frac{1}{\sigma_T\sigma_S}\right)-\frac{1}{3}\left(\frac{R_T}{\sigma_T}+\frac{R_S}{\sigma_S}\right)\right)\lambda - \frac{1}{\sigma_T\sigma_S}\left(\frac{27}{8}-\frac{1}{2}(R_T+R_S)\right). \tag{4-186}$$

Temporarily define the coefficients in the above equation by

$$0 = -\lambda^3 + b\lambda^2 - c\lambda + d. \tag{4-187}$$

Comparing equations (4-184) and (4-187) gives

$$c = \lambda_1\lambda_2+\lambda_2\lambda_3+\lambda_3\lambda_1 = \lambda_2\lambda_3 + O(\lambda_1) \tag{4-188}$$

$$d = \lambda_1\lambda_2\lambda_3, \tag{4-189}$$

so that

$$\lambda_1 = \frac{d}{\lambda_2\lambda_3} = \frac{d}{c+O(\lambda_1)} = \frac{d}{c}\left[1+O(\lambda_1)\right]. \tag{4-190}$$

Using the values of c and d in equation (4-186), one finds

$$\lambda_1 = \frac{(R_T+R_S-\frac{27}{4})}{2\sigma_T\sigma_S\left(\frac{9}{4}\left(\frac{1}{\sigma_T}+\frac{1}{\sigma_S}+\frac{1}{\sigma_T\sigma_S}\right)-\frac{1}{3}\left(\frac{R_T}{\sigma_T}+\frac{R_S}{\sigma_S}\right)\right)} + O(\lambda_1{}^2). \tag{4-191}$$

When evaluated at $R_T+R_S = \frac{27}{4}$, the denominator in the above expression is equal to $\mathbf{X}_0^l\cdot\mathbf{X}_0^r$. Therefore the coefficient in equation (4-182) has been found:

$$\dot{z}_1 = \frac{(R_T+R_S-\frac{27}{4})}{(\mathbf{X}_0^l\cdot\mathbf{X}_0^r)} z_1 + \cdots. \tag{4-192}$$

4.4.2. The approximation of the center manifold

Equations (4-181) and (4-192) suggest a rescaling to eliminate the denominator:

$$t \to (\mathbf{X}_0^l\cdot\mathbf{X}_0^r)\, t\,. \tag{4-193}$$

The connection between the dimensional time and the newly scaled time is

$$t = \frac{2}{3}(R_T\sigma_T+R_S\sigma_S+\tfrac{27}{4})\frac{\pi^2\nu}{d^2}t_{dim}\,. \tag{4-194}$$

The ODE for z_1 is now

$$\dot{z}_1 = (R_T+R_S-\tfrac{27}{4})z_1+\mathbf{X}_0^1\cdot\begin{pmatrix}N_w\\N_\vartheta\\N_\xi\end{pmatrix}+O\left[(R_T+R_S-\tfrac{27}{4})^2\varepsilon\right]+O\left[(R_T+R_S-\tfrac{27}{4})\varepsilon^3\right]+O(\varepsilon^5). \quad (4\text{-}195)$$

In order to continue, the nonlinear terms N_w, N_ϑ, and N_ξ must be evaluated on the center manifold, when $R_T+R_S=\frac{27}{4}$. The second order modes are approximated by setting their time derivative to zero. This is justified as follows: on the center manifold,

$$\mathbf{c}_{1,1,2}\sim z_1z_2, \quad (4\text{-}196)$$

and the time derivative is

$$\dot{\mathbf{c}}_{1,1,2}\sim(z_1z_2)^{\cdot}\sim\dot{z}_1z_2+z_1\dot{z}_2\sim O(\lambda\varepsilon^2)+O(\varepsilon^4). \quad (4\text{-}197)$$

(Recall that the center manifold is evaluated *at* $\lambda=0$.) A similar argument applies to the $\mathbf{c}_{0,0,2}$ modes. Thus, equation (4-161) implies that

$$\vartheta_{0,0,2}=-\frac{\sigma_S}{4}i(w_{1,0,1}\vartheta_{-1,0,1}+w_{-1,0,1}\vartheta_{1,0,1}+w_{0,1,1}\vartheta_{0,-1,1}+w_{0,-1,1}\vartheta_{0,1,1})+O(\varepsilon^4). \quad (4\text{-}198)$$

Using equation (4-172) and the constraints (4-50) and (4-54), one finds

$$\begin{aligned}&w_{1,0,1}=3z_1+O(\varepsilon^3)\\&w_{-1,0,1}=-\overline{w}_{1,0,1}=-3\overline{z}_1+O(\varepsilon^3)\\&\vartheta_{-1,0,1}=-\overline{z}_1+O(\varepsilon^3),\text{ etc.}\end{aligned} \quad (4\text{-}199)$$

$\vartheta_{0,0,2}$ can be evaluated on the center manifold. The result is

$$\vartheta_{0,0,2}=\tfrac{3}{2}i\sigma_T(A^2)+O(\varepsilon^4), \quad (4\text{-}200)$$

where

$$A^2\equiv|z_1|^2+|z_2|^2. \quad (4\text{-}201)$$

Using the $[T\leftrightarrow S]$ pseudo-symmetry, the equation for $\xi_{0,0,2}$ is

$$\xi_{0,0,2}=\tfrac{3}{2}i\sigma_S(A^2)+O(\varepsilon^4). \quad (4\text{-}202)$$

The other second order amplitudes are more difficult to compute. The equations are

$$\begin{bmatrix} \dot{w}_{1,1,2} \\ \dot{\vartheta}_{1,1,2} \\ \dot{\xi}_{1,1,2} \end{bmatrix} = \mathbf{L}_{1,1,2} \begin{bmatrix} w_{1,1,2} \\ \vartheta_{1,1,2} \\ \xi_{1,1,2} \end{bmatrix} - \tfrac{1}{2} i(1-\varphi) \begin{bmatrix} 3(5+\varphi)^{-1} w_{1,0,1} w_{0,1,1} \\ w_{1,0,1}\vartheta_{0,1,1} + w_{0,1,1}\vartheta_{1,0,1} \\ w_{1,0,1}\xi_{0,1,1} + w_{0,1,1}\xi_{1,0,1} \end{bmatrix} = O(\varepsilon^4), \quad (4\text{-}203)$$

where

$$\mathbf{L}_{1,1,2} = \begin{bmatrix} -(5+\varphi) & \dfrac{R_T}{(5+\varphi)} & \dfrac{R_S}{(5+\varphi)} \\ \dfrac{(1+\varphi)}{\sigma_T} & -\dfrac{(5+\varphi)}{\sigma_T} & 0 \\ \dfrac{(1+\varphi)}{\sigma_S} & 0 & -\dfrac{(5+\varphi)}{\sigma_S} \end{bmatrix}. \quad (4\text{-}204)$$

On the center manifold, this becomes

$$\begin{bmatrix} w_{1,1,2} \\ \vartheta_{1,1,2} \\ \xi_{1,1,2} \end{bmatrix} = \tfrac{3}{2} i(1-\varphi) z_1 z_2 \mathbf{L}_{1,1,2}{}^{-1} \begin{bmatrix} 9(5+\varphi)^{-1} \\ 2 \\ 2 \end{bmatrix} + O(\varepsilon^4), \quad (4\text{-}205)$$

It is straightforward to invert the 3×3 matrix,

$$\mathbf{L}_{1,1,2}{}^{-1} = \frac{1}{\sigma_S \sigma_T \mathrm{Det}\, \mathbf{L}_{1,1,2}} \mathbf{M} = \frac{-1}{[(5+\varphi)^3 - \frac{27}{4}(1+\varphi)]} \mathbf{M}, \quad (4\text{-}206)$$

where

$$\mathbf{M} = \begin{bmatrix} (5+\varphi)^2 & R_T\sigma_T & R_S\sigma_S \\ (1+\varphi)(5+\varphi) & \sigma_T\left[(5+\varphi)^2 - \dfrac{R_S(1+\varphi)}{(5+\varphi)}\right] & R_S\sigma_S \dfrac{(1+\varphi)}{(5+\varphi)} \\ (1+\varphi)(5+\varphi) & R_T\sigma_T \dfrac{(1+\varphi)}{(5+\varphi)} & \sigma_S\left[(5+\varphi)^2 - \dfrac{R_T(1+\varphi)}{(5+\varphi)}\right] \end{bmatrix}. \quad (4\text{-}207)$$

Substituting $\mathbf{L}_{1,1,2}{}^{-1}$ into equation (4-205) gives

$$\begin{bmatrix} w_{1,1,2} \\ \vartheta_{1,1,2} \\ \xi_{1,1,2} \end{bmatrix} = z_1 z_2 \frac{-\frac{3}{2} i(1-\varphi)}{[(5+\varphi)^3 - \frac{27}{4}(1+\varphi)]} \begin{bmatrix} 9(5+\varphi) + 2(R_T\sigma_T + R_S\sigma_S) \\ 9(1+\varphi) + 2\sigma_T(5+\varphi)^2 + 2R_S(\sigma_S - \sigma_T)\dfrac{(1+\varphi)}{(5+\varphi)} \\ 9(1+\varphi) + 2\sigma_S(5+\varphi)^2 + 2R_T(\sigma_T - \sigma_S)\dfrac{(1+\varphi)}{(5+\varphi)} \end{bmatrix}. \quad (4\text{-}208)$$

These second order modes can now be inserted into the nonlinear terms (4-176) and (4-177):

$$N_w = -i(1+\varphi)(1-\varphi) w_{1,1,2}(3\bar{z}_2) + [\varphi \to -\varphi] \quad (4\text{-}209)$$

$$N_\vartheta = -\tfrac{1}{2}i(1-\varphi)\vartheta_{1,1,2}(3\bar{z}_2)+[\varphi \to -\varphi]-i\vartheta_{0,0,2}(-3z_1) \tag{4-210}$$

$$N_\xi = (-\tfrac{3}{2}i(1-\varphi)\xi_{1,1,2}\bar{z}_2)+[\varphi \to -\varphi]+(3i\xi_{0,0,2}z_1)\,. \tag{4-211}$$

The pseudo-symmetry (4-105) has been used so that the contributions of the $\mathbf{c}_{1,-1,2}\mathbf{c}_{0,1,-1}$ terms don't have to be calculated. They are found by replacing φ with $-\varphi$ in the $\mathbf{c}_{1,1,2}\mathbf{c}_{0,-1,-1}$ terms. (Since ψ does not appear in the ODEs, the $[\psi \to -\psi]$ is dropped from equation (4-105).)

Combining (4-195), (4-208), and the nonlinear terms listed above, the normal form can be written

$$\dot{z}_1 = z_1\big[(R_T+R_S-\tfrac{27}{4})+[\hat{a}(\varphi)+\hat{a}(-\varphi)]\,|z_2|^2+bA^2\big], \tag{4-212}$$

where the $\hat{a}(\varphi)$ terms come from $\mathbf{c}_{1,1,2}\mathbf{c}_{0,-1,-1}$:

$$\begin{aligned}\hat{a}(\varphi)z_1|z_2|^2 = \Big(\tfrac{3}{2}\big[-3i(1+\varphi)(1-\varphi)w_{1,1,2}\bar{z}_2\big]+\tfrac{2}{3}R_T\sigma_T\big[-\tfrac{3}{2}i(1-\varphi)\vartheta_{1,1,2}\bar{z}_2\big]\\ +\tfrac{2}{3}R_S\sigma_S\big[-\tfrac{3}{2}i(1-\varphi)\xi_{1,1,2}\bar{z}_2\big]\Big),\end{aligned} \tag{4-213}$$

and the term proportional to b comes from $\mathbf{c}_{0,0,2}\mathbf{c}_{1,0,-1}$:

$$bz_1A^2 = \Big(\tfrac{3}{2}\cdot 0+\tfrac{2}{3}R_T\sigma_T(3i\vartheta_{0,0,2}z_1)+\tfrac{2}{3}R_S\sigma_S(3i\xi_{0,0,2}z_1)\Big). \tag{4-214}$$

When the $\mathbf{c}_{1,1,2}$ modes are inserted into (4-213), a little algebra yields

$$\begin{aligned}\hat{a}(\varphi) = -3f(\varphi)\Big(\tfrac{81}{4}(1+\varphi)(5+\varphi)+9(1+\varphi)(R_T\sigma_T+R_S\sigma_S)\\ +(5+\varphi)^2(R_T\sigma_T{}^2+R_S\sigma_S{}^2)-\frac{(1+\varphi)}{(5+\varphi)}R_TR_S\,|\sigma_T-\sigma_S|^2\Big),\end{aligned} \tag{4-215}$$

where

$$f(\varphi) \equiv \frac{(1-\varphi)^2}{[(5+\varphi)^3-\frac{27}{4}(1+\varphi)]}. \tag{4-216}$$

When the $\mathbf{c}_{0,0,2}$ modes are inserted into (4-214), one finds

$$b = -3(R_T\sigma_T{}^2+R_S\sigma_S{}^2). \tag{4-217}$$

The equations can be rescaled to simplify the coefficients; let

$$R_T = \tfrac{27}{4}r_T,\ \ R_S = \tfrac{27}{4}r_S,\ \ (z_1)_{old} = \frac{(z_1)_{new}}{\sqrt{3}},\ \text{and} \tag{4-218}$$

$$\frac{d}{dt}_{old} = \frac{27}{4}\frac{d}{dt}_{new}. \tag{4-219}$$

The rescaled normal form is

$$\dot{z}_1 = (r_T+r_S-1)z_1+a_{\varphi^2}z_1|z_2|^2+bz_1(|z_1|^2+|z_2|^2), \tag{4-220}$$

where

$$a_{\varphi^2} \equiv \left[\hat{a}(\varphi)+\hat{a}(-\varphi)\right], \tag{4-221}$$

with

$$\begin{aligned}\hat{a}(\varphi) = -f(\varphi)\Big[&3(1+\varphi)(5+\varphi)+9(1+\varphi)(r_T\sigma_T+r_S\sigma_S)\\ &+(5+\varphi)^2(r_T\sigma_T{}^2+r_S\sigma_S{}^2)-\tfrac{27}{4}\frac{(1+\varphi)}{(5+\varphi)}r_Tr_S|\sigma_T-\sigma_S|^2\Big],\end{aligned} \tag{4-222}$$

$$b = -(r_T\sigma_T{}^2+r_S\sigma_S{}^2), \tag{4-223}$$

where $f(\varphi)$ is defined in equation (4-216). The dimensionless time used in this scaling of the normal form is

$$t = \frac{9}{2}(R_T\sigma_T+R_S\sigma_S+\tfrac{27}{4})\frac{\pi^2\nu}{d^2}t_{dim}, \tag{4-224}$$

and the amplitude is

$$z_1 = \frac{\sqrt{3}}{\sigma_T}\frac{\pi}{\Delta T}(\vartheta_{1,0,1})_{dim}. \tag{4-225}$$

The above equations are perhaps the simplest expression of the result, but there is some redundancy because $r_S+r_T = 1$ at the pitchfork bifurcation. The thermal Rayleigh number can be eliminated using $r_T = (1-r_S)$. This corresponds to an experiment where R_S is fixed, and R_T is the control parameter:

$$\begin{aligned}a(\varphi) = -f(\varphi)\Big[&3(1+\varphi)(5+\varphi)+9(1+\varphi)\left[\sigma_T+r_S(\sigma_S-\sigma_T)\right]\\ &+(5+\varphi)^2[\sigma_T{}^2+r_S(\sigma_S{}^2-\sigma_T{}^2)]-\tfrac{27}{4}\frac{(1+\varphi)}{(5+\varphi)}(r_S-r_S{}^2)|\sigma_T-\sigma_S|^2\Big]\end{aligned} \tag{4-226}$$

$$b = -\left[\sigma_T{}^2+r_S(\sigma_S{}^2-\sigma_T{}^2)\right]. \tag{4-227}$$

In the literature a different scaling and different parameters are usually used. (See the discussion in chapter 1.) The traditional notation hides the sym-

metry between heat and solute, but the symmetry is destroyed anyway when τ_T is eliminated. The amplitude is rescaled by

$$(z_1)_{new} = \sigma_T (z_1)_{old}, \tag{4-228}$$

and the new parameters are

$$\tilde{r}_S \equiv -r_S \tau, \quad \tau \equiv \frac{\sigma_T}{\sigma_S}, \text{ and } \sigma \equiv \sigma_T. \tag{4-229}$$

In terms of these new variables,

$$\hat{a}(\varphi) = -f(\varphi)\left\{\frac{3}{\sigma^2}(1+\varphi)(5+\varphi) + \frac{9}{\sigma}(1+\varphi)\left[1+\tilde{r}_S\left(\frac{1}{\tau}-\frac{1}{\tau^2}\right)\right]\right.$$
$$\left.+(5+\varphi)^2\left[1+\tilde{r}_S\left(\frac{1}{\tau}-\frac{1}{\tau^3}\right)\right] + \frac{27}{4}\frac{(1+\varphi)}{(5+\varphi)}\left[\frac{\tilde{r}_S}{\tau}+\left(\frac{\tilde{r}_S}{\tau}\right)^2\right]\left|1-\frac{1}{\tau}\right|^2\right\}, \tag{4-230}$$

$$b = -\left[1+\tilde{r}_S\left(\frac{1}{\tau}-\frac{1}{\tau^3}\right)\right], \tag{4-231}$$

where $f(\varphi)$ is defined in equation (4-216). The value of $\tilde{r}_S$ where the pitchfork bifurcation of the rolls is degenerate is

$$(\tilde{r}_S)_{b=0} = \frac{\tau^3}{1-\tau_2}. \tag{4-232}$$

Note that this does not depend on σ.

This concludes the calculation of the coefficients in the normal form for doubly diffusive convection.

4.4.3. Analysis of the results

Now the results of the calculation must be analyzed to see what convection patterns they predict. The analysis is done with the parameters $\tilde{r}_S$, τ, and σ to simplify comparison with other work. The parameters can be restricted to the region

$$\begin{aligned} &-\infty < \tilde{r}_S < \frac{\tau^2}{(1-\tau)}\frac{(1+\sigma)}{\sigma} \equiv (\tilde{r}_S)_{\omega^2=0} \\ &0 < \tau \le 1 \\ &\sigma > 0, \end{aligned} \tag{4-233}$$

without essential loss of generality. The upper limit of $\tilde{r}_S$ is at the

codimension-two bifurcation where the Hopf and pitchfork bifurcations coalesce. For $\tilde{r}_S > (\tilde{r}_S)_{\omega^2=0}$, the Hopf bifurcation occurs before the pitchfork, as r_T is increased. Note that $(\tilde{r}_S)_{\omega^2=0} > (\tilde{r}_S)_{b=0}$ for all σ and τ. The case where $\tau \geq 1$ can be transformed to the above region by interchanging S and T, which changes the new parameters as follows:

$$\tilde{r}_S \to -r_T\tau = -(1-r_S)\tau = -\tau-\tilde{r}_S \tag{4-234}$$

$$\sigma \to \frac{\sigma}{\tau} \tag{4-235}$$

$$\tau \to \frac{1}{\tau}. \tag{4-236}$$

Theorem: There are no stable, small amplitude, three-dimensional, stationary solutions of the equations for doubly diffusive convection in the Boussinesq approximation (equations (1-46)ff). Rolls are the only possible stable, small amplitude, stationary solution.

Proof: According to the results of Chapter Two, the hexagons, rectangles, or squares can only be stable when

$$a_{\varphi^2} = \left[\hat{a}(\varphi)+\hat{a}(-\varphi)\right] > 0, \text{ and} \tag{4-237}$$

$$b = < 0, \tag{4-238}$$

for the value of φ corresponding to the hexagonal, rhombic, or square lattice. (This is necessary but not sufficient for there to be stable three-dimensional patterns; the coefficients must be in region II of fig. 2-7, 2-23 or 2-32) However, the above combination is impossible. The expression (4-230) for a can be written

$$\hat{a}(\varphi) = neg.+neg.\left[1+\tilde{r}_S\left(\frac{1}{\tau}-\frac{1}{\tau^2}\right)\right]+neg.\left[1+\tilde{r}_S\left(\frac{1}{\tau}-\frac{1}{\tau^3}\right)\right]+neg., \tag{4-239}$$

where "*neg.*" represents negative semidefinite terms. Note that

$$\frac{1}{\tau}-\frac{1}{\tau^3} \leq \frac{1}{\tau}-\frac{1}{\tau^2} \leq 0. \tag{4-240}$$

Since both of these combinations are negative, $a(\varphi)$ is always negative when $\tilde{r}_S$ is negative. Furthermore, when $\tilde{r}_S$ is positive,

$$-b = \left[1+\tilde{r}_S\left(\frac{1}{\tau}-\frac{1}{\tau^3}\right)\right] \leq \left[1+\tilde{r}_S\left(\frac{1}{\tau}-\frac{1}{\tau^2}\right)\right]. \tag{4-241}$$

Therefore, when b is negative, every term in $\hat{a}(\varphi)$ is less than or equal to zero. QED

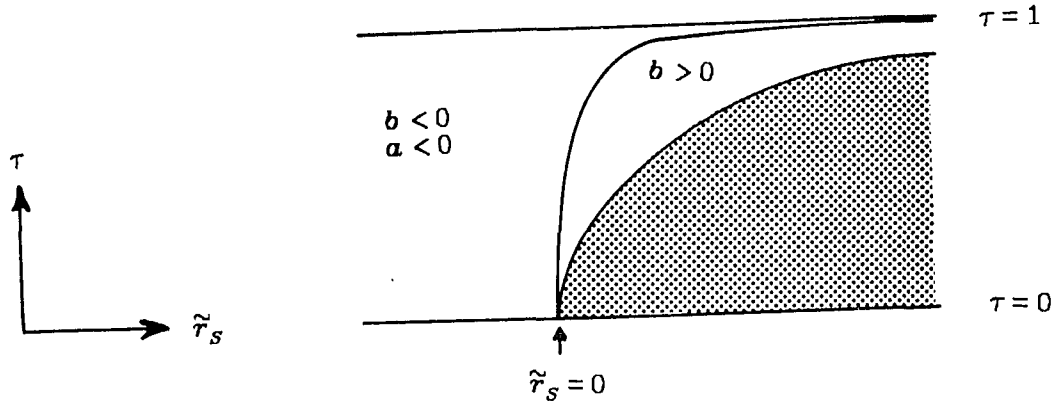

Fig. 4-2. The $\tilde{r}_s$-τ parameter space of doubly diffusive convection, where σ is fixed.. (The qualitative results are independent of σ.) The rolls are subcritical in the region where $b > 0$, and therefore there are no stable small amplitude solutions. The rolls are supercritical when $b < 0$, and the rolls are the only stable solution in this region since $a \leq 0$ for all lattices when $b < 0$. In the shaded region, the Hopf bifurcation occurs before the pitchfork. The dividing lines in this figure are $(\tilde{r}_s)_{b=0}$ and $(\tilde{r}_s)_{\omega^2=0}$.

Fig. 4-3 shows the lattice function (equation (4-221), combined with (4-230)) for the parameters σ and τ of salt water.

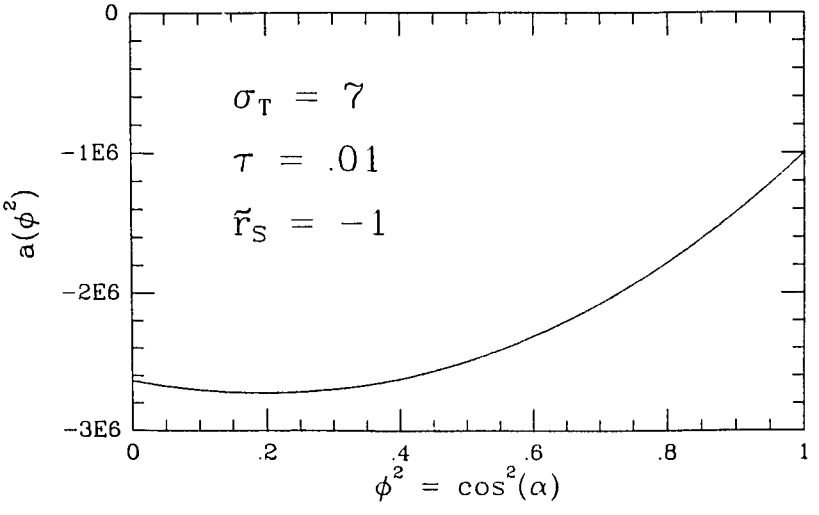

fig. 4-3(a)

Fig. 4-3. The lattice function, (4-221) and (4-230), for thermohaline convection (doubly diffusive convection in salt water). Fig. 4-3(a) shows the lattice function in the salt-finger regime, where $\tilde{r}_S$ is negative: rolls are the only stable solution here since $a<0$ for all lattices. Fig. 4-3(b) and Fig. 4-3(c) are in the range $(\tilde{r}_S)_{b=0} < \tilde{r}_S < (\tilde{r}_S)_{\omega^2=0}$. (These endpoints are defined in equations (4-232) and (4-233).) Note that $b = a_{\varphi^2=1} > 0$ in figs. (b) and (c), so that rolls are subcritical and there are no stable, small amplitude solutions. In fig. (b), the dotted line is at $a = 0$, the dashed line is at $a+2b = 0$ (where the rectangles bifurcate vertically), and the triangle is at $2a_H+3b = 0$ (where the hexagons and regular triangles bifurcate vertically). In fig. (c), the arrow indicates that $2a_H > 0$, $b > 0$, so that region IV of figs. 2-23 and 2-24 are relevant to Boussinesq convection on a hexagonal lattice with these parameters.

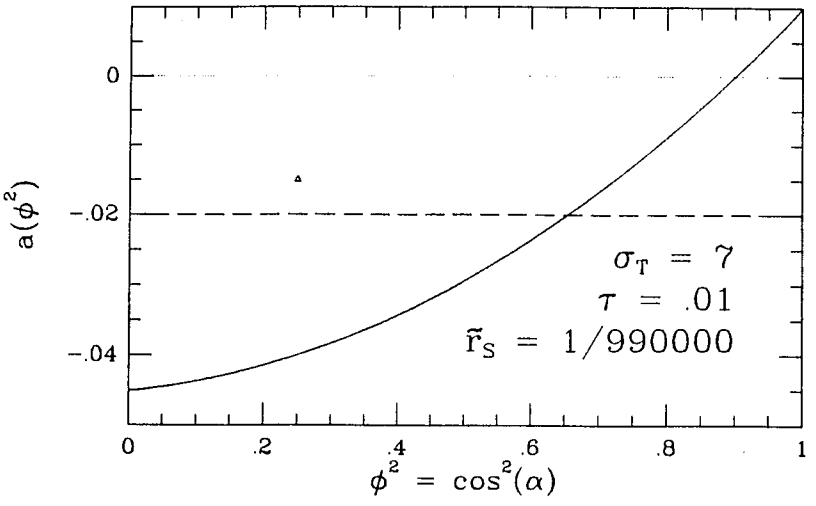

fig. 4-3(b)

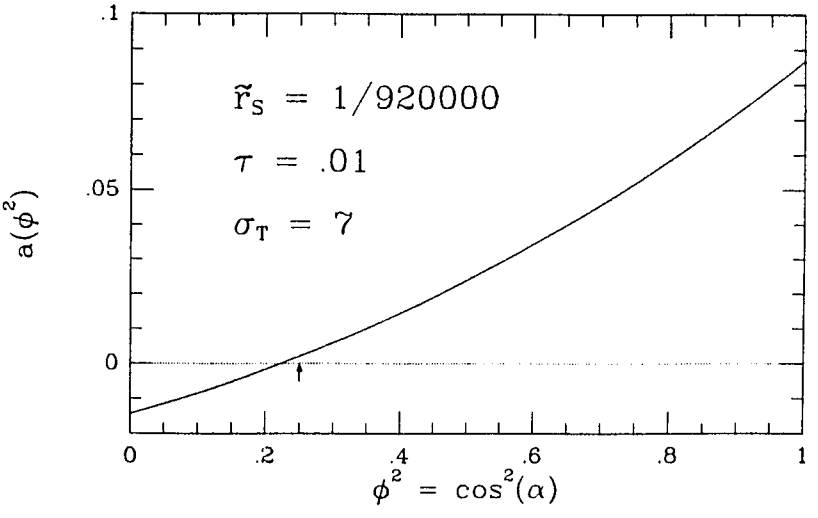

fig. 4-3(c)

Nagata and Thomas (1983) have calculated what is usually called R_2 in the literature, (see equation (2-461)) although they cannot determine the stability of the rolls to three-dimensional disturbances. However, the preprint results of Nagata and Thomas do not agree with Schlüter, Lortz, and Busse (1965) in the limiting case of purely thermal convection.

The limiting case of Rayleigh-Bénard convection can be reached in two ways: either by setting $\tilde{r}_S = 0$, or by setting $\tau = 1$. The nonlinear terms are

$$\hat{a}(\varphi) = -f(\varphi)\left[\frac{3}{\sigma^2}(1+\varphi)(5+\varphi)+\frac{9}{\sigma}(1+\varphi)+(5+\varphi)^2\right] \tag{4-242}$$

$$b = -1 \tag{4-243}$$

Therefore the rolls are always supercritical ($b < 0$), and they are the only small amplitude stable solution ($a < 0$).

This final form agrees with the appendix of Schlüter, Lortz, and Busse (1965), where the calculation was first done. The correspondence with their notation is:

$$\hat{a}(\varphi) = c\,\mathrm{L}(\varphi,-\varphi)\,, \quad b = c\,\mathrm{L}(-1,1)\,, \tag{4-244}$$

where c is a constant.

There is some experimental indication that squares are preferred in the salt finger regime, where $\tilde{r}_S \ll 0$ (Shirtcliffe & Turner 1970). It is well known, however, that nonlinear effect are important for salt fingers. The small amplitude analysis used here cannot be expected to work.

Chapter Five

The Hopf bifurcation in doubly diffusive convection

In this section the bifurcation of the standing and traveling waves is computed for doubly diffusive convection. A major result is that the bifurcation of the traveling waves is degenerate: The cubic damping coefficient is identically zero for all parameter values. This fact was known to Bretherton and Spiegel (1983), although they did not emphasize it. The focus of their paper is how the slowly varying amplitudes (varying on a slow spatial scale as in Newell and Whitehead (1969)) can check the growth of the waves.

The traveling waves have generally been ignored in the literature. Analytical studies as well as numerical integrations of the partial differential equations usually impose "no flux" boundary conditions at the side walls which forbid the traveling waves. With periodic boundary conditions the traveling waves are allowed. The results of section 2.8.1, where the degenerate bifurcation with $b=0$ is studied, apply to this problem. In particular, when the standing waves are supercritical, one of the diagrams in fig. 2-13 (with $b=0$) is appropriate. The traveling waves are the preferred mode of oscillatory convection when the standing waves are supercritical. (Near the bifurcation, the traveling waves are sure to have a larger amplitude than the standing waves.)

In this chapter the cubic damping coefficient of the standing waves is calculated. This is not a new result but the techniques are new. The complex notation used here particularly appropriate for Hopf bifurcations. For simplicity, the calculations are restricted to two-dimensional convection.

5.1. The Third Order Calculation

The ODEs needed are an extension of the Lorenz (1963) equations, where

the solute modes are included and the amplitudes are complex.

For two-dimensional convection the notation for the amplitudes is

$$\mathbf{c}_{l,n} \equiv \mathbf{c}_{l\mathbf{k}_1,n}\ ,\quad |\mathbf{k}_1|^2 = k_c{}^2. \tag{5-1}$$

It follows from equations (4-155)-(4-162), neglecting the $\mathbf{c}_{l,m,n}$ modes with $m \neq 0$, that the ODEs are

$$\dot{w}_{1,1} = -\tfrac{3}{2}w_{1,1} + \tfrac{2}{3}[R_T\vartheta_{1,1} + R_S\xi_{1,1}] \tag{5-2}$$

$$\dot{\vartheta}_{1,1} = \frac{1}{2\sigma_T}w_{1,1} - \frac{3}{2\sigma_T}\vartheta_{1,1} - iw_{1,-1}\vartheta_{0,2} \tag{5-3}$$

$$\dot{\xi}_{1,1} = \frac{1}{2\sigma_S}w_{1,1} - \frac{3}{2\sigma_S}\xi_{1,1} - iw_{1,-1}\xi_{0,2} \tag{5-4}$$

$$\dot{\vartheta}_{0,2} = \frac{-4}{\sigma_T} - i(w_{1,1}\vartheta_{-1,1} + w_{-1,1}\vartheta_{1,1}) \tag{5-5}$$

$$\dot{\xi}_{0,2} = \frac{-4}{\sigma_S} - i(w_{1,1}\xi_{-1,1} + w_{-1,1}\xi_{1,1}). \tag{5-6}$$

These equations can be scaled to eliminate the numerical coefficients. Let

$$\frac{d}{dt} \to \tfrac{3}{2}\frac{d}{dt}\text{, so that } \omega \to \tfrac{3}{2}\omega\text{,} \tag{5-7}$$

$$R_T \to \tfrac{27}{4}r_T\text{, and } R_S \to \tfrac{27}{4}r_S\text{,} \tag{5-8}$$

$$w_{l,n} \to \tfrac{3}{2}iw_{l,n}\ , \tag{5-9}$$

$$\vartheta_{l,n} \to \tfrac{1}{2}i\vartheta_{l,n}\text{, and } \xi_{l,n} \to \tfrac{1}{2}i\xi_{l,n}\ . \tag{5-10}$$

In terms of the new variables, on the right hand side, the ODEs are

$$\dot{w}_{1,1} = -w_{1,1} + r_T\vartheta_{1,1} + r_S\xi_{1,1} \tag{5-11}$$

$$\dot{\vartheta}_{1,1} = \frac{1}{\sigma_T}(w_{1,1} - \vartheta_{1,1}) + w_{1,-1}\vartheta_{0,2} \tag{5-12}$$

$$\dot{\vartheta}_{0,2} = \frac{-1}{\sigma_T}\frac{8}{3}\vartheta_{0,2} + (w_{1,1}\vartheta_{-1,1} + w_{-1,1}\vartheta_{1,1}), \tag{5-13}$$

and the equations for $\dot{\xi}_{1,1}$ and $\dot{\xi}_{0,2}$, which follow from the pseudo-symmetry

$$\vartheta_{l,n} \leftrightarrow \xi_{l,n}\ ,\quad [\sigma_S \leftrightarrow \sigma_T\text{, } r_S \leftrightarrow r_T]. \tag{5-14}$$

For a general wavenumber, the factor of $\frac{8}{3}$ in the $\dot{\vartheta}_{0,2}$ equation is replaced by

$$\nu \equiv \frac{4}{1+|\mathbf{k}|^2}. \tag{5-15}$$

Note that $0 < \nu < 4$. Of course, $\nu = \frac{8}{3}$ is the most interesting case, since it corresponds to the first wavelength to go unstable. The result that the traveling waves aren't damped to third order is independent of the wavelength.

The system of five complex equations ((5-11)ff) is the complexification of the five dimensional real system which was first derived by Veronis (1965). The real system was studied extensively by Da Costa *et al.* (1981), where many interesting bifurcations were found. The five dimensional real system describes doubly diffusive convection in a box, where traveling waves are not allowed. The behavior of the complex system is certainly more complicated, and should be studied numerically. However, the five dimensional complex system is degenerate and more modes must be included to properly study the traveling waves.

WARNING: The change of variables of equations (5-9) and (5-10) involved multiplication by i. This changes the symmetries of the ODEs which involve complex conjugation. In terms of the new variables, the symmetries which preserve the boundary condition give the constraints :

$$\mathbf{c}_{l,n} = -\mathbf{c}_{l,-n} = -\bar{\mathbf{c}}_{-l,-n} = \bar{\mathbf{c}}_{-l,n} \tag{5-16}$$

The other symmetries are

$$\mathbf{c}_{l,n} \to \bar{\mathbf{c}}_{l,n} = -\mathbf{c}_{-l,n} \tag{5-17}$$

$$\to (-1)^n \mathbf{c}_{l,n} \tag{5-18}$$

$$\to e^{il\mathbf{k}_1 \cdot \mathbf{d}} \mathbf{c}_{l,n}. \tag{5-19}$$

The vertical vorticity modes have not been included here, since the symmetry (4-152),

$$\begin{aligned} \mathbf{c}_{l,n} &\to \mathbf{c}_{l,n} \\ \zeta_{l,n} &\to -\zeta_{l,n}, \end{aligned} \tag{5-20}$$

forces the vertical vorticity to be identically zero on the center manifold.

5.1.1. Linear theory

The linear problem of the first order modes involves finding the eigenvectors of the matrix

$$\mathbf{L}_{1,1} \equiv \begin{bmatrix} -1 & r_T & r_S \\ \frac{1}{\sigma_T} & \frac{-1}{\sigma_T} & 0 \\ \frac{1}{\sigma_S} & 0 & \frac{-1}{\sigma_S} \end{bmatrix}. \tag{5-21}$$

At the Hopf bifurcation, the eigenvalues of $\mathbf{L}_{1,1}$ are

$$i\omega, \quad -i\omega, \quad \text{and} \quad -\left(1+\frac{1}{\sigma_S}+\frac{1}{\sigma_T}\right). \tag{5-22}$$

The third eigenvalue is the trace of $\mathbf{L}_{1,1}$, since the sum of the other two eigenvalues is zero. The right eigenvectors for these eigenvalues are:

$$\mathbf{X}_{i\omega} = \begin{bmatrix} 1 \\ \frac{1}{(1+i\omega\sigma_T)} \\ \frac{1}{(1+i\omega\sigma_S)} \end{bmatrix}, \quad \mathbf{X}_{-i\omega} = \begin{bmatrix} 1 \\ \frac{1}{(1-i\omega\sigma_T)} \\ \frac{1}{(1-i\omega\sigma_S)} \end{bmatrix} = \bar{\mathbf{X}}_{i\omega}, \text{ and} \tag{5-23}$$

$$\mathbf{X}_{-\left(1+\frac{1}{\sigma_T}+\frac{1}{\sigma_S}\right)} = \begin{bmatrix} \sigma_T\sigma_S(1+\sigma_T)(1+\sigma_S) \\ -\sigma_S{}^2(1+\sigma_T) \\ -\sigma_T{}^2(1+\sigma_S) \end{bmatrix}. \tag{5-24}$$

The linear change of variables which diagonalizes $\mathbf{L}_{1,1}$ is therefore

$$\begin{bmatrix} w_{1,1} \\ \vartheta_{1,1} \\ \xi_{1,1} \end{bmatrix} = \mathbf{S} \begin{bmatrix} z \\ w \\ q \end{bmatrix}, \tag{5-25}$$

where z is the complex amplitude of the left-going traveling wave, w is the amplitude of the right-going traveling wave, and q is the amplitude of the third order mode associated with the real eigenvalue. The columns of $\mathbf{S}$ are the eigenvectors listed above:

$$\mathbf{S}=\begin{bmatrix} 1 & 1 & \sigma_T\sigma_S(1+\sigma_T)(1+\sigma_S) \\ \dfrac{1}{(1+i\omega\sigma_T)} & \dfrac{1}{(1-i\omega\sigma_T)} & -\sigma_S{}^2(1+\sigma_T) \\ \dfrac{1}{(1+i\omega\sigma_S)} & \dfrac{1}{(1-i\omega\sigma_S)} & -\sigma_T{}^2(1+\sigma_S) \end{bmatrix}. \tag{5-26}$$

The matrix $\mathbf{S}$ diagonalizes the linear ODE:

$$\begin{bmatrix} \dot{z} \\ \dot{w} \\ \dot{q} \end{bmatrix} = \mathbf{S}^{-1}\mathbf{L}_{1,1}\mathbf{S}\begin{bmatrix} z \\ w \\ q \end{bmatrix} + \mathbf{S}^{-1}\begin{bmatrix} 0 \\ w_{1,-1}\vartheta_{0,2} \\ w_{1,-1}\xi_{0,2} \end{bmatrix}, \tag{5-27}$$

where

$$\mathbf{S}^{-1}\mathbf{L}_{1,1}\mathbf{S}=\begin{bmatrix} i\omega & 0 & 0 \\ 0 & -i\omega & 0 \\ 0 & 0 & -\left(1+\dfrac{1}{\sigma_T}+\dfrac{1}{\sigma_S}\right) \end{bmatrix}. \tag{5-28}$$

The inverse of $\mathbf{S}$ can be calculated from the usual method of determinants and cofactors. Note that this is a different approach than was used for the pitchfork bifurcation. There, the left eigenvectors were computed in lieu of the full matrix $\mathbf{S}$. The left eigenvectors of $\mathbf{L}_{1,1}$ involve r_T and r_S, but in the Hopf bifurcation it is more convenient to eliminate these parameters in favor of ω^2 using equation (1-122). After this substitution the left eigenvectors are messy, and the dot product of the left and right eigenvectors for the same eigenvalue is neither purely real nor purely imaginary.

The method used here is convenient since all three eigenvalues are known. In addition, $\mathbf{S}$ has some nice properties; for instance its determinant is pure imaginary:

$$\mathrm{Det}\,\mathbf{S}=i\omega(\sigma_S-\sigma_T)\frac{\omega^2\sigma_S{}^2\sigma_T{}^2+(\sigma_S\sigma_T+\sigma_S+\sigma_T)^2}{(1+\omega^2\sigma_S{}^2)(1+\omega^2\sigma_T{}^2)}. \tag{5-29}$$

The first three factors are necessary since $i \to -i$ or $\omega \to -\omega$ interchange the first two columns of $\mathbf{S}$, and $\sigma_S \leftrightarrow \sigma_T$ interchanges the second and third rows, thus

changing the sign of the determinant. The other factors are positive definite, and invariant under $[S \leftrightarrow T]$.

It is easy to see that z is the amplitude of the traveling wave going in the direction opposite $\mathbf{k}_1$: This will be called the left-going wave. The ODE for z is

$$\dot{z} = i\omega z + O(z^3), \text{ so that } z(t) = \varepsilon e^{i\omega t} + O(\varepsilon^3), \tag{5-30}$$

where ε is the amplitude, assumed small, which is undetermined by the linear ODE. When ε is real, the vertical velocity field is

$$w(\mathbf{x}, t) \propto \varepsilon \sin(\hat{\mathbf{z}}\cdot\mathbf{x})\cos(\mathbf{k}_1\cdot\mathbf{x}+\omega t)+O(\varepsilon^3), \tag{5-31}$$

which is indeed a traveling wave.

It is necessary to find how the amplitudes (z, w, and q) transform under the symmetries. The symmetry between right- and left-going waves is

$$\mathbf{c}_{l,n} \to \mathbf{c}_{-l,n} = \bar{\mathbf{c}}_{l,n}. \tag{5-32}$$

This transformation is the same as

$$z \to \bar{w}, \quad w \to \bar{z}, \quad q \to \bar{q} \tag{5-33}$$

since $\bar{\mathbf{X}}_{i\omega} = \mathbf{X}_{-i\omega}$, which implies

$$\begin{bmatrix} \bar{w}_{1,1} \\ \bar{\vartheta}_{1,1} \\ \bar{\xi}_{1,1} \end{bmatrix} = \mathbf{S} \begin{bmatrix} \bar{w} \\ \bar{z} \\ \bar{q} \end{bmatrix}. \tag{5-34}$$

The translational symmetry (5-19) gives

$$\begin{bmatrix} z \\ w \\ q \end{bmatrix} \to e^{is} \begin{bmatrix} z \\ w \\ q \end{bmatrix}, \text{ where } s = \mathbf{k}_1\cdot\mathbf{d}. \tag{5-35}$$

In addition, the critical modes have a *time translation* symmetry, which corresponds to the freedom of assigning $t = 0$. This has no effect in stationary bifurcations, but here it yields the symmetry

$$\begin{aligned} z &\to e^{i\varphi_t} z \\ w &\to e^{-i\varphi_t} w. \end{aligned} \tag{5-36}$$

These two symmetries can be combined to give two space-time translational symmetries which follow the left- and right-going traveling waves, respectively:

$$z \to z\,,\ w \to e^{2is}w\,,\ \text{and} \tag{5-37}$$

$$z \to e^{2is}z\,,\ w \to w\,. \tag{5-38}$$

The time translation symmetry is different than the others, since it is not a transformation of all the amplitudes, just the critical ones. The higher order amplitudes are damped in the linear ODEs, and the critical amplitudes are damped at higher order. The details of this rather subtle symmetry are given in Golubitsky and Stewart (1984).

5.1.2. The center manifold

The only second order modes are $\vartheta_{0,2}$ and $\xi_{0,2}$. These modes are invariant under spatial translations (5-19), and the left-right symmetry (5-33). This forces the center manifold function to be of the form

$$\begin{aligned}\vartheta_{0,2}(z,w) &= \alpha_T z\bar{w} + \bar{\alpha}_T \bar{z} w + \beta_T(A^2) + O(A^4)\\ \xi_{0,2}(z,w) &= \alpha_S z\bar{w} + \bar{\alpha}_S \bar{z} w + \beta_S(A^2) + O(A^4)\,,\end{aligned} \tag{5-39}$$

where β_T and β_S are real, and $A^2 \equiv |z|^2 + |w|^2$. Due to the $[S \leftrightarrow T]$ pseudo-symmetry, the coefficients satisfy

$$\begin{aligned}\alpha_T &= \alpha_T[\sigma_T,\sigma_S]\\ \alpha_S &= \alpha_T[\sigma_S,\sigma_T]\,,\\ &\text{and}\\ \beta_T &= \beta_T[\sigma_T,\sigma_S]\\ \beta_S &= \beta_T[\sigma_S,\sigma_T]\,.\end{aligned} \tag{5-40}$$

Equation (5-39) can be differentiated with respect to time,

$$\dot{\vartheta}_{0,2} = 2i\omega\alpha_T z\bar{w} - 2i\omega\bar{\alpha}_T\bar{z}w + O(A^4). \tag{5-41}$$

Then this equation can be inserted into the ODE for $\vartheta_{0,2}$ to solve for α and β:

$$\begin{aligned}\dot{\vartheta}_{0,2} &= \frac{-1}{\sigma_T}\frac{8}{3}\vartheta_{0,2} + (w_{1,1}\vartheta_{-1,1} + w_{-1,1}\vartheta_{1,1})\\ &= \frac{-1}{\sigma_T}\frac{8}{3}\left(\alpha_T z\bar{w} + \bar{\alpha}_T\bar{z}w + \beta_T(A^2)\right] + (w_{1,1}\bar{\vartheta}_{1,1} + \bar{w}_{1,1}\vartheta_{1,1}) + O(A^4).\end{aligned} \tag{5-42}$$

The nonlinear terms can be written in terms of z and w:

$$w_{1,1}\bar{\vartheta}_{1,1}+\bar{w}_{1,1}\vartheta_{1,1}=(z+w)\left[\frac{\bar{z}}{(1-i\omega\sigma_T)}+\frac{\bar{w}}{(1+i\omega\sigma_T)}\right]+c.c.$$
$$=\frac{2}{(1+\omega^2\sigma_T{}^2)}(A^2)+\left[\frac{2z\bar{w}}{(1+i\omega\sigma_T)}+c.c.\right], \tag{5-43}$$

where the "c.c." stands for the complex conjugate of the proceeding term. When the two equations for $\dot{\vartheta}_{0,2}$ are set equal to each other, the coefficients of $z\bar{w}$ and $|z|^2$ match independently:

$$2i\omega\alpha_T=\frac{-1}{\sigma_T}\frac{8}{3}\alpha_T+\frac{2}{(1+i\omega\sigma_T)}, \tag{5-44}$$

$$0=\frac{-1}{\sigma_T}\frac{8}{3}\beta_T+\frac{2}{(1+\omega^2\sigma_T{}^2)}. \tag{5-45}$$

These are solved to give

$$\alpha_T=\frac{\sigma_T}{(\frac{4}{3}+i\omega\sigma_T)(1+i\omega\sigma_T)}, \tag{5-46}$$

$$\beta_T=\frac{3}{4}\frac{\sigma_T}{(1+\omega^2\sigma_T{}^2)}. \tag{5-47}$$

The second order modes can now be inserted into the equation for z and w:

$$\dot{z}=i\omega z+\mathbf{S}^{-1}{}_{1,2}\,w_{1,-1}\vartheta_{0,2}+\mathbf{S}^{-1}{}_{1,3}\,w_{1,-1}\xi_{0,2} \tag{5-48}$$

$$\dot{w}=i\omega z+\mathbf{S}^{-1}{}_{2,2}\,w_{1,-1}\vartheta_{0,2}+\mathbf{S}^{-1}{}_{2,3}\,w_{1,-1}\xi_{0,2}. \tag{5-49}$$

It can be verified that $\mathbf{S}^{-1}$ has the symmetry properties,

$$\begin{aligned}\mathbf{S}^{-1}{}_{i,2}&=\mathbf{S}^{-1}{}_{i,2}[\sigma_T,\sigma_S]\\ \mathbf{S}^{-1}{}_{i,3}&=\mathbf{S}^{-1}{}_{i,2}[\sigma_S,\sigma_T],\text{ and}\end{aligned} \tag{5-50}$$

$$\mathbf{S}^{-1}{}_{1,j}=\bar{\mathbf{S}}^{-1}{}_{2,j}. \tag{5-51}$$

This last property insures that the normal form is equivariant under the symmetry ($z\leftrightarrow\bar{w}$). The ODE for z is

$$\dot{z}=i\omega z+\left[\mathbf{S}^{-1}{}_{1,2}\left[-(z+w)\right]\left[\alpha_T z\bar{w}+\bar{\alpha}_T\bar{z}w+\beta_T(|z|^2+|w|^2)\right]+[S\leftrightarrow T]\right]. \tag{5-52}$$

As discussed in Chapter Two, the beauty of the complex notation is that all the cubic terms which are not in the normal from can be eliminated with a near identity change of coordinates. Because of the symmetry, there are no quadratic terms; therefore the normal form is

$$\dot{z} = i\omega z + az\,|w|^2 + bz(A^2) + O(zA^4) \tag{5-53}$$

$$\dot{w} = -i\omega w + \bar{a}w\,|w|^2 + \bar{b}w(A^2) + O(wA^4), \tag{5-54}$$

where

$$a = \hat{a}_T + \hat{a}_S\ ,\ \ b = \hat{b}_T + \hat{b}_S, \tag{5-55}$$

and in turn,

$$\hat{a}_T = -\mathbf{S}^{-1}{}_{1,2}\alpha_T, \text{ and } \hat{b}_T = -\mathbf{S}^{-1}{}_{1,2}\beta_T. \tag{5-56}$$

All that remains is to substitute the value of $\mathbf{S}^{-1}{}_{1,2}$:

$$\mathbf{S}^{-1}{}_{1,2} = \frac{1}{\mathrm{Det}\,\mathbf{S}}\left[\frac{\sigma_T\sigma_S(1+\sigma_T)(1+\sigma_S)(1+i\omega\sigma_S)}{(1+\omega^2\sigma_S{}^2)} + \sigma_T{}^2(1+\sigma_S)\right]. \tag{5-57}$$

The normal form (5-53) and (5-54) was discussed in Chapter Three. The results are simply stated: Only the real parts of a and b are important for the qualitative behavior of the bifurcation diagrams. The real part of $\frac{1}{2}a+b$ determines whether the standing waves are subcritical ($\mathrm{Re}(\frac{1}{2}a+b)>0$), or supercritical ($\mathrm{Re}(\frac{1}{2}a+b)<0$) ; the real part of b determines whether the traveling waves are subcritical ($\mathrm{Re}(b)>0$), or supercritical ($\mathrm{Re}(b)<0$). If both standing waves and traveling waves are supercritical, the one with the larger amplitude A^2 is stable.

5.1.3. Traveling waves

It turns out that the real part of b is zero. Since β_T is real, only the real part of $\mathbf{S}^{-1}{}_{1,2}$ contributes to $\mathrm{Re}(b)$ (see equation (5-56)). Also, in determining the sign of b, one can neglect all positive factors which are symmetric under the interchange of temperature and solute variations. Referring to equation (5-29) for the determinant, which is pure imaginary,

$$\mathrm{Re}(\mathbf{S}^{-1}{}_{1,2}) = \frac{1}{\mathrm{Det}\,\mathbf{S}}\frac{i\omega\sigma_S}{(1+\omega^2\sigma_S{}^2)} \propto \frac{1}{i\omega(\sigma_S-\sigma_T)}\frac{i\omega\sigma_S}{(1+\omega^2\sigma_S{}^2)} = \frac{\sigma_S}{(\sigma_S-\sigma_T)(1+\omega^2\sigma_S{}^2)}. \tag{5-58}$$

In the above equation and elsewhere, the $\propto$ symbol means that the constant of proportionality is positive and symmetric under $[T \leftrightarrow S]$. Using equation (5-47)

for β_T,

$$\mathrm{Re}(\hat{b}_T) \propto \frac{\sigma_T \sigma_S}{(\sigma_S - \sigma_T)(1+\omega^2\sigma_T)(1+\omega^2\sigma_S)}, \tag{5-59}$$

which is antisymmetric under $[T \leftrightarrow S]$. Therefore

$$\mathrm{Re}(b) = \mathrm{Re}(\hat{b}_T + \hat{b}_S) = 0. \tag{5-60}$$

In other words, the damping coefficient of the standing waves vanishes to third order. When the wavelength of $\mathbf{k}_1$ is varied, the $\frac{8}{3}$ in equation (5-42) is replaced by ν, which changes β_T and β_S by a factor of $\nu/\frac{8}{3}$. The real part of b is therefore zero for all wavelengths.

The result that $\mathrm{Re}(b) = 0$ is not forced by the $[T \leftrightarrow S]$ symmetry; therefore one would expect that any perturbation of the system will break the degeneracy. For instance, doubly diffusive convection with rigid boundary conditions would most likely *not* have $\mathrm{Re}(b) = 0$, even if the symmetry between heat and solute were perfectly preserved.

The degeneracy in the third order system seems to be truly accidental. The view is perhaps naive; it is dogma that all degeneracies of this type, which hold for a wide range of parameter values, are caused by some symmetry of the system. However, if the degeneracy were caused in some simple way by a symmetry, they the real part of *all* the coefficients in the ODE would be zero. This is physically impossible, because it would imply that the amplitude of the traveling wave grows without bound when the critical Rayleigh number is exceeded.

There may be some more subtle symmetry which causes the cubic degeneracy, similar to the symmetry which forces the vertical vorticity modes to vanish at second order (but not higher order) on the center manifold in three-dimensional Bénard convection. For instance, the fact that the $\mathbf{c}_{0,2}$ modes are invariant under the right-left symmetry, $z \leftrightarrow \overline{w}$, may be important.

5.1.4. Standing waves

The coefficient which determines the criticality of the standing waves is

$$\mathrm{Re}(\tfrac{1}{2}a+b)=\tfrac{1}{2}\mathrm{Re}(a), \tag{5-61}$$

where

$$a=-\mathbf{S}^{-1}{}_{1,2}\,\alpha_T+[T\leftrightarrow S]. \tag{5-62}$$

The result is that $\mathrm{Re}(a)$ has the same sign as

$$\begin{aligned}&9(\sigma_S\,\sigma_T\,\omega)^4\\&-(\sigma_S\,\sigma_T\,\omega)^2\left[37\,(\sigma_S+\sigma_T)+49\,\sigma_S\,\sigma_T+12\,(\sigma_S{}^2+\sigma_T{}^2+\sigma_S{}^2\sigma_T+\sigma_S\,\sigma_T{}^2)\right]\\&-16\,(\sigma_S+\sigma_T+\sigma_S\,\sigma_T)\left[\sigma_S{}^2+\sigma_T{}^2+\sigma_S\,\sigma_T(1+\sigma_S+\sigma_T)\right].\end{aligned} \tag{5-63}$$

For fixed σ_S and σ_T this is a quadratic in ω^2, of the form

$$(pos.)\omega^4+(neg.)\omega^2+(neg.). \tag{5-64}$$

where the coefficients are positive or negative as indicated. When $\omega=0$, at the codimension two bifurcation, the real part of a is negative for all Prandtl numbers. Therefore the standing waves are always supercritical when ω^2 is sufficiently small, and subcritical at large enough ω^2.

Before plotting the results, it is best to convert to the standard parameters used in the literature,

$$\sigma_T,\quad \tau=\frac{\sigma_T}{\sigma_S},\quad \text{and}\quad \tilde{\omega}=\frac{\omega}{\sigma_T}. \tag{5-65}$$

The frequency is rescaled since the thermal time scale is used. In terms of these parameters, $\mathrm{Re}(b)$ has the same sign as

$$\begin{aligned}&9\sigma_T\tilde{\omega}^4\\&-\left[(12\sigma_T+37)\tau^2+(12\sigma_T{}^2+49\sigma_T+37)\tau+12\sigma_T(\sigma_T+1)\right]\tilde{\omega}^2\\&-16\tau(\tau+\sigma_T+1)(\tau^2+\sigma_T\tau+\tau+\sigma_T+1).\end{aligned} \tag{5-66}$$

This result agrees with Da Costa *et al.* (1981).

The derivative of the above expression for $\mathrm{Re}(b)$ with respect to τ is negative definite (for $\tau>0$), since the coefficient of $\tilde{\omega}^4$ does not involve τ and the other coefficients are negative. Therefore, when the zero set is mapped for fixed σ_T, $\tilde{\omega}^2$ is monotonically increasing with τ.

The zero set of $\mathrm{Re}(\alpha)$ is drawn for various fixed values of σ_T in fig. 5-1.

Note that the value of $\tilde{\omega}^2$ where $\mathrm{Re}(\alpha)$ is zero stays finite and non-zero in the limit that $\tau \to 0$ or $\tau \to 1$. The lower limit gives a particularly simple result:

$$\lim_{\tau \to 0} \tilde{\omega}^2 \Big|_{\mathrm{Re}(\alpha)=0} = \frac{4}{3}(1+\sigma_T). \tag{5-67}$$

There is no Hopf bifurcation when $\tau = 1$, so it is at first surprising that this limit is also well behaved. The value of $\tilde{\omega}^2$ determines the Rayleigh numbers at which the Hopf bifurcation occurs (see equation (1-122)). In terms of the standard notation, these equations are

$$r_T = \frac{(\sigma_T+\tau)}{\sigma_T}\frac{(1+\tilde{\omega}^2)}{(1-\tau)} \tag{5-68}$$

$$\tilde{r}_S = \frac{(1+\sigma_T)}{\sigma_T}\frac{(\tau^2+\tilde{\omega}^2)}{(1-\tau)}. \tag{5-69}$$

The singularity at $\tau = 1$ is apparent in these formulas.

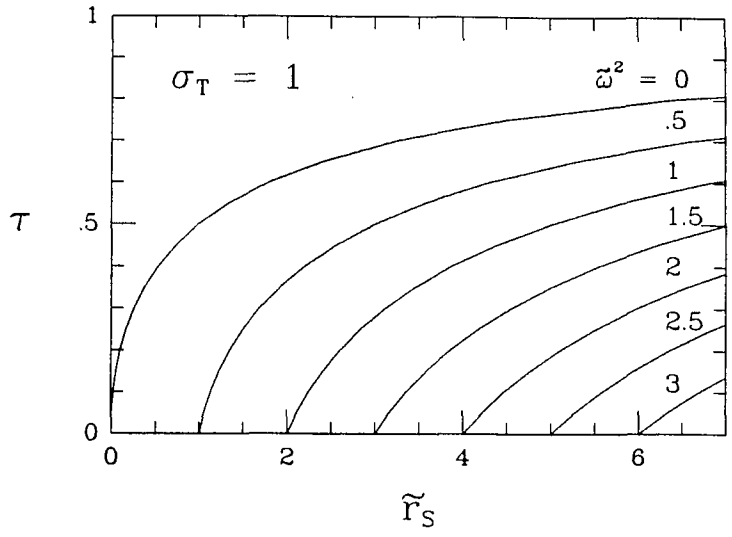

Fig. 5-2. $\tilde{r}_S$ vs. τ (equation (5-69), with $\sigma_T = 1$), for various values of $\tilde{\omega}^2$. The codimension two bifurcation is at $\tilde{\omega}^2 = 0$. This figure is simply expanded in the horizontal direction when σ_T is different than one.

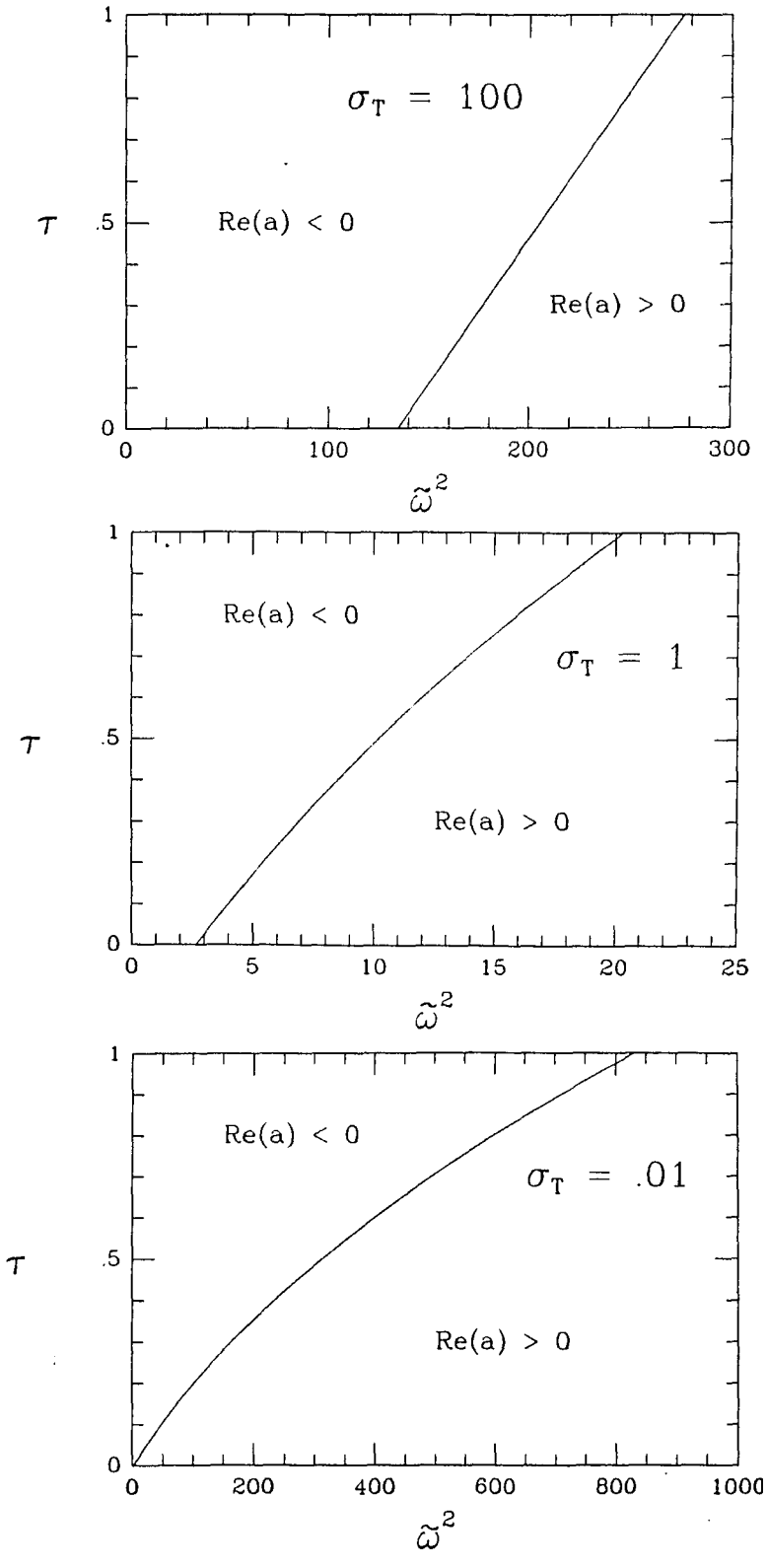

Fig 5-1. The sign of Re(a) is plotted as a function of $\tilde{\omega}^2$ and τ for fixed thermal Prandtl number. The curve is qualitatively the same for all Prandtl numbers.

Conclusion

This dissertation has used the modern theory of dynamical systems to investigate pattern selection in thermal convection. The method used here unifies the perturbation expansion technique of Malkus & Veronis (1958) with the abstract approach of Sattinger (1979), which is based solely on symmetry considerations. The symmetry of the critical modes is used to find the normal forms, which contain undetermined coefficients, for many convection examples. The coefficients are then calculated for doubly diffusive convection using the center manifold approach (Marsden & McCracken 1976, Guckenheimer & Knobloch 1983). The symmetries and psuedosymmetries of the problem are fully exploited in the center manifold reduction.

The bifurcation with the symmetry of the square ($\mathbf{D}_4$ symmetry) is a unifying element in this work. It contains the essential symmetry of steady convection on a square or rhombic lattice, and oscillatory two-dimensional convection.

The steady state bifurcations on the hexagonal lattice are much more complicated that those on a square or rhombic lattice. The analysis of the ordinary differential equations (ODEs) describing this case is included here in detail for the first time. This analysis is made possible by considering the restriction of the ODEs to two invariant subspaces: the equal amplitude subspace and the real subspace. When symmetries are present, higher dimensional systems can often be analyzed using this technique.

Chapter Four provides a complete analysis of three-dimensional stationary bifurcations in doubly diffusive convection with periodic boundary conditions. (The Boussinesq approximation is assumed in these calculations.) The only stable, stationary, small amplitude solutions are the rolls. Two-dimensional oscillatory convection is treated in Chapter Five. When periodic boundary con-

ditions are assumed, it is found that traveling waves are the only small amplitude, stable, two-dimensional solution. In much of the parameter regime there are no stable small amplitude solutions due to subcritical instabilities.

There are two general directions in which this work can be extended: the first is the mathematical analysis of more complicated bifurcations, and the second is the calculation of the normal form coefficients in more examples.

- The complete analysis of three-dimensional oscillatory convection should be possible with more work. In addition, the normal forms for higher-dimensional critical eigenspaces, such as the 8-dimensional representation of fig. mmm, could also be analyzed.

- The calculation of the coefficients in the normal form for rotating convection is completed (in preliminary form). Magnetoconvection has rich symmetries and pseudo-symmetries, and this example should prove to be very interesting. The combination of effects, such as doubly diffusive convection in a rotating layer, provides many examples where the techniques of Chapter Four are applicable.

Appendix A

Notation

(Tildes indicate standard notation)

Rayleigh number

$$R = R_T = \frac{\alpha g \Delta T d^3}{\nu \kappa \pi^4} = \frac{1}{\pi^4}\tilde{R}$$

$$r_T = \frac{R_T}{(\frac{27}{4})}$$

Solute Rayleigh number

$$R_S = \frac{g \Delta \rho d^3}{\nu \kappa_S \pi^4} = \frac{-\kappa_S}{\kappa}\frac{\tilde{R}_S}{\pi^4} = \frac{-1}{\pi^4}\frac{\tilde{R}_S}{\tau}$$

$$r_S = \frac{R_S}{(\frac{27}{4})}$$

$$\tilde{r}_S = \frac{\tilde{R}_S}{\frac{27}{4}} = -r_S \tau$$

Non-dimensional rotation vector

$$\Omega = \frac{2\,\Omega_{dim}\, d^2}{\pi^2 \nu}$$

Taylor number (for vertical rotation vector only)

$$T = |\Omega|^2 = \frac{1}{\pi^4}\tilde{T}$$

Prandtl number

$$\sigma = \frac{\nu}{\kappa} \quad [= \sigma_T]$$

Solute Prandtl number (Schmidt number)

$$\sigma_S = \frac{\nu}{\kappa_S}$$

Viscous time scale

$$t = t_{dim}\,\frac{\pi^2 \nu}{d^2}$$

Thermal time scale

$$t = t_{dim}\,\frac{\pi^2 \kappa}{d^2}$$

Wavevector

$$\mathbf{k} = \frac{\tilde{\mathbf{k}}}{\pi}$$

Exponential

$$e_{\mathbf{k},n} = e^{i(\mathbf{k}\cdot\mathbf{x}+nz)}$$

Temperature variation

$$\vartheta = \sum_{n=-\infty}^{\infty} \sum_{\mathbf{k}} (\vartheta_{\mathbf{k},n}\, e_{\mathbf{k},n})$$

Solute variation

$$\xi = \sum_{n=-\infty}^{\infty} \sum_{\mathbf{k}} (\xi_{\mathbf{k},n}\, e_{\mathbf{k},n})$$

Velocity field

$$\mathbf{u} = \sum_{n=-\infty} \sum_{\mathbf{k}} \left[w_{\mathbf{k},n}\, \mathbf{W}_{\mathbf{k},n} + \zeta_{\mathbf{k},n}\, \mathbf{Z}_{\mathbf{k},n} \right]$$

Vertical velocity mode

$$\mathbf{W}_{\mathbf{k},n} = (-\mathbf{k}n + |\mathbf{k}|^2 \hat{\mathbf{z}})\, e_{\mathbf{k},n}$$

Appendix B

Convection in a Rotating Fluid Layer

This appendix is a reprint of the paper, "Convection in a rotating fluid layer" (Swift 1984), which originally appeared in the conference proceedings: "Geometry and Dynamics: Fluids and Plasmas", Jerry Marsden, ed. (1984). This paper describes the effect of non-Boussinesq terms added to a model, due to Busse and Clever (1979), of convection in a rotating fluid layer. The Busse-Clever model is a degenerate dynamical system; the degeneracy is removed when the non-Boussinesq terms are added.

This paper is a natural extension of the work in Chapter Two on the nonrotating problem, and the previous appendix on the Boussinesq rotating problem. In Chapter Two, the analysis of ODE was done in two steps; the phase space $\{(z_1, z_2, z_3) \in \mathbb{C}^3\}$ was restricted to two invariant subspaces:

(i) The *real solutions*, where z_1, z_2, and z_3 are real, and

(ii) The *equal amplitude solutions*, where $z_1 = z_2 = z_3 \equiv z \in \mathbb{C}$.

The analysis of these two subspaces allows an understanding of the full six dimensional phase space.

In this appendix the analysis of the real solutions (i) is done in the rotating case. The analysis of the equal amplitude solutions (ii), which finds the bifurcations of hexagon and triangle solutions, is the same in the rotating and nonrotating cases. The proof follows:

When restricted to the equal amplitude solutions, the symmetries of the dynamical system are generated by:

$$z \to e^{i\frac{2\pi}{3}} z \quad \text{and}$$
$$z \to \bar{z}$$

in the non-Boussinesq case, and the additional transformation

$$z \to -z$$

in the Boussinesq case. These symmetries are the same in the rotating and nonrotating cases; therefore the results of Chapter Two of this dissertation carry over to the rotating case.

(Recall that the symmetry of the nonrotating case which is *not* present in the rotating case is

$$(z_1, z_2, z_3) \to (z_1, z_3, z_2).$$

This has no effect on the equal amplitude solutions (*ii*).)

Ken Rimey used the Macsyma computer algebra program to help with some of the calculations. He has written a paper (Rimey, 1984) on the computer aided calculation of the general solutions (see Swift 1984, p. 444).

CONVECTION IN A ROTATING FLUID LAYER

James W. Swift[1]

ABSTRACT. A model for convection in a rotating fluid layer, due to Busse and Clever [1], is modified to include non-Boussinesq effects. The three dimensional ODE of the new model has saddle-node, pitchfork, Hopf, and global bifurcations.

1. INTRODUCTION. Thermal convection in a fluid layer heated uniformly from below and rotating about a vertical axis can undergo an unusual instability. Kuppers and Lortz [2] have shown that, if the rotation rate exceeds a critical value, any convection roll is unstable to a new roll oriented preferentially at 58° to the original roll, as measured in the direction of rotation. The subsequent time evolution is somewhat puzzling since there are no stable, steady solutions of small amplitude. Kuppers and Lortz argued that the flow would become turbulent. They did not consider the possibility of limit cycle behavior, perhaps because they considered parameters where the convective instability is direct rather than oscillatory.

Busse and Clever [1] analyzed a system of three rolls, mutually oriented at 60°. They found that the rolls cyclically replace each other due to the Kuppers-Lortz instability, but the transition time from one roll to the next grows exponentially as time goes on. The reason is that there is a heteroclinic cycle connecting the rolls, which are saddle points in the three dimensional phase space of time dependent roll amplitudes. (See Fig. 3). This heteroclinic cycle is like an attracting limit cycle of "infinite period" and the transition time from one roll orientation to the next increases as the trajectory approaches the heteroclinic cycle. Busse and Clever predicted that experimental noise would keep the transition time finite, fluctuating about some mean value depending on the noise level.

Heikes and Busse [3,4] performed experiments on a rotating system using shadowgraph visualization and found that the rolls aligned themselves in

1980 Mathematics Subject Classification. 76E15.

[1] Supported by the California Space Institute under Grant No. CS13-83

Reprinted from Contemporary Mathematics, "Convection in a Rotating Fluid Layer", James W. Swift, (1984) Volume 28, pp. 435-448, by permission of the American Mathematical Society.

randomly oriented patches about 5 to 10 rolls wide. There is a beautiful film of this experiment which shows one patch of rolls growing at the expense of another, with the net effect of rotating the roll orientation at a given point by approximately 60° as predicted.

The experiments of Heikes and Busse were done with methyl alcohol, which satisfies the Boussinesq approximation [5] well, however this approximation is poor in many geophysical and astrophysical examples of rotating convection.

The purpose of this paper is to examine the model of Busse and Clever [1] when non-Boussinesq effects are included and there is no noise. The Boussinesq approximation causes a symmetry in the system of ODE's which forces the saddle connections of the heteroclinic cycle. When the Boussinesq symmetry is broken, the saddle connections are broken to yield a long period limit cycle.

The three dimensional ODE with non-Boussinesq effects included has many secondary bifurcations. The bifurcations of fixed points are computed explicitly, but there is also a global bifurcation of a limit cycle which has not yet been analyzed completely, but which may indicate deterministic chaotic dynamics.

In section 2 the three dimensional system of ODE's is derived from the convection PDE's, and the symmetries of the two systems are related. In section 3 the ODE's are analyzed and the bifurcation diagrams are drawn.

2. FROM PDE's TO ODE's. The equations describing convection in a rotating fluid layer, suitably non-dimensionalized, are [2]:

$$\nabla \cdot \vec{u} = 0$$

$$\frac{1}{P}\left(\frac{\partial \vec{u}}{\partial t} + (\vec{u} \cdot \nabla)\vec{u}\right) = -\nabla\pi + (\theta + \varepsilon\theta^2)\hat{z} + \vec{u} \times \tau\hat{z} + \nabla^2\vec{u} \qquad (1)$$

$$\frac{\partial\theta}{\partial t} + \vec{u} \cdot \nabla\theta = R\,\vec{u} \cdot \hat{z} + \nabla^2\theta.$$

The dependent variables are the fluid velocity $\vec{u}$, the deviation from a linear temperature profile θ, and a generalized pressure π which gives all gradient forces, including the centrifugal force.

The dimensionless parameters are the Prandtl number $P = \nu/\kappa$, the Taylor number $\tau^2 = (4\Omega^2 d^4)/\nu^2$, and the Rayleigh number $R = (\alpha g \Delta T d^3)/\nu\kappa$, where ν is the kinematic viscosity, κ is the thermal conductivity, $\vec{\Omega}$ is the rotation rate about a vertical axis, d is the thickness of the fluid layer, α is the thermal expansion coeffiecient, ΔT is the temperature difference between the top and bottom plates, and $-g\hat{z}$ is the acceleration due to gravity.

The equations (1) have the symmetry of the proper Euclidean group in the horizontal (x,y) plane, that is, the semi-direct product of proper rotations and translations $SO(2) \times R^2$. The rotations are

$$\begin{pmatrix} x \\ y \\ z \end{pmatrix} \to \begin{pmatrix} \cos\phi & \sin\phi & 0 \\ -\sin\phi & \cos\phi & 0 \\ 0 & 0 & 1 \end{pmatrix} \begin{pmatrix} x \\ y \\ z \end{pmatrix} ; \quad \begin{pmatrix} u_x \\ u_y \\ u_z \end{pmatrix} \to \begin{pmatrix} \cos\phi & \sin\phi & 0 \\ -\sin\phi & \cos\phi & 0 \\ 0 & 0 & 1 \end{pmatrix} \begin{pmatrix} u_x \\ u_y \\ u_z \end{pmatrix} \tag{2a}$$

$$\theta \to \theta , \quad \pi \to \pi$$

The translations are

$$\begin{pmatrix} x \\ y \\ z \end{pmatrix} \to \begin{pmatrix} x + D_x \\ y + D_y \\ z \end{pmatrix} ; \quad \vec{u} \to \vec{u}, \quad \theta \to \theta, \quad \pi \to \pi \tag{2b}$$

Note that the Coriolis force term ($\vec{u} \times \tau\hat{z}$) is not symmetric under orientation reversing transformations in the horizontal plane.

In addition, when $\varepsilon = 0$, the equations (1) have the Boussinesq Symmetry, which is a midplane reflection coupled to a temperature inversion.

$$\begin{pmatrix} x \\ y \\ z \end{pmatrix} \to \begin{pmatrix} x \\ y \\ -z \end{pmatrix} , \quad \begin{pmatrix} u_x \\ u_y \\ u_z \end{pmatrix} \to \begin{pmatrix} u_x \\ u_y \\ -u_z \end{pmatrix} , \quad \theta \to -\theta , \quad \pi \to \pi \tag{3}$$

This symmetry requires the validity of the Boussinesq approximation, which says that all material properties, such as ν and κ, are independent of temperature. For real fluids the Boussinesq symmetry is often broken because the viscosity depends on temperature, but the term proportional to ε in (1) also breaks the symmetry and is mathematically simpler.

When the Prandtl number is greater than 1 the convective instability of a roll is due to a single eigenvalue λ passing through zero as the Rayleigh number is increased beyond R_c. As in Golubitsky et. al. [5], and Busse and Clever [1], assume that the bifurcating solutions to the linear problem are a linear combination of three rolls

$$\theta(\vec{x},t) = \mathrm{Re}\Big(\sum_{j=1}^{3} a_j(t) e^{i\vec{k}_j \cdot \vec{x}} f(z) \Big), \quad \vec{x} \equiv (x,y,z)$$

where a_i $(i = 1,2,3)$ are complex amplitudes and $\vec{k}_i$ are three critical wavevectors, mutually oriented at 120° in the horizontal plane, so that $\vec{k}_1 + \vec{k}_2 + \vec{k}_3 = 0$ and $\vec{k}_i \cdot \hat{z} = 0$.

With these assumptions, the Center Manifold Theorem [6] allows a reduction of the PDE's (1) to a system of ODE's for the amplitudes $a_i(t)$,

$$\dot{a}_i = g_i(a_j, \lambda, \varepsilon, \tau, P) = \lambda a_i + \text{higher order terms.}$$

As a result of the rotational symmetry (2a) the vector field g commutes with a cyclic permutation of the a_i's (120° rotation in the x-y plane),

$$g_1(a_2, a_3, a_1) = g_2(a_1, a_2, a_3), \text{ etc.},$$

and the complex conjugation of the a_i's (180° rotation in the x-y plane)

$$g_i(\bar{a}_j) = \overline{g_i(a_j)}$$

A reflection through a vertical plane, coupled with a reversal of the rotation direction leaves (1) invariant, and the consequence for g is

$$g_1(a_1, a_3, a_2, -\tau) = g_1(a_1, a_2, a_3, \tau),$$

however this is not a true symmetry unless $\tau = 0$.

The invariance of (1) under translations in the horizontal plane $\vec{x} \to \vec{x} + \vec{D}$ implies that

$$g_i(e^{i\vec{k}_j \cdot \vec{D}} a_j) = e^{i\vec{k}_i \cdot \vec{D}} g_i(a_j)$$

Finally, the Boussinesq symmetry (3), if it holds, gives an inversion symmetry

$$g_i(-a_j) = -g_i(a_j).$$

The most general ODE with these symmetries is

$$\dot{a}_1 = \lambda a_1 + \varepsilon \bar{a}_2 \bar{a}_3 - a_1(|a_1|^2 + \alpha|a_2|^2 + \beta|a_3|^2) + O(a^4, a^2\lambda, \lambda^2) \qquad (4)$$

plus cyclic permutations for a_2 and a_3, where $\varepsilon = 0$ if the Boussinesq symmetry holds, and $\alpha = \beta$ if there is no rotation.

One effect of the ε term is to cause the a_i's to become real. Let $\phi = \arg(a_1) + \arg(a_2) + \arg(a_3)$, then

$$\dot{\phi} = \frac{\bar{a}_1\dot{a}_1 - a_1\dot{\bar{a}}_1}{2i|a_1|^2} + \frac{\bar{a}_2\dot{a}_2 - a_2\dot{\bar{a}}_2}{2i|a_2|^2} + \frac{\bar{a}_3\dot{a}_3 - a_3\dot{\bar{a}}_3}{2i|a_3|^2} + O(a^3) + O(a\lambda)$$

$$\dot{\phi} = -\varepsilon \sin\phi \left(\frac{|a_2||a_3|}{|a_1|} + \frac{|a_1|a_3|}{|a_2|} + \frac{|a_1||a_2|}{|a_3|} \right) + O(a^3) + O(a\lambda)$$

Therefore ϕ approaches 0 or π, depending on the sign of ε, and we can choose a displacement $\vec{D}$ in (2b) that makes all the a_i's real. Much of Golubitsky et. al. [5] concerned the subtle effects on the phase ϕ when ε is perturbed from zero. These complications also exist in the rotating problem, however the bifurcations that occur for $\lambda = O(\varepsilon^2)$ and $\sum_{i=1}^{3} |a_i|^2 = O(\varepsilon^2)$ can be studied by letting a_i be real and truncating the ODE to third order. Let

$a_1 = x$, $a_2 = y$, $a_3 = z$, and truncate (4) to obtain

$$\begin{aligned} \dot{x} &= \lambda x + \varepsilon yz - x(x^2 + \alpha y^2 + \beta z^2) \\ \dot{y} &= \lambda y + \varepsilon zx - y(y^2 + \alpha z^2 + \beta x^2) \\ \dot{z} &= \lambda z + \varepsilon xy - z(z^2 + \alpha x^2 + \beta y^2). \end{aligned} \tag{5}$$

These equations have the symmetry of a tetrahedron T, a 12 element group of proper rotations about the origin in R^3, generated as the semi-direct product of

$$(x,y,z) \to (y,z,x), \quad (x,y,z) \to (-x,-y,z), \text{ and } (x,y,z) \to (x,-y,-z) \tag{6}$$

When there is no rotation of the fluid layer $\alpha = \beta$ and the equations (5) have the full symmetry of a tetrahedron T_d, a 24 element group generated by (6) plus a reflection through the $x = y$ plane:

$$(x,y,z) \to (y,x,z). \tag{7}$$

The reflection symmetries severely limit the dynamic behavior possible in (5) since a trajectory cannot pass through a hyperplane of reflection. The case where $\alpha = \beta$ was studied by Buzano and Golubitsky [7], and Golubitsky et. al. [5], where the parameter α is replaced by $a = \alpha/1-\alpha$.

When the Boussinesq symmetry holds $\varepsilon = 0$ and the system (5) has the symmetry T_h, generated by (6) and

$$(x,y,z) \to (-x,-y,-z). \tag{8}$$

The 24 element group T_h includes 3 reflections through hyperplanes, such as

$$(x,y,z) \to (-x,y,z).$$

When $\alpha = \beta$ and $\varepsilon = 0$ the equations (5) have the full symmetry of a cube (or octagon), O_h, which is a 48 element group generated by (6), (7), and (8).

Finally, when $\alpha = \beta = 1$ and $\varepsilon = 0$, the equations (5) have spherical symmetry, O(3).

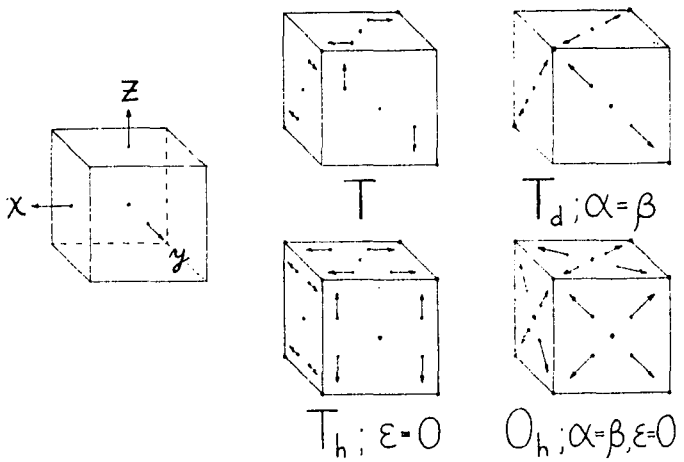

Fig. 1 The symmetries of (5) as represented on a cube. Planes of reflection are indicated by dotted lines.

3. THE BIFURCATION DIAGRAMS. First consider the Boussinesq system ($\varepsilon = 0$), which was studied by May and Leonard [8] as a model of population dynamics. This special case is important because it is an organizing center. For a generic system the non-degeneracy condition $\varepsilon \neq 0$ is likely to hold. In the non-degenerate bifurcation, however, only the solutions which branch off the conduction solution (i.e. $x=y=z=0$) are captured by a local analysis. Therefore one studies the degenerate bifurcation, with $\varepsilon = 0$, and the unfolding, where ε is perturbed from zero. Secondary bifurcations can be analyzed when $\varepsilon \neq 0$, and these bifurcations are guaranteed to occur when ε is sufficiently small. In practice this often gives qualitatively correct behavior even when ε is quite large.

The stationary solutions of (5), when $\varepsilon = 0$, are of four types:

Name	Multiplicity	Equation	Eigenvalues
Conduction (C)	1	$x=y=z=0$	$-\lambda,-\lambda,-\lambda$
Roll (R)	6	$x^2=\lambda,\ y=z=0$	$-2x^2,(1-\beta)x^2,(1-\alpha)x^2$
Hexagon (H)	8	$x^2=y^2=z^2=\frac{\lambda}{1+\alpha+\beta}$	$-2\lambda,(\alpha+\beta-2)x^2\pm i\sqrt{3}(\alpha-\beta)x^2$
General Solution (G)	12	$x^2 = \frac{\lambda(\alpha-1)}{\alpha\beta-1}$	$-2\lambda,\ \frac{2\lambda(\alpha-1)(\beta-1)}{\alpha\beta-1}$,
		$y^2 = \frac{\lambda(\beta-1)}{\alpha\beta-1}$	$\frac{-\lambda[(\alpha-1)(\beta-1)+(\alpha-\beta)^2]}{\alpha\beta-1}$
		$z^2 = 0$	

For rolls and general solutions there are additional solutions related to those listed by the symmetry (see Fig. 1). The eigenvalues of the Jocobian matrix of (5), evaluated at the stationary solution, determine the linear stability of each solution type. A negative eigenvalue is stable.

The general solutions only exist when $(\alpha-1)(\beta-1) > 0$. In the complementary parameter region there are instead the heteroclinic cycles (HC) mentioned in the introduction, which connect 3 rolls as shown in the phase portraits accompanying the bifurcation diagrams (see Fig. 3).

The qualitative behavior of the system (5) can be summarized by drawing bifurcation diagrams for various fixed values of the parameters α and β. The bifurcation diagrams plot $(x^2 + y^2 + z^2)$ as a function of λ. The quantity $x^2 + y^2 + z^2$ is proportional to the convective heat flux (Nusselt # - 1) and λ is proportional to the amount of temperature difference above critical $(R - R_c)$. These bifurcation diagrams describe an experiment where the temperature difference is quasistatically increased.

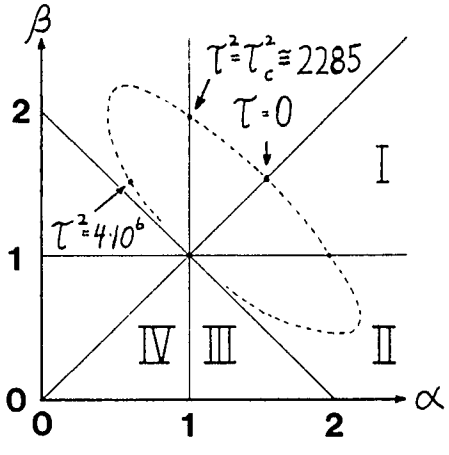

Figure 2. The $\alpha - \beta$ parameter space is divided into open regions by the lines $\alpha = \beta$, $\alpha = 1$, $\beta = 1$, and $\alpha = \beta$, and $\alpha + \beta = 2$. (Only α and β positive are considered for simplicity). Within each region the behavior of the system (5) is qualitatively similar. A reversal of the rotation rate ($\tau \to -\tau$) interchanges α and β, so only $\alpha > \beta$ need be considered. The dotted line summarizes the results of Kuppers and Lortz [2] for infinite Prandtl number and stress-free boundary conditions. Regions III and IV may be relevant for other convection systems.

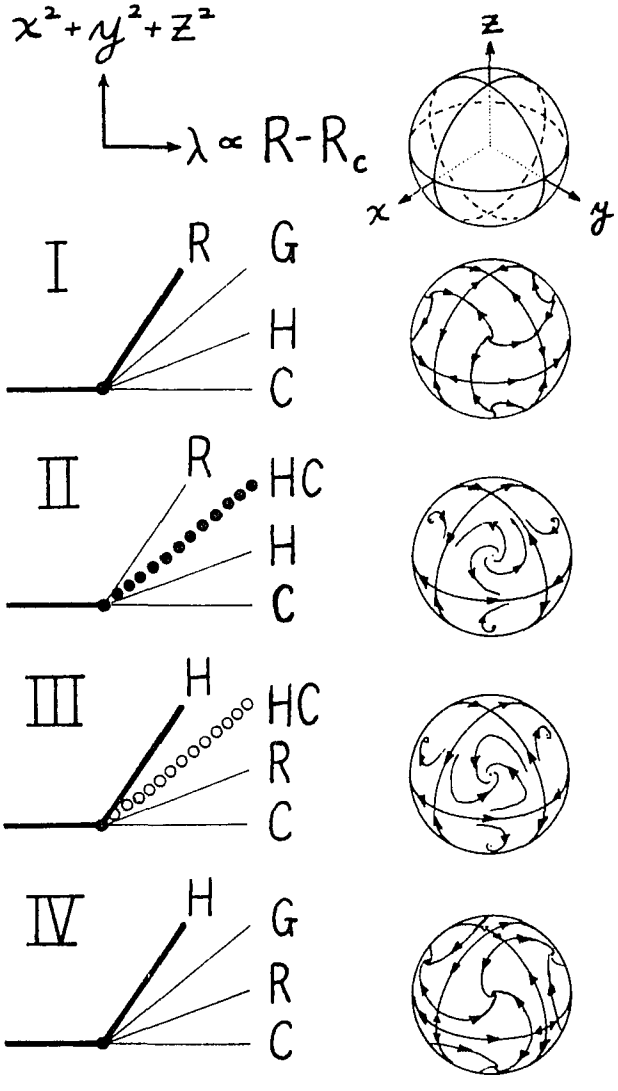

Fig. 3 The bifurcation diagrams of (5) when $\varepsilon = 0$. The Roman numerals correspond to the regions in the $\alpha - \beta$ plane shown in fig. 2. The solution types are: R = roll, H = hexagon, G = general, and HC = heteroclinic cycle. The stable solutions are drawn with a bold line, or solid dots. The phase portraits are schematically drawn for $\lambda > 0$, where x, y, z are the time dependent roll amplitudes. The spheres represent attracting invariant surfaces. These surfaces are not smooth unless $\alpha + \beta = 2$.

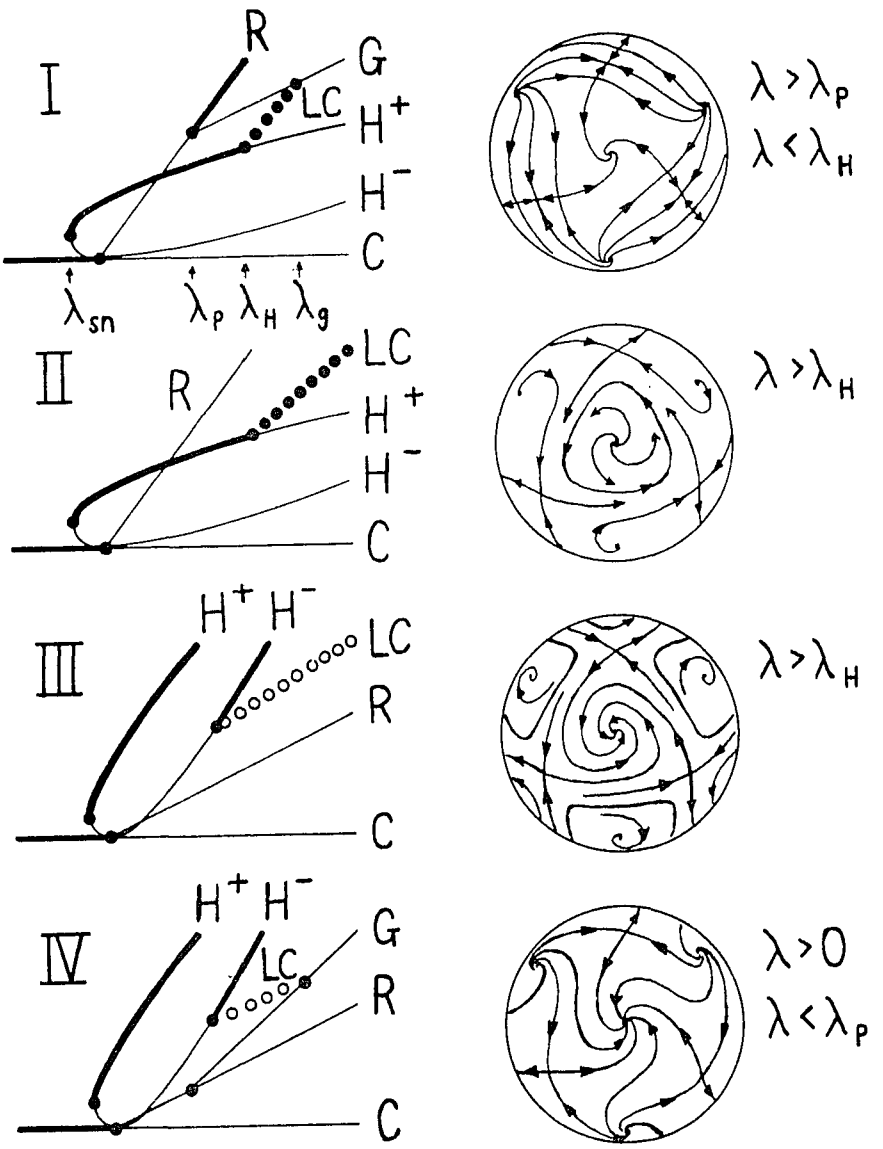

Fig. 4 The bifurcation diagrams of (5) for $\varepsilon > 0$, along with phase portraits at selected values of λ. The solution types are abbreviated as in fig. 3, except LC = limit cycle. In regions I and IV both $\lambda_p > \lambda_H$ and $\lambda_p < \lambda_H$ are possible, although only the latter is drawn. When $\varepsilon \neq 0$ the two types of hexagons, H^+ and H^-, are inequivalent. The four H^+ solutions, related by the symmetry (6), are situated on the vertices of a tetrahedron in phase space. In the original fluid layer H^+ solutions have flow up in the center of the hexagon and down on the sides. The cell walls form a honeycomb pattern.

When $\varepsilon \neq 0$, the stationary solution types are as follows:

Name	Multiplicity	Equation	Eigenvalues
Conduction (C)	1	$x=y=z=0$	$-\lambda,-\lambda,-\lambda$
Roll (R)	6	$x^2=\lambda, y=z=0$	$-2x^2$, $\frac{2-\alpha-\beta}{2}x^2 \pm \sqrt{1/4(\alpha-\beta)^2x^4+\varepsilon^2x^2}$
Hexagon (H^+ or H^-)	4 or 2	$x=y=z=\frac{\varepsilon \pm \sqrt{\varepsilon^2+4\lambda(1+\alpha+\beta)}}{2(1+\alpha+\beta)}$	$-2\lambda-\varepsilon$, $2\lambda-(\alpha+\beta+4)x^2 \pm i\sqrt{3}\,(\alpha-\beta)x^2$
H^+ if sgn(x)>1			
H^- if sgn(x)<1			
General (G)	12	$x^2 \neq y^2 \neq z^2$	Unknown
		$x^2+y^2+z^2 = \frac{\varepsilon^2+(\alpha+\beta-2)\lambda}{\alpha\beta-1}$	

The values of x^2, y^2, and z^2 for the general solution are the three roots of the cubic in x^2:

$$x^6 - \frac{[\varepsilon^2 + (\alpha+\beta-2)\lambda]}{(\alpha\beta - 1)} x^4 + \frac{\delta}{(\alpha\beta-1)^2} \frac{[(1+\alpha+\beta)\varepsilon^2 + \gamma\lambda]}{\gamma} x^2 - \frac{\varepsilon^2\delta^2}{(\alpha\beta-1)^2\gamma^2} = 0.$$

where $\gamma = 1/2\,[(\alpha - \beta)^2 + (\alpha - 1)^2 + (\beta - 1)^2]$
$\delta = (\alpha - 1)(\beta - 1)\,\lambda - \varepsilon^2$

This expression was found by Ken Rimey, using Vaxima and some clever tricks. Vaxima is a Berkeley variant of Macsyma, a computer program developed at MIT for doing algebraic calculations. The eigenvalues of the general solution have not been computed, but they are known when $\varepsilon^2 << \lambda$(same as $\varepsilon = 0$), and when the general solutions are created at the pitchfork bifurcation of the rolls, to be discussed below.

There are many secondary bifurcations:

1) Saddle-node of hexagons. As λ is increased past λ_{sn} two hexagons appear with nonzero amplitude.

$$\lambda_{sn} = \frac{-\varepsilon^2}{4(1+\alpha+\beta)} \qquad x_{sn} = \frac{\varepsilon}{2(1+\alpha+\beta)}$$

2) Pitchfork of a roll, creating two general solutions at

$$\lambda_p = x_p^2 = \frac{\varepsilon^2}{(\alpha-1)(\beta-1)}$$

The general solutions exist for $\lambda > \lambda_p$, and have the same stability near the bifurcation as the rolls have for $\lambda < \lambda_p$.

3) Hopf of a hexagon, creating a limit cycle at

$$\lambda_H = \frac{2\varepsilon^2(\alpha+\beta+4)}{(\alpha+\beta-2)^2} \qquad x_H = \frac{2\varepsilon}{(\alpha+\beta-2)}$$

The sub- or supercriticality of the Hopf bifurcation can be computed relatively simply by exploiting the Z_3 symmetry about the x=y=z axis. Rotate and translate to the coordinates (u,v,w), where the Hopf bifurcation is at the origin and w is the axis of 3-fold symmetry. Let $\xi = u + iv$, then the vector field has the symmetry $\xi \to e^{i2\pi/3}\xi$, $w \to w$, and consequently the Taylor expansion about the fixed point at $\lambda = \lambda_H$, is:

$$\dot{\xi} = i\omega\xi + \sigma\bar{\xi}^2 + \mu\xi|\xi|^2 + \nu w\xi + \ldots$$

$$\dot{w} = -dw + e|\xi|^2 + \ldots$$

where ω, d, and e are real, and σ, μ, and ν are complex.

The center manifold calculation is trivial due to the symmetry: $w = e/d|\xi|^2$. On the bowl shaped center manifold one can change coordinates so that the radial coordinate satisfies

$$\dot{r} = \mathrm{Re}(\mu + \nu e/d)r^3 \equiv -ar^3.$$

When $a > 0$ the bifurcation is supercritical, meaning that there is a stable limit cycle created as λ is varied (assuming $d > 0$). When $a < 0$ the bifurcation is subcritical, and there is an unstable limit cycle near the bifurcation [6].

For the Hopf bifurcation in (5) one finds

$$a = \frac{2}{9}\,\frac{(\alpha+\beta-2)(\alpha+\beta+4)}{(\alpha+\beta+2)}$$

The linear stability of the hexagon and the sign of a determine the stability of the limit cycles, and indicate that the limit cycles exist for $\lambda > \lambda_H$.

4) A global bifurcation occurs when the limit cycle collides with three general solutions. The period of the limit cycle increases until three general solutions are connected in a heteroclinic cycle at λ_g. As λ is increased beyond λ_g the saddle connections are broken and there is no more limit cycle. Assuming the eigenvalues of the general solution are real, the

global bifurcation proceeds as shown in fig. 5. This is sure to be the case near $\alpha = \beta$ since the trajectories in the neighborhood of the hexagon are strongly attracted to the plane normal to the x=y=z axis.

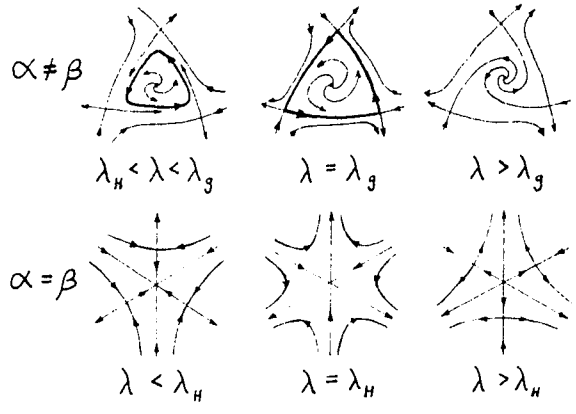

Fig. 5. The global bifurcation when the eigenvalues of the general solution are real. When $\alpha = \beta$ the three general solutions pass through the hexagon solution at λ_H and there is no Hopf bifurcation nor global bifurcation.

Since the ODE is actually three dimensional rather than two dimensional, there is the possibility of chaotic dynamics. As the limit cycle grows it could period double and become "strange". This would be particularly likely if the two attracting eigenvalues of the general solution are complex. Then the saddle connections, or heteroclinic cycle, would appear as in figure 6. Given certain conditions on the eigenvalues [9] there would be chaotic solutions near the heteroclinic cycle. This chaos is, however, very subtle since most trajectories escape to one of the roll solutions.

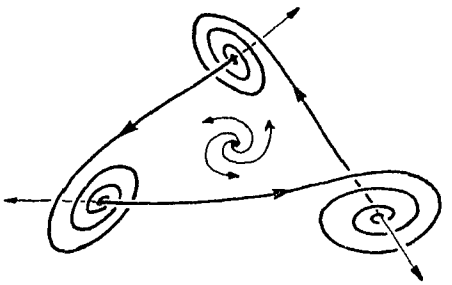

Fig. 6. Possible heteroclinic cycle, an alternative to fig. 5.

4. CONCLUSION. The idea that turbulence may be described as a strange attractor in the dynamical system of the fluid equations has been around for two decades now [10], and there is some experimental verification of this notion [11], however this has never been rigorously demonstrated for any real system. The transition to turbulence in a rotating fluid layer is well suited to small amplitude investigation, although much work remains to be done. In particular, the spatial dependence (i.e. patch structure) has been ignored.

Rotating convection has three properties which may be generally useful in searching for systems where deterministic chaos is present in the center manifold ODE's. First, there is a high degree of symmetry, which forces the center manifold to be multidimensional. Second, when a portion of the symmetry is broken the secondary bifurcations can be analyzed in the unfolding of the degenerate bifurcation. Finally, the symmetry does not include hyperplanes of reflection which would severely limit the possible dynamical behavior.

I would like to thank Edgar Knobloch for encouraging and supporting this work, and Ken Rimey for performing or verifying many of the calculations using Vaxima.

BIBLIOGRAPHY

1. F.H. Busse and R.M. Clever, "Nonstationary Convection in a Rotating System," in Recent Developments in Theoretical and Experimental Fluid Mechanics, ed. U. Muller, K.G. Roesner, and B. Schmidt, Springer, Berlin, 1969, 376-385.

1974 2. G. Kuppers and D. Lortz, "Transition from Laminar Convection to Thermal Turbulence in a Rotating Fluid Layer," J. Fluid Mech., 35 (1969), 609-620.

3. K.E. Heikes and F.H. Busse, "Weakly Nonlinear Turbulence in a Rotating Convection Layer," Ann. N.Y. Acad. Sciences, 357 (1980), 28-36.

4. F.H. Busse and K.E. Heikes, "Convection in a Rotating Layer: A Simple Case of Turbulence," Science, 208 (1980), 173-175.

5. M. Golubitsky, J.W. Swift, and E. Knobloch, "Symmetries and Pattern Selection in Rayleigh-Benard Convection," Physica D, to appear.

6. J. Marsden and M.C. McCracken, "The Hopf Bifurcation and its Applications," Appl. Math. Sci., 19, Springer-Verlag, New York, 1976.

7. E. Buzano and M. Golubitsky, "Bifurcation on the Hexagonal Lattice and the Planar Benard Problem," Phil. Trans. R. Soc. Lond. A, 308 (1983), 617-667.

8. R.M. May and W.J. Leonard, "Nonlinear Aspects of Competition between Three Species," SIAM J. Appl. Math., 29 (1975), 243-253.

9. A. Arneodo, P. Coullet, and C. Tresser, "Oscillators with Chaotic Behavior: An Illustration of a Theorem by Shil'nikov," J. Stat. Phys., 27 (1982), 171-182.

10. E.N. Lorenz, "Deterministic Non-Periodic Flows," J. Atmos. Sci., 20 (1963), 130-141.

11. H.L. Swinney, "Geometry and Dynamics in Experiments on Chaotic Systems," in this volume.

DEPARTMENT OF PHYSICS
UNIVERSITY OF CALIFORNIA
BERKELEY, CA 94720

Note: A further reference should be included.

A. M. Soward, "Bifurcation and Stability of Finite Amplitude Convection in a Rotating Fluid Layer," preprint, University of Newcastle-upon-Tyne.

Dr. Soward also investigates the effect of vertical asymmetries and gets very similar results. Dr. Soward's preprint was in existance when my paper was independently prepared. I thank him for allowing me to publish this anyway.

ABCDEFGHIJ-AMS-8987654

Appendix C

Hopf Bifurcations with $\mathbb{Z}_3$ Symmetry

In general, a tedious but straightforward calculation is needed to determine whether a Hopf bifurcation is subcritical or supercritical. The calculation is made simpler by exploiting the symmetry of the problem. This appendix describes techniques that simplify the calculation when the bifurcation occurs on the axis of a 3-fold rotational symmetry. This $\mathbb{Z}_3$ symmetry comes about in a natural way when there is a cyclic permutation symmetry in a three dimensional ODE:

$$\begin{aligned} \dot{x} &= f(x,y,z) \\ \dot{y} &= f(y,z,x) \\ \dot{z} &= f(z,x,y) \end{aligned} \tag{1}$$

The line $x = y = z$ is invariant, and the permutation

$$(x,y,z) \rightarrow (y,z,x)$$

is a rotation of 120° about this axis (x, y, and z are assumed to be real Cartesian coordinates). When there is no further symmetry, a fixed point on the invariant axis will typically lose stability via a saddle-node bifurcation when the null eigenvector is along the axis, or a Hopf bifurcation when the two dimensional null eigenspace is perpendicular to the invariant axis.

One can in general choose the coordinate system so that the bifurcating fixed point is at the origin. It is usually more efficient to rotate the coordinate system to take advantage of the symmetry before translating the system. Therefore it is not assumed that the bifurcation is at the origin.

This work is motivated by the Hopf bifurcations which occur in two systems of ordinary differential equations which arise in the study of convection in a rotating fluid layer;

$$\dot{x} = \lambda x + \varepsilon yz - x(x^2 + \alpha y^2 + \beta z^2) \tag{2}$$

and

$$\dot{x} = \lambda x - x(x + \alpha y + \beta z) + x(C_1 x^2 + C_2 y^2 + C_3 z^2 + C_4 xy + C_5 xz + C_6 yz). \tag{3}$$

Each equation has two partners which are related by the permutation symmetry (1).

This appendix describes how to efficiently transform from the Cartesian coordinates to a coordinate system where the sub- or supercriticality of the Hopf bifurcation is more easily computed.

The change of variables

Consider the following linear change of coordinates:

$$\begin{pmatrix} u \\ v \\ w \end{pmatrix} = \frac{1}{3} \begin{pmatrix} \sqrt{2} & -\sqrt{\frac{1}{2}} & -\sqrt{\frac{1}{2}} \\ 0 & \sqrt{\frac{3}{2}} & -\sqrt{\frac{3}{2}} \\ 1 & 1 & 1 \end{pmatrix} \begin{pmatrix} x \\ y \\ z \end{pmatrix}. \tag{4}$$

Now the w axis is the axis of three-fold symmetry. It is useful to use a complex coordinate in the perpendicular plane. Let

$$\xi = \frac{1}{\sqrt{2}}(u - iv), \quad \bar{\xi} = \frac{1}{\sqrt{2}}(u + iv).$$

The change of coordinates is now

$$\begin{pmatrix} \xi \\ \bar{\xi} \\ w \end{pmatrix} = \frac{1}{3} \begin{pmatrix} 1 & \bar{\sigma} & \sigma \\ 1 & \sigma & \bar{\sigma} \\ 1 & 1 & 1 \end{pmatrix} \begin{pmatrix} x \\ y \\ z \end{pmatrix}, \tag{5}$$

where

$$\sigma \equiv e^{i2\pi/3}. \tag{6}$$

The following relationships are useful:

$$1 + \sigma + \bar{\sigma} = 0,$$
$$\sigma^2 = \bar{\sigma}, \quad \bar{\sigma}^2 = \sigma,$$
$$\sigma\bar{\sigma} = \sigma^3 = 1, \quad \text{etc.}$$

The inverse of this transformation is

$$\begin{pmatrix} x \\ y \\ z \end{pmatrix} = \begin{pmatrix} 1 & 1 & 1 \\ \sigma & \bar{\sigma} & 1 \\ \bar{\sigma} & \sigma & 1 \end{pmatrix} \begin{pmatrix} \xi \\ \bar{\xi} \\ w \end{pmatrix}. \tag{7}$$

Note that equation (4) is an orthogonal transformation and equation (5) is a unitary transformation, aside from factors of $\sqrt{3}$ and $-i\sqrt{3}$, respectively. The normalization used here is more convenient.

The three-fold rotation about the w axis is

$$\begin{bmatrix} x \\ y \\ z \end{bmatrix} \to \begin{bmatrix} y \\ z \\ x \end{bmatrix} = \begin{bmatrix} 0 & 1 & 0 \\ 0 & 0 & 1 \\ 1 & 0 & 0 \end{bmatrix} \begin{bmatrix} x \\ y \\ z \end{bmatrix}.$$

In the new coordinates this is

$$\begin{bmatrix} \xi \\ \bar{\xi} \\ w \end{bmatrix} \to \frac{1}{3} \begin{bmatrix} 1 & \bar{\sigma} & \sigma \\ 1 & \sigma & \bar{\sigma} \\ 1 & 1 & 1 \end{bmatrix} \begin{bmatrix} 0 & 1 & 0 \\ 0 & 0 & 1 \\ 1 & 0 & 0 \end{bmatrix} \begin{bmatrix} 1 & 1 & 1 \\ \sigma & \bar{\sigma} & 1 \\ \bar{\sigma} & \sigma & 1 \end{bmatrix} \begin{bmatrix} \xi \\ \bar{\xi} \\ w \end{bmatrix} = \begin{bmatrix} \sigma & 0 & 0 \\ 0 & \bar{\sigma} & 0 \\ 0 & 0 & 1 \end{bmatrix} \begin{bmatrix} \xi \\ \bar{\xi} \\ w \end{bmatrix}.$$

The result is that

$$\begin{array}{lll} x \to y & & \xi \to \sigma\xi \\ y \to z & \text{is equivalent to} & \bar{\xi} \to \bar{\sigma}\bar{\xi}. \\ z \to x & & w \to w \end{array} \tag{8}$$

The ODE is equivariant under the $\mathbb{Z}_3$ symmetry, which gives

$$\begin{aligned} \dot{\xi}(\sigma\xi,\bar{\sigma}\bar{\xi},w) &= \sigma\dot{\xi}(\xi,\bar{\xi},w) \\ \dot{\bar{\xi}}(\sigma\xi,\bar{\sigma}\bar{\xi},w) &= \bar{\sigma}\dot{\bar{\xi}}(\xi,\bar{\xi},w) \\ \dot{w}(\sigma\xi,\bar{\sigma}\bar{\xi},w) &= \dot{w}(\xi,\bar{\xi},w). \end{aligned}$$

So far, ξ and $\bar{\xi}$ are treated as independent variables. There is another symmetry of the complex system due to the fact that it is derived from a real system. The ODE is equivariant under the $\mathbb{Z}_2$ symmetry of complex conjugation which gives

$$\xi \to \bar{\xi},\ \bar{\xi} \to \xi,\ w \to w,\ \text{and}$$
$$\alpha \to \bar{\alpha},\ \text{where } \alpha \text{ is any complex constant.}$$

The resulting equivariance of the vector field is

$$\begin{aligned} \dot{\xi}(\bar{\xi},\xi,w;\bar{\alpha}) &= \dot{\bar{\xi}}(\xi,\bar{\xi},w;\alpha) \\ \dot{\bar{\xi}}(\bar{\xi},\xi,w;\bar{\alpha}) &= \dot{\xi}(\xi,\bar{\xi},w;\alpha) \\ \dot{w}(\bar{\xi},\xi,w;\bar{\alpha}) &= \dot{w}(\xi,\bar{\xi},w;\alpha) \end{aligned}$$

The constant α is appended to the arguments of the ODE to describe how complex numbers are treated by the symmetry. Because of the $\mathbb{Z}_2$ symmetry ξ and

$\bar{\xi}$ are no longer independent. The equation for $\dot{\bar{\xi}}$ is superfluous since it is just the complex conjugate of the equation for $\dot{\xi}$.

The invariant functions

Clearly any function of w is invariant, but the monomials of ξ and $\bar{\xi}$ transform under the $\mathbb{Z}_3$ symmetry as

$$\xi^n \bar{\xi}^m \rightarrow \sigma^n \bar{\sigma}^m \xi^n \bar{\xi}^m .$$

This is $\mathbb{Z}_3$-invariant provided

$$(n-m)(mod\,3) = 0.$$

The $\mathbb{Z}_3$-invariant functions (these are not the true invariant functions) can be written as

$$f(|\xi|^2, \xi^3, w), \tag{9}$$

where f is any complex function. In addition, the invariant functions must be real. Therefore, the invariant functions are of the form

$$\mathrm{Re}[f(|\xi|^2, \xi^3, w)]. \tag{10}$$

This includes terms like

$$a\xi^3 + \bar{a}\bar{\xi}^3.$$

The equivariant vector fields

Since w itself is an invariant function, $\dot{w}$ is an invariant function:

$$\dot{w} = \mathrm{Re}[f_0(|\xi|^2, \xi^3, w)].$$

The equivariance condition for monomials in ξ and $\bar{\xi}$ which occur in $\dot{\xi}$ is

$$\xi^n \bar{\xi}^m \rightarrow \sigma^n \bar{\sigma}^m \xi^n \bar{\xi}^m = \sigma \xi^n \bar{\xi}^m, \text{ therefore } \sigma^n \bar{\sigma}^m = \sigma.$$

If $n > m$ then $\sigma^n \bar{\sigma}^m = \sigma^{(n-m)(mod\,3)}$, therefore $(n-m)(mod\,3) = 1$.

If $m > n$ then $\sigma^n \bar{\sigma}^m = \bar{\sigma}^{(m-n)(mod\,3)}$, therefore $(m-n)(mod\,3) = 2$.

Each equivariant monomial can be multiplied by an invariant function to obtain the set of equivariant vector fields:

$$\dot{\xi} = \xi f_1(|\xi|^2, w) + \bar{\xi}^2 f_2(|\xi|^2, w) + \xi^4 f_4(|\xi|^2, w) + \bar{\xi}^5 f_5(|\xi|^2, w) + \cdots .$$

The functions f_n could also be the general invariant functions (10), but this is

unnecessary. The definition used here is somewhat simpler since the f_n are uniquely defined for a given vector field.

An alternate description is

$$\dot{\xi} = \xi g_1(|\xi|^2, \xi^3, w) + \bar{\xi}^2 g_2(|\xi|^2, \xi^3, w),$$

where g_1 and g_2 are complex functions (9).

Hopf bifurcations

The Taylor expansion of an equivariant ODE about a fixed point is

$$\begin{aligned} \dot{\xi} &= \lambda\xi + i\omega\xi + c_1\xi w + c_2\bar{\xi}^2 + c_3\xi|\xi|^2 + O(\xi w^2, \bar{\xi}^2, \xi^4) \\ \dot{w} &= d_1 w + d_2|\xi|^2 + O(w^2, w|\xi|^2, \xi^3) \end{aligned} \tag{11}$$

where $c_n \in \mathbb{C}$ and $\lambda, \omega, d_n \in \mathbb{R}$.

At a Hopf bifurcation $\lambda = 0$ and $\omega \neq 0$. There is a near-identity change of coordinates,

$$\tilde{\xi} = \xi + \frac{c_2}{3i\omega}\bar{\xi}^2,$$

such that the ODE is

$$\dot{\tilde{\xi}} = i\omega\tilde{\xi} + c_1\xi w + c_3\tilde{\xi}|\tilde{\xi}|^2 + \cdots.$$

Note that the quadratic term, $\dot{\xi} = c_2\bar{\xi}^2$, has been eliminated.

The approximate calculation of the center manifold is trivial due to the symmetry: w must be an invariant function of ξ which is zero at $\xi = 0$. The only possible choice is

$$w = -\frac{d_2}{d_1}|\xi|^2 + O(\xi^3).$$

This part of the calculation can be extremely tedious without the symmetry. Therefore, on the center manifold and near $\lambda = 0$, the ODE is

$$\dot{\tilde{\xi}} = \lambda\tilde{\xi} + i\omega\tilde{\xi} + (c_3 - c_1\frac{d_2}{d_1})\tilde{\xi}|\tilde{\xi}|^2 + \cdots.$$

It is illuminating to write this ODE in polar coordinates. Let $\xi = re^{i\vartheta}$, then

$$\dot{r} = \lambda r - ar^3$$

$$\dot{\vartheta} = \omega - br^2$$

$$\text{where } a = -\mathrm{Re}\left(c_3 - c_1\frac{d_2}{d_1}\right) \tag{12}$$

$$\text{and } b = -\mathrm{Im}\left(c_3 - c_1\frac{d_2}{d_1}\right).$$

At a subcritical bifurcation an unstable limit cycle is swallowed up by the fixed point as λ increases past zero. In a supercritical bifurcation a stable limit cycle exists for $\lambda > 0$ (assuming the flow is attracting in the w direction). Which of these occurs depends on the sign of the Hopf parameter (a).

$$\text{The bifurcation is } \begin{cases} \textit{supercritical} \text{ if } a > 0. \\ \textit{subcritical} \text{ if } a < 0. \end{cases}$$

The change of variables (revisited)

All that remains is to change variables from (x,y,z) to (ξ,w). Then a translation along the w axis may be necessary to put the bifurcation at the origin.

From equation (5) the ODE is

$$\dot{\xi} = \tfrac{1}{3}(\dot{x} + \bar{\sigma}\dot{y} + \sigma\dot{z}) \tag{13}$$
$$\dot{w} = \tfrac{1}{3}(\dot{x} + \dot{y} + \dot{z})$$

where the right hand side must be written in terms of ξ, $\bar{\xi}$, and w using equation (7).

This section describes an efficient procedure for changing variables. It is only necessary to transform the $\dot{x}$ equation into the new variables. The full system can then be recovered as follows: The first equation of system (1) can be written as

$$\begin{aligned} \dot{x} = {} & \mathrm{Re}[f_0(|\xi|^2,\xi^3,w)] \\ & + \xi f_1(|\xi|^2,w) + \bar{\xi}\overline{f_1(|\xi|^2,w)} \\ & + \bar{\xi}^2 f_2(|\xi|^2,w) + \xi^2\overline{f_2(|\xi|^2,w)} \\ & + \xi^4 f_4(|\xi|^2,w) + \bar{\xi}^4\overline{f_4(|\xi|^2,w)} + \cdots \end{aligned} \tag{14}$$

since the right hand side is an arbitrary real function. The change of variables (7) transforms system (14) into

$$\dot{\xi} = \xi f_1(|\xi|^2,w)+\bar{\xi}^2 f_2(|\xi|^2,w)+\xi^4 f_4(|\xi|^2,w)+\cdots \qquad (15)$$
$$\dot{w} = \mathrm{Re}[f_0(|\xi|^2,\xi^3,w)].$$

Therefore one can pick out the terms that are necessary to calculate the criticality of the Hopf bifurcation, namely f_0 and f_1.

To prove this, use the fact (equation [8]) that the permutation $x \to y \to z$ is equivalent to $(\xi \to \sigma\xi,\ w \to w)$. Therefore the expression (13) for $\dot{x}$ implies that

$$\begin{aligned}\dot{y} = {} & \mathrm{Re}[f_0(|\xi|^2,\xi^3,w)] \\ & +\sigma\xi f_1(|\xi|^2,w)+\bar{\sigma}\bar{\xi}\overline{f_1(|\xi|^2,w)} \\ & +\sigma\bar{\xi}^2 f_2(|\xi|^2,w)+\bar{\sigma}\xi^2\overline{f_2(|\xi|^2,w)} \\ & +\sigma\xi^4 f_4(|\xi|^2,w)+\bar{\sigma}\bar{\xi}^4\overline{f_4(|\xi|^2,w)}+\cdots \\ \dot{z} = {} & \mathrm{Re}[f_0(|\xi|^2,\xi^3,w)] \\ & +\bar{\sigma}\xi f_1(|\xi|^2,w)+\sigma\bar{\xi}\overline{f_1(|\xi|^2,w)} \\ & +\bar{\sigma}\bar{\xi}^2 f_2(|\xi|^2,w)+\sigma\xi^2\overline{f_2(|\xi|^2,w)} \\ & +\bar{\sigma}\xi^4 f_4(|\xi|^2,w)+\sigma\bar{\xi}^4\overline{f_4(|\xi|^2,w)}+\cdots .\end{aligned} \qquad (16)$$

Equation (15) follows easily from (13), (14), and (16), using $1+\sigma+\bar{\sigma}=0$ and $1+\sigma\bar{\sigma}+\bar{\sigma}\sigma=3$.

Tables of nonlinear terms

More can be done to aid the calculations. It is relatively simple to construct tables of all the information needed to compute the Hopf bifurcation parameter (12) for a bifurcation occurring anywhere on the symmetry axis, when the original system (1) is cubic. The right hand side of $\dot{x} = f(x,y,z)$ must be written in terms of ξ and w. A simple calculation gives

$$\begin{aligned} x^2 &= (2\xi w+2|\xi|^2+w^2)+(\bar{\xi}^2+\xi^2+2\bar{\xi}w) \\ y^2 &= (2\sigma\xi w+2|\xi|^2+w^2)+(\bar{\sigma}^2\bar{\xi}^2+\sigma^2\xi^2+2\bar{\sigma}\bar{\xi}w) \\ z^2 &= (2\bar{\sigma}\xi w+2|\xi|^2+w^2)+(\sigma^2\bar{\xi}^2+\bar{\sigma}^2\xi^2+2\sigma\bar{\xi}w) \\ &\text{etc.}\end{aligned} \qquad (17)$$

Only the first three terms are needed for the calculation of the Hopf parameter. The ξw and w^2 terms are necessary if the bifurcation is not at the origin, as in the motivating equations (2) and (3). In addition, only the real part of the

coefficients of ξw are needed.

In this way, all the essential elements can be computed for all the quadratic monomials in (x, y, z). For instance

$$y^2 \sim -1\xi w + 2|\xi|^2 + w^2,$$

where the $\sim$ represents the equivalence relation obtained when the unnecessary terms are dropped.

	ξw	$\lvert\xi\rvert^2$	w^2
x^2	2	2	1
$y^2 \sim z^2$	-1	2	1
$xy \sim xz$	$\frac{1}{2}$	-1	1
yz	-1	-1	1

The first two rows give the essential information of equations (17), and the other rows are similar. In producing these tables, it helpful to use the "symmetry"

$$x \to x, \quad y \to z, \quad z \to y$$
$$\sigma \to \bar{\sigma}, \text{ but } \xi \to \xi.$$

which corresponds to changing the handedness of the system. For instance z^2 is obtained from y^2 by interchanging σ and $\bar{\sigma}$, but since $\mathrm{Re}(\sigma) = \mathrm{Re}(\bar{\sigma}) = -\frac{1}{2}$ the two rows in the table are identical (i.e. $y^2 \sim z^2$).

The cubic monomials can be tabulated in the same way.

	$\xi\|\xi\|^2$	ξw^2	$\|\xi\|^2 w$	w^3
x^3	3	3	6	1
$xy^2 \sim xz^2$	$\frac{3}{2}$	0	0	1
$x^2y \sim x^2z$	$-\frac{3}{2}$	$\frac{3}{2}$	0	1
xyz	0	0	−3	1
$y^3 \sim z^3$	$-\frac{3}{2}$	$-\frac{3}{2}$	6	1
$y^2z \sim yz^2$	0	$\frac{3}{2}$	0	1

The important terms in the general monomial can be calculated as follows. Use the binomial theorem to expand

$$x^n = [w + (\xi + \bar{\xi})]^n$$
$$= w^n + nw^{n-1}(\xi + \bar{\xi}) + \frac{n(n-1)}{2} w^{n-2}(\xi + \bar{\xi})^2 + \frac{n(n-1)(n-2)}{3!} w^{n-3}(\xi + \bar{\xi})^3 + \cdots .$$

The Z_3 permutation symmetry implies

$$y^n = x^n{}_{[\xi \to \sigma\xi]}$$

and

$$z^n = x^n{}_{[\xi \to \bar{\sigma}\xi]}.$$

Let $N = n_x + n_y + n_z$, then a bit of algebra yields

$$x^{n_x} y^{n_y} z^{n_z} \sim w^N + A_{N-1} w^{N-1} \xi + A_{N-2} w^{N-2} |\xi|^2 + A_{N-3} w^{N-3} \xi |\xi|^2,$$

where

$$A_{N-1} = n_x + \sigma n_y + \bar{\sigma} n_z$$

$$A_{N-2} = n_x(n_x - 1) + n_y(n_y - 1) + n_z(n_z - 1) - (n_x n_y + n_y n_z + n_z n_x)$$

and

$$A_{N-3} = f(n_x, n_y, n_z) + \sigma f(n_y, n_z, n_x) + \bar{\sigma} f(n_z, n_x, n_y),$$

where

$$f(n_x, n_y, n_z) = \frac{n_x(n_x - 1)(n_x - 2)}{2} + n_x[n_y(n_y - 1) + n_z(n_z - 1)]$$
$$+ n_y \frac{n_z(n_z - 1)}{2} + n_z \frac{n_y(n_y - 1)}{2}$$

Example 1

When there is a Hopf bifurcation at the origin of the system (1) written in

Cartesian coordinates, one must evaluate the Taylor series to third order to get all the terms which contribute to the Hopf parameter. The arbitrary $\mathbb{Z}_3$ invariant ODE is

$$\begin{aligned}\dot{x} &= L_1x + L_2y + L_3z \\ &\quad + Q_1x^2 + Q_2y^2 + Q_3z^2 + Q_4xy + Q_5xz + Q_6yz \\ &\quad + x(C_1x^2 + C_2y^2 + C_3z^2 + C_4xy + C_5xz + C_6yz) \\ &\quad + C_7y^3 + C_8z^3 + C_9y^2z + C_{10}yz^2 + \cdots,\end{aligned}$$

where the *L*inear, *Q*uadratic, and *C*ubic coefficients are real. The linear part of $\dot{x}$, written in terms of ξ and w, is

$$\begin{aligned}\dot{x} &= L_1(\xi+\bar{\xi}+w) + L_2(\sigma\xi+\bar{\sigma}\bar{\xi}+w) + L_3(\bar{\sigma}\xi+\sigma\bar{\xi}+w) \\ &= \xi(L_1+\sigma L_2+\bar{\sigma}L_3) + \bar{\xi}(L_1+\bar{\sigma}L_2+\sigma L_3) + w(L_1+L_2+L_3).\end{aligned}$$

Therefore, using (14) and (15),

$$\begin{aligned}\dot{\xi} &= \xi(L_1+\sigma L_2+\bar{\sigma}L_3) \\ \dot{w} &= w(L_1+L_2+L_3).\end{aligned}$$

The condition for a Hopf bifurcation is that

$$L_1 - \tfrac{1}{2}(L_2+L_3) = 0 \quad (\lambda = 0)$$

and

$$L_2 \neq L_3 \quad (\omega \neq 0).$$

The important terms can be read off the tables:

$$\begin{aligned}\dot{\xi} &= [2Q_1 - (Q_2+Q_3) + \tfrac{1}{2}(Q_4+Q_5) - Q_6]\xi w \\ &\quad + [3C_1 + \tfrac{3}{2}(C_2+C_3) - \tfrac{3}{2}(C_4+C_5+C_7+C_8)]\xi|\xi|^2 \\ &\quad + i\xi(Real) + O(\xi^2, \xi w^2, \xi|\xi|^4)\end{aligned}$$

$$\dot{w} = (L_1+L_2+L_3)w + [2(Q_1+Q_2+Q_3) - (Q_4+Q_5+Q_6)]|\xi|^2 + O(w^2, |\xi|^2 w).$$

From equations (11) and (12), the Hopf parameter is

$$\begin{aligned}a = \frac{[2(Q_1+Q_2+Q_3) - (Q_4+Q_5+Q_6)]}{(L_1+L_2+L_3)}&[2Q_1 - (Q_2+Q_3) + \tfrac{1}{2}(Q_4+Q_5) - Q_6] \\ &- [3C_1 + \tfrac{3}{2}(C_2+C_3) - \tfrac{3}{2}(C_4+C_5+C_7+C_8)]\end{aligned}$$

This concludes the calculation for the general system (1) when the Hopf bifurcation is at the origin.

Example 2

Consider the Hopf bifurcation in system (2),

$$\dot{x} = \lambda x + \varepsilon yz - x(x^2 + \alpha y^2 + \beta z^2)$$

Using the tables, the ODE transforms to

$$\dot{\xi} = \lambda\xi - \varepsilon\xi w - 3\xi w^2 - [3 + \tfrac{3}{2}(\alpha+\beta)]\xi|\xi|^2 + i\xi(Real) + O(\bar{\xi}^2, \xi|\xi|^4).$$

$$\dot{w} = \lambda w + \varepsilon w^2 - (1+\alpha+\beta)w^3 - 6|\xi|^2 w - \varepsilon|\xi|^2$$

The Hopf bifurcation is at the simultaneous solution of two conditions. First, the bifurcation is at a fixed point ($\dot{w} = 0$)

$$0 = \lambda + \varepsilon w - (1+\alpha+\beta)w^2. \tag{18}$$

Second, the linearization about the fixed point must be $\dot{\xi} = i\omega\xi$

$$0 = \lambda - \varepsilon w - 3w^2. \tag{19}$$

The parameters ε, α, and β are considered fixed, while w and λ are adjusted to satisfy equations (18) and (19). The solution is

$$w_H = \frac{2\varepsilon}{(\alpha+\beta-2)}, \quad \lambda_H = \frac{2\varepsilon^2(\alpha+\beta+4)}{(\alpha+\beta-2)^2}.$$

When the origin is translated to $w = w_H$, the following partial derivatives must be calculated for the Taylor expansion of the ODE:

$$\left.\frac{\partial\dot{\xi}}{\partial w}\right|_{\substack{\lambda=\lambda_H \\ w=w_H}} = -\varepsilon\xi - 6\xi w_H$$

$$= -\varepsilon\xi\,\frac{(\alpha+\beta+10)}{(\alpha+\beta-2)}$$

$$\left.\frac{\partial\dot{w}}{\partial w}\right|_{\substack{\lambda=\lambda_H \\ w=w_H}} = \lambda_H + 2\varepsilon w_H - 6|\xi|^2 - 3(1+\alpha+\beta)w_H^2$$

$$-6\varepsilon^2\frac{(\alpha+\beta-2)^2}{(\alpha+\beta+2)} - 6|\xi|^2.$$

Let $\tilde{w} = w - w_H$. At $\lambda = \lambda_H$, the ODE has a Taylor expansion

$$\dot{\xi} = -\tfrac{1}{3}\varepsilon\,\frac{(\alpha+\beta+10)}{(\alpha+\beta-2)}\xi\tilde{w} - [3 + \tfrac{3}{2}(\alpha+\beta)]\xi|\xi|^2 + O(\bar{\xi}^2, \xi\tilde{w}^2)$$

$$\dot{\tilde{w}} = -6\varepsilon^2\,\frac{(\alpha+\beta+2)}{(\alpha+\beta-2)^2}\tilde{w} - \varepsilon|\xi|^2 - 6|\xi|^2 w_H + O(|\xi|^2\tilde{w}, \tilde{w}^2)$$

$$= -6\varepsilon^2 \frac{(\alpha+\beta+2)}{(\alpha+\beta-2)^2}\tilde{w} - \varepsilon \frac{(\alpha+\beta+10)}{(\alpha+\beta-2)}|\xi|^2 + \cdots .$$

Therefore, the approximation to the center manifold is

$$\tilde{w} = -\frac{1}{6\varepsilon}\frac{(\alpha+\beta+10)(\alpha+\beta-2)}{(\alpha+\beta+2)}|\xi|^2$$

At $\varepsilon = 0$ the planes $x = 0$, $y = 0$, and $z = 0$ are invariant. Therefore, as $\varepsilon \to 0$ the center manifold approaches the shape of the corner of a cube, and the curvature at the fixed point approaches infinity. For any $\varepsilon \neq 0$ this singularity does not effect the Hopf parameter, which is

$$a = -\left[-\frac{\varepsilon}{3}\frac{(\alpha+\beta+10)}{(\alpha+\beta-2)}\right]\left[-\frac{1}{6\varepsilon}\frac{(\alpha+\beta+10)(\alpha+\beta-2)}{(\alpha+\beta+2)}\right] - \frac{3}{2}(\alpha+\beta+2)$$

$$= -\frac{4}{3}\frac{(\alpha+\beta+4)(\alpha+\beta-2)}{(\alpha+\beta+2)}.$$

This calculation could have been done using the results of example 1. The system would first have to be translated (in Euclidean coordinates) to put the bifurcation at the origin. The method used here is much more efficient.

Example 3

The third example arises from a special case of equation (2), when the quadratic (and all even power) terms are zero due to an inversion symmetry

$$(x,y,z) \to -(x,y,z).$$

Assume $\alpha \neq \beta$ (this means that the fluid layer is indeed rotating). When $\alpha+\beta < 2$ the complex pair of eigenvalues of the fixed point at $x = y = z$ has negative real part, and when $\alpha+\beta > 2$ the eigenvalue pair has positive real part. There must be a Hopf bifurcation as $\alpha+\beta$ is increased past two. However, the case when $\alpha+\beta = 2$ is degenerate, and higher order terms must be added. In addition, an unfolding parameter

$$\mu \equiv \alpha+\beta-2$$

is needed to describe the dynamics near the degenerate bifurcation. The following analysis is only valid when $\mu \ll 1$, since otherwise the secondary bifurca-

tions predicted are at too large an amplitude.

When x replaces x^2, etc., and the time derivative is rescaled by a factor of two, the fifth order system obtained from extending equation (2) can be written as the third order system (3)

$$\dot{x} = \lambda x - x(x + \alpha y + \beta z) + x(C_1 x^2 + C_2 y^2 + C_3 z^2 + C_4 xy + C_5 xz + C_6 yz).$$

While a complete understanding of this ODE is too difficult at present, it is useful to analyze the Hopf bifurcation that accompanies the change of stability of the fixed point at $x = y = z$. Using the tables, the system (3) is equivalent to

$$\dot{\xi} = \lambda\xi - (2 + \tfrac{1}{2}\alpha + \tfrac{1}{2}\beta)w\,\xi + [3C_1 + \tfrac{3}{2}(C_2 + C_3) - \tfrac{3}{2}(C_4 + C_5)]\xi\,|\xi|^2 + [3C_1 + \tfrac{3}{2}(C_4 + C_5)]\xi w^2$$
$$\dot{w} = \lambda w - (2 - \alpha - \beta)\,|\xi|^2 - (1 + \alpha + \beta)w^2 + (6C_1 - 3C_6)\,|\xi|^2 w + (C_1 + C_2 + \cdots + C_6)w^3.$$

The Hopf bifurcation occurs when $\dot{w} = 0$ at $\xi = 0$

$$0 = \lambda - (1 + \alpha + \beta)w + (C_1 + C_2 + \cdots + C_6)w^2,$$

and $\dot{\xi} =$ (pure imaginary)$\xi + \cdots$.

$$0 = \lambda - [2 + \tfrac{1}{2}(\alpha + \beta)]w + [3C_1 + \tfrac{3}{2}(C_4 + C_5)]w^2.$$

Subtract these two equations to eliminate λ:

$$\mu = \alpha + \beta - 2 = -[4C_1 - 2(C_2 + C_3) + C_4 + C_5 - 2C_6]w_H,$$

or

$$w_H = \frac{-\mu}{2[2C_1 - C_2 - C_3 + \frac{1}{2}(C_4 + C_5) - C_6]} \equiv \frac{-\mu}{A}.$$

A necessary non-degeneracy condition is that the denominator does not vanish. Therefore assume that

$$A \neq 0, \quad w_H = O(\mu).$$

The corresponding value of λ is

$$\lambda_H = (\mu + 3)w_H + (C_1 + C_2 + \cdots + C_6)w_H^2.$$

Since μ is small,

$$\lambda_H = 3w_H + O(\mu^2)$$

and the $O(\mu^2)$ terms can be neglected. It must be remembered that x, y, and z are non-negative, since they are the square of the original coordinates. This

implies that

$$w_H, \lambda_H > 0.$$

The Taylor expansion is obtained using

$$\dot{\xi}\Big|_{\substack{\lambda=\lambda_H \\ w=w_H}} = [3C_1 + \tfrac{3}{2}(C_2+C_3-C_4-C_5)]\xi|\xi|^2$$

$$\frac{\partial \dot{\xi}}{\partial w}\Big|_{\substack{\lambda=\lambda_H \\ w=w_H}} = -[2+\tfrac{1}{2}(\alpha+\beta)]\xi + 2[3C_1+\tfrac{3}{2}(C_4+C_5)]\xi w_H$$

$$= -3\xi + O(\mu\xi)$$

$$\dot{w}\Big|_{\substack{\lambda=\lambda_H \\ w=w_H}} = (6C_1-3C_6)|\xi|^2 w_H + \mu|\xi|^2$$

$$\frac{\partial \dot{w}}{\partial w}\Big|_{\substack{\lambda=\lambda_H \\ w=w_H}} = -(1+\alpha+\beta)w_H + (6C_1-3C_6)|\xi|^2 + (C_1+C_2+\cdots+C_6)2w_H{}^2$$

$$= -3w_H + O(\mu^2) + O(|\xi|^2).$$

The Taylor expansion about $\xi = 0$, $w = w_H$ is

$$\dot{\xi} = [3C_1 + \tfrac{3}{2}(C_2+C_3-C_4-C_5)]\xi|\xi|^2 - 3\xi\tilde{w} + O(\mu)\xi\tilde{w}$$

$$\dot{\tilde{w}} = (6C_1-3C_6)|\xi|^2\left(\frac{-\mu}{A}\right) + \mu|\xi|^2 - 3\left(\frac{-\mu}{A}\right)\tilde{w} + O(\mu^2 w_H)$$

where $\tilde{w} = w - w_H$. The equation for the center manifold is

$$\tilde{w} = \tfrac{2}{3}[C_1+C_2+C_3-\tfrac{1}{2}(C_4+C_5+C_6)]|\xi|^2$$

and the Hopf parameter is

$$\alpha = -C_1 + \tfrac{1}{2}(C_2+C_3+C_4+C_5) - C_6.$$

Therefore, at $\lambda_H \approx -3\mu/A > 0$ there is a Hopf bifurcation which is subcritical or supercritical depending on the sign of α. The ultimate fate of this limit cycle as it grows is harder to figure out, since this involves a global calculation.

Conclusion

This appendix provides a recipe for calculating the Hopf bifurcation parameter which takes full advantage of the $\mathbb{Z}_3$ symmetry in systems defined by

equation (1). The resulting formulas are remarkably simple considering the complexity of the calculation without the symmetry.

Heikes, K. E. and F. H. Busse, "Weakly nonlinear turbulence in a rotating convection layer," *Ann. N. Y. Acad. Sciences*, vol. 357, pp. 28-36, 1980.

Hirsch, M., C. Pugh, and M. Schub, *Invariant manifolds*, 583, Springer lecture notes, 1967.

Huppert, H. E. and P. C. Manins, "Limiting conditions for salt-fingering at an interface," *Deep-Sea Res.*, vol. 20, pp. 315-323, 1973.

Huppert, H. E. and D. R. Moore, "Nonlinear double-diffusive convection," *J. Fluid Mech.*, vol. 78, pp. 821-854, 1976.

Jeffreys, H., "The instability of a compressible fluid heated below," *Proc. Camb. Phil. Soc.*, vol. 26, pp. 170-172, 1930.

Joseph, D. D., "Global stability of the conduction-diffusion solution," *Arch. Rational Mech. Anal.*, vol. 36, pp. 285-292, 1970.

Joseph, D. D., *Stability of Fluid Motions I*, Springer Tracts in Natural Philosophy, 27, Springer-Verlag, Berlin, 1976.

Joseph, D. D., *Stability of Fluid Motions II*, Springer Tracts in Natural Philosophy, 28, Springer-Verlag, Berlin, 1976.

Knobloch, E. and M. R. E. Proctor, "Nonlinear periodic convection in double-diffusive systems," *J. Fluid Mech.*, vol. 108, pp. 291-316, 1981.

Krishnamurti, R., "Finite Amplitude convection with changing mean temperature. Part 1. Theory," *J. Fluid Mech.*, vol. 33, no. 4, pp. 445-455, 1968.

Krishnamurti, R., "Finite Amplitude convection with changing mean temperature. Part 2. An experimental test of the theory," *J. Fluid Mech.*, vol. 33, no. 4, pp. 457-463, 1968.

Krishnamurti, R., "On the transition to turbulent convection. Part I. The transition from two- to three-dimensional flow," *J. Fluid Mech.*, vol. 42, pp. 205-307, 1970a.

Krishnamurti, R., "On the transition to turbulent convection. Part II. The transition from two- to three-dimensional flow," *J. Fluid Mech.*, vol. 42, pp. 309-320, 1970b.

Küppers, G. and D. Lortz, "Transition from laminar convection to thermal turbulence in a rotating fluid layer," *J. Fluid Mech.*, vol. 35, pp. 609-620, 1969.

Küppers, G., "The stability of steady finite amplitude convection in a rotating fluid layer," *Physics Letters*, vol. 32A, no. 1, pp. 7-8, 1970.

Malkus, W. V. R. and G. Veronis, "Finite amplitude cellular convection," *J. Fluid Mech.*, vol. 4, pp. 225-260, 1958.

Marsden, J. and M. McCracken, *The Hopf Bifurcation and Its Applications*, Springer-Verlag, 1976.

Nagata, W. and J. W. Thomas, "Bifurcation in doubly-diffusive systems: Equilibrium Solutions I," *Preprint, Colorado State University*, 1983.

Newell, A. C. and J. A. Whitehead, "Finite bandwidth, finite amplitude convection," *J. Fluid Mech.*, vol. 38, no. 2, pp. 279-303, 1969.

Palm, E., "On the tendency towards hexagonal cells in steady convection," *J. Fluid Mech.*, vol. 8, no. 2, pp. 183-192, 1960.

Pearlstein, A. J., "Effect of rotation on the stability of a doubly diffusive fluid layer," *J. Fluid Mech.*, vol. 103, pp. 389-412, 1981.

Rayleigh, Lord, "On convective currents in a horizontal layer of fluid when the higher temperature is on the under side," *Phil. Mag.*, vol. 32, pp. 529-46, 1916.

Riahi, N., "Nonlinear convection in a porous layer with finite conducting boundaries," *J. Fluid Mech.*, vol. 129, pp. 153-171, 1983.

Rimey, K., "A system of polynomial eauations and their solution by an unusual method," *SIGSAM*, May 1984.

Sattinger, D. H., "Group Theoretic Methods in Bifurcation Theory," *Lecture Notes in Mathematics*, vol. 762, Springer-Verlag, Berlin, 1979.

Schlüter, A., D. Lortz, and F. Busse, "On the stability of finite amplitude convection," *J. Fluid Mech.*, vol. 23, pp. 129-144, 1965.

Segel, L. A. and J. T. Stuart, "On the question of the preferred mode in cellular thermal convection," *J. Fluid Mech.*, vol. 13, no. 2, pp. 289-306, 1962.

Segel, L. A., "Distant side-walls cause slow amplitude modulation of cellular convection," *J. Fluid Mech.*, vol. 38, no. 1, pp. 203-224, 1969.

Shirtcliffe, T. G. L. and J. S. Turner, "Observations of cell structure of salt fingers," *J. Fluid Mech.*, vol. 41, no. 4, pp. 707-719, 1970.

Spiegel, E. A. and G. Veronis, "On the Boussinesq approximation for a compressible fluid," *Astrophys. J.*, vol. 131, pp. 442-447, 1960.

Stommel, H., A. B. Arons, and D. Blanchard, "An oceanographic curiosity: the perpetual salt fountain," *Deep-Sea Res.*, vol. 3, pp. 152-153, 1956.

Swift, J. W., "Convection in a rotating fluid layer," in *Contemporary Mathematics, vol. 28*, ed. J. Marsden, pp. 435-448, American Mathematical Society, 1984.

Veronis, G., "Cellular convection with finite amplitude in a rotating system," *J. Fluid Mech.*, vol. 5, pp. 401-435, 1959.

Veronis, G., "On finite amplitude instability in themohaline convection," *J. Mar. Res.*, vol. 23, pp. 1-17, 1965.

Veronis, G., "Motions at subcritical values of the Rayleigh number in a rotating fluid," *J. Fluid Mech.*, vol. 24, pp. 545-554, 1966.

Veronis, G., "Effect of a stabilizing gradient of solute on thermal convection," *J. Fluid Mech.*, vol. 34, pp. 315-336, 1968.

Veronis, G., "Large-amplitude Bénard convection in a rotating fluid," *J. Fluid Mech.*, vol. 31, pp. 113-139, 1968.

Walden, R. W. and G. Ahlers, "Non-Boussinesq and penetrative convection in a cylindrical cell," *J. Fluid Mech.*, vol. 109, pp. 89-114, 1981.

Weiss, N. O., "Convection in the presence of restraints," *Phil. Trans. Roy. Soc. Lon. A*, vol. 256, pp. 99-147, 1964.

White, D., "The planforms and onset of convection with temperature-dependent viscosity," *Preprint, Bullard Laboratories, Cambridge University*, 1983.

Whitehead, J. A. and B. Parsons, "Observations of convection at Rayleigh numbers up to 760,000 in a fluid with large Prandtl number," *Geophys. Astrophys. Fluid Dyn.*, vol. 9, pp. 201-217, 1978.

Whitehead, J. A., "Dislocations in convection and the onset of chaos," *Phys. Fluids*, vol. 26, no. 10, pp. 2899-2904, 1983.